STUDY OF UNSTEADY ANNULAR FLOWS BETWEEN ECCENTRIC CYLINDERS

by

Woo-Gun, Sim

Department of Mechanical Engineering
McGill University
Montreal, Canada.

September, 1991

A Thesis submitted to the Faculty of Graduate Studies and Research
in partial fulfillment of the requirements for the degree of
Doctor of Philosophy.

Abstract

A new numerical method has been developed to evaluate the fluid-dynamic forces acting on a cylinder immersed in flowing or quiescent fluid for eccentric configurations, in connection with the flow-induced-vibration problem. The fluid-dynamic forces, generated by translational motion in quiescent fluid or by a flexural motion in axial(laminar) flow, have been formulated based on a spectral collocation method. This numerical method is capable of taking fully into account unsteady viscous effects and of predicting viscous forces rigorously rather than approximately, in contrast with existing theories.

This approach uses suitable spectral expansions for fluid-dynamic parameters, involving Chebyshev polynomials, Fourier series and exponential functions; in these expansions, the *a priori* unknown coefficients are determined through a collocation method. A variant of the spectral collocation method was developed for the three-dimensional problem of flexural motions of the cylinder, with the aid of the finite-difference method in a hybrid scheme. The method has been validated by applying it to several types of steady and unsteady flows for which analytical solutions are available. Considering the numerical results, semi-analytical and simplified analytical approaches have been developed for estimating the fluid-dynamic forces. Good agreement with the numerical results was found.

Experiments have been conducted to further test the validity of the numerical method, involving oscillations of the outer cylinder in an annular configuration. The unsteady pressure generated in either rocking or translational motion of this cylinder was measured on the wall of the fixed inner cylinder at various axial and azimuthal locations. The theoretical model was found to be in good agreement with the experiments designed to test it.

It was found that the present numerical method may be used to evaluate the fluid-dynamic forces rigorously. The contribution of unsteady viscous forces to the overall unsteady forces is significant for low values of the oscillatory Reynolds number, especially in very narrow annuli.

Résumé

Une nouvelle méthode numérique est développée afin d'évaluer les forces hydrodynamiques agissant sur un cylindre immergé dans un fluide en écoulement et au repos, pour des configurations éccentrées, en relation au problème de vibrations induites par l'écoulement. Les forces hydrodynamiques, généreés par le mouvement de translation dans un fluide au repos, ou par le mouvement en flexion dans un écoulement axial(laminaire), ont été formulées en se basant sur une méthode spectrale de collocation. Cette méthode numérique prend en compte tous les effets de viscosité instable et, contrairement aux théories existantes, prédit précisément les forces visqueuses.

Cette approche utilise des développements spectraux appropriés pour les paramètres hydrodynamiques, faisant appel aux polynômes de Chebyshev, aux séries de Fourier et aux fonctions exponentielles. Dans ces développements, les coefficients *a priori* inconnus sont déterminés par une la méthode de collocation. Cependant, la méthode spectrale de collocation a été modifiée pour le problème tri-dimensionnel des mouvements en flexion du cylindre à l'aide de la méthode des différences finies utilisant un schéma hybride. La méthode a été validée en l'appliquant à différents types d'écoulements stationnaires et instationnaires pour lesquels des solutions analytiques sont disponibles. Au vu des résultats numériques, des approches semi-analytiques et analytiques simplifiées ont été développées pour estimer les forces hydrodynamiques. Un bon accord avec les résultats numériques a été trouvé.

Des expériences ont été menées avec le cylindre extérieur étant en oscillation dans une configuration annulaire afin de confirmer la validité de la méthode numérique. La pression instable générée par le mouvement de translation et de pivot du cylindre a été mesurée sur la paroi intérieure du cylindre fixe et à différents points axiaux et circonférentiels. Un bon accord des résultats a été trouvé entre le modèle théorique et les expériences.

La présente méthode numérique peut être utilisée afin d'évaluer de façon précise les forces hydrodynamiques. La contribution des forces visqueuses instationnaires aux forces instationnaires totales est siguificative pour de faibles valeurs du nombre de

Reynolds oscillatoire et particulièrement pour les configuration annulaires étroites.

Acknowledgements

The author would like to express his sincere appreciation and thanks to Professors M. P. Païdoussis and D. Mateescu, for their guidance and encouragement during the course of this research work. Their suggestions, with great insight and experience in the field of flow-induced vibration, played a most important role in this work.

Special thanks are extended to Mr Steve Markhauser for the excellent work he did in fabricating the experimental apparatus.

The author is also grateful to, and acknowledges the financial support from, the NSERC and FCAR grants of his research directors.

Finally, the author offers his heartfelt appreciation to his family.

Contents

Nomenclature

ORDINARY SYMBOLS

a	Radius of the centre-body
A, B, C, D	Variables derived from the coordinate transformations, defined in equation (4.5)
A_s	Cross-sectional area of the centre-body
b	Radius of the outer cylinder
c_f	Friction coefficient
C_m	Added mass coefficient, defined in equation (5.47)
C_v	Damping coefficient, defined in equation (5.47)
D_H	Hydraulic diameter, $2H$
ϵ	Eccentricity of annulus
e_I, e_O	Lateral displacements of the moving cylinders for oscillations in the plane of symmetry
e_r	Radial displacements of the moving cylinders
EI	Rigidity of flexible cylinder(Young's modulus × moment of inertia)
f	General fluid-dynamic paremeter or oscillation frequency
$\bar{f}$	Mean value of fluid-dynamic parameter
$\hat{f}$	Nondimensional fluid-dynamic parameter
f_b	Equation of body surface
$\mathbf{f}_v$	Velocity of oscillating structure
F	Fluid-dynamic forces for oscillations in the plane of symmetry
$F_k(\theta)$	Fourier expansions
g_I, g_O	Lateral displacements of the moving cylinders for oscillations normal to the symmetry plane
G	Fluid-dynamic forces for oscillations normal to the symmetry plane
G_{1k}, G_{2k}	Equivalent added mass coefficients, defined in eqation (2.38)
H	Annular gap between two cylinders

$\Im$	Imaginary component of complex value
$\vec{i}_x, \vec{i}_r, \vec{i}_\Theta$	Unit vectors associated with the coordinate system
k	Fluidelastic stiffness
L	Length of cylinder
M	Virtual mass, defined in equation (2.7)
P_∞	Stagnation pressure
P_{2k}, P_{1k}, P_{0k}	Inertia, damping and stiffness components of fluid force, defined in equation (2.40)
$\Re$	Real component of complex value
Re	Reynolds number based on the hydraulic diameter
Re_s	Oscillatory Reynolds number
t	Time
U, V, W, P	Steady flow velocities and pressure
U^*, V^*, W^*, P^*	Flow velocities and pressure including unsteady component
u^*, v^*, w^*, p^*	Unsteady flow velocities and pressure
u_τ	Friction velocity, $\sqrt{\tau_o/\rho}$
$T_j(Z)$	Chebyshev polynomials

COORDINATE SYSTEMS

x_1, x_2, x_3	General coordiates
x, r, Θ	Cylindrical coordinates
X, Z, θ	Nondimensional coordinates

GREEK LETTERS

α_{ij}	Added mass coefficients for oscillation in the plane of symmetry
β_{ij}	Added mass coefficients for oscillations normal to the symmetry plane
β_k	Eigenvalues
δ_{ij}	Kronecker delta

δ_p	Penetration depth, $\sqrt{2\nu/\omega}$
θ	Azimuthal angle, defined in computational domain – see Figure 3.1.
ϑ	Direction of the total mean flow velocity oscillating, defined in equation (2.46)
ι	Complex value, $\sqrt{-1}$
μ	Viscosity of fluid
ν	Kinematic viscosity of fluid
ρ	Density of fluid
τ	Shear stress
Φ	Velocity potential
$\hat{\phi}$	Reduced-motion potential, defined in equation (2.32)
φ	Phase angle, $\arctan[\Im(f)/\Re(f)]$
ψ_{1k}, ψ_{2k}	Eigenfunctions of the beam, defined in equation (2.31)
ω	Circular frequency

SUPERSCRIPTS AND SUBSCRIPTS

d	refers to viscous damping effect
I, O	stand for the inner and outer cylinders, respectively
l	stands for steady longitudial force
p	refers to inviscid effect
vl	stands for unsteady lateral viscous force
v	refers to viscous effects
$', ''$	derivatives of the corresponding variable
$\bullet$	refers to fluid parameters containing unsteady components

List of Figures

Chapter 1

Introduction

1.1 DEFINITION OF THE PROBLEM AND PREVIOUS WORK

When a structure submerged in fluid oscillates, the surrounding fluid must be displaced to accommodate the motion of the structure. As a result, fluid-dynamic forces are produced by the integrated effects of the pressure and skin friction, so that there is generally fluid-structure coupling and interaction. The fluid-dynamic forces acting on an oscillating structure have an important effect on the dynamics of a structure surrounded by quiescent or flowing fluid. In general, fluid flow around the structure has the potential to cause destructive vibrations. Hence, the study of flow-induced vibrations is of great interest for design. The interested reader is referred to Chen's [1, 2] and Païdoussis's [3, 4] reviews on flow-induced vibration and instabilities.

Depending on the flow orientation relative to the structure, *e.g.* flow within or over the structure, the vibrations are classified into different categories. For external flows, for instance, flow-induced vibration arises from cross flow or from axial flow. The main distinction between flow-induced-vibration phenomena depends on the fluid mechanism involved; for cross-flow, as an example, the phenomena are affected by separation of the fluid and vortex shedding. Although, in very few cases is the fluid stream truly axial or normal to the structure, nevertheless, for most studies in the field, the idealization is made that the flow is either purely axial or normal (*e.g.* to a cylindrical structure); this may be fully justifiable for the purposes of research into

the phenomena involved, but not necessarily for design purposes. The present work is concerned with vibration of cylindrical structures in axial flow or in still fluid in an annular passage, with the fluid being assumed to be incompressible.

Cylindrical structures subjected to annular flow are widely used in many engineering constructions; *e.g.*, control rods in guide tubes of PWR-reactors, feed water spargers in BWR-type reactors, fuel-cluster stringers in AGR-type reactors, tubes in the baffle regions of some kinds of heat exchangers and certain types of valves and pistons. For sufficiently high flow velocities, the cylinders in such arrangements have often developed self-excited oscillations, sometimes severe and occasionally destructive. For this reason, increasingly more effort has recently been devoted to research in this area. Work in the field can generally be classified as pertaining to either (a) the study of stability related to the effect of the mean fluid flow on the system, or (b) the study of the unsteady fluid-dynamic forces acting on an oscillating structure surrounded by fluid or fluid flow. The present work belongs to the last class of problems.

The dynamics and stability of a cylinder in confined flow represent a coupled fluid-structure interaction problem. Hence, it is essential to formulate the hydrodynamic forces associated with the motion of the cylinder. In a linear analysis, the unsteady, motion-related, fluid-dynamic forces may be conveniently separated into inertia, damping and stiffness components. Therefore, it is a logical first step to develop analytical tools which may be used to predict the inertial added-mass and damping forces in flow or just in quiescent fluid. As is well-known, added mass and damping are dependent on fluid parameters and system geometry. Studies of added mass can be traced to Stokes [5] and a brief survey was presented by Muga and Wilson [6]. In general, in a flowing fluid, the total damping is expressed as the sum of the damping in stationary fluid plus flow-velocity-dependent damping. However, it is true that the latter is dominant when the axial flow velocity is large or the viscosity of the fluid is small. The papers in this area of interest to the present work will now be reviewed.

A considerable amount of work has been done on the dynamics of a cylinder immersed in stationary confined viscous or inviscid fluid. Fritz developed a method for

calculating the inertial forces [7], in which an appropriate ideal-flow solution was proposed, and then generalized forces were obtained via Lagrange's equations of motion. The fluid-dynamic forces acting on oscillating rods in a stationary confined fluid have been studied by potential-flow theory [8, 9, 10] and by viscous theory based on the linearized Navier-Stokes equations of motion [11, 12, 13]. The systems studied were a cylindrical beam or clustered beams within a rigid container, a cylindrical beam within a cylindrical shell and two coaxial shells. The added-mass effect, which results from the accelerations suffered by the fluid, becomes larger as the annular space is decreased. As a result, the natural frequencies of the coupled system in stationary confined fluid are lower than those of the system without fluid. The effect of fluid viscosity on the system natural frequencies is negligibly small in most practical systems, and the added-mass effect can be estimated rather easily by potential-flow theory. However, the modal damping ratio is noticeably increased in some cases when the fluid viscosity is included, especially for low natural frequencies, and the effect on the inertial forces is not negligible in this case. Of course, the viscous damping component of fluid-dynamic forces, specially when the gap is small, is always important and cannot be neglected;

For narrow annular configurations, where the viscous damping is specially important, in stationary confined fluid, three-dimensional effects on the hydrodynamic forces, considering the end effect due to a finite-length annular region where both ends of the annulus are open, have been studied by Mulcahy [14] using simplified Navier-Stokes equations. The theory was formulated for various viscous penetration depths(to be defined later) in the narrow annular space. As the ratio of length to radius of the inner cylinder is decreased, this three-dimensional effect becomes significant. It was also found that the added mass is insensitive to this ratio, while damping is sensitive to variations of the viscous penetration depth when the gap is small.

In most of the studies mentioned before, the effect of steady axial flow was not considered. The dynamics of a flexible cylinder subjected to steady axial flow was first investgated by Païdoussis, both theoretically [15] and experimentally [16], for the system in unconfined flow. The coupled-hydrodynamic forces acting on the cylinder were

formulated according to slender-body theory, as proposed by Lighthill [17] for inviscid fluid, and the viscous forces were formulated by simple linearized relationships, earlier proposed by Taylor [18]. The elastic and inertia forces on the cylinder as well as the tension induced by drag forces were taken into account, and systems with various boundary conditions (pinned-pinned, clamped-clamped, clamped-free) were considered. It was demonstrated that small flow velocities damp free motions of the cylinder and generally diminish its natural frequencies as compared to those in still fluid. For sufficiently high flow velocities, however, fluid-elastic instabilities may occur; both buckling (divergence) and oscillatory instabilities (flutter) are possible, the former generally occurring at lower flow velocities than the latter. It was shown that, in the case of cylinders supported at both ends, oscillatory instabilities are specifically caused by frictional forces and that, without fluid-dynamic drag, only buckling is possible. In general, the added mass, which is associated with inertia forces, has a significant effect on the natural frequencies of system, while hydrodynamic stiffness effects are responsible for the onset of fluid-elastic instability by divergence. On the other hand, negative flow-induced damping is responsible for flutter; in this case, the critical flow velocity is defined as the point where the energy extracted from the flow is equal to the energy of dissipation. For a towed cylinder, the dynamics of the system display a more intricate dynamical behaviour [19, 20].

In a subsequent paper [21], the theory was extended to confined viscous flow, considering the effect of confinement of the fluid flow by a duct, in which the formulation of the viscous forces was adjusted appropriately and the gravity and pressurization effects were taken into account. If the flow about the cylinder is confined by a conduit or by an adjacent structure, the virtual mass of the fluid associated with the lateral motions of the system becomes large and the system loses stability much earlier, but the fundamental behaviour is not altered. The theory was validated by comparison with the experimental results [22], where it was found that, with increasing flow velocity, the cylinder is subject, sequentially, to instabilities of increasing mode number; confinement severely destabilizes the system. By taking into account both inviscid [23] and viscous

hydrodynamic [21] coupling of small arbitary motions of cylinders, the dynamics of a cluster of flexible cylinders was studied [24].

The system with steady axial flow in an annulus was later studied further and more completely [25]. With the help of the generalized Fourier-transform techniques developed by Dowell and Widnall [26], the inviscid forces for confined flow were derived by the full (linear) potential-flow theory, rather than the slender-body approximation; nevertheless, the viscous force formulation based on an adaptation of Taylor's expressions for unconfined flow was retained. The analysis was capable of estimating the dynamics of a body of relatively small length-to-radius ratio, since the inviscid force was not derived via the slender-body assumption. It was found that the potential-flow refinement effectively raised the critical flow velocities for instability, since slender-body theory overestimates the fluid-dynamic forces on a cylinder of relatively small length-to-radius ratio. Interestingly, the effect of compressibility on stability was found to be small in the subsonic regime and once again the fundamental behaviour of the system was found to be almost the same as described in the foregoing.

In parallel to the foregoing, similar and notable research on the dynamics and flow-induced vibration of cylinders in axial flow was conducted by Chen and co-workers [1, 27]. The experimental data for the turbulent-boundary-layer pressure [28] were introduced in the theory [27] and the mechanisms of damping and virtual mass were investigated for a rod with arbitrary end conditions.

In situations involving very narrow annular flows, the viscous effects, formulated approximately by an adaptation of Taylor's expression, are no longer reliable, casting some doubt on the validity of that aspect of the model; however, the inviscid model is clearly applicable for relatively narrow annuli. The viscous forces based on Taylor's expressions are associated with skin friction and pressure drop and are therefore passive in the sense that they do not influence the unsteady flow around an oscillating cylinder. Although this is quite reasonable for unconfined and weakly confined flows, it is clearly not realistic for highly confined annular flows. Thus, an appropriate model for evaluating viscous effects was necessary.

The first attempt to generate an analytical viscous model for cylindrical geometry was made by Hobson and co-workers [29, 30]. The model was formulated for dealing with situations of sudden constriction or enlargement in an approximate manner, *i.e.* with the help of some empirical relationships. The dynamics of a rigid cylinder subjected to axial flow in very narrow passages of non-uniform cross-sectional area was studied, for a rigid centre-body hinged at one point, neglecting the radial variation of fluid velocity. The analysis was extended to predict the dynamical behaviour of an actual fuel assembly oscillating in a channel of arbitrary shape [31]. It was shown that, at sufficiently high flow velocities of the annular fluid, oscillatory instability occurs via a negative-damping mechanism.

A more rigorous and purely analytical model was developed by Mateescu and Païdoussis [32] for a rigid centre-body motion hinged at one point, where axial variations of the narrow passage were restricted to be gradual and smooth. The model was based on potential-flow theory. It was then extended to take into account unsteady coupled viscous effects [33] (*i.e.*, the viscous-related modification of the unsteady pressure) by a systematic, albeit approximate, solution of the Navier-Stokes equations, which considered the unsteady viscous effects much more fully than heretofore. In those studies, the radial variations in the unsteady annular flow were taken into account, despite the assumption of small annular clearance with respect to centre-body radius. The fluid-dynamic pressures acting on a cylinder having rocking motion were measured and compared with the theoretical ones [34]. Good agreement between the two results was found.

In subsequent papers, the theory has been modified in order to develop the model for the turbulent-flow regime, based on a power-law velocity profile that fits the logarithmic form fairly well [35]. The dynamical behaviour of the system of a flexible cylinder with fixed ends subjected to axial flow in a narrow annulus was then studied [36, 37], by assuming the annular space to have constant cross-sectional area. The analytical unsteady-flow solutions for the unsteady pressure, based on potential-flow theory or simplified viscous theory in laminar or turbulent regimes, were shown to be

in good agreement with the experimental results. It was found that, as the annular gap becomes narrower, the system loses stability by divergence at progressively smaller flow velocities, provided the gap size is such that inviscid-fluid effects are dominant. However, this monotonic destabilizing effect of the inviscid forces (eventually predicting instability at infinitesimally small flow velocity for very narrow annuli) cannot be physically correct. It is thus very interesting that the theory predicts that, for very narrow annuli, viscous forces predominate, and this trend is reversed; thus, further narrowing of the annular gap has a stabilizing effect on the system. In some cases the system loses stability by flutter rather than divergence. Similar behaviour for a biological system has been reported by Grotberg and Reiss [39], where the inclusion of fluid-friction effects could alter the mode of loss of stability from divergence to flutter; however, the physical system involved was quite different.

1.2 ANALYTICAL VERSUS NUMERICAL SOLUTIONS OF THE UNSTEADY FLOWS

The fundamental mechanism of annular-flow-induced instabilities is fairly well understood and can be fairly well predicted. This is not true, however, for complex geometries. To be able to treat such system with complex geometries, especially cases involving area discontinuities, diffuser sections and eccentric configurations in the annular passage, some drastic simplifications or semi-empirical relationships have to be used for analytical treatment of the problem. To improve on that, for complex geometries, but also for more accurate formulations of the unsteady viscous forces in purely cylindrical geometries, recourse has to be taken to numerical solution techniques.

In the past, exact solutions have been obtained for a few problems by direct integration of the differential equations. This was accomplished by separation of variables or with the help of transformations that make the variables separable, leading to a similarity solution; moreover, a number of simplifying assumptions were made in order to make the problem tractable. The big advantage of an analytical solution is that clean and general information, which is usually in closed form, can be obtained. In this

way, one gets a much clearer understanding and better appreciation of the underlying physical assumptions and limitations of the solution obtained. However, the number of problems amenable to analytical solution is limited.

In an increasing number of engineering situations today, it is obvious that, to obtain an approximate but realistic solution to complex problems, the numerical rather than the analytical approach should be used. The numerical method is fast becoming a new and powerful tool in solving solid-fluid interaction problems. For example, Païdoussis and co-workers [40] presented a finite-element method for the free vibration of cylinder clusters in still fluid and the hydrodynamic pressure exerting on a dam due to small-amplitude seismic motion was proposed by Zienkiewicz and Nath [41]. Comparisons with the classical method of solution showed that, although it is less efficient, the finite-element technique is able to solve more complex geometries. The ready availability of previously unimaginable computer power has stimulated many changes in research laboratories where the need to solve complex problems is important. With the advent of high-speed computers, it is now possible to get an approximate solution of high accuracy to problems in modern engineering practice, by numerical methods; *e.g.* the finite-difference methods, the finite-element method, so on. Chenault [42] and Newton *et al.* [43] used a finite-element method to study the frequency-dependent added mass and damping effects in a two-dimensional ship-vibration problem. In order to predict the response of a system conveying fluid, a numerical method that considered the non-linear terms appearing in the equation of motion of the structure was presented [44].

By the use of the finite-element method, viscous damping and added mass coefficients were obtained by Yang and Moran [45] for eccentric configurations, where the system of discretized equations was obtained from the appropriate Navier-Stokes equations and continuity equation through Galerkin's method. The analysis was conducted for the system having translational motion in stationary confined flow. It was found that a finite-element method has limitations when the penetration depth is small.

A comprehensive research effort to develop numerical methods for unsteady vis-

cous flow has been initiated at McGill University, for annular-flow configurations involving generally variable annular spaces and concentric or eccentric cylinders oscillating in laminar or turbulent viscous flows – not purely uniform flows. For concentric configurations, an unsteady viscous model has been developed with a time-integration method (a finite-difference formulation) based on a three-point-backward implicit time-discretization scheme with a factored ADI scheme [46].

The numerical approach has the potential of providing information not accessible by analytical methods. On the other hand, the numerical approach has disadvantages such as truncation errors and round-off errors. Round-off errors can accumulate when a large number of arithmetic operations are involved. In some types of calculations, the magnitude of the round-off error is proportional to the number of grid points in the problem domain. In this case, refining the grid may decrease truncation errors but increase round-off errors. Thus, clearly one has to choose the right tool for the task at hand: an analytical, albeit idealized, solution for insight and ease of interpretation; or a numerical method for a more realistic solution(especially for complex geometries), but always with proper attention to its practical limitations.

1.3 THE CONTENT OF THIS THESIS

The scope of the research program undertaken in the present work is to develop a numerical solution for unsteady flow problems generated by forced or self-excited oscillations of the structure in axial or annular flow in non-uniform configurations, such as eccentricities. These unsteady-flow solutions can also be used in the analysis of various flow-induced-vibration vibration problems, as discussed before.

In order to investigate the hydrodynamic forces acting on a cylinder, a numerical approach will be developed for both potential and viscous flows in an annular passage. This is based on a spectral collocation method for solving the steady and unsteady confined flows and is completely different from the numerical methods mentioned before. This approach uses suitable spectral expansions for the fluid-dynamic parameters, involving Chebyshev polynomials, Fourier series and exponential functions. The

discretized system equations are obtained through a collocation method, where the governing equations and the boundary conditions are rigorously satisfied at specified collocation points within the computational domain and on its boundary.

In most applications of the spectral methods [47, 48, 49, 50, 51] recently developed for fluid-dynamic problems, a spatial discretization is used in conjuction with a temporal discretization based on a finite-difference approach. For example, Marcus successfully developed a spectral approach using a time-splitting method based on a finite-difference method for the study of the Taylor-Couette flow. The present spectral collocation method takes a different approach for the study of the unsteady flow generated by oscillating boundaries at a specified frequency, which is consistently based on spectral expansions for both time and space discretizations, by using Chebyshev polynomials, Fourier expansions and exponential functions, as already mentioned.

In an attempt to predict the fluid-dynamic forces acting on a cylinder surrounded by a viscous or an inviscid fluid in an eccentric annulus, the spectral collocation method has first been applied to a system having "translational motion" in quiescent fluid, where "translational motion" is understood to mean motion transverse to the flow, such that the sides of the two cylindrical bodies remain parallel to each other. Then, this method was used to solve the three-dimensional problem for a system having flexural motion in a concentric annulus conveying viscous axial flow; in this case, the spectral collocation method has been modified and used together with the finite-difference method in a hybrid scheme. The finite-difference method based on the hybrid scheme is used only for the axial variations of fluid parameters, while the axial domain is subdivided into a finite number of mesh points at which the spectral collocation method is used for the radial and circumferential variations; in this Thesis, this method is called the collocation-finite-difference method. As a result, the fluid-dynamic forces including the viscous effects can be evaluated rigorously rather than approximately, in contrast with existing theories.

In Chapter 2, the equations of unsteady potential and viscous flows are derived in a general form. To understand the mechanism involved in flow-induced vibration,

the previous analytical solutions for unsteady annular flows developed by the author are presented, for the case of the self-excited flexural motion of a cylinder treated as a clamped-clamped beam as an example. The fluid-dynamic forces acting on the inner cylinder can be evaluated by the theory.

In Chapter 3, for the problem of steady and unsteady flow, the spectral collocation method is formulated. With the aid of a coordinate transformation, the problem is transformed into a convenient computational domain, before the spectral collocation method is applied.

In Chapter 4, the spectral collocation method is applied for validation to several typical flow problems, such as the unsteady viscous motion between two oscillating parallel plates, the annular viscous flow generated by a steady or oscillatory rotation of one of its cylindrical boundaries, and the steady viscous flow between two eccentric cylinders. In all these typical problems, the present spectral solutions will be shown to compare favourably with the analytical solutions; *e.g.*, for the steady viscous flow between two eccentric cylinders, developed by Piercy et al. [52] and more recently by Snyder & Goldstein [53].

In Chapter 5, the fluid-dynamic forces acting on a cylinder oscillating in an eccentric annulus filled with a quiescent viscous or inviscid fluid are obtained by the spectral collocation method, when the cylinder executes translational motion. Then, typical results for added mass and viscous damping coefficients are determined and compared with the existing analytical results for potential flow [7, 9].

In Chapter 6, the unsteady viscous flow theory based on the collocation finite-difference method is developed to formulate the three-dimensional problem. The system under consideration undergoes flexural motions, as an example, and is subjected to a steady axial flow (laminar flow), the solution of which is obtained in Chapter 4. The fluid-dynamic forces, as influenced by the steady axial flow, are calculated by this collocation finite-difference method. Utilizing the spectral collocation method, with the aid of a separation of variables method, the unsteady fluid dynamic forces acting on a flexible cylinder subjected to axial flow is investigated, and then compared with the

previous analytical results presented in Chapter 2 for narrow annular configurations. This semi-analytical method is less restricted to very narrow annuli, as compared to the analytical solution refered to in the foregoing. The numerical results are discussed and compared with the semi-analytical results.

In Chapter 7, simplified analytical solutions for viscous damping are obtained, with the help of the results obtained by the numerical method presented in previous chapters. In terms of computational efficiency, it is better to obtain the viscous damping forces for very narrow configurations by this approximate method. The inviscid-fluid model for added mass is acceptable; however, viscous damping cannot be neglected and must be obtained by the methods of either Chapter 6 or Chapter 7. The general results are compared with those obtained by the present numerical method.

In Chapter 8, experimental results, in which the unsteady pressure generated by translational motion or rocking motion have been measured, are presented and compared with the present numerical results. In the equilibrium configurations, the cylinders are either concentric or eccentric, in the plane of oscillation or normal to it.

Finally, Chapter 9 is devoted to discussion and conclusions, as well as suggestions for future work.

Chapter 2

Problem Formulation and Approximate Analytical Solutions

The principal aim of this chapter is to present the basic equations of fluid motion, in general form, for flow-induced-vibration problems; they will eventually be used for estimating the fluid-dynamic forces acting on a cylinder in annular configurations. The fluid-dynamic forces, which have inertia, damping and stiffness components, can be evaluated by potential or viscous theory. The forces, obtained by integrating skin friction and pressure around the circumference of the cylinder, are expressed in terms of steady and unsteady components. Even though the steady viscous forces, which are mainly due to the steady skin friction and the mean pressure acting on the cylinder, must be considered for predicting the dynamical behaviour of the system, it is a secondary problem at this stage. Thus, only the unsteady forces due to the oscillatory motion of the cylinder will be discussed in the present numerical analysis.

As a step toward estimating fluid-dynamic forces for two eccentrically located cylinders in quiescent fluid or annular flow, the basic equations of fluid motion for potential and viscous flows are formulated for harmonic oscillatory motion of the cylinder. At this stage, the annular flow is assumed to be fully developed laminar flow. The time-dependent lateral displacement of the oscillating centre body is assumed to be small. Furthermore, the effect of flow separation can then considered to be negligible. As a result, the equations of fluid flow can be expressed in linearized form.

In the study of flow-induced vibrations, it is essential to understand the coupled

fluid-structure interaction mechanism. For this purpose, the self-excited flexural motion of a cylindrical beam subject to annular flow, which was undertaken analytically for concentric configurations by the author [54], is presented in this chapter as an example. The basic principles used in formulating the fluid problem for inviscid and viscous flows are investigated.

The differential equation of motion of the flexible centre body constitutes a boundary-value problem together with the boundary conditions, used to derive a typical eigenvalue problem. The normal-mode-expansion theorem based on the separation-of-variable method can play a major role in the transformation of the boundary value problem into eigenvalue problem. By Galerkin's method, the system equations can be discretized, which eventually leads to the determination of the mass, damping and stiffness matrices of the system. The dynamics of a flexible cylinder in an annulus are presented by the previous analytical theory [37, 54] in this chapter as typical results. In the present analysis based on the spectral method, the solution of the eigenvalue problem remains to be done.

2.1 BASIC EQUATIONS OF FLUID MOTION

Most theoretical investigations in the field of fluid dynamics are based on a perfect, *i.e.* frictionless and incompressible, fluid. In the motion of such a perfect fluid, two contacting fluid layers experience no tangential force(shearing stress) but act on each other with normal forces(pressure) only. However, the theory of perfect fluids fails completely to account for the drag of a body. Because of the tangential or friction forces between a fluid and solid wall, there exists no difference in relative tangential velocity, *i.e.* there is no slip.

The existence of tangential stresses and the condition of no slip near solid walls constitute the essential difference between a perfect fluid and a real fluid. In many instances, the motion of certain fluids, such as water and air, agrees well with that of a perfect fluid, because the shearing stresses are very small. As a result, the problem can be simplified so as to become tractable. However, the viscous effects on the fluid-

dynamic forces cannot be neglected in some cases, for example for unsteady fluid motion due to the low-frequency oscillatory motion of a cylinder in a narrow annulus.

The equations of the unsteady potential flow and the steady and unsteady viscous flows will be discussed, and then adapted to the present problem in the following chapters. In the unsteady flow generated by the oscillatory motion of a cylinder with either high frequency or low fluid viscosity (*i.e.*, with high oscillatory Reynolds number which will be defined later), the viscous effects are limited to a region near the surface of the oscillating cylinder. According to the results given by Chen *et al.* [11] for a viscous fluid and Chung *et al.* [9] for an inviscid fluid, the difference between the fluid-dynamic forces acting on a cylinder in an annulus, obtained by the two theories for the case of high oscillatory Reynolds number, is very small. The effects of fluid viscosity, which may be of secondary importance in some cases, are neglected in a first attempt to predict the fluid-dynamic forces acting on the cylinder by means of potential-flow theory. Then the viscous effects on the fluid-dynamic forces are investigated by the present viscous theory.

The system considered in the present analysis consists of a centre body located concentrically or eccentrically in a cylindrical duct as shown in Figure 2.1. The radius of the inner cylinder is a and the annular space between two cylinders is $H(\Theta)$; thus, for the case of a constant H, the radius of the outer cylinder is $b = a + H$. The flexible or rigid cylinder, immersed in quiescent fluid or in a steady flow, generally executes oscillatory motion. The fluid-dynamic forces exerted on the inner and/or outer cylinders are evaluated numerically based on the spectral method, which will be presented in the following chapters.

2.1.1 Unsteady Potential Flow

In this section, the flow is presumed to be irrotational and incompressible, in addition to being inviscid, so that motion of the fluid is governed by Laplace's equation which is derived from the continuity equation. The boundary conditions state that the normal velocity of the body is equal to that of the fluid at the boundary surface between fluid

and body. Without the complication of viscosity, the momentum equation is reduced to the Bernoulli-Lagrange equation, from which the unsteady pressure force acting on the cylinder can be obtained.

The Laplace equation in terms of the unsteady velocity potential Φ is

$$\nabla^2\Phi(x_1, x_2, x_3, t) = 0\,, \tag{2.1}$$

subject to boundary conditions

$$\frac{\partial f_b}{\partial t} + \nabla\Phi \cdot \nabla f_b = 0\,, \tag{2.2}$$

on $f_b = 0$, where x_1, x_2, x_3 represent geometrical coordinates, *e.g.* r, Θ and x for cylindrical coordinates as will be shown in the form of Laplace equation in equation (2.27), and $f_b(x_1, x_2, x_3, t) = 0$ is the equation of the body surface. In the unsteady motions with moving boundaries, the fluid domain deforms with time. The system is usually employed in conjuction with a time-dependent coordinate transformation. However, by the assumption of small-amplitude oscillations of the moving boundaries, the geometrical effects of deformation of the fluid domain are of second order and will be neglected in the present analysis.

The velocity potential, $\Phi(x_2, x_2, x_3, t)$, may be separated into steady and unsteady components:

$$\Phi(x_1, x_2, x_3, t) = \phi_s(x_1, x_2, x_3) + \phi(x_1, x_2, x_3, t)\,. \tag{2.3}$$

Considering the velocity potential, steady and unsteady velocities, $\mathbf{V}_s$ and $\mathbf{v}^*$, are defined by

$$\mathbf{V}_s(x_1, x_2, x_3) = \nabla\phi_s(x_1, x_2, x_3)\,,$$

$$\mathbf{v}^*(x_1, x_2, x_3, t) = \nabla\phi(x_1, x_2, x_3, t)\,. \tag{2.4}$$

For concentric-flow passages, the steady-state component simply gives, because of cylindrical symmetry, $\partial\phi_s/\partial x = \bar{U}$, where $\bar{U}$ denotes the mean axial-flow velocity.

In order to obtain the inviscid-fluid dynamic force exerted on the surface, the unsteady pressure may be written in the following form, usually known as the Bernoulli-

Lagrange equation deduced from the momentum equation:

$$P - P_\infty = \frac{1}{2}\rho\bar{U}^2 - \frac{1}{2}\rho \mid \nabla\Phi \mid^2 - \rho\frac{\partial\Phi}{\partial t} , \tag{2.5}$$

where ρ is the fluid density and P_∞ is the stagnation pressure. Thus, the inviscid fluid dynamic force, acting on the inner cylinder of radius a, can be obtained by integrating the above equation around the circumference of the cylinder, as

$$F_p = -\int_0^{2\pi} a(P - P_\infty)|_{r=a} \cos\Theta \, d\Theta , \tag{2.6}$$

which can be expressed in the general form as

$$F_p = -\left(M\frac{\partial^2 e_I}{\partial t^2} + C_v\frac{\partial e_I}{\partial t} + ke_I\right) , \tag{2.7}$$

where e_I represents the displacement of the oscillating inner cylinder(the subscript I stands for the inner cylinder); C_v is the damping coefficient, k is the fluidelastic stiffness coefficient, and M is the virtual mass. In Appendix A, these coefficients are presented based on the slender-body theory [21] and then the critical flow velocity where a system loses stability by divergence(buckling) are estimated in order to compare the results with the analytical results obtained by the inviscid-flow theory, which will be presented in Section 2.2.

2.1.2 Steady and Unsteady Viscous Flows

The basic equations of mass and momentum conservation are applied to the analysis of viscous-fluid flow to get a complete and fundamental understanding of the fluid-dynamic problem. In the study of viscous incompressible flow, it is necessary to obtain the three components of velocity and pressure, as functions of space and time. These four unknowns can be determined in principle from the governing equations, *i.e.* the continuity equation based on the conservation of mass and the Navier-Stokes equations based on the conservation of momentum. However, the complete general solution is still not possible because of insurmountable mathematical difficulties.

Ideally, the hydrodynamic forces should be calculated from the governing equations together with boundary conditions. In viscous fluids, the surface forces acting on

an element of fluid are considerably more complicated than in an inviscid fluid. These are of two types: there is a normal force or normal stress similar to the pressure, but it may not be the same in all directions and there are shear forces whose direction is tangent to the surface on which they act.

In the present analysis, the viscosity and density of the fluid are assumed to be constant. Thus, the Navier-Stokes equations, without body forces, and the continuity equation are written as

$$\frac{D\mathbf{V}}{Dt} = -\frac{1}{\rho}\nabla P + \nu\nabla^2\mathbf{V}\,, \tag{2.8}$$

$$\nabla\cdot\mathbf{V} = 0\,, \tag{2.9}$$

where ν is the kinematic viscosity of fluid and

$$\frac{D\mathbf{V}}{Dt} = \frac{\partial\mathbf{V}}{\partial t} + (\mathbf{V}\cdot\nabla)\mathbf{V}\,,$$

in which the first and second terms on the right-hand side denote the local and convective derivatives, respectively, and $\mathbf{V}(x_1, x_2, x_3, t)$ represents the velocity vector of the fluid.

For cylindrical coordinates (r, Θ, x), the above equations are rewritten as

$$\frac{\partial U^*}{\partial t} + V^*\frac{\partial U^*}{\partial r} + \frac{W^*}{r}\frac{\partial U^*}{\partial \Theta} + U^*\frac{\partial U^*}{\partial x} + \frac{1}{\rho}\frac{\partial P^*}{\partial x} = \nu\left[\frac{1}{r}\frac{\partial}{\partial r}\left(r\frac{\partial U^*}{\partial r}\right) + \frac{1}{r^2}\frac{\partial^2 U^*}{\partial \Theta^2} + \frac{\partial^2 U^*}{\partial x^2}\right]\,,$$

$$\frac{\partial W^*}{\partial t} + V^*\frac{\partial W^*}{\partial r} + \frac{W^*}{r}\frac{\partial W^*}{\partial \Theta} + U^*\frac{\partial W^*}{\partial x} + \frac{W^*V^*}{r} + \frac{1}{\rho r}\frac{\partial P^*}{\partial \Theta} =$$

$$\nu\left[\frac{1}{r}\frac{\partial}{\partial r}\left(r\frac{\partial W^*}{\partial r}\right) + \frac{1}{r^2}\frac{\partial^2 W^*}{\partial \Theta^2} + \frac{\partial^2 W^*}{\partial x^2} - \frac{W^*}{r^2} + \frac{2}{r^2}\frac{\partial V^*}{\partial \Theta}\right]\,,$$

$$\frac{\partial V^*}{\partial t} + V^*\frac{\partial V^*}{\partial r} + \frac{W^*}{r}\frac{\partial V^*}{\partial \Theta} + U^*\frac{\partial V^*}{\partial x} - \frac{W^{*2}}{r} + \frac{1}{\rho}\frac{\partial P^*}{\partial r} =$$

$$\nu\left[\frac{1}{r}\frac{\partial}{\partial r}\left(r\frac{\partial V^*}{\partial r}\right) + \frac{1}{r^2}\frac{\partial^2 V^*}{\partial \Theta^2} + \frac{\partial^2 V^*}{\partial x^2} - \frac{V^*}{r^2} - \frac{2}{r^2}\frac{\partial W^*}{\partial \Theta}\right]\,, \tag{2.10}$$

$$\frac{\partial U^*}{\partial x} + \frac{\partial W^*}{\partial \Theta} + \frac{\partial}{\partial r}(rV^*) = 0\,, \tag{2.11}$$

where U^*, V^* and W^* denote the flow velocities, including the unsteady components, in the axial, radial and circumferential directions, respectively.

For small-amplitude periodic motions of the structure, the fluid executes periodic motions, and it is possible to separate the flow velocity into steady and unsteady components, as follows:

$$\mathbf{V}^*(x,\, r,\, \Theta,\, t) = \mathbf{V}_s(x,\, r,\, \Theta) + \mathbf{v}^*(x,\, r,\, \Theta,\, t)\,. \tag{2.12}$$

The pressure can also be expressed as the sum of steady and unsteady terms

$$P^*(x,\, r,\, \Theta,\, t) = P_s(x,\, r,\, \Theta) + p^*(x,\, r,\, \Theta,\, t)\,. \tag{2.13}$$

The equations for the steady viscous flow are

$$(\mathbf{V}_s \cdot \nabla)\mathbf{V}_s = -\frac{1}{\rho}\nabla P_s + \nu\nabla^2\mathbf{V}_s\,, \tag{2.14}$$

$$\nabla \cdot \mathbf{V}_s = 0\,. \tag{2.15}$$

By subtracting the steady-flow equations from the full Navier-Stokes equations, the remained unsteady-flow equations can be expressed as

$$\frac{\partial \mathbf{v}^*}{\partial t} + (\mathbf{V}_s \cdot \nabla)\mathbf{v}^* + (\mathbf{v}^* \cdot \nabla)\mathbf{V}_s = -\frac{1}{\rho}\nabla p^* + \nu\nabla^2\mathbf{v}^*\,, \tag{2.16}$$

$$\nabla \cdot \mathbf{v}^* = 0\,, \tag{2.17}$$

where the product terms between the unsteady components are neglected by the assumption of small-amplitude motion of the structure. The boundary conditions based on the no-slip condition can be expressed as

$$\mathbf{v}^* = \mathbf{f}_v\,, \tag{2.18}$$

where $\mathbf{f}_v$ denotes the velocity of the oscillating structure.

The resultant forces acting on the structure per unit length, including unsteady components, can be calculated by considering the following stress component:

$$\tau_{ij} = -P\delta_{ij} + \mu\left(\frac{\partial V_i}{\partial x_j} + \frac{\partial V_j}{\partial x_i}\right)\,, \tag{2.19}$$

where $\partial V_i/\partial x_j$ denotes j–component derivative of the i directional flow velocity, μ is the fluid viscosity and δ_{ij} represents the Kronecker delta.

The fluid-dynamic forces per unit length can be obtained by integrating the above equation along the structure. Thus,

$$F_v = -\int_\ell \tau_{ij} n_j d\ell \,, \tag{2.20}$$

which will be rewritten for cylindrical coordinates.

The viscous forces acting on a cylinder in confined flow may be separated into steady and unsteady components. The steady viscous forces, which are dependent on the derivatives of the motion with respect to the axial direction, are derived from the longitudinal frictional force and from the pressurization of the flow to overcome the pressure drop. The steady forces, obtained by a previous analytical method, will be reviewed in this chapter as an example, but in the present numerical analysis they are not considered. The unsteady viscous forces arise from the tangential friction forces containing the effect of the viscous pressure distribution along the circumference in a direction normal to the wall. Thus, free oscillations of a flexible centre body are influenced by both steady and unsteady viscous forces.

The unsteady forces, acting on the inner cylinder per unit length, due to its oscillatory motion can be obtained by

$$F_I(x,t) = \int_0^{2\pi} a \left(\tau_{rr}\,|_{r=a} \cos\Theta - \tau_{r\Theta}\,|_{r=a} \sin\Theta + \tau_{rx}\,|_{r=a} \frac{de_I}{dx} \right) d\Theta \,, \tag{2.21}$$

where e_I denotes the displacement of the moving cylinder and the stress components can be rewritten

$$\begin{aligned}
\tau_{rr}(x,r,\Theta,t) &= -p^* + 2\mu \frac{\partial v^*}{\partial r} \,, \\
\tau_{r\Theta}(x,r,\Theta,t) &= \mu \left\{ \frac{\partial w^*}{\partial r} + \frac{w^*}{r} + \frac{1}{r}\frac{\partial v^*}{\partial \Theta} \right\} \,, \\
\tau_{rx}(x,r,\Theta,t) &= \mu \left\{ \frac{\partial u^*}{\partial r} + \frac{\partial v^*}{\partial x} \right\} \,,
\end{aligned} \tag{2.22}$$

in terms of the axial, radial and circumferential components of unsteady-flow velocity, u^*, v^* and w^*, and the unsteady pressure p^*.

In the present analysis, motion of either the inner cylinder(centre body) or the outer containing cylinder is considered. The forces acting on cylinder i, due to motions

of cylinder j oscillating in the plane of symmetry e_j and in the normal to that plane g_j, can be written as

$$\begin{aligned} F_i &= -\left(\alpha_{ij}\frac{\partial^2 e_j}{\partial t^2} + \alpha'_{ij}\frac{\partial e_j}{\partial t} + \alpha''_{ij}e_j\right) = \rho\pi a^2\omega^2 e_j[\Re(\hat{F}_i) + \imath\Im(\hat{F}_i)] \,, \\ G_i &= -\left(\beta_{ij}\frac{\partial^2 g_j}{\partial t^2} + \beta'_{ij}\frac{\partial g_j}{\partial t} + \beta''_{ij}g_j\right) = \rho\pi a^2\omega^2 g_j[\Re(\hat{G}_i) + \imath\Im(\hat{G}_i)] \,, \end{aligned} \quad (2.23)$$

where $\Re$ and $\Im$ stand for the real and imaginary parts, respectively, of the nondimensional fluid-dynamic forces, $\hat{F}_i$ or $\hat{G}_i$. Physically, the forces associated with unprimed, primed and double-primed coefficients in the above equations can be interpreted as the fluid inertial force, the fluid damping force and the fluidelastic stiffness force, respectively; note that α_{ij} and β_{ij} are added mass matrices; α'_{ij} and β'_{ij} are viscous damping matrices; α''_{ij} and β''_{ij} are fluidelastic stiffness matrices. For translational motion in annular space without axial flow, it was found that the unsteady forces can be expressed in terms of Bessel functions [11].

2.2 ANALYTICAL APPROXIMATE SOLUTIONS FOR UNSTEADY ANNULAR FLOWS

The system considered in the previous analysis [37] consists of a flexible cylindrical centre-body, coaxially located in a narrow cylindrical annulus conveying fluid. The flexible centre-body, of which both ends are supposed to be clamped, is free to oscillate in flexure inside the duct. Only planar motions are considered. The system is coupled by the fluid-dynamic forces acting on the flexible centre-body, due to the annular flow, which is obviously unsteady.

A simplified analytical approach was developed in order to estimate the dynamical behaviour of the system in a narrow annular passage in the presence of a fully-developed laminar flow. The potential-flow solution obtained in the first stage of the analysis was modified by adding a laminar-perturbation solution to account for the viscous effects.

The inner cylinder, which has length L and radius a, is considered to be an Euler-Bernoulli beam characterized by flexural rigidity EI, cross-section area A_s and density

ρ_s. The annular gap is H, hence the radius of the outer cylinder is $b = a + H$. The annular flow is characterized by the mean-flow velocity $\bar{U}$, static pressure P_∞ in the annulus upstream and the fluid density ρ, which is considered constant; see Figure 2.2.

In order to simplify the solution, the following two flow fields were considered: (a) a potential flow, representing the perturbation-flow field according to inviscid-flow theory, and (b) a viscous-flow field, whose axial flow, far upstream, is considered fully developed and laminar, and which includes the steady and unsteady viscous effects.

The equations of motion with the following principal differences to the existing theory [21] were formulated. First, without using slender-body theory, the potential-flow theory was developed, based on the assumption of a small annular gap with respect to cylinder radius, so that the inviscid forces acting on cylinders of small length-to-radius can be predicted. Second, the unsteady viscous forces are formulated by considering the simplified Navier-Stokes equations instead of Taylor's expressions, the applicability of which is doubtful.

The equations of small lateral motions can be derived by considering the equilibrium of forces acting on a differential segment of the flexible centre-body subjected to distributed external forces, based on Hamilton's principle. In this case, the distributed forces are due to the fluid motion. The equation of motion of the flexible centre-body motion is expressed, as follows:

$$EI\frac{\partial^4 e_I}{\partial x^4} + \rho_s A_s \frac{\partial^2 e_I}{\partial t^2} = F_p + F_{vl} + F_{vs} \,, \tag{2.24}$$

subject to boundary conditions (at the fixed ends of the flexible cylinder)

$$e_I(0,t) = 0 \,, \qquad e_I(L,t) = 0 \,, \qquad \frac{\partial e_I(0,t)}{\partial x} = 0 \,, \qquad \frac{\partial e_I(L,t)}{\partial x} = 0 \,, \tag{2.25}$$

where $e_I(x,t)$ is the lateral displacement of the inner cylinder, F_p the inviscid-fluid force, F_{vl} the unsteady lateral viscous force and F_{vs} the steady viscous force due to longitudial steady skin friction and the mean pressure, acting on the centre-body per unit length. For the case where the cylinder, although laterally fixed at both ends, can slide axially at the downstream end, the steady viscous forces may be expressed in the

following form [21]

$$F_{vs} = \left[-\frac{\partial P_m}{\partial x} A_s (L - x) + \int_x^L F_l dx \right] \frac{\partial^2 e_I}{\partial x^2} + \frac{\partial P_m}{\partial x} A \frac{\partial e_I}{\partial x} , \qquad (2.26)$$

where P_m is the mean pressure in the duct, $F_l(x)$ is the longitudinal steady viscous-fluid force per unit length due to the longitudinal component of skin friction on the inner cylinder.

The unsteady fluid-dynamic forces arise from the resultant of the unsteady pressure forces and of the unsteady viscous shear stresses acting on the centre-body surface. This analysis has as its principal aim the determination of the unsteady fluid-dynamic forces, firstly for the case of an unsteady potential(inviscid) flow and then considering also the main effects of fluid viscosity on the forces. A full account of the procedure to develop the steady and unsteady forces may be found in refs [37, 54].

2.2.1 Derivation of the Inviscid Forces

Based on the assumption of small-amplitude motion of the oscillating inner cylinder, the inviscid forces were derived by potential flow theory. For incompressible fluid, the governing equation is expressed, as the Laplace equation shown in equation (2.1), in cylindrical coordinates, as follows:

$$\nabla^2 \Phi = \frac{\partial^2 \Phi}{\partial x^2} + \frac{\partial^2 \Phi}{\partial r^2} + \frac{1}{r} \frac{\partial \Phi}{\partial r} + \frac{1}{r^2} \frac{\partial^2 \Phi}{\partial \Theta^2} = 0 , \qquad (2.27)$$

subject to the boundary conditions, which are obtained by substituting the equations of body surface ($f_b(r,t) = r - a - e_r$ for the inner oscillating cylinder and $f_b(r,t) = r - b$ for the outer fixed cylinder) into equation (2.2),

$$\left.\frac{\partial \Phi}{\partial r}\right|_{r=a} = \frac{\partial e_r}{\partial t} + \left[\frac{\partial \Phi}{\partial x} \frac{\partial e_r}{\partial x} + \frac{1}{r} \frac{\partial \Phi}{\partial \Theta} \frac{1}{r} \frac{\partial e_r}{\partial \Theta} \right] ,$$
$$\left.\frac{\partial \Phi}{\partial r}\right|_{r=b} = 0 , \qquad \left.\frac{\partial \Phi}{\partial x}\right|_{x=-\infty} = \bar{U} , \qquad (2.28)$$

where the radial displacement, e_r, at the azimuthal angle Θ is expressed in terms of the lateral displacement, $e_l(x,t) = E(x)e^{i\omega t}$, of the inner cylinder as

$$e_r(x, \Theta, t) = e_l(x,t) \cos \Theta = E(x) \cos \Theta e^{i\omega t} . \qquad (2.29)$$

Based on the normal-mode expansion for the motion of the clamped-clamped cylinder, $E(x)$ can be expressed in terms of the eigenfunctions, ψ_k,

$$E(x) = \sum_k a_k \psi_k(x) = \sum_k a_k [\psi_{1k}(x) + \psi_{2k}(x)] \,, \tag{2.30}$$

where ψ_{1k} and ψ_{2k} denote the trigonometric and hyperbolic components of these eigenfunctions, respectively,

$$\psi_{1k} = -\cos\beta_k x + \sigma_k \sin\beta_k x \,, \quad \psi_{2k} = \cosh\beta_k x - \sigma_k \sinh\beta_k x \,, \tag{2.31}$$

and $\sigma_k = (\cosh\beta_k L - \cos\beta_k L)/(\sinh\beta_k L - \sin\beta_k L)$, the $\beta_k L$ being the corresponding eigenvalues of a clamped-clamped beam.

In view of equations (2.3) and (2.30), reduced potentials $\hat{\phi}_k(x,r)$ may be introduced as follows:

$$\phi(x,r,\Theta,t) = \sum_k a_k \, \hat{\phi}_k(x,r) \cos\Theta \, e^{\iota\omega t} \,, \tag{2.32}$$

where by the separation of variables, $\phi_k(x,r)$ may be written as

$$\hat{\phi}_k(x,z) = f_k(x) \, F_k(z) \,, \tag{2.33}$$

in terms of the new coordinate z instead of r, defined by

$$z = r - a \,. \tag{2.34}$$

Thus, the analytical solution, which is restricted to very narrow annuli where $r - a \ll a$ and $1/r \simeq 1/a$, can be obtained by considering the following reduced form of equation (2.27) as

$$\frac{\partial^2 \hat{\phi}_k}{\partial x^2} + \frac{\partial^2 \hat{\phi}_k}{\partial z^2} + \frac{1}{a}\frac{\partial \hat{\phi}_k}{\partial z} - \frac{1}{a^2}\hat{\phi}_k = 0 \,, \tag{2.35}$$

with the boundary conditions

$$\left.\frac{\partial \hat{\phi}_k}{\partial z}\right|_{z=hs} = 0 \,, \qquad \left.\frac{\partial \hat{\phi}_k}{\partial z}\right|_{z=0} = \iota\omega\psi_k(x) + \bar{U}\psi_k'(x) \,, \tag{2.36}$$

where the prime denotes differentiation with respect to x, and $h = (b-a)/a = H/a$.

For brevity, the procedure for obtaining the solution for the reduced potential, $\hat{\phi}_k(x,z)$, effected by equation (2.33) is not given here. The solution of reduced potential $\hat{\phi}_k$, evaluated on the surface of the cylinder ($z = 0$), is found to be

$$\hat{\phi}_k(x,0) = -a \sum_{s=1}^{2} G_{sk} \left[\iota\omega\psi_{sk}(x) + \bar{U}\psi_{sk}(x) \right] , \tag{2.37}$$

where

$$G_{1k} = \frac{q_k - 1/2 \tanh(q_k h)}{(q_k^2 - 1/4)\tanh(q_k h)} ,$$

$$G_{2k} = \frac{-c_k^\dagger + 1/2 \tan(c_k^\dagger h)}{(c_k^{\dagger 2} + 1/4)\tan(c_k^\dagger h)}, \quad \text{for } \beta_k^2 a^2 > 5/4 ,$$

and

$$G_{2k} = \frac{c_k - 1/2 \tanh(c_k h)}{(c_k^2 - 1/4)\tanh(c_k h)} , \quad \text{for } \beta_k^2 a^2 < 5/4 , \tag{2.38}$$

in which q_k, c_k and $c_k^\dagger$ are

$$q_k = [5/4 + \beta_k^2 a^2]^{1/2} , \quad c_k = [5/4 - \beta_k^2 a^2]^{1/2} , \quad c_k^\dagger = [-5/4 + \beta_k^2 a^2]^{1/2} . \tag{2.39}$$

Having determined ϕ, and hence Φ, the pressure on the surface of the cylinder may be found, after suitable linearization, through the unsteady Bernoulli equation (2.5). Therefore, the unsteady inviscid forces on the cylinder may be obtained by integration, as shown in equation (2.6). Substituting the solution for the unsteady velocity potential into the unsteady Bernoulli equation with the aid of $d\phi_s/dx = \bar{U}$, the unsteady inviscid force is found to be

$$F_p(x,t) = -\rho\pi a^2 e^{\iota\omega t} \sum_k a_k(-\omega^2 P_{k2} + \iota\omega P_{k1} + P_{k0}) , \tag{2.40}$$

where P_{k2}, P_{k1}, and P_{k0} are the components of fluid force associated with inertial, damping and stiffness effects, respectively, in the same form of equation (2.7); these components are given by

$$P_{k2} = \sum_{s=1}^{2} G_{sk}\psi_{sk}, \quad P_{k1} = 2\bar{U} \sum_{s=1}^{2} G_{sk}\psi'_{sk}, \quad P_{k0} = \bar{U}^2\beta_k^2 \sum_{s=1}^{2}(-1)^s G_{sk}\psi_{sk} . \tag{2.41}$$

As shown in the above equation, the effect of mean flow on the inviscid forces is to produce a centrifugal force due to the curvature of the flexible cylinder, and a Coriolis

force due to the combined flow and rotation of the fluid element. The centrifugal and Coriolis forces are associated with the stiffness and damping components of the inviscid forces, respectively.

2.2.2 Determination of the Viscous Forces

The unsteady potential flow, which is of course irrotational, is expressed in terms of the velocity potential $\Phi(x, r, \Theta, t)$, as shown in the previous section. The analytical solution of the potential flow, under consideration, is used to develop the approximate method of the viscous flow with the simplified Navier-Stokes equations, based on the following assumptions: the frequency of oscillation is not very high and the Reynolds number, based on the hydraulic diameter of the annulus, $D_H = 2H = 2ha$, is relatively small.

Taking into consideration the two flow fields, potential and viscous, the velocity vector associated with the potential flow may be written as $\tilde{U}[(1+\check{u}_p)\vec{i}_x + \check{v}_p\vec{i}_r + \check{w}_p\vec{i}_\Theta]$, where the unsteady flow velocity can be obtained using the unsteady velocity potential as shown in equation (2.4), and the associated perturbation pressure as $\check{p}_p = (P - P_\infty)/(\rho\tilde{U}^2)$: $\check{u}$, $\check{v}$, and $\check{w}$ stand for the corresponding components of the nondimensional flow velocity with respect to $\tilde{U}$. Then, one may write

$$\check{u}(x, r, \Theta, t) = \check{u}_v(x, r; \Theta, t) + \check{u}_p(x, r, \Theta, t), \tag{2.42}$$

and similarly, for $\check{v}$, $\check{w}$ and $\check{p}$ where the components associated with viscous effects, $\check{u}_v$, $\check{v}_v$, $\check{w}_v$, and $\check{p}_v$, are considered to be dependent only slightly on Θ and t.

Using an approach similar to the one used in the previous section to develop the unsteady equations (2.16) and (2.17), the Navier-Stokes equations are simplified drastically by subtracting the potential terms from the full equations for narrow annuli, based on a set of assumptions, similar to those made in boundary-layer theory, which are valid, because of the narrowness of the annular passage, namely: (a) the radial component of viscous motion $\check{v}_r$ is negligible and (b) the circumferential and axial variations in $\check{u}$ and $\check{w}$ are also negligible, compared to the radial variations in the same

components. Taking the foregoing assumptions into account, the governing equations for unsteady viscous flow reduce to the following equations in terms of nondimensional parameters:

$$\frac{\partial^2 \breve{u}}{\partial Y^2} = \frac{Re}{2h}\frac{1}{l}\frac{\partial \breve{p}_v}{\partial X}\,, \quad \frac{\partial^2 \breve{w}}{\partial Y^2} = \frac{Re}{2h}\frac{1}{R}\frac{\partial \breve{p}_v}{\partial \Theta}\,, \quad 0 \simeq \frac{\partial \breve{p}_v}{\partial Y}\,, \tag{2.43}$$

where the nondimensional coordinates are defined by

$$X = \frac{x}{a}\,, \quad R = \frac{r}{a}\,, \quad h = \frac{H}{a}\,, \quad l = \frac{L}{a}\,, \quad Y = \frac{z}{a} = R - 1\,. \tag{2.44}$$

With the aid of Figure 2.3, the total mean dimensionless velocity(over the gap height) may be approximated by

$$\bar{V}(X, \Theta, t) = \bar{u}\cos\vartheta + \bar{w}\sin\vartheta\,, \tag{2.45}$$

where ϑ may be expressed as

$$\sin\vartheta = \bar{w}/\bar{V} \simeq \bar{w}(X, \Theta, t)\,, \tag{2.46}$$

since the dimensionless total mean velocity is approximately equal to unity. This is the key to this simplified treatment of unsteady viscous effects: the magnitude of the total mean flow velocity remains approximately constant, but its direction fluctuates circumferentially through a small angle ϑ, associated with the circumferential mean flow velocity.

In order to simplify the analysis, the average circumferential velocity across the annular space, $\bar{w}$, can be calculated from the potential flow obtained in the previous section with the relationship $\breve{w} = (\partial\phi/\partial\Theta)/(\bar{U}r)$, as follows:

$$\bar{w} = \frac{1}{h}\int_0^h \breve{w}\,dZ = \sum_k \frac{a_k}{\bar{U}h}\left[\sum_{s=1}^{2} f_{sk} W_{sk}\right]\sin\Theta e^{i\omega t}\,, \tag{2.47}$$

where

$$f_{sk} = G_{sk}[i\psi_{sk}(x) + \bar{U}\psi_{sk}(x)]\,,$$

and the W_{sk} are expressed as integral forms as

$$W_{1k} = \int_0^h \frac{1}{1+Y}[\cosh(q_k Y) + R_1\sinh(q_k Y)]e^{1/Y}\,dY\,,$$

$$W_{2k} = \begin{cases} \int_0^h \frac{1}{1+Y}[\cos(c_k^\dagger Y) + R_2^\dagger \sin(c_k^\dagger Y)]e^{1/Y}dY\,, & \text{for } (\beta_k a)^2 > 5/4\,, \\ \int_0^h \frac{1}{1+Y}[\cosh(c_k Y) + R_2 \sinh(c_k Y)]e^{1/Y}dY\,, & \text{for } (\beta_k a)^2 < 5/4\,, \end{cases} \tag{2.48}$$

where

$$R_1 = \frac{q_k \sinh(q_k h) - 1/2\,\cosh(q_k h)}{-q_k \cosh(q_k h) + 1/2\,\sinh(q_k h)}\,,$$

$$R_2^\dagger = \frac{c_k^\dagger \sin(c_k^\dagger h) + 1/2\,\cos(c_k^\dagger h)}{c_k^\dagger \cos(c_k^\dagger h) - 1/2\,\sin(c_k^\dagger h)}\,, \qquad R_2 = \frac{-c_k \sinh(c_k h) + 1/2\,\cosh(c_k)}{c_k \cosh(c_k h) - 1/2\,\sinh(c_k h)}\,, \tag{2.49}$$

where c_k, $c_k^\dagger$, and q_k, are shown in equation (2.39).

Using the chain rule of differentiation, the first two equations of equation (2.43) may be combined in terms of the new coordinates shown in Figure 2.3 leading to

$$\frac{\partial^2 V(Y)}{\partial Y^2} = \frac{Re}{2h}\frac{1}{l}\frac{\partial \check{p}_v}{\partial \xi}\,. \tag{2.50}$$

The solution to the above equation for velocity distribution is obtained based on the no-slip condition on the wall, giving the parabolic shape

$$V(Y) = -\frac{Re}{2h}\frac{\check{p}_v}{\partial \xi}\left[\frac{1}{2}Y(h-Y)\right]\,. \tag{2.51}$$

Considering the total nondimensional flow rate, which is calculated by integration of the above equation over the narrow annulus – the flow rate is approximately equal to the cross-section area of annular passage since the total mean nondimensional flow velocity is equal to 1 – and recalling that $h \ll 1$, the nondimensional pressure drop is expressed

$$\frac{\partial \check{p}_v}{\partial \xi} = -\frac{24}{h}\frac{1}{Re} = -\frac{c_f}{h} \simeq \frac{\partial P_m}{\partial x}\frac{a}{\rho \bar{U}^2}\,, \tag{2.52}$$

where $(\partial P_m)/(\partial x)$ denotes the dimensional pressure drop per unit length and the nondimensional friction coefficient c_f is defined by

$$c_f = \frac{24}{Re}\,, \tag{2.53}$$

which is equal to that for laminar flow between concentric cylinders or between two parallel plates. Hence, the dimensional shear stress on the cylinder may be separated into two components: an axial and a circumferential one,

$$\tau_x = \tau \cos\vartheta, \qquad \tau_\Theta = \tau \sin\vartheta\,, \tag{2.54}$$

where the time-independent shear stress on the surface of the cylinder, τ, is given by

$$\tau = \rho\bar{U}^2\frac{12}{Re} = c_f\frac{1}{2}\rho\bar{U}^2. \tag{2.55}$$

The steady longitudinal force F_l and the unsteady lateral viscous force F_{vl} can now be evaluated using

$$\begin{aligned} F_l &= \int_0^{2\pi} \tau_z a\, d\Theta = c_f \pi a \rho \bar{U}^2 , \qquad (2.56) \\ F_{vl} &= \int_0^{2\pi} [\tau_\Theta \sin\Theta + \rho\bar{U}^2 p_v \cos\Theta] a\, d\Theta , \\ &= -\rho\pi a^2 e^{\iota\omega t} \sum_k a_k(\iota\omega\bar{P}_{k1} + \bar{P}_{k0}) , \qquad (2.57) \end{aligned}$$

where

$$\bar{P}_{k1} = -\frac{c_f\bar{U}}{2}\frac{2+h}{ah^2}\sum_{s=1}^{2} G_{sk}W_{sk}\psi_{sk} , \quad \bar{P}_{k0} = -\frac{c_f\bar{U}^2}{2}\frac{2+h}{ah^2}\sum_{s=1}^{2} G_{sk}W_{sk}\psi'_{sk} . \tag{2.58}$$

Thus, the steady and unsteady forces, including the inviscid forces, can be expressed as the general forms shown in equation (2.23). In the above equations, the first and second terms of the numerator, $2+h$, are associated with the viscous perturbation pressure and shear stress, respectively.

Although the foregoing analysis applies to laminar flow, its extension to turbulent flow, *e.g.*, using an eddy-viscosity model, is quite feasible. The unsteady dynamic pressure generated by rocking motion was predicted by the viscous theory for turbulent flow under the same assumptions [35]. The analysis can be adapted to the problem of flexural motion of a cylinder, in order to obtain the nondimensional friction coefficient, c_f, eventually used in predicting the viscous hydrodynanic forces. For turbulent flows in narrow annular passages, the power law for the velocity distribution in the half-width of annular space is

$$\frac{V(y)}{u_\tau} = C\left[\frac{u_\tau}{\nu}(H/2 - y)\right] , \tag{2.59}$$

where y, which is a coordinate normal to the surface of cylinder, is measured from mid-distance between two cylinders and the friction velocity, u_τ, is expressed in terms of the shear stress on the surface, $\tau_o = -\mu\partial V/\partial y\,|_{y=H/2}$, as

$$u_\tau = \sqrt{\frac{\tau_o}{\rho}} . \tag{2.60}$$

Considering the relationship between the total mean flow velocity and the maximum flow velocity at the mid-point between two cylinders and recalling equation (2.60), the nondimensional pressure drop is expressed in the same form as for laminar flow

$$\frac{\partial p_v}{\partial \xi} = -\frac{c_f}{h} \simeq \frac{\partial P_m}{\partial x}\frac{a}{\rho \bar{U}^2}\,, \tag{2.61}$$

where

$$c_f = KRe^{-\frac{2}{n+1}}\,, \tag{2.62}$$

with

$$K = 2\left[4^{1/n}\frac{n+1}{n}\frac{1}{C}\right]^{\frac{2n}{n+1}}\,.$$

Taking $n = 7$ and $C = 8.56$ specfied by Blasius [55] for $Re < 10^5$, the resultant value of K is 0.084. For an eccentric annular flow passage, the friction coefficient, which is related to the steady shear stresses on the walls, is estimated by a more complicated method, based on the law of the wall or the velocity defect law [57, 58].

Utilizing the nondimensional friction coefficient for turbulent flow, the steady and unsteady forces can be evaluated in the same forms as those for laminar flow shown in foregoing.

2.2.3 Typical Result of Dynamics and Stability

Introducing now nondimensional parameters

$$\eta = \frac{e_I}{a}\,, \qquad \hat{T} = \left(\frac{EI}{\rho_s A_s}\right)^{1/2}\frac{t}{L^2}\,, \qquad \Omega = \left(\frac{\rho_s A_s}{EI}\right)\omega L^2\,,$$

$$\sigma = \frac{\rho \pi L^2}{\rho_s A_s}\,, \qquad \Pi = \frac{\bar{P} A_s L^2}{EI}\,, \qquad \hat{U} = \left(\frac{\rho \pi a^2 L^2}{EI}\right)^{\frac{1}{2}}\bar{U}\,, \tag{2.63}$$

together with equation (2.44), and considering the unsteady lateral forces with end condition, the following dimensionless equation of motion of the flexible centre-body is obtained from equation (2.24)

$$\eta^{iv} - c_f \hat{U}^2 l\left(1+\frac{1}{h}\right)\left[\left(1-\frac{1}{2}\delta\right) - \lambda\right]\eta'' - (1-2v)\delta(2-\delta)\Pi\eta''$$

$$+ c_f \hat{U}^2 \frac{l}{h}\eta' + \ddot{\eta} = \left(\frac{L}{aEI}\right)^4 (F_p + F_{vl})\,, \tag{2.64}$$

where $\delta = 0$ corresponds to the case of an axially-sliding downstream end, $\delta = 2$ to a sliding upstream end, and $\delta = 1$ to no axial sliding at either end; υ is Poisson's ratio, $\bar{P}$ is the overpressure at the midpoint of the cylinder, and the prime and dot denote differentiation by X and $\hat{T}$, respectively.

In order to investigate the dynamics and stability of the system, the system of equation (2.64) was discretized by Galerkin's method, utilizing the eigenfunctions ψ_k as comparison functions, and transformed into a standard eigenvalue problem, from which the dimensionless eigenfrequencies, Ω_n, may be obtained. A typical result obtained in this manner is presented. The fluid-dynamic forces acting on the inner cylinder, which executes a flexural motion, are presented in Chapter 6 and a comparison is undertaken between analytical and numerical results.

The dynamical behaviour of the system is illustrated in Figure 2.4, where $l = L/a = 20$, $h = 0.1$, $\sigma = 323.7$, $EI/(\rho\pi a^2 L^2) = 1.33$ m/s , and $\mu = 0.007$ pa s; μ is relatively large here(typical for oil) to highlight the effects of viscous flow. The real and imaginary components of the lowest three eigenfrequencies as functions of $\hat{U}$, calculated according to (a) entirely inviscid (potential) theory, $\mu = 0$, and (b) unsteady viscous flow, but excluding the steady viscous effects (*i.e.*, pressurization effects, surface traction and related pressure drop, which are time-independent). It is recalled that the system loses stability if $\Im(\Omega_n) < 0$, by divergence when $\Re(\Omega_n) = 0$ and by flutter otherwise.

According to potential theory for this case, the system loses stability at $\hat{U} = 2.13$ (point A) in its first mode by divergence. At high flow this mode is restabilized at $\hat{U} = 3.21$(point B) and then the first and second mode loci coalesce and the system loses stability by coupled-mode flutter at point C ($\hat{U} = 3.5$). At higher $\hat{U}$ the system is subject to a succession of coupled-mode flutter and divergence instability, as may be seen in the figure. The critical flow velocity, obtained by an approximate method based on slender-body theory for potential flow, is presented in Appendix A.

The presence of unsteady viscous forces has the following effects on the dynamics of the system. The eigenfrequencies, in the stable region, are complex, rather than

purely real as in the potential case:*i.e.* the system is subject to damping due to the prescence of fluid in the annulus (sometimes refered to as squeeze-film damping). As a result, it takes a higher flow to precipitate divergence; the system loses stability at point A′ (not point *a*) for $\hat{U} = 2.29$. Similarly, coupled-mode flutter occurs at a higher flow velocity, $\hat{U} = 3.56$. Neverthless, the fundamental dynamical hehaviour of the system remains the same as for potential flow. In this respect it is significant that almost up to the point of loss of stability, the $\Im(\Omega_n)$ remain essentially constant with $\hat{U}$.

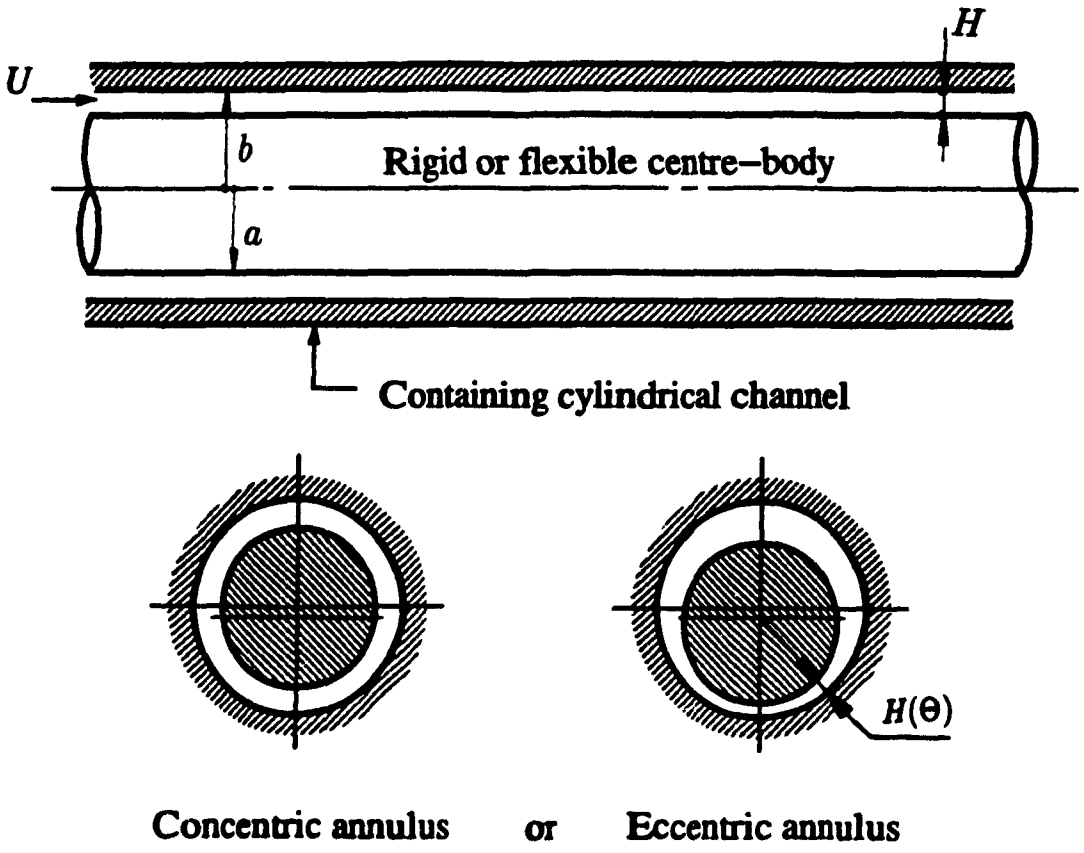

Figure 2.1: Geometry of the centre-body in the cylindrical duct

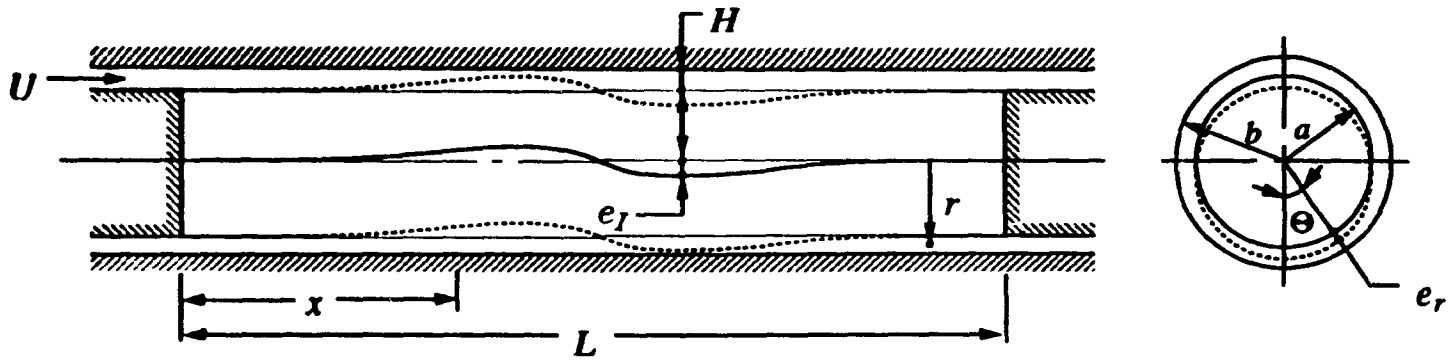

Figure 2.2: Geometry of the flexible centre-body oscillating in a duct with annular flow

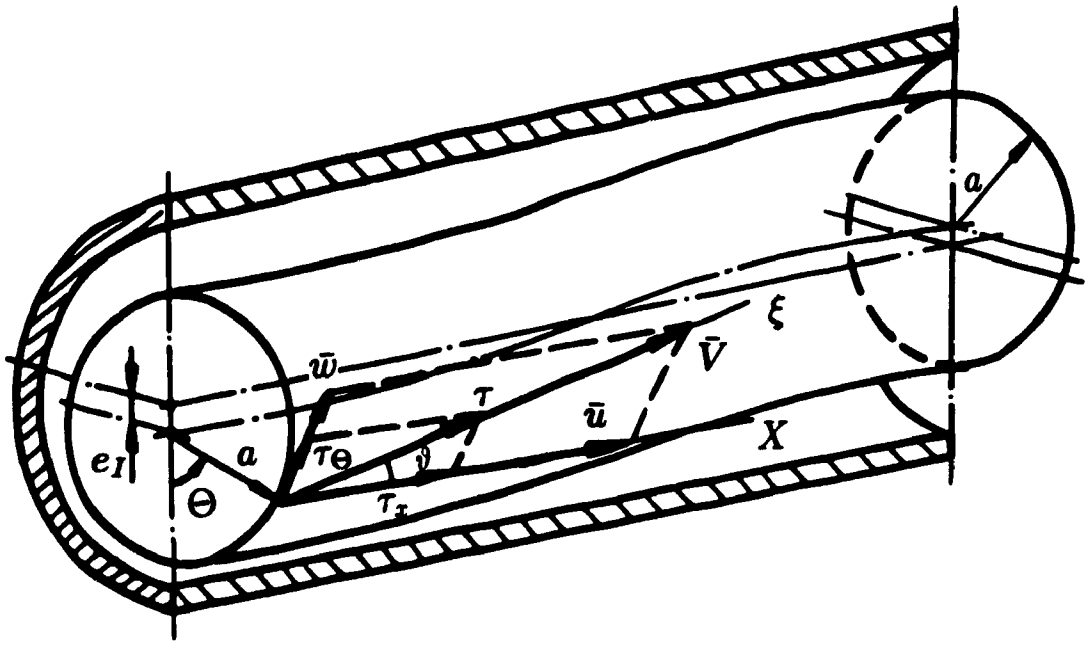

Figure 2.3: Diagram showing transformation of coordinates and definition of the angle ϑ

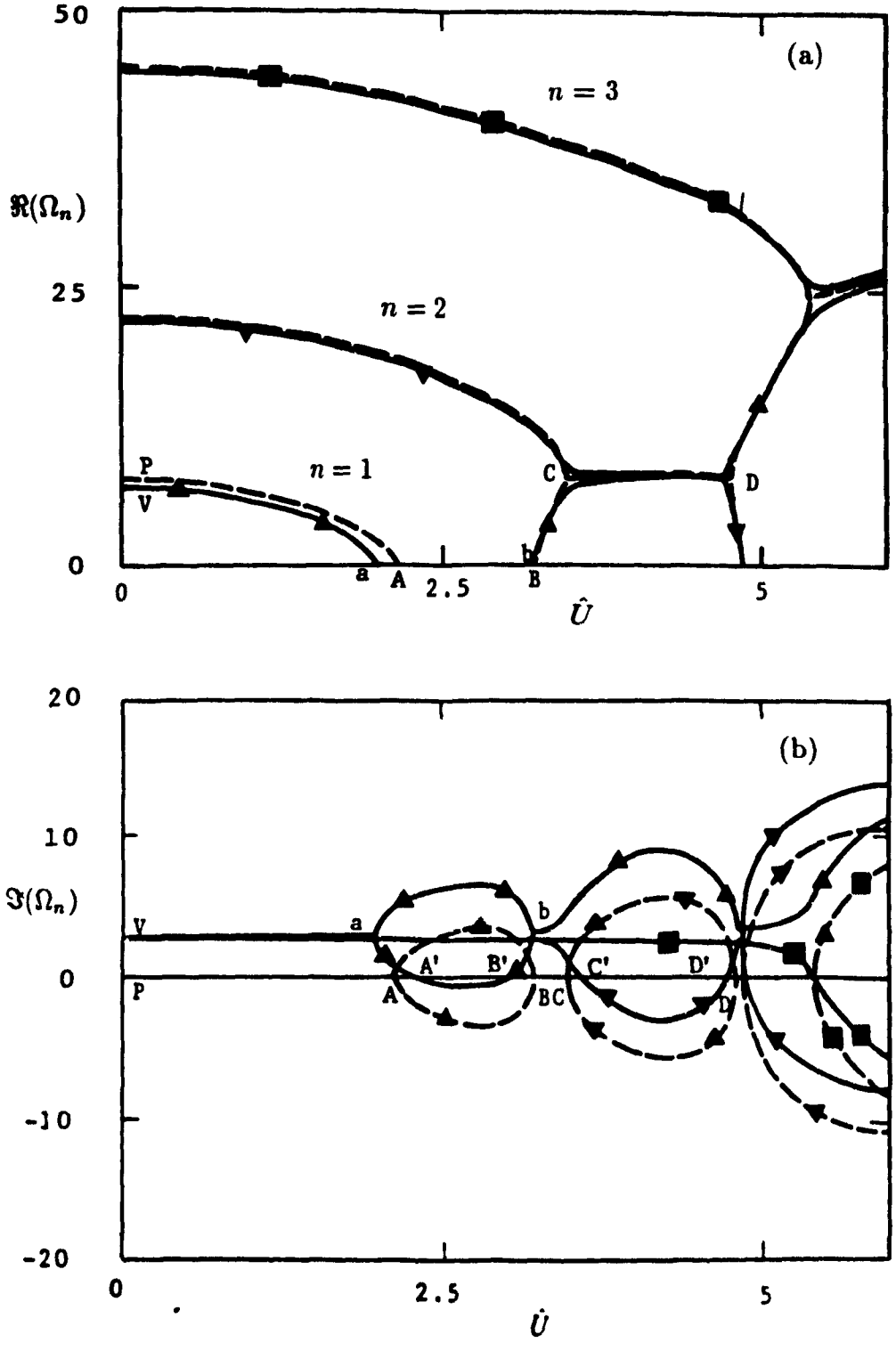

Figure 2.4: The (a) real and (b) imaginary components of the nondimensional eigenfrequencies versus the nondimensional flow velocity, for potential flow(- - - -) and viscous flow(——): ▲, first mode; ▼, second mode; ■, third mode

Chapter 3

Formulation of the Spectral Collocation Method

3.1 GENERAL CONSIDERATION OF THE NUMERICAL METHOD

As seen in the previous chapter for unsteady annular flow as an example, the fluid-dynamic forces have been formulated analytically, leading to a closed-form solution; however, the model is restricted by the assumptions used in the formulation. Using a numerical approach, solutions of wider applicability can be obtained by eliminating such limitations. The present analysis is mainly concerned with numerical solutions for steady and unsteady flows in annular constructions involving eccentricity. The presence of eccentricity in annular configurations considerably adds to the complexity of the problem. For this reason, very few accurate analytical solutions have been obtained and then only for simplified cases. Because of the special interest in dynamical systems involving eccentricity, sudden expansion, contraction, or diffuser sections and even in the case of concentric configurations, it is desirable to provide more accurate solutions for viscous flows than the existing analytical solutions.

For the study of steady and unsteady flows, a newly developed spectral method will be presented. The numerical method is completely different from the recently developed method based on time-integration by a finite-difference formulation [46].

Using convenient expansions, the fluid dynamic parameters can be expressed in

terms of interpolation functions such as Chebyshev and Legendre polynomials and Fourier series etc. containing *a priori* unknown coefficients. In this procedure, the governing equations and boundary conditions are discretized in terms of unknown coefficients, using a collocation method. In the present work, a linear boundary-value problem, based on small-amplitude motion of the oscillating cylinder, is considered.

In order to discretize the fluid-dynamic governing equations, two numerical approaches have been formulated for two-dimensional problems of flow between two parallel plates or two eccentric cylinders and for the three-dimensional problems of flow between cylinders. In the present work for eccentric configurations, the fluid parameters are expressed in the radial and circumferential domains as interpolation functions. In general, the unknown coefficients of expanded parameters confined in the radial and circumferential coordinates are also dependent variables in the axial domain. For two-dimensional problems, these coefficients are constant in the axial direction. The governing equations expanded by the spectral method are imposed on a finite number of collocation points in the radial and circumferential domains.

For three-dimensional problems, the collocation method is restricted to the radial and circumferential domains, while a finite-difference approximation based on the hybrid scheme is used to discretize the problem for axial variations, where the axial region is subdivided into a finite number of axial points. Eventually, the problem of self-excited motions of flexible bodies in fluid flow in eccentric geometries will be tackled, where the motion of the cylinder in time and space is not known *a priori*.

A similar hybrid scheme under the name "high-lateral-flux modification" was introduced by Spalding for the finite-difference method [56]. The main principles and application of the collocation finite-difference method will be presented in Chapter 6.

Similarly to any other numerical approach, the solution of a continuum problem by the collocation method follows an orderly step-by-step process. To summarize in general terms how the collocation method works, the steps will be succinctly listed as follows. The first step is to *choose suitable interpolation functions* to represent the variations of a field variable over the given domain. The second step is to *transform*

the coordinates by considering the property of the polynomial functions selected in the first step. The next step is to *determine the degree of the interpolation functions.* In general, an approximate solution of high accuracy can be obtained by increasing the degree(order) of these functions. But, with increasing the degree, it is obvious that the system of discretized equations becomes larger, which can reduce the computational efficiency of the method; sometimes, this may also have a detrimental effect on the solution due to round-off errors, as mentioned before. It is therefore necessary to optimize the degree of the interpolation functions. The final step is to *select the collocation points.* In order to get a solution of high accuracy with a given degree of the interpolation functions, it is required to assign more collocation points in the regions where the variations are larger than at other regions. Generally, a pseudo-singularity problem in the system equation may arise because of the inadequate number of collocation points and/or unsuitable selection of the collocation points.

In summary, the nature of the solution depends not only on the interpolation function, but also on its degree. Most often, the choice is a matter of engineering judgement based on accumulated experience. Generally, the approximation improves with increasing the size of the family of interpolation functions, as long as the pseudo-singularity problem is not encountered. If by chance, the exact solution is contained in the family of interpolation functions, this procedure gives the exact solution. At the same time, it is very impotant that the numerical method utilized be as computationally efficient and frugal as possible, in terms of memory requirements and time.

This newly developed spectral collocation method will first be applied to the study of steady and unsteady flow between two parallel plates and two eccentric cylinders. The spectral solutions will be validated by comparison with the available analytical solutions in Chapter 4.

In two dimensional problems such as steady and unsteady flows between two eccentric cylinders or two parallel plates, any fluid-dynamic parameters, at any location in the physical domain, are dependent variables in the computational domain related to the selected interpolation functions; they may also be functions of time, when the flow

is unsteady. The specific form of the spectral expansion is chosen in accordance with the physical problem involved. Considering a convenient coordinate transformation, the problem can be defined in the computational domain, where the algebraic system of equations is obtained from the governing equations, in addition to the boundary conditions. Using the collocation method, the equations are discretized in terms of the unknown coefficients. Using the Gauss-Seidel iteration method based on a pivot point, the unknown coefficients can be determined. The solutions obtained in the computational domain can be converted back to the physical domain by a coordinate transformation.

3.2 SPECTRAL COLLOCATION METHOD FORMULATIONS

The governing equations of the steady and the unsteady flows, represented by the Navier-Stokes and continuity equations subjected to specific boundary conditions, form systems of partial differential equations which can be expressed in matrix form as

$$\mathbf{E}\left(\mathbf{f}, \frac{\partial \mathbf{f}}{\partial x_1}, \frac{\partial \mathbf{f}}{\partial x_2}, \cdots, \frac{\partial \mathbf{f}}{\partial x_m}, \frac{\partial^2 \mathbf{f}}{\partial x_1^2}, \frac{\partial^2 \mathbf{f}}{\partial x_2^2}, \cdots, \frac{\partial^2 \mathbf{f}}{\partial x_m^2}\right) = 0\,, \quad \mathbf{E} = (E_1, E_2, \cdots, E_n)^{\mathrm{T}}\,, \quad (3.1)$$

where $x_1, x_2, \cdots, x_m$ are the independent variables, such as the geometrical coordinates and times, and $\mathbf{f} = (f_1, f_2, \cdots, f_n)^{\mathrm{T}}$ is the vector of fluid-dynamic parameters, such as the velocity components and pressure.

In the present spectral collocation method, the following type of expansion is considered for any fluid dynamic parameter $\mathbf{f}_n$ (where $n = 1, 2, \cdots, N$), in the form

$$\mathbf{f}_n(x_1, x_2, \cdots, x_m) = \sum_{j,k,l} A^{(n)}_{j,k,l}\, T_j(x_J)\, F_k(x_K)\, exp(\omega_l x_L)\,, \quad (3.2)$$

where $A^{(n)}_{j,k,l}$ are *a priori* unknown coefficients. The appropriate interpolation functions for the expansions must be chosen in accordance with the physical problem involved. This is completely illustrated in Chapter 4 for typical unsteady and steady flow problems. In the present work for eccentric configurations, T_j and F_k represent, respectively, Chebyshev polynomials and Fourier series functions. The exponential functions are

used for the time variable in unsteady flow with harmonically oscillating boundaries, in which case the coefficients ω_l are related to the radian frequency of the oscillation, ω.

The choice of Fourier series as an interpolation function in the circumferential direction stems from the obvious periodic character of the flow field with respect to the azimuthal angle, while no such periodic character is obvious in the radial direction. The Chebyshev expansion method defined in the direction normal to the wall is particularly suitable because of its fast convergence (exponential convergence as compared to the algebraic convergence of the finite-difference solution) and capability to resolve especially thin layer-penetration depth, $\delta_p = \sqrt{2\nu/\omega}$, in an unsteady viscous flow.

In the present spectral collocation method, the governing equations of the steady or unsteady flow and the associated boundary conditions reduce to a system of algebraic equations, where the coefficients of the flow variable expansions are the unknowns. The solution of this system of equations determines completely the entire flow field (steady or unsteady). To get the system equation with this spectral expansion, the governing equations are imposed at M collocation points, $x_{1m}, x_{2m}, ..., x_{qm}$ where $m = 1, 2, ...M$, which leads, together with boundary conditions, to an algebraic system of equations expressed in the general form

$$\mathbf{E}_m \left(\sum_{n=1}^{N} \sum_{j,k,l} A_{j,k,l}^{(n)} \, T_j(x_{Jm}) \, F_k(x_{Km}) \, exp(\omega_l x_{Lm}) \right) = 0 \, , \quad m = 1, 2, \cdots, M \, . \qquad (3.3)$$

In the determination of the unknown coefficients, $A_{j,k,l}^{(n)}$, of the spectral expansions, it is necessary to assign more collocation points in regions with sharp gradients than in other regions, in order to converge to the solution more easily: for example, when the unsteady flow fields are generated by the oscillatory motion of a wall or a cylinder with relatively small penetration depth.

Galerkin's approach in the spectral method for discretizing the fluid dynamic governing equation was tried first, to be used instead of the present collocation method. However, Galerkin's approach did not provide good accuracy and computing efficiency, especially for unsteady problems where large velocity variations exist near the wall.

Galerkin's method cannot put weight on particular regions of the domain since the governing equations are discretized by integration over the whole domain.

The present spectral-collocation method will be shown to provide accurate results with good computing efficiency for a considerable range of unsteady and steady problems. This method permits clustering of the collocation points in important regions so as reduce the number of terms in the spectral expansion for a desired accuracy.

3.3 COORDINATE TRANSFORMATION

For steady and unsteady flows in eccentric annular configurations, any fluid dynamic properties are variables dependent on the radial and circumferential coordinates, r and Θ shown in Figure 3.1, and also on time when the flow is unsteady. In this figure, a and b denote the inner and outer cylinder radii, ha is the annular gap and e is the eccentricity.

In order to generalize the problem by using the spectral collocation method, it is necessary to transform the annular space (r and Θ) between the eccentric cylinders into the rectangular computational domain (Z and θ). For this purpose, it is convenient to define the following nondimensional coordinates:

$$Z = 1 - 2\frac{r - a}{a\, h(\Theta)}, \qquad \theta = \Theta, \tag{3.4}$$

where

$$H = a\, h(\Theta) = bE^{1/2} - e\, \cos\Theta - a, \tag{3.5}$$

with

$$E = 1 - \left(\frac{e}{b}\right)^2 \sin^2\Theta .$$

All functions having continuous partial derivatives in the cylindrical domain can be expressed in the form of functions in the computational domain by the chain rule. Thus, by considering equation (3.4), the derivatives of a function f in the radial direction can be written as

$$\frac{\partial f}{\partial r} = -\frac{2}{ah}\frac{\partial f}{\partial Z}, \qquad \frac{\partial^2 f}{\partial r^2} = \left(\frac{2}{ah}\right)^2 \frac{\partial^2 f}{\partial Z^2} . \tag{3.6}$$

Let the fluid dynamic property $f = f(Z,\theta)$ and the nondimensional coordinate $Z = Z(r,\Theta)$; then by the chain rule the new coordinate Z has derivatives

$$\frac{\partial Z}{\partial \theta} = \frac{\partial Z}{\partial \Theta}\frac{\partial \Theta}{\partial \theta} = \frac{1-Z}{h}\frac{\partial h}{\partial \Theta},$$

$$\frac{\partial^2 Z}{\partial \theta^2} = \frac{\partial}{\partial \theta}\left(\frac{\partial Z}{\partial \theta}\right) = -\frac{1-Z}{h^2}\left(\frac{\partial h}{\partial \Theta}\right)^2 + \frac{1-Z}{h}\frac{\partial^2 h}{\partial \Theta^2}, \tag{3.7}$$

where

$$\frac{\partial h}{\partial \Theta} = \frac{e}{a}\sin\theta - \frac{1}{2}\frac{b}{a}\left(\frac{e}{b}\right)^2 \sin 2\theta\, E^{-\frac{1}{2}},$$

$$\frac{\partial^2 h}{\partial \Theta^2} = \frac{e}{a}\cos\theta - \frac{b}{a}\left(\frac{e}{b}\right)^2 \cos 2\theta\, E^{-\frac{1}{2}} - \frac{1}{4}\frac{b}{a}\left(\frac{e}{b}\right)^4 \sin^2 2\theta\, E^{-\frac{3}{2}}, \tag{3.8}$$

The partial derivatives of the fluid-dynamic property in the circumferential direction can then be expressed in term of the computational domain as

$$\frac{\partial f}{\partial \Theta} = \frac{\partial f}{\partial \theta} + \frac{1-Z}{h}\frac{\partial h}{\partial \Theta}\frac{\partial f}{\partial Z},$$

$$\frac{\partial^2 f}{\partial \Theta^2} = \frac{\partial^2 f}{\partial \theta^2} + \left[\frac{1-Z}{h}\frac{\partial^2 h}{\partial \Theta^2} - \frac{1-Z}{h^2}\left(\frac{\partial h}{\partial \Theta}\right)^2\right]\frac{\partial f}{\partial Z} + 2\frac{1-Z}{h}\frac{\partial h}{\partial \Theta}\frac{\partial^2 f}{\partial Z\,\partial \theta}$$
$$+ \left(\frac{1-Z}{h}\frac{\partial h}{\partial \Theta}\right)^2 \frac{\partial^2 f}{\partial Z^2} - \frac{1-Z}{h^2}\left(\frac{\partial h}{\partial \Theta}\right)^2 \frac{\partial f}{\partial Z}. \tag{3.9}$$

In this manner, the partial-differential equation defined in physical domain for eccentric configurations can be discretized in the computational domain with the spectral collocation method.

For the unsteady viscous motion between oscillating and fixed parallel plates (Figure 3.2), the derivatives in the normal direction of a fluid dynamic property f can be expressed in the computational domain $(-1 < Z < 1)$ as

$$\frac{\partial f}{\partial y} = \frac{1}{H}\frac{\partial f}{\partial Z}, \qquad \frac{\partial^2 f}{\partial y^2} = \frac{1}{H^2}\frac{\partial^2 f}{\partial Z^2}, \tag{3.10}$$

where Z denotes the nondimensional parameter defined by $Z = y/H$, y is a coordinate normal to the plates, which is measured from mid-distance between them, and $2H$ represents the distance between two parallel plates.

Let us consider the properties of Chebyshev polynomials in order to expand their derivatives in series form. The following formulae relate the expansion coefficients a_n in the series

$$f(Z) = \sum_{n=0}^{\infty} a_n T_n(Z) \tag{3.11}$$

to the expansion coefficients b_n of

$$Lf(Z) = \sum_{n=0}^{\infty} b_n T_n(Z)\,, \tag{3.12}$$

for various linear operators. The formulae for the derivatives are

$$Lf(Z) = f'(Z) \quad : \quad c_n b_n = 2 \sum_{p=n+1}^{\infty} p a_p\,, \qquad n+p = \text{odd}\,,$$

$$Lf(Z) = f''(Z) \quad : \quad c_n b_n = \sum_{p=n+2}^{\infty} p(p^2 - n^2) a_p\,, \qquad n+p = \text{even}\,, \tag{3.13}$$

where $c_0 = 2$ and $c_n = 1$ $(n > 0)$.

As a result, it is possible to express the solutions of fluid parameters in expansion form of Chebyshev polynomials and Fourier series in the computational domain $(-1 < Z < 1,\ 0 < \theta < 2\pi)$.

The spectral collocation method can now be applied to several specific problems for steady and unsteady flows, in order to validate the method, in Chapter 4. Then, the method is extended in order to solve more complicated problems – for example, the unsteady viscous flow problem of a cylinder subject to axial flow, which will be studied in Chapter 6.

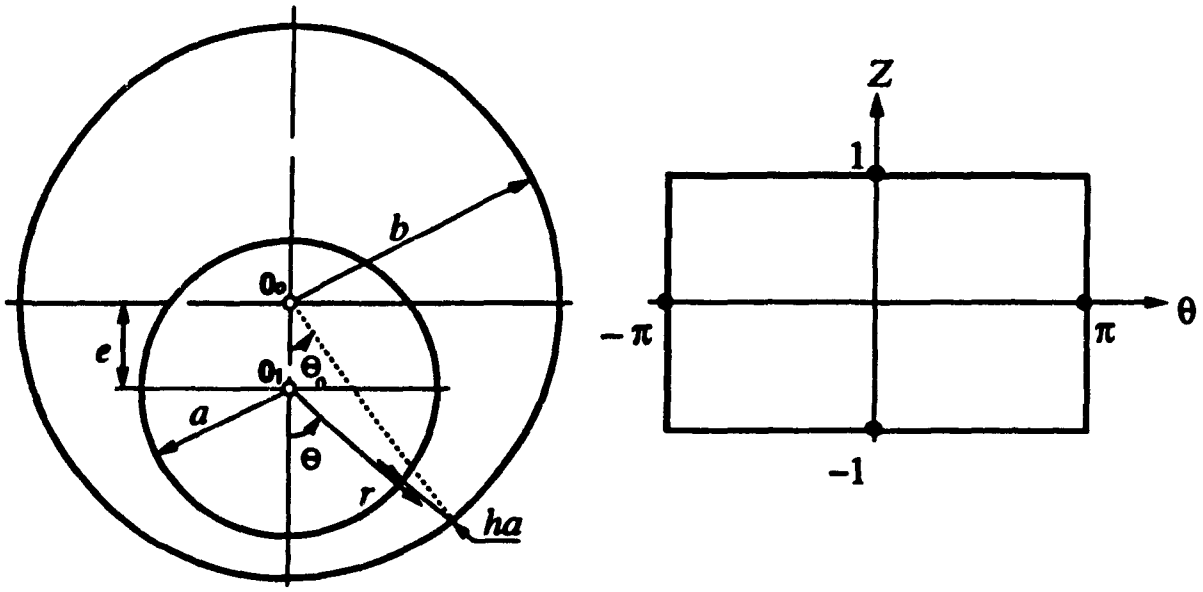

Figure 3.1: Geometry of the annular space between two eccentric cylinders in the physical plane (r, Θ) and in the computational domain (Z, θ)

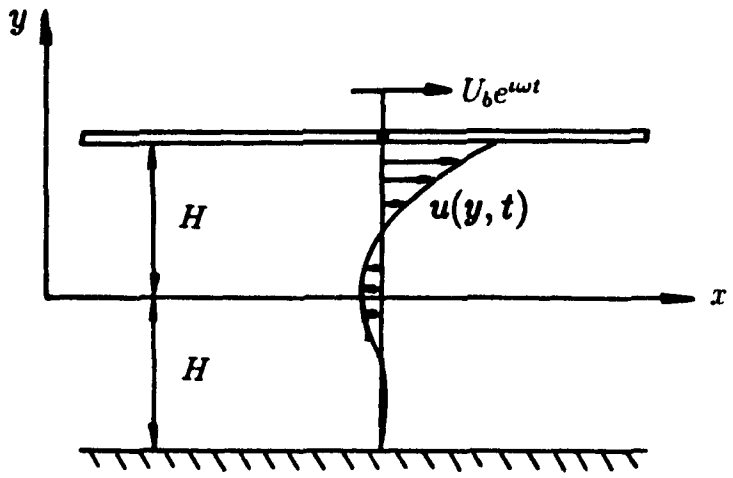

Figure 3.2: Unsteady viscous flow between two parallel plates

Chapter 4

Validation of the Spectral Method

A spectral collocation method has been developed in the previous chapter of unsteady flows in an annulus. Before applying it to problems, the method will be validated by comparison with available analytical solutions for typical steady and unsteady fluid flow problems. The dynamic characteristics of the fluid motions obtained for the typical problems may be useful to judge numerical results given for more complicated but similar problems.

Thus, for the validation purposes, the spectral collocation method is first applied to the problems of (i) fully-developed laminar flow in an eccentric annulus and (ii) the steady flow generated by cylinders rotating in a concentric annulus. The analytical solutions are presented in Appendices B and C. Considering the steady viscous flow, generated by rotational motion of one or both of the cylinders in a concentric annulus, it should be mentioned that this method can be extended to the problem of oil lubricated bearings in an eccentric annulus, where extremely large pressure differences are obtained at high flow velocities. The velocity distributions along the radial direction are presented by the numerical and the analytical methods.

In order to validate the spectral collocation method for unsteady flow problems, the theory is also applied to simple problems of unsteady viscous flows, where analytical solutions are known: unsteady viscous flows between two parallel plates oscillating harmonically and between concentric cylinders undergoing harmonic oscillatory rotation. The numerical results are then compared to the analytical ones given in Appendices C

and D.

In general, the accuracy of the numerical solution given by this method is dependent on the number of the selected collocation points. In other words, it is possible to get higher accuracy in the numerical solution by increasing the degree of the polynomials considered, when singularity problems are not encountered. The influence of the number of collocation points, m, or n and m, on accuracy of the present spectral method is investgated by comparing the numerical results obtained for various values of m, or n and m, with the exact analytical solutions. For this purpose, a *rms* average error is calculated for each set of m, or n and m, values:

$$\overline{rms} = \left[\frac{1}{N}\sum_{j}^{N}(1 - f_{num}/f_{ana})_j^2\right]^{\frac{1}{2}} , \tag{4.1}$$

where N denotes the number of points, uniformly distributed in the domain, in which the numerical solution, f_{num}, is compared with the analytical solution, f_{ana}.

The velocity profile for unsteady viscous flow has the form of a damped harmonic oscillation, the fluid velocity, $f(x,t)$, at a certain point x, has a phase lag φ with respect to the motion of the wall. The nondimensional velocity amplitude, $|\hat{f}|$, and the phase angle φ have been calculated for the unsteady viscous flow between two parallel plates and two concentric cylinders, as

$$|\hat{f}(x)| = \frac{|f(x,t)|}{f_b e^{i\omega t}} , \qquad \varphi = \arctan\frac{\Im(\hat{f}(x))}{\Re(\hat{f}(x))} , \tag{4.2}$$

where $f_b\, e^{i\omega t}$ represents the velocity of the moving structure, and $\Re$ and $\Im$ stand for real and imaginary components, respectively.

4.1 STEADY VISCOUS FLOWS

4.1.1 Fully Developed Laminar Flow Between Two Eccentric Cylinders

In the present work, the fully developed laminar-flow velocity distribution in an eccentric annulus is obtained by the spectral collocation method, for comparison with the analytical solution given by Piercy *et al.* [52]. This analytical method was developed

based on a conformal transformation of the annular space from the physical coordinates to bipolar ones. The cross-sectional geometry considered in the present problem is shown in Figure 3.1.

The equation of motion for fully developed laminar flow, essentially a two dimensional problem in r and Θ, reduces to Poisson's equation

$$\frac{\partial^2 U}{\partial r^2} + \frac{1}{r}\frac{\partial U}{\partial r} + \frac{1}{r^2}\frac{\partial^2 U}{\partial \Theta^2} = 4\frac{Q}{a^2}\,, \tag{4.3}$$

where $U(r,\Theta)$ is the fully developed axial flow velocity and Q is related to the pressure drop by

$$Q = \frac{a^2}{4\mu}\frac{dP}{dx} = \text{constant}\,, \tag{4.4}$$

where $P(x)$ is the pressure and μ is the fluid viscosity.

Considering equations (3.7) and (3.9) defined for the nondimensional computational domain (Z,θ) by the coordinate transformation, Poisson's equation becomes

$$A\frac{\partial^2 U}{\partial Z^2} + B\frac{\partial U}{\partial Z} + C\frac{\partial^2 U}{\partial Z \partial \theta} + D\frac{\partial^2 U}{\partial \theta^2} = Qh^2\,, \tag{4.5}$$

where

$$\begin{aligned} A &= 1 + D[(1-Z)h'/h]^2\,, \\ B &= -\sqrt{D} + D(1-Z)[h''/h - 2(h'/h)^2]\,, \\ C &= 2D(1-Z)h'/h\,, \\ D &= \{h/[2+(1-Z)h]\}^2\,, \end{aligned}$$

where $h(\theta)$ represents the nondimensional annular space defined in equation (3.5) and $h'(\theta)$ and $h''(\theta)$ denote its derivatives defined in equation (3.8).

The boundary conditions, based on the no-slip condition, on the inner and outer cylinders ($Z = \pm 1$), can be rewritten as

$$U(1,\theta) = 0 \qquad \text{and} \qquad U(-1,\theta) = 0\,. \tag{4.6}$$

In this spectral collocation method, the following expansion in terms of Chebyshev polynomials and Fourier series may be considered for the axial flow velocity

$$U(Z,\theta) = \sum_{j=0}^{m}\sum_{k=0}^{n} U_{jk}\, T_j(Z)\, F_k(\theta)\,, \tag{4.7}$$

where $F_k = \cos k\theta$, due to flow symmetry with respect to the plane $\theta = 0$ in this case. With this expansion, the governing equation (4.5) and the boundary conditions can formally be expressed as

$$\sum_{j=0}^{m}\sum_{k=0}^{n} U_{jk}\left[A\,T_j''(Z)\,F_k(\theta) + B\,T_j'(Z)\,F_k(\theta) + C\,T_j'(Z)\,F_k'(\theta) + D\,T_j(Z)\,F''(\theta)\right] = Qh^2(\theta)\,, \tag{4.8}$$

and

$$\begin{aligned}\sum_{j=0}^{m}\sum_{k=0}^{n} U_{jk}\,T_j(1)\,F_k(\theta) &= 0\,,\\ \sum_{j=0}^{m}\sum_{k=0}^{n} U_{jk}\,T_j(-1)\,F_k(\theta) &= 0\,,\end{aligned} \tag{4.9}$$

where the prime denotes differentiation with respect to the concerned coordinates; for example, $T' = dT/dZ$ and $F'' = d^2F/d\theta^2$.

Considering the properties of Chebyshev polynomials and their derivatives given in equation (3.13), the governing equation is expressed as

$$\sum_{j=0}^{m}\sum_{k=0}^{n}\left\{A\,T_j\,F_k(\theta)\frac{1}{c_j}\sum_{p=j+2}^{m} p(p^2-j^2)\,U_{pk} + T_j(Z)\left[B\,F_k(\theta) + C\,F_k'(\theta)\right]\frac{2}{c_j}\sum_{p=j+1}^{m} p\,U_{pk} + D\,T_j(Z)\,F''(\theta)\,U_{jk}\right\} = Qh^2(\theta)\,. \tag{4.10}$$

Using the collocation method, equations (4.9) and (4.10) can be formulated as a system of algebraic equations, with unknowns U_{jk} and U_{pk}. At the collocation points, equation (4.10) is rigorously satisfied, specifically at $(n+1)$ circumferential positions corresponding to the angular coordinates $\theta_k (k = 0, 1, 2, \cdots, n)$ and also at $(m-1)$ radial positions corresponding to the nondimensional coordinates $Z_J (J = 1, 2, \cdots, m-1)$. The boundary conditions are imposed on $(2n+2)$ angular positions on the wall $Z = \pm 1$. The solution of this algebraic system of $(n+1)\times(m+1)$ equations completely determines the flow in the annular space.

The present solution is compared in Figure 4.1 with the analytical solution, obtained by Piercy *et al.* [52] and Snyder and Goldstein [53], which is derived in Appendix

B; it is noted that the results of the two analytcal solutions are identical. The numerical solution is obtained with $n = m = 6$ collocation points which are uniformly distributed radially and azimuthally. The ratio of the radii of the inner and outer culinders, a/b, is 0.5, the relative eccentricity, $e/(b-a)$, is 0.6 and the relative pressure drop per unit length, defined by equation (4.4), is -0.17m/s. The variation of the calculated average *rms* error, $\overline{rms}$, defined in equation (4.1), is shown in Table 4.1 for $N = 180$.

Table 4.1 The variation of the calculated *rms* average error with the number of collocation points, n and m, for fully developed laminar flow [$a/b = 0.5$, $e/(b-a) = 0.6$, $Q = -0.17$m/s and$N = 180$]

$n = m$	3	5	7
$\overline{rms}$ %	29.11	0.34	0.02

As shown in Figure 4.1, the laminar flow velocity in a strongly eccentric annular space is highly asymmetrical; the maximum axial velocity in the azimuthal plane $\Theta = 180°$ being more than ten times larger than the maximum one in the $\Theta = 0°$ plane. This strong asymmetry is due to the large viscous stresses near the wall. By physical intuition, the flow rate discharged per second may increase with the eccentricity and the local shear stress around the wall may vary along the circumferential direction, as compared to concentric ones. As a result, the effects of the steady axial flow due to the eccentricity on the fluid dynamic forces acting on the cylinder are different from those for concentric configurations.

Considering the results shown in Table 4.1 and Figure 4.1, excellent agreement is found to exist between the present and the analytical solutions for n and m greater than 5. It was found that the accuracy of the numerical solution converges relatively fast, namely exponentially, with the number of collocation points.

4.1.2 Steady Viscous Flow in An Annulus Generated by Rotating Concentric Cylinders

In this problem, the steady viscous flow between two concentric cylinders is generated by steady rotational motion of the inner or outer cylinder. The spectral collocation

method is used to solve the problem, and the numerical results are compared to the analytical ones presented in Appendix C.

For this two-dimensional problem, any fluid dynamic parameters are dependent only on the radial coordinate. The radial flow velocity and the circumferential variation of fluid-dynamic parameters can be eliminated. Thus, the Navier-Stokes equations reduce drastically to

$$\frac{d^2W}{dr^2} + \frac{d}{dr}\left(\frac{W}{r}\right) = 0 , \tag{4.11}$$

subject to the boundary condition on the surface of the rotating cylinder:

$$W = a\omega \qquad \text{at} \quad r = a ,$$

when the inner cylinder rotates; or when the outer one is rotating,

$$W = b\omega \qquad \text{at} \quad r = b ;$$

and $W = 0$ on the stationary cylinder. In these equaions, $W(r)$ represents the circumferential flow velocity and ω denotes the angular velocity of the rotating cylinder.

Using the convenient coordinate transformation based on the nondimensional parameter $Z = 1 - 2(r - a)/H$, the problem is defined in the computational domain, Z, in which the governing equation (4.11) can be expressed as

$$\frac{d^2\hat{w}}{dZ^2} - \sqrt{D}\frac{d\hat{w}}{dZ} - D\hat{w} = 0 , \tag{4.12}$$

subject to the boundary conditions

$$\hat{w}\,|_{Z=1} = 1 - \delta ,$$

$$\hat{w}\,|_{Z=-1} = \delta ,$$

where D, defined in equation (4.5), is constant for a concentric annulus, δ is 0 or 1 accordingly as the inner or outer cylinder is rotating, and the nondimensional flow velocity is $\hat{w}(Z) = W'/(a\omega)$ for inner cylinder motion or $\hat{w}(Z) = W'/(b\omega)$ for outer cylinder motion.

Using Chebyshev polynimials, $\hat{w}(Z)$ is expanded as

$$\hat{w}(Z) = \sum_{j=0}^{m} W_j T_j(Z) . \tag{4.13}$$

Substituting this equation into equation (4.12), an algebraic system of $(m+1)$ equations is obtained in the form

$$\sum_{j=0}^{m} W_j [T_j''(Z) - \sqrt{D} T_j'(Z) - D T_j(Z)] = 0 , \tag{4.14}$$

which is to be rigorously satisfied at $(m-1)$ collocation points, $Z_J (J = 0, 1, 2, \cdots, m-1)$, and by two boundary conditions,

$$\sum_{j=0}^{m} W_j T_j(1) = 1 - \delta ,$$

$$\sum_{j=0}^{m} W_j T_j(-1) = \delta .$$

The unknown coefficients W_j are then determined from a set of algebraic equations consisting of the discretized governing equation and the boundary conditions.

For the viscous flow generated by rotational motion of a cylinder, the analytical and numerical solutions are studied: when (a) the inner cylinder rotates and (b) the outer cylinder rotates. By inspection of equation (4.14), the principal nondimensional parameter characterizing the system is D, which is dependent only on the nondimensional annular space, $h = H/a = b/a - 1$.

In Figure 4.2, the velocity distributions are presented for various values of a/b (0.4, 0.6 and 0.8), in cases (a) and (b) with $m = 7$. To investigate the influence of the number of collocation points, m, uniformly distributed in the radial direction, the calculated average *rms* error is presented in Table 4.2 for $a/b = 0.6$ with $N = 40$.

Table 4.2 The variation of the calculated *rms* average error with the number of collocation points, m, for steady viscous flow generated by the rotational motion of the cylinder $[a/b = 0.6]$

	inner cylinder rotates		outer cylinder rotates	
m	3	5	3	5
rms %	7.30	0.05	3.54	0.03

Taking account of the results shown in Figure 4.2, it is noted that the velocity distribution is less affected by the ratio of two radii in case (b) than in case (a). With decreasing a/b, both cases tend to the linear velocity distribution of Couette flow, as it occurs between two flat plates.

Excellent agreement between the present numerical solution and the analytical results is obtained for m greater than 5, and the accuracy of the present solutions converges very fast as the number of collocation points is increased, as shown in Table 4.2 and in Figure 4.2.

4.2 UNSTEADY VISCOUS FLOWS

4.2.1 Unsteady Viscous Motion between Oscillating Parallel Plates

The first test for unsteady viscous flow problems is the unsteady motion between two infinitely long parallel plates, one of which executes an oscillatory motion in its plane with periodic harmonic motion, while the other is fixed or has an oscillatory motion in antiphase. As shown in Figure 4.3, the distance between the two plates is $2H$, and y denotes the coordinate measured from the centerline. The velocity of the oscillating plate is $U_b\, e^{\omega t}$.

By eliminating the derivatives of the fluid dynamic parameters in the tangential direction to the plate as well as the flow velocity normal to the plate, the governing equation , derived from the Navier-Stokes equations, is expressed as

$$\frac{\partial u^*}{\partial t} = \nu \frac{\partial^2 u^*}{\partial y^2} , \tag{4.15}$$

where ν is the kinematic viscosity of fluid and $u^*(y,t)$ is unsteady flow velocity in the tangential direction to the plates, which can be defined by

$$u^*(y,t) = U(y)\, e^{\omega t} , \tag{4.16}$$

where ω represents the circular frequency of the oscillations.

In order to generalize the problem, it is convenient to define the following nondimensional parameters;

$$Z = \frac{y}{H}\,, \qquad \hat{u} = \frac{U}{U_b}\,, \qquad Re_s = \frac{\omega H^2}{\nu}\,, \tag{4.17}$$

where Re_s is called the oscillatory Reynolds number, defined as the product of the Reynolds number based on the plate velocity amplitude, $Re = (U_b H)/\nu$, and the reduced frequency, $\Omega = (\omega H)/U_b$.

In this case, the following spectral expansion, based on Chebyshev polynomials, can be considered for the nondimensional complex amplitude of velocity, $\hat{u}$, as

$$\hat{u}(Z) = \sum_{j=0}^{m} [\, \Re(U_j) + \imath\, \Im(U_j)\,]\, T_j(Z)\,, \tag{4.18}$$

where $\Re$ and $\Im$ stand for the real and imaginary components, respectively, of the complex unknown U_j. Hence, considering the equation (4.17), the governing equation can be rewritten as

$$\frac{\partial^2 \hat{u}}{\partial Z^2} = \imath\, Re_s \hat{u}\,, \tag{4.19}$$

subject to the boundary conditions

$$\begin{aligned} \hat{u}\,|_{Z=-1} &= \delta\,, \\ \hat{u}\,|_{Z=1} &= 1\,, \end{aligned} \tag{4.20}$$

where $\delta = 0$ when only the upper plate oscillates, and $\delta = -1$ when the lower plate also oscillates in antiphase with the upper one.

With the spectral expansion, the governing equation (4.19) is expanded as

$$\sum_{j=0}^{m} [\, \Re(U_j) + \imath\, \Im(U_j)\,]\, [T_j''(Z) - \imath Re_s T_j(Z)] = 0\,, \tag{4.21}$$

where the prime denotes the differentiation with respect to Z. The no-slip boundary conditions are also rewritten in the expanded form

$$\sum_{j=0}^{m} [\Re(U_j) + \imath \Im(U_j)]\, T_j(1) = 1\,,$$

$$\sum_{j=0}^{m}[\Re(U_j) + \iota\Im(U_j)]\, T_j(-1) = \delta\ . \tag{4.22}$$

It is worth noting that both real and imaginary parts have to be satisfied in each of the above equations.

The *a priori* unknown coefficients U_j, which are now complex variables, are determined using the same procedure utilized in previous sections for steady viscous flows; however, in this case it is necessary to select the collocation points more carefully, as discussed in Chapter 3. To obtain good accuracy and computing efficiency in the case of relatively high Re_s, the collocation points need to be clustered near the wall, where the largest velocity variations occur; they are assigned in the present analysis by

$$Z_J = 2\sin\frac{(J-1)\pi}{2(m-2)} - 1\ , \qquad J = 1, 2, \cdots, m-1, \tag{4.23}$$

when only the upper plate oscillates, and

$$Z_J = \sin\frac{(2J-m)\pi}{2(m-2)}\ , \qquad J = 1, 2, \cdots, m-1, \tag{4.24}$$

when the two plates oscillate in antiphase; since, the penetration depth ($\delta_p = \sqrt{2\nu/\omega}$), regarded as a kind of viscous wavelength, is small relative to the space between the two walls. For this case, the oscillatory Reynolds number, $Re_s = (\omega H^2)/\nu$, which is proportional to the square of the ratio of the annular gap to the penertation depth, is a principal characteristic parameter, as shown in the nondimensional governing equations.

The radial variations of the amplitude and the phase angle are presented in Figures 4.3(a,b) for viscous flow between two plates for the following cases; (a) the upper plate oscillates with $Re_s = 8.37$ and (b) both plates oscillate with $Re_s = 52.3$. In the latter case, the variation of $\mid \hat{u}(Z) \mid$ and $\varphi(Z)$ are shown only for $Z \geq 0$, the flow being antisymmetric with respect to the plane $Z = 0$

As expected, the numerical solutions converge to the analytical ones as the number of the collocation points is increased. It was found that very good accuracy has already been achieved for $m = 10$ in case (a) and $m = 20$ in case (b). For the plates oscillating in antiphase, more collocation points ($m = 20$) are required for good accuracy,

since the nondimensional penetration depth of the viscous wave (nondimensionalized with respect to the distance between plates and defined by $2\pi\sqrt{2/Re_s}$) is 2.5 times smaller than in the case (a).

4.2.2 Unsteady Rotational Motion between Two Concentric Cylinders

The unsteady viscous flow between two concentric cylinders is generated by the harmonic rotational motion $w^*(r,t) = W_o\, e^{\iota\omega t}$ of one cylinder while the other is fixed. On the basis of the considerations discussed in Section 4.1.2 and shown in Appendix C for concentric configurations, the Navier-Stokes equations reduce to

$$\frac{d^2w^*}{dr^2} + \frac{d}{dr}\left(\frac{w^*}{r}\right) - \frac{1}{\nu}\frac{dw^*}{dt} = 0\,, \tag{4.25}$$

where the unsteady flow velocity can be expressed in an expansion form as

$$w^*(r,t) = W(r)\, e^{\iota\omega t} = W_o \sum_{j=0}^{m} [\,\Re(W_j) + \iota\,\Im(W_j)]\, T_j(Z)\, e^{\iota\omega t}\,, \tag{4.26}$$

where T_j denotes Chebyshev polynominals.

Taking account of the coordinate transformation, given in Chapter 3 for cylindrical coordinates, to get the solution in the computational domain, the governing equation is expressed in terms of the nondimensional complex amplitude of velocity, $\hat{w} = W/W_o$, as

$$\frac{d^2\hat{w}}{dZ^2} - \sqrt{D}\frac{d\hat{w}}{dZ} + D\hat{w} - \iota\frac{Re_s}{4}\hat{w} = 0\,, \tag{4.27}$$

where Re_s denotes the oscillatory Reynolds number defined as $Re_s = \omega H^2/\nu$, and Z is the nondimensional parameter as $Z = 1 - 2(r-a)/H$. Based on the no-slip condition at the wall, the boundary conditions can be expressed in nondimensional form as

$$\hat{w}\,|_{Z=1} = 1 - \delta\,,$$

$$\hat{w}\,|_{Z=-1} = \delta\,,$$

where $\delta = 0$ when the inner cylinder oscillates and $\delta = 1$ when the outer one oscillates.

The unknown complex coefficients, W_j, are obtained by solving the algebraic system of equations, obtained from the governing equation and the boundary conditions, defined by

$$\sum_{j=0}^{m}[\,\Re(W_j)+\iota\,\Im(W_j)]\left\{T_j''(Z)-\sqrt{D}T_j'(Z)+\left(D-\iota\frac{Re_s}{4}\right)T_j(Z)\right\}=0 \qquad (4.28)$$

which is to be rigorously satisfied at $(m-1)$ collocation points, and

$$\sum_{j=0}^{m}[\,\Re(W_j)+\iota\,\Im(W_j)]\,T_j(1)=1-\delta\,,$$

$$\sum_{j=0}^{m}[\,\Re(W_j)+\iota\,\Im(W_j)]\,T_j(-1)=\delta\,. \qquad (4.29)$$

With the same procedure shown in the previous section for unsteady flow velocity between two plates, the solutions of the unknown complex coefficients, W_j, can be obtained.

In Figures 4.4 and 4.5, the distribution of amplitude and phase angle are presented when (a) the inner cylinder oscillates and (b) the outer cylinder oscillates. The present results have been obtained for various values of the ratio $a/b = 0.98$, 0.8 and 0.4 with constant $Re_s = 33.5$ in Figure 4.4 and of the oscillatory Reynolds number $Re_s = 33.5\,(a/b = 0.8)$, $75.4\,(a/b = 0.7)$ and $134.1\,(a/b = 0.6)$ with constant $b = 0.1$ m in Figure 4.5. The analytical solutions, derived for infinitesimally small clearance $H \simeq 0$ in Appendix C, are presented here for $Re_s = 33.5$ for comparison with the present numerical results.

Considering the results, it is noted that the nondimensional amplitude and the phase angle are strongly affected by the oscillatory Reynolds number, Re_s; however they are almost independent on the ratio a/b for a constant Re_s. By increasing the oscillatory Reynolds number, the viscous wavelength, which is related to the phase angle , becomes smaller. In Figure 4.4, good agreement in the velocity profiles is shown with the analytical results for $a/b = 0.98$ and $Re_s = 33.5$ with $m = 20$ and the analytical results. In case of $a/b \simeq 1$, the results tend to converge to those for unsteady viscous flow between two parallel plates.

4.3 REMARKS

The spectral collocation method developed in Chapter 3 has been presented here for the study of steady and unsteady flows and for the validation of the method. Utilizing suitable expansions, involving Chebyshev polynomials, Fourier series and exponential functions for fluid-dynamic parameters, the *a priori* unknown coefficients in these expansions are determined from the governing equations and boundary conditions, which are rigorously satisfied at conveniently chosen collocation points.

This method has been applied to several typical problems for which analytical solutions exist. Excellent agreement has been found, in all the flow problems considered, between the spectral solutions and the exact analytical ones. One can conclude that the present numerical method has been validated by these comparisons.

In subsequent chapters, this method will be applied to the analysis of unsteady eccentric annular flows generated by an oscillating rigid cylinder with confidence, as well as to the study of flexural motions of a cylinder subjected to axial flow in a narrow annular flow.

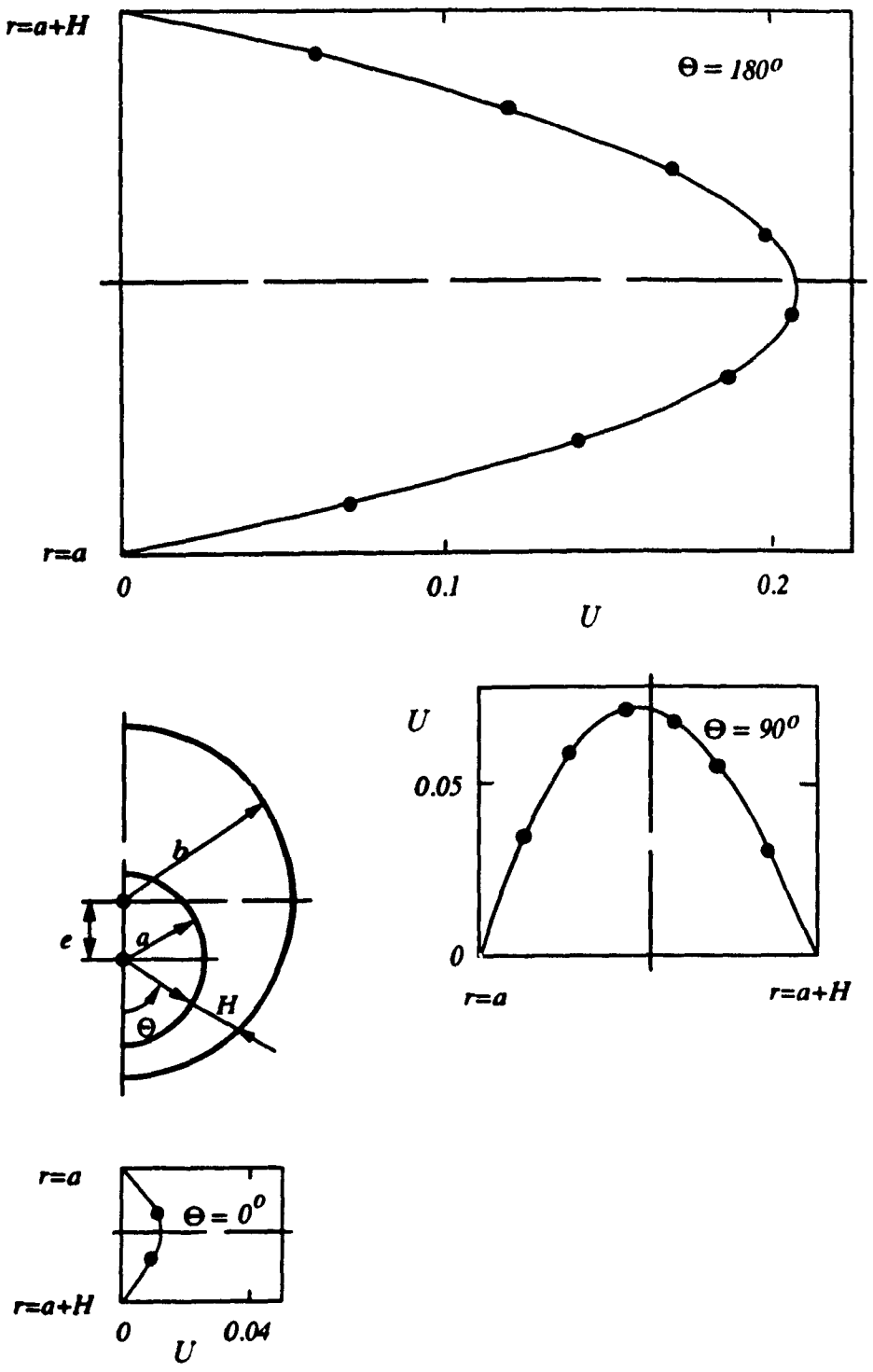

Figure 4.1: Comparison of the present spectral method with the analytical solution for the steady axial laminar flow between two eccentric cylinders (for $b/a = 2$, $e/a = 0.6$ and $Q = -0.17$ m/s), in terms of the radial variation of the axial velocity, U m/s, at various azimuthal planes ($\Theta = 0°$, $90°$, and $180°$). •, present solution; —, Snyder & Goldstein's analytical solution.

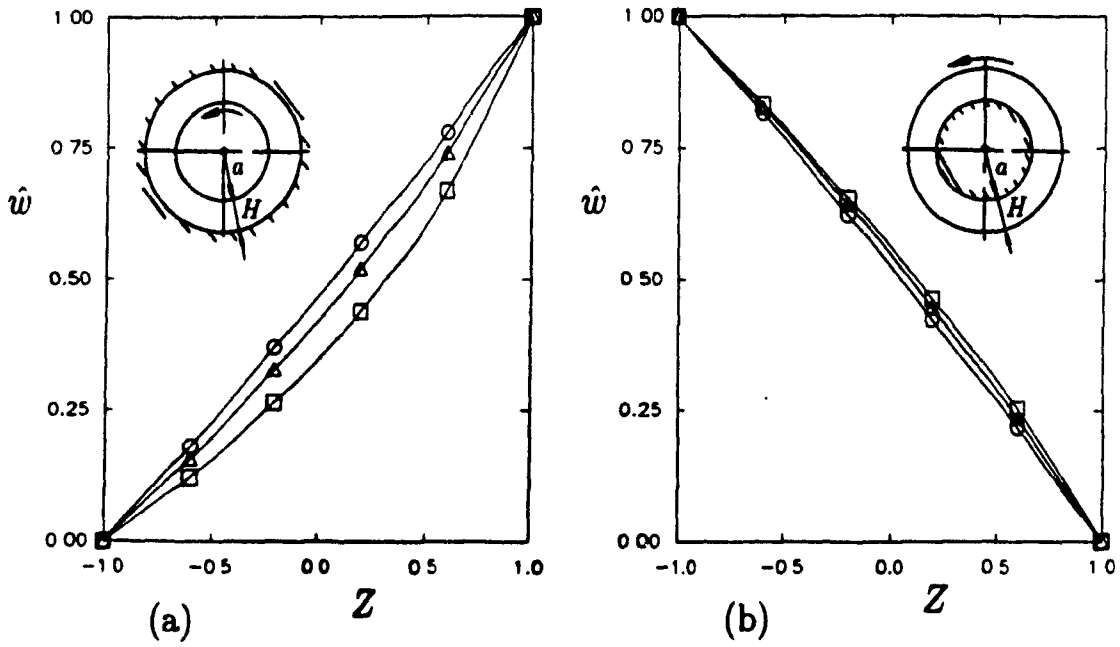

Figure 4.2: Comparison of the present spectral method with the analytical solution for the viscous flow between two concentric cylinders, one of which is steady rotation, in terms of the radial variation of the nondimensional velocoty $\hat{w}(Z)$: (a) with the inner cylinder rotating, $\delta = 0$, and (b) with the outer cylinder rotating, $\delta = 1$. Present solutions calculated for various values of the ratio of the radii: □, $a/b = 0.4$; △, $a/b = 0.6$ and o, $a/b = 0.8$; —, analytical solution.

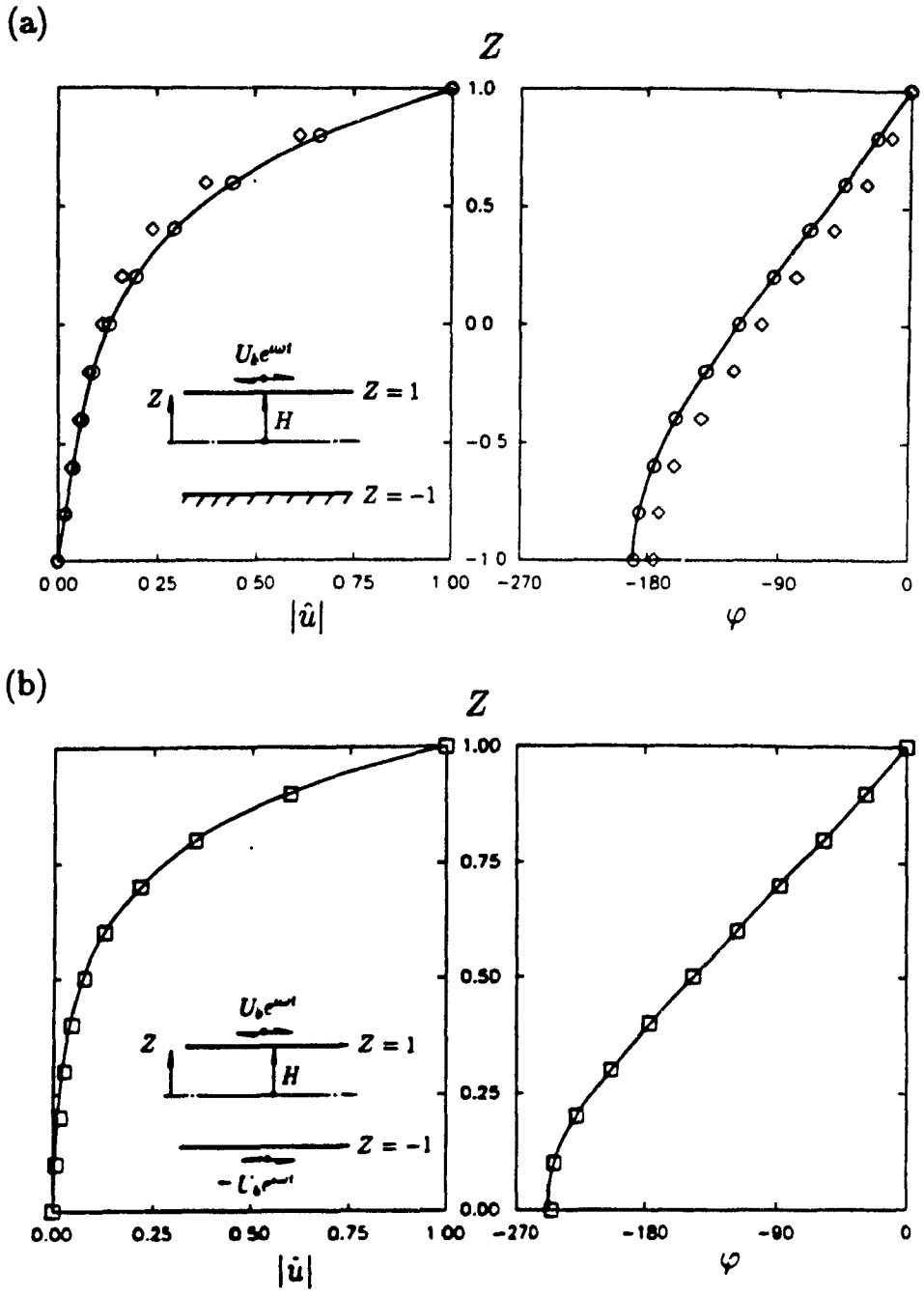

Figure 4.3: Comparison of the present spectral method with the analytical solution for the unsteady viscous motion between two oscillating parallel plates, in terms of nondimensional fluid velocity amplitude $| \hat{u}(Z) |$ and phase φ, with respect to the upper plate oscillation: (a) the lower is fixed, $\delta = 0$; (b) the lower plate oscillates in antiphase, $\delta = 1$. ◇, ○, □, present solutions calculated with $m = 5$, 10 and 20, respectively; ——, analytical solution.

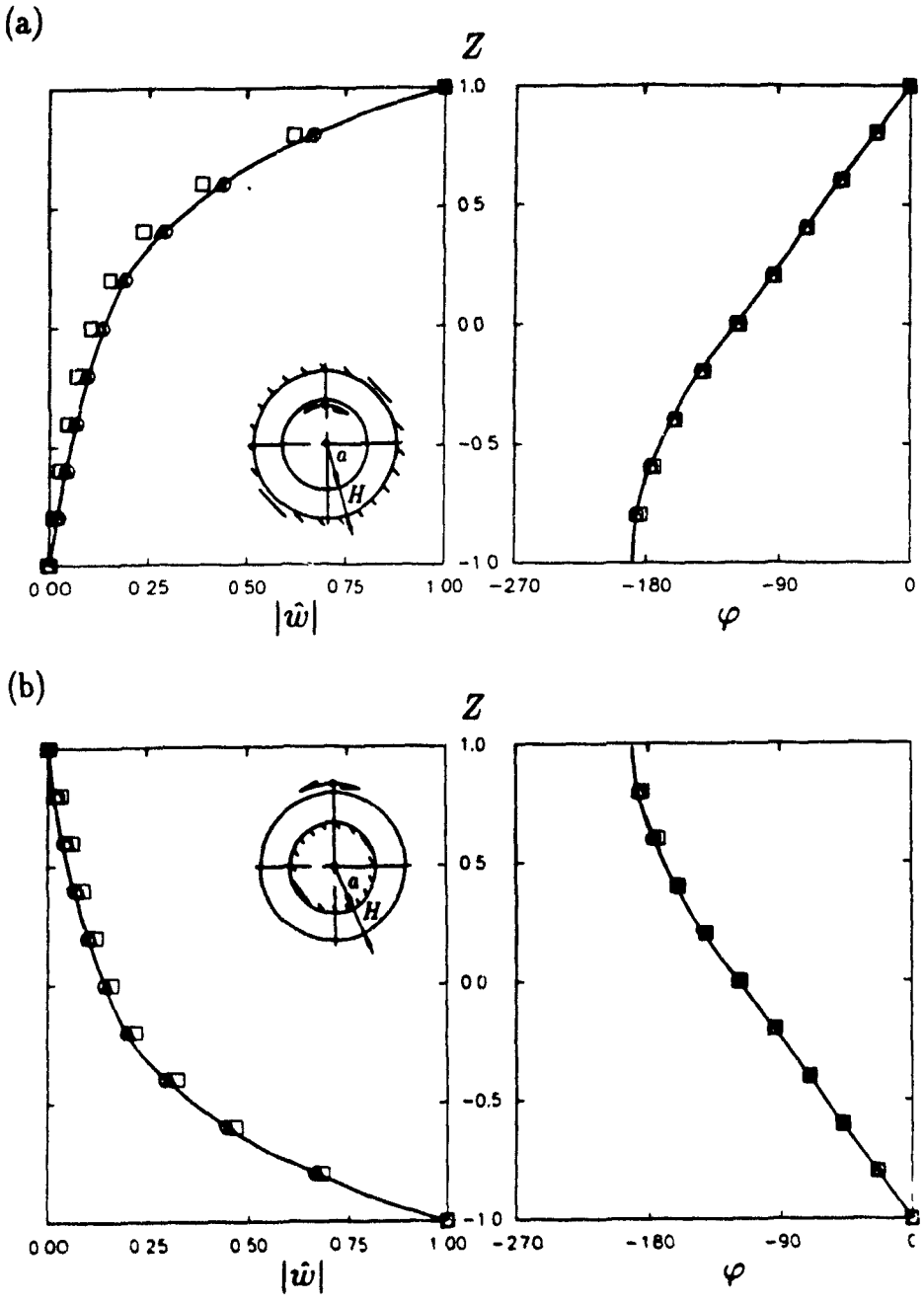

Figure 4.4: Comparison of the present spectral method with the analytical solution for the unsteady viscous motion between two concentric cylinders, when the inner cylinder oscillates, in terms of the radial variation of the nondimensional velocity amplitude, $| \hat{w}(Z) |$ and phase φ, for an oscillatory Reynolds number $Re_s = 33.5$: (a) with the inner cylinder oscillating, $\delta = 0$; (b) with the outer cylinder oscillating, $\delta = 1$. Present solutions calculated (a) for various values of the radii: o, $a/b = 0.98$; Δ, $a/b = 0.8$; $\square$, $a/b = 0.4$;—, analytical solution for $H \simeq 0$.

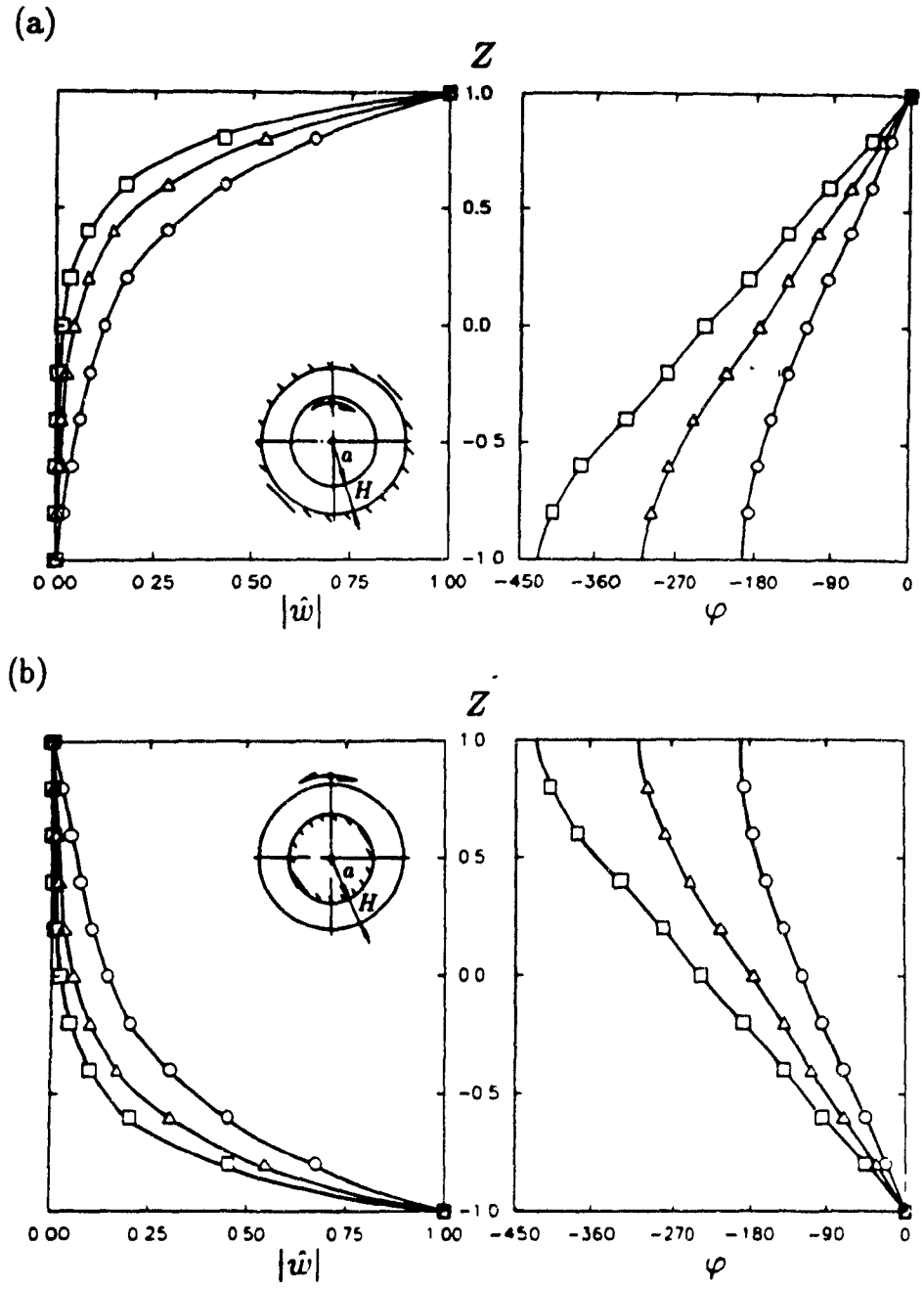

Figure 4.5: Influence of the oscillatory Reynolds number $Re_s = \omega H^2/\nu$, on the nondimensional velocity amplitude, $\mid \hat{w}(Z) \mid$, and phase, φ, calculated with the present spectral method for constant outer radius $b = 0.1$ m: (a) case of oscillating inner cylinder, $\delta = 0$, and (b) case of oscillating outer cylinder, $\delta = 1$. —o—, $Re_s = 33.5$ and $a/b = 0.8$; —△—, $Re_s = 75.4$ and $a/b = 0.7$; —□—, $Re_s = 134.1$ and $a/b = 0.6$.

Chapter 5

Study of Two-dimensional Unsteady Annular Flows

The unsteady fluid motion generated by the harmonic motion of a cylinder in an annular passage has an important effect on the hydrodynamic forces acting on it. To determine the hydrodynamic forces, it is necessary to obtain first the unsteady pressure distribution and skin friction generated by the vibrating cylinder in the annulus. In general, this is a three-dimensional problem; however, the three-dimensional effect is small when the radius of the cylinder is small compared to its length. In this case, a two-dimensional formulation can provide a good approximation.

In flow-induced vibration studies, it is of interest to evaluate the added mass and viscous damping coefficients, which are dependent on fluid properties as well as geometry. In predicting the stability of a system in a confined fluid, the added mass and damping are important considerations, as shown in Chapter 2. The spectral method has first been applied to the unsteady potential flow and then to the unsteady viscous flow, generated by periodic translational motion of a cylinder in an eccentric annulus.

The final aim of this chapter is to provide the formulae and the results for added mass and fluid damping when a cylinder undergoes oscillatory motion in the plane of symmetry and normal to the plane of the symmetry in an eccentric annulus. The potential theory has been developed to obtain the added mass for incompressible, inviscid and irrotational fluid. For the viscous fluid, the added mass, in phase with the acceleration of the moving cylinder, and the viscous damping, in phase with the

its velocity, are presented.

When a cylinder, immersed in viscous fluid, has oscillatory motion in an annluar space, the viscous damping effect becomes important with decerasing annular space, even though the viscosity of the fluid may be relatively small, as discussed in Chapter 1. However, the added mass can be estimated rather easily for a narrow annulus by potential-flow theory. In the present study, the viscous effect on the added mass can be evaluated by comparing the results obtained by potential-flow theory with those obtained by viscous-flow theory, and viscous damping is investigated.

The results obtained by the potential-flow theory will also be used to validate the present spectral method against the avaible analytical solutions of Chung and Chen [9] for eccentric configurations and of Fritz [7] for concentric configurations. To have meaningful comparisons with the available solutions, the same considerations are used to solve this unsteady problem with the spectral collocation method. In the present analysis, the problem is formulated based on the following assumptions: (a) the flow is two dimensional with no axial-flow velocity and (b) the amplitude of the oscillatory motion of the cylinder is small.

5.1 UNSTEADY POTENTIAL FLOW

By definition, the penetration depth, $\delta_p = \sqrt{2\nu/\omega}$, is very small when the viscosity of fluid, ν, is very small or the circular frequency of the motion of the cylinder, ω, is very large. In this case, the fluid flow can be assumed to be irrotational and inviscid.

The velocity potential associated with the motion of the inner or outer cylinder can be solved in the computational domain by the spectral collocation method through a coordinate transformation. Using the present numerical method, the self-added mass of the moving cylinder and the mutual-added mass of the fixed cylinder are obtained by integrating the unsteady pressure around the circumference for various eccentricities.

5.1.1 Formulation of the Basic Equations

Let us consider an infinitely long cylinder undergoing a periodic translational motion in an annular space, which is filled with incompressible and inviscid fluid, as shown in Figure 3.1. In the unsteady potential-flow problem, the continuity equation reduces to the Laplace equation in terms of the unsteady velocity potential $\phi(x_1, x_2, x_3, t)$ given in equation (2.3). In cylindrical coordinates, r and Θ, the governing equation when there is no axial flow can be expressed as

$$\frac{\partial^2\phi}{\partial r^2} + \frac{1}{r}\frac{\partial\phi}{\partial r} + \frac{1}{r^2}\frac{\partial^2\phi}{\partial\Theta^2} = 0\,. \tag{5.1}$$

Considering equations (3.6) and (3.9), the Laplace equation, after transformation into the computational domain (Z,θ), becomes

$$A\,\frac{\partial^2\phi}{\partial Z^2} + B\,\frac{\partial\phi}{\partial Z} + C\,\frac{\partial^2\phi}{\partial Z\partial\theta} + D\,\frac{\partial^2\phi}{\partial\theta^2} = 0\,, \tag{5.2}$$

where A, B, C, and D are functions of $Z = 1 - 2(r-a)/H$ and $h(\theta)$, as defined in equation (4.5).

Assuming the frequency of the periodic motion of translation has circular frequency ω, the unsteady velocity potential $\phi(Z,\theta,t)$ is expressed by a set of expansions in terms of Chebyshev polynomials, $T_j(Z)$, and Fourier series functions, $F_k(\theta)$:

$$\phi(Z,\theta,t) = \iota\,\omega\,\epsilon\,a^2\,e^{\iota\omega t}\sum_{j=0}^{m}\sum_{k=0}^{n}\Phi_{jk}\,T_j(Z)\,F_k(\theta)\,, \tag{5.3}$$

where $a\epsilon e^{\iota\omega t}$ denotes the displacement of the oscillating cylinder, ϵ being a nondimensional amplitude.

With this spectral expansion, equation (5.2) can be rewritten in terms of the selected interpolation functions as

$$\sum_{j=0}^{m}\sum_{k=0}^{n}\Phi_{jk}\left[A\,T_j''(Z)\,F_k(\theta) + B\,T_j'(Z)\,F_k(\theta) + C\,T_j'(Z)\,F_k'(\theta) + D\,T_j(Z)\,F_k''(\theta)\right] = 0\,, \tag{5.4}$$

where the prime symbols denote differentiations with respect to Z for the Chebyshev polynomials and with respect to θ for Fourier series functions.

In order to formulate the problem completely, the boundary conditions on the moving and fixed cylinders are added to the above governing equation. As shown in equation (2.2) for unsteady potential flow, the normal flow velocities at the boundary surfaces are equal to those of the moving and the fixed cylinders. Because of the eccentricity, the normal-flow velocity can be decomposed into radial and the circumferential components, v^* and w^*, in terms of the unsteady velocity potential, as

$$\begin{aligned} v^* &= \frac{\partial \phi}{\partial r} = -\frac{2}{ah}\frac{\partial \phi}{\partial Z} = -\frac{2a}{h}\,\iota\,\omega\,\epsilon\,e^{\iota\omega t}\sum_{j=0}^{m}\sum_{k=0}^{n}\Phi_{jk}\,T_j'(Z)\,F_k(\theta)\,, \\ w^* &= \frac{1}{r}\frac{\partial \phi}{\partial \Theta} = 2\frac{\sqrt{D}}{ah}\left[\frac{\partial \phi}{\partial \theta} + (1-Z)\frac{h'(\theta)}{h(\theta)}\frac{\partial \phi}{\partial Z}\right] \\ &= \sqrt{D}\,\frac{2a}{h}\,\iota\,\omega\,\epsilon\,e^{\iota\omega t}\sum_{j=0}^{m}\sum_{k=0}^{n}\Phi_{jk}\left[T_j(Z)\,F_k'(\theta) + (1-Z)\frac{h'(\theta)}{h(\theta)}\,T_j'(Z)\,F_k(\theta)\right]. \end{aligned} \tag{5.5}$$

In the present analysis for eccentric configurations, the boundary conditions are more complicated than those for concentric configurations. Let us consider oscillatory motion; (a) in the plane of the symmetry and (b) normal to the plane of the symmetry, $\Theta = 0$. For both cases, the inner or outer cylinders execute the oscillatory motion, identified by e_O or g_I, where e and g stand for case (a) and (b), respectively. The subscripts O and I represent the inner and the outer cylinder, respectively; for example, e_O denotes the oscillatory displacement of the outer cylinder in the plane of symmetry.

(a) Oscillatory motions in the plane of symmetry, $\Theta = 0$.

Let us consider small oscillatory motion of the outer cylinder executing oscillatory translation in the plane of symmetry $\Theta = 0$, containing the axes of the two cylinders. While the inner cylinder is fixed, the outer cylinder is oscillating with lateral displacement, $e_O(t)$, which may be expressed as

$$e_O(t) = a\,\dot{e}\,e^{\iota\omega t}\,. \tag{5.6}$$

The boundary conditions on the fixed and moving cylinders can be expressed as

$$\begin{aligned} &[v^*(r,\Theta)]_{r=a} = 0\,, \\ &[v^*(r,\Theta)\cos(\Theta-\Theta_o) - w^*(r,\Theta)\sin(\Theta-\Theta_o)]_{r=b} = \frac{de_O}{dt}\cos\Theta_o\,, \end{aligned} \tag{5.7}$$

where

$$\cos\Theta_o = [1 + h(\Theta)]\ \frac{a}{b}\ \cos\Theta + \frac{e}{b}\,,$$

see Figure 3.1.

Using equation (5.5), these boundary conditions can be expanded as follows:

$$\sum_{j=0}^{m}\sum_{k=0}^{n} \Phi_{jk}\, T_j'(1)\, F_k(\theta) = 0\,,$$

$$\sum_{j=0}^{m}\sum_{k=0}^{n} \Phi_{jk}\, \left[A_0\, T_j'(-1)\, F_k(\theta) + B_0\, T_j(-1)\, F_k'(\theta)\right] = \cos\Theta_o\,, \tag{5.8}$$

where

$$A_0 = -\frac{2}{h(\theta)}\ \cos(\Theta - \Theta_o) + 2B_0\, h'(\theta)/h(\theta)\,, \qquad B_0 = -\frac{1}{1 + h(\theta)}\ \sin(\Theta - \Theta_o)\,.$$

When the inner cylinder executes an oscillatory translation in the plane of symmetry $\Theta = 0$ while the outer cylinder is fixed, the displacement on the moving cylinder can be written as

$$e_I(t) = a\ \hat{e}\ e^{\omega t}\,, \tag{5.9}$$

and the corresponding boundary conditions in this case are

$$-\frac{2}{h(\theta)}\sum_{j=0}^{m}\sum_{k=0}^{n} \Phi_{jk}\, T_j'(1)\, F_k(\theta) = \cos\theta\,,$$

$$\sum_{j=0}^{m}\sum_{k=0}^{n} \Phi_{jk}\, \left[A_0\, T_j'(-1)\, F_k(\theta) + B_0\, T_j(-1)\, F_k'(\theta)\right] = 0\,. \tag{5.10}$$

It is obvious that in both cases when the translational motion takes place in the plane of symmetry, the unsteady flow in the eccentric annular space is symmetric with respect to $\Theta = 0$. Hence, $F_k(\theta)$, which will be used in the expansion form of the governing equation (5.1) for the velocity potential, may be defined by

$$F_k(\theta) = \cos k\theta\,. \tag{5.11}$$

The collocation method can be applied now, as described in Chapter 4 for the steady viscous flow between eccentric cylinders, to equations (5.4) and (5.8) or (5.10), which will reduce these differential equations to an algebraic system of $(n+1)\times(m+1)$

equations. The solution for the coefficients Φ_{jk} of the velocity potential in expanded form can then be obtained by the Gauss-Seidel iteration method based on pivot points.

(b) Oscillatory motions normal to the plane of symmetry, $\Theta = 0$.

If the inner cylinder is fixed and the outer cylinder executes the translational motion perpendicular to the plane of symmetry, $\Theta = 0$, with displacement

$$g_0(t) = a\,\hat{g}\,e^{\iota\omega t}\,, \tag{5.12}$$

the boundary conditions on the fixed inner cylinder and on the moving outer cylinder can be expressed as

$$\sum_{j=0}^{m}\sum_{k=0}^{n}\Phi_{jk}\,T_j'(1)\,F_k(\theta) = 0\,,$$

$$\sum_{j=0}^{m}\sum_{k=0}^{n}\Phi_{jk}\left[A_0\,T_j'(-1)\,F_k(\theta) + B_0\,T_j(-1)\,F_k'(\theta)\right] = \sin\Theta_o\,, \tag{5.13}$$

where A_0 and B_0 have the same expressions given in equation (5.8).

Similarly, when the outer cylinder is fixed and the inner cylinder axis has an oscillatory displacement

$$g_I(t) = a\,\hat{g}\,e^{\iota\omega t}\,, \tag{5.14}$$

the boundary condition on the fixed outer cylinder is given by equation (5.10), while that on the moving inner cylinder can be expressed as

$$-\frac{2}{h(\theta)}\sum_{j=0}^{m}\sum_{k=0}^{n}\Phi_{jk}\,T_j'(1)\,F_k(\theta) = \sin\theta\,. \tag{5.15}$$

In both cases, when the translational motion is normal to the plane $\Theta = 0$, the unsteady flow in the eccentric annular space can be considered (when the oscillation amplitude is small) to be antisymmetric with respect to $\Theta = 0$; hence, in such cases the Fourier functions $F_k(\theta)$ used in the velocity-potential expansion (5.3) can be defined as

$$F_k(\theta) = \sin k\theta\,. \tag{5.16}$$

The governing equation (5.4) together with the boundary conditions will also be reduced to an algebraic system of $(n+1)\times(m+1)$ equations, leading to the solutions for the coefficients Φ_{jk} of the velocity potential expansion.

5.1.2 Unsteady Pressure Distribution and Resultant Pressure Force

With the coefficients Φ_{jk} determined from the solution of the equations, the entire flow field in the eccentric annular space is completely determined. Considering the governing equations and the boundary conditions in expanded forms, which are linearized with respect to the amplitude of the displacement of oscillatory motion (based on the small amplitude of motion assumption), it is obvious that the solution of the velocity potential Φ_{jk} is independent on the amplitude of oscillatory motion; however, the fluid parameters are linearly dependent on the amplitude of translational motion.

The unsteady pressure may be calculated now in the annular space by the Bernoulli-Lagrange equation (2.5),

$$P - P_\infty = -\rho \left[\frac{\partial \phi}{\partial t} + \frac{1}{2} \left(\frac{\partial \phi}{\partial r} \right)^2 + \frac{1}{2} \left(\frac{1}{r} \frac{\partial \phi}{\partial \Theta} \right)^2 \right] , \tag{5.17}$$

where P_∞ denotes the stagnation pressure in the fluid (existing in the absence of any oscillatory motion). Assuming small-amplitude oscillations, so as to have a meaningful comparison with Chung and Chen's (1976) results, the second and third terms of the right-hand side in the above equation can be neglected and the unsteady pressure can be expressed in simple-harmonic-oscillation form,

$$P - P_\infty = \rho \, \omega^2 a^2 \, \hat{p}(Z, \theta) \, \epsilon \, e^{\iota \omega t} , \tag{5.18}$$

where $\hat{p}(Z, \theta)$ is a nondimensional reduced pressure defined by

$$\hat{p}\,(Z, \theta) = \sum_{j=0}^{m} \sum_{k=0}^{n} \Phi_{jk} \, T_j(Z) \, F_k(\theta) , \tag{5.19}$$

and where $\epsilon = \hat{e}$ or $\hat{g}$, respectively, for oscillation in the plane of symmetry or normal to it. The circumferential variation of the nondimensional reduced pressure $\hat{p}(1, \theta)$ on the oscillatory inner cylinder ($Z = 1$), when its axis oscillates in the plane of symmetry, or normal to it, can be calculated for various relative eccentricities.

The resultant unsteady force, acting on the moving or fixed cylinder, in the direction of oscillatory motion can be obtained by integrating the unsteady pressure along

the circumference of the cylinder. The unsteady force normal to the motion equals zero: since, the pressure distribution around the circumference of cylinder is symmetric with respect to the plane of the motion for oscillation in the plane of symmetry; for the other case, the pressure distribution includes the antisymmetric components, but its integrated effect is zero. The resultant unsteady force acting on the inner cylinder in the direction of the motion per unit length, for oscillation in the plane of symmetry, is given by

$$F_I(t) = -\int_0^{2\pi} a\, p(1,\Theta)\, \cos\Theta\, d\Theta\,, \tag{5.20}$$

and, for oscillation normal to the plane of symmetry, it is given by

$$G_I(t) = -\int_0^{2\pi} a\, p(1,\Theta)\, \sin\Theta\, d\Theta\,, \tag{5.21}$$

where the subscript I stands for the inner cylinder.

Similarly, the resultant unsteady force per unit length acting on the outer cylinder, when the inner or outer cylinder oscillates in the plane of symmetry or normal to the plane of symmetry, is given, respectively, by

$$F_O(t) = \int_0^{2\pi} b\, p(-1,\Theta)\, \cos\Theta_o\, d\Theta_o\,,$$

and

$$G_O(t) = \int_0^{2\pi} b\, p(-1,\Theta)\, \sin\Theta_o\, d\Theta_o\,, \tag{5.22}$$

where the subscript O stands for the outer cylinder.

These integrals can be calculated in the computational domain $(Z, \theta = \Theta)$, taking account of equation (5.7) with the aid of Figure 3.1, by the following relationship:

$$\cos\Theta_o d\Theta_o = \frac{a}{b}[1 + h(\theta)]\cos\theta d\theta + \frac{a}{b}h'(\theta)\sin\theta d\theta = \frac{a}{b}\sum_k C_k \cos k\theta d\theta\,,$$

$$\sin\Theta_o d\Theta_o = \frac{a}{b}\,[1 + h(\theta)]\sin\theta d\theta\, + \frac{a}{b}\,h'(\theta)\cos\theta d\theta = \frac{a}{b}\sum_k S_k \sin k\theta d\theta\,, \tag{5.23}$$

since $h(\theta)$ and $h'(\theta)$ are even and odd functions of the Fourier expansion, respectively.

In general, the hydrodynamic forces, acting on cylinder i in the direction of the motion, due to the translational motion of cylinder j are expressed in terms of added-

mass coefficients, α_{ij} for motions in the plane of symmetry and β_{ij} for motions normal to the plane of symmetry:

$$F_i = -\rho\pi\left(\frac{r_i^2+r_j^2}{2}\right)\alpha_{ij}\frac{\partial^2 e_j}{\partial t^2}\,,$$
$$G_i = -\rho\pi\left(\frac{r_i^2+r_j^2}{2}\right)\beta_{ij}\frac{\partial^2 g_j}{\partial t^2}\,, \qquad (5.24)$$

where r_i and r_j denote the radii of cylinders, i and j. For example, α_{IO} and β_{OI} denote the mutual-added-mass coefficients for the force acting on the inner cylinder due to the outer-cylinder oscillation in the plane of the symmetry and for the force acting on the outer cylinder due to the inner-cylinder oscillation normal to the symmetry, respectively, where the subscripts I stands for the inner and O for outer cylinder. Hence, *e.g.*, the fluid-dynamic force acting on the inner cylinder due to its motion in the plane of symmetry can be calculated by considering the self-added-mass coefficients α_{II}.

Substituting equation (5.18) into equations (5.20) and (5.21), the added-mass coefficients for the resultant forces acting on the inner cylinder can be obtained

$$\alpha_{II} = -\sum_{j=0}^{m}\Phi_{j1}T_j(1)\,, \qquad \alpha_{IO} = \frac{-2a^2}{a^2+b^2}\sum_{j=0}^{m}\Phi_{j1}T_j(1)\,,$$
$$\beta_{II} = -\sum_{j=0}^{m}\Phi_{j1}T_j(1)\,, \qquad \beta_{IO} = \frac{-2a^2}{a^2+b^2}\sum_{j=0}^{m}\Phi_{j1}T_j(1)\,, \qquad (5.25)$$

where Φ_{jk} are obtained from the corresponding algebraic equation for each case.

Similarly, substituting equation (5.18) into (5.22) with the aid of equation (5.23), the added-mass coefficients for the resultant forces acting on the outer cylinder can be expressed as

$$\alpha_{OO} = \frac{a^2}{b^2}\sum_{j=0}^{m}\sum_{k=0}^{n}\Phi_{jk}C_kT_j(-1)\,, \qquad \alpha_{OI} = \frac{2a^2}{a^2+b^2}\sum_{j=0}^{m}\sum_{k=0}^{n}\Phi_{jk}C_kT_j(-1)\,,$$
$$\beta_{OO} = \frac{a^2}{b^2}\sum_{j=0}^{m}\sum_{k=0}^{n}\Phi_{jk}S_kT_j(-1)\,, \qquad \beta_{OI} = \frac{2a^2}{a^2+b^2}\sum_{j=0}^{m}\sum_{k=0}^{n}\Phi_{jk}S_kT_j(-1)\,, \qquad (5.26)$$

where C_k and S_k are defined in equation (5.23).

By inspection of the expansion forms of the velocity potential, which are expressed in terms of even or odd Fourier functions according to the direction of oscillatory motion, the hydrodynamic forces normal to the direction of motion (calculated by circumferential integration involving $\sin\Theta d\Theta$ and $\cos\Theta d\Theta$ instead of $\cos\Theta d\Theta$ and $\sin\Theta d\Theta$ in equations (5.20) and (5.21), respectively) are zero; this is because the even and odd terms of the Fourier-series functions are orthogonal to each other over the domain in the circumferential direction.

5.1.3 Numerical Results for Inviscid Fluid-dynamic Forces

The numerical results for an inviscid fluid are presented to evaluate the fluid-dynamic forces. For this purpose, the unsteady pressure on the surface of the cylinder and the fluid-dynamic force have been expressed in terms of added mass coefficients.

The circumferential variation of the nondimensional reduced pressure $\hat{p}(Z=1,\theta)$ on the inner cylinder ($Z=1$), when the inner cylinder has translational motion (a) in the plane of symmetry or (b) normal to the plane of symmetry, is shown in Figure 5.1 for various relative eccentrities $e/(b-a) = 0,\ 0.4$ and 0.8, and for $b/a = 1.25$. The unsteady pressure distributions are symmetric in case (a) and antisymmetric in case (b) about $\Theta = 0°$, as expected by considering equations (5.11), (5.16) and (5.18). It is of interest to find that the maximum values of $|\,\hat{p}(1,\theta)\,|$, which become larger with the eccentricity, are on the axis of oscillatory motion ($\Theta = 0°$ or 180°) in case (a); and they are near the axis ($\Theta = 90°$) in case (b), but gradually move to the narrow region with increasing eccentricity.

Before discussing the subsequent figures, the terms "self-added" and "mutual-added mass" should be defined. Self-added mass is that associated with the moving component, and mutual-added mass is that associated with another component due to the motion of the first. Thus, for the case of two concentric cylinders, let us consider that the inner one is moving while the outer is stationary; then we talk about the self-added mass on the moving cylinder and the mutual-added mass on the stationary one.

In Figure 5.2, the self-added mass and mutual-added mass coefficients of the inner cylinder oscillating, obtained by the present method for concentric configuration with various ratios b/a ($m = 20$), are compared with Fritz's analytical results [7] which are shown in Appendix E in detail for concentric configurations. In order to check the rate of convergence of the solutions, the number of terms taken in the Chebyshev polynomial expansion was varied; the results are shown in Table 5.1 and are also compared with the Fritz's results. The rate of convergence is faster in the case of the narrower annulus than in the case of the wider one. Also the difference between the numerical results and the analytical results appears to decrease faster with an increasing number of collocation points, m. As a resut, a slight increase in the number of terms m taken in the calculation is found to be needed for larger b/a, in order to obtain the same accuracy. The agreement between the numerical and analytical results is very good.

Table 5.1 Variation of the calculated mass coefficients a_{II} and a_{IO} with the number of collocation points, m, and their relative difference with respect to Fritz's analytical results.

b/a	m	a_{II}	$-a_{IO}$	Comparison with Fritz's analytical results	
				$1 - a_{II}/a_{II_{F_r}}$	$1 - a_{IO}/a_{IO_{F_r}}$
1.25	3	4.3117	4.1457	5.35%	4.39%
	5	4.5549	4.3355	0.01%	0.01%
	7	4.5556	4.3360	0.0001%	0.0001%
2	5	1.6409	1.0564	1.54%	0.96%
	7	1.6654	1.0662	0.07%	0.04%
	9	1.6666	1.0666	0.0001%	0.0001%

The added-mass coefficients, defined in equation (5.24), are calculated with the present spectral-collocation method for various relative eccentricities $e/(b-a)$, and the results are shown in Figures 5.3 and 5.4. To further validate the present method, the results are compared with the analytical results obtained by Chung and Chen (1976) in Figure 5.3 (b). The agreement between the present solution and the solution of Chung and Chen is very good. (For the sake of this comparison, the same assumptions as those made by Chung and Chen were also used in the application of the present

spectral collocation method.)

The variation with the relative eccentricity $e/(b-a)$ of the nondimensional unsteady force coefficients β_{ij} in the case of oscillatory translation normal to the plane of symmetry is shown for $b/a = 2$ in Figure 5.4; one can notice that this variation is almost identical with that of the coefficients α_{ij} in Figure 5.3 (a), although the corresponding resultant unsteady forces act in directions perpendicular to each other. Note that the self-added-mass and mutual-added-mass coefficients of the two cylinders are strongly influenced by eccentricity for narrow annular configurations ($b/a = 1.25$); however, in case $b/a = 2$, the self-added-mass coefficients of the outer cylinders with eccentricity is relatively small while both coefficients of the inner cylinder are still influenced by eccentricity.

5.2 UNSTEADY VISCOUS FLOW

This section presents the numerical analysis for the inner cylinder, which has the translational motion in the plane of symmetry or normal to the plane of symmetry in a confined viscous fluid. A system of discretized equations is obtained from the appropriate Navier-Stokes and continuity equations and the boundary conditions through the spectral collocation method. As shown in Chapter 2, the nonlinearity in the Naver-Stokes equations can be disregarded for small-amplitude motions of the cylinder.

Although for many engineering applications, the viscosity is small and the fluid may be considered inviscid as a first approximation, near the surface of the cylinder there exists a thin layer of rotational flow, as mentioned before. This flow region, where the viscous effect is significant, is of great concern to the dynamic response of the system for annular configurations. In paticular, when the annular gap is small, the viscous effect becomes pronounced.

The hydrodynamic forces acting on the inner cylinder, due to the oscillatory motion of the inner cylinder, will be obtained through line integration of stresses and pressures around the circumference of the cylinder. In general for this problem, the resultant hydrodynamic forces have simple harmonic forms, based on the assumption

of small-amplitude oscillations, and are decomposed into two parts, one in phase with the acceleration and the other with the velocity of the motion. Thus, they can be expressed in terms of added-mass and damping coefficients, which will be obtained by considering the definitions shown in equation (2.23).

5.2.1 Formulation of the Basic Equations

We consider the inner cylinder of the system, surrounded by viscous incompressible fluid, and undergoing periodic translational motion in an eccentric annulus. The motion of the inner cylinder is assumed to be simple harmonic with circular frequency, ω, and its amplitude small. For this kind of two-dimensional problem without steady axial flow, it is possible to eliminate the convective terms and the axial-component terms from the governing equations, shown in equation (2.16) for unsteady fluid flow. The linearized Naver-Stokes equations and the continuity equation in cylindrical coordinates can be reduced to

$$\begin{aligned}
\frac{\partial w^*}{\partial t} + \frac{1}{\rho}\frac{1}{r}\frac{\partial p^*}{\partial \Theta} &= \nu\left[\frac{1}{r}\frac{\partial}{\partial r}\left(r\frac{\partial w^*}{\partial r}\right) + \frac{1}{r^2}\frac{\partial^2 w^*}{\partial \Theta^2} - \frac{w^*}{r^2} + \frac{2}{r^2}\frac{\partial v^*}{\partial \Theta}\right], \\
\frac{\partial v^*}{\partial t} + \frac{1}{\rho}\frac{\partial p^*}{\partial r} &= \nu\left[\frac{1}{r}\frac{\partial}{\partial r}\left(r\frac{\partial v^*}{\partial r}\right) + \frac{1}{r^2}\frac{\partial^2 v^*}{\partial \Theta^2} - \frac{v^*}{r^2} - \frac{2}{r^2}\frac{\partial w^*}{\partial \Theta}\right], \qquad (5.27)
\end{aligned}$$

$$\frac{\partial w^*}{\partial \Theta} + \frac{\partial}{\partial r}(rv^*) = 0\,, \qquad (5.28)$$

where v^* and w^* denote the unsteady flow velocities in the radial and circumferential directions, respectively.

Based on the no-slip condition at the interface between fluid and cylinder, the boundary conditions on the fixed ($r = b$) and moving ($r = a$) cylinders can be expressed, in cases of oscillatory motion (a) in the plane of symmetry and (b) normal to the plane of symmetry, as

$$v^*(b,\Theta) = w^*(b,\Theta) = 0\,,$$

$$\begin{aligned}
v^*(a,\Theta) &= e_r\cos\Theta = \frac{e_I}{\partial t}\cos\Theta\,, \\
w^*(a,\Theta) &= -e_r\sin\Theta = -\frac{e_I}{\partial t}\sin\Theta\,, \qquad \text{in case (a),}
\end{aligned}$$

$$v^*(a,\Theta) = g_v \sin\Theta = \frac{g_I}{\partial t}\sin\Theta\,,$$
$$w^*(a,\Theta) = g_v \cos\Theta = \frac{g_I}{\partial t}\cos\Theta\,, \qquad \text{in case (b)}, \tag{5.29}$$

where e_v and g_v represent the lateral velocity of the vibrating inner cylinder in cases (a) and (b), respectively, and e_I and g_I denote the corresponding displacement of the moving cylinder.

In order to generalize the present problem, it is convenient to define the following nondimensional parameters

$$\hat{v} = \frac{v^*}{\iota a\omega\epsilon e^{\iota\omega t}}\,, \qquad \hat{w} = \frac{w^*}{\iota a\omega\epsilon e^{\iota\omega t}}\,, \qquad \hat{p} = \frac{p^*}{\rho a^2\omega^2\epsilon e^{\iota\omega t}}\,, \qquad h = \frac{H}{a}\,,$$
$$\hat{e} = \frac{e_v}{\iota a\omega e^{\iota\omega t}}\,, \qquad \hat{g} = \frac{g_v}{\iota a\omega e^{\iota\omega t}}\,, \qquad Re_s = \frac{\omega a^2}{\nu}\,, \tag{5.30}$$

where $\hat{e}$ and $\hat{g}$ denote the nondimensional amplitudes [equations (5.9) and (5.14)], of the displacement of the oscillating inner cylinder, and $\epsilon = \hat{f}$ when the inner cylinder has oscillatory motion in the plane of symmetry, or $\epsilon = \hat{g}$ when it has oscillatory motion normal to the plane of symmetry.

Considering the coordinate transformation with the above nondimensional papameters, it is not difficult to reformulate the governing equations (5.27) and (5.28) in the computational domain (Z,θ) in a nondimensional form:

$$\iota\frac{Re_s}{4}h^2\hat{w} - \iota\frac{Re_s}{2}h\sqrt{D}\,L(\hat{p}) = \left[A\frac{\partial^2\hat{w}}{\partial Z^2} + B\frac{\partial\hat{w}}{\partial Z} + C\frac{\partial^2\hat{w}}{\partial Z\partial\theta} + D\frac{\partial^2\hat{w}}{\partial\theta^2} - D\,(\hat{w} - 2L(\hat{v}))\right],$$
$$\iota\frac{Re_s}{4}h^2\hat{v} + \iota\frac{Re_s}{2}h\,\frac{\partial\hat{p}}{\partial Z} = \left[A\frac{\partial^2\hat{v}}{\partial Z^2} + B\frac{\partial\hat{v}}{\partial Z} + C\frac{\partial^2\hat{v}}{\partial Z\partial\theta} + D\frac{\partial^2\hat{w}}{\partial\theta^2} - D(\hat{v} + 2L(\hat{w}))\right] \tag{5.31}$$

$$\frac{\partial\hat{v}}{\partial Z} - \sqrt{D}\hat{v} - \sqrt{D}\,L(\hat{w}) = 0\,, \tag{5.32}$$

where the operator $L(f)$ is

$$L(f) = \left[\frac{\partial}{\partial\theta} + (1-Z)\,\frac{h'(\theta)}{h(\theta)}\,\frac{\partial}{\partial Z}\right] f\,.$$

Considering the order of magnitude of A, B, C and D in the above equation with the aid of equation (4.5), A is dominant as compared to the others for narrow annular

passages, and the unsteady pressure drop in the circumferential direction is mainly due to the radial variation and time derivative of the circumferential unsteady flow velocity.

In this spectral method, the nondimensional fluid parameters can be expressed in terms of Chebyshev polynomials and Fourier expansions, as shown in the potential theory. By inspection of the boundary conditions and consideration of the properties of symmetry and antisymmetry of fluid parameters with respect to the plane of symmetry $\Theta = 0$, the fluid parameters can be expressed in terms of only even functions ($\cos k\theta$) or only in odd functions ($\sin k\theta$), according to the direction of the oscillatory motion of cylinder; in case (a) or in case (b), as mentioned before.

(a) Oscillatory motions in the plane of symmetry, $\Theta = 0$.

Using the spectral expansion for the oscillatory motion of the inner cylinder in the plane of symmetry, the following types of expansions can be considered for the fluid-dynamic properties in two-dimensional annular space

$$\begin{aligned} \hat{w} &= \sum_{j=0}^{m}\sum_{k=0}^{n} W_{jk}\, T_j(Z)\, s(k\theta)\,, \\ \hat{v} &= \sum_{j=0}^{m}\sum_{k=0}^{n} V_{jk}\, T_j(Z)\, c(k\theta)\,, \\ \hat{p} &= \sum_{j=0}^{m-2}\sum_{k=0}^{n} P_{jk}\, T_j(Z)\, c(k\theta)\,, \end{aligned} \tag{5.33}$$

where $c(k\theta)$ and $s(k,\theta)$ stand for the even terms ($\cos k\theta$) and odd terms ($\sin k\theta$) of the Fourier expansions, respectively, and the unknown coefficients W_{jk}, V_{jk} and P_{jk} are in complex forms due to the viscosity. In the above equations, the degree of the Chebyshev polynomials for unsteady velocity is considered two degrees higher than that for unsteady pressure in the present analysis because, generally the degree of the interploation functions for the unsteady velocity components is higher than that for the pressure distribution [59].

Taking account of the expansion forms shown in the above equations, the governing equations and the continuity equation can be expanded as

$$\sum_{j=0}^{m}\sum_{k=0}^{n} W_{jk} \left[A\, T_j''(Z)\, s(k\theta) + B\, T_j'(Z)\, s(k\theta) + C\, T_j'(Z)\, s'(k\theta) + D\, T_j(Z)\, s''(k\theta)\right.$$

$$
\begin{aligned}
& -D\,T_j(Z)\,s(k\theta) - \iota\,\frac{Re_s}{4}h^2\,T_j(Z)\,s(k\theta)\Big] \\
+ \quad & 2V_{jk}\left[T_j(Z)\,c'(k\theta) + (1-Z)\frac{h'(\theta)}{h(\theta)}\,T_j'(Z)\,c(k\theta)\right] \\
+ \quad & \iota P_{jk}\frac{Re_s}{2}h(\theta)\sqrt{D}\left[T_j(Z)\,c'(k\theta) + (1-Z)\frac{h'(\theta)}{h(\theta)}\,T_j'(Z)\,c(k\theta)\right] = 0\,, \\
\sum_{j=0}^{m}\sum_{k=0}^{n} \quad V_{jk} \quad & \Big[A\,T_j''(Z)\,c(k\theta) + B\,T_j'(Z)\,c(k\theta) + C\,T_j'(Z)\,c'(k\theta) + D\,T_j(Z)\,c''(k\theta) \\
& -D\,T_j(Z)\,c(k\theta) - \iota\,\frac{Re_s}{4}h^2\,T_j(Z)\,c(k\theta)\Big] \\
- \quad & 2W_{jk}\left[T_j(Z)\,s'(k\theta) + (1-Z)\frac{h'(\theta)}{h(\theta)}\,T_j'(Z)\,s(k\theta)\right] \\
- \quad & \iota P_{jk}\frac{Re_s}{2}h(\theta)\,T_j'(Z)\,c(k\theta) = 0\,, \qquad (5.34)
\end{aligned}
$$

$$
\begin{aligned}
\sum_{j=0}^{m}\sum_{k=0}^{n} \quad V_{jk} \quad & \left[T_j'(Z)\,c(k\theta) - \sqrt{D}T_j(Z)\,c(k\theta)\right] \\
-W_{jk} \quad & \left[T_j(Z)\,s'(k\theta) + (1-Z)\frac{h'(\theta)}{h(\theta)}\,T_j'(Z)\,s(k\theta)\right] = 0\,. \qquad (5.35)
\end{aligned}
$$

subject to the boundary conditions

$$
\begin{aligned}
\sum_{j=0}^{m}\sum_{k=0}^{n} V_{jk}\,T_j(1)\,c(k\theta) &= \cos\theta\,, \\
\sum_{j=0}^{m}\sum_{k=0}^{n} W_{jk}\,T_j(1)\,s(k\theta) &= -\sin\theta\,, \\
\sum_{j=0}^{m}\sum_{k=0}^{n} V_{jk}\,T_j(-1)\,c(k\theta) &= 0\,, \\
\sum_{j=0}^{m}\sum_{k=0}^{n} W_{jk}\,T_j(-1)\,s(k\theta) &= 0\,, \qquad (5.36)
\end{aligned}
$$

where $()'$ and $()''$ denote the first and second-order differentiations, respectively, with respect to the concerned parameter; for example, $T' = dT/dZ$ and $c'' = d^2c/d\theta^2$. In the present analysis, the unknown coefficients can be determined by the collocation method, whereby the governing equations and the continuity equation are satisfied at a certain number of distinct locations within in the computional domain, say $(3m-1)\times(n+1)$. As a result, the discretized set of equations can be obtained from the governing equations and the boundary conditions $2\times(n+1)$. Thus, the solutions of the algebraic system of

$(3m+1)\times(n+1)$ equations can be obtained completely in the computational domain, which are convertible back to the physical domain.

(b) Oscillatory motions normal to the plane of symmetry $\Theta = 0$.

In the spectral expansion when the inner cylinder has oscillatory motion normal to the plane of symmetry, while the outer cylinder is fixed, the following types of expansions can be considered for the fluid-dynamic properties in the two-dimensional annular space by inspection of the boundary conditions and the properties of symmetry and antisymmetry of fluid parameters:

$$\begin{aligned}
\hat{w} &= \sum_{j=0}^{m}\sum_{k=0}^{n} W_{jk}\, T_j(Z)\, c(k\theta)\,, \\
\hat{v} &= \sum_{j=0}^{m}\sum_{k=0}^{n} V_{jk}\, T_j(Z)\, s(k\theta)\,, \\
\hat{p} &= \sum_{j=0}^{m-2}\sum_{k=0}^{n} P_{jk}\, T_j(Z)\, s(k\theta)\,,
\end{aligned} \tag{5.37}$$

in terms of unknown coefficients, W_{jk}, V_{jk} and P_{jk}, which are separated into real and imaginary components.

Considering the above equations in expansion form, the governing equations and continuity equation can be written as

$$\begin{aligned}
\sum_{j=0}^{m}\sum_{k=0}^{n} W_{jk} & \left[A\,T_j''(Z)\,c(k\theta) + B\,T_j'(Z)\,c(k\theta) + C\,T_j'(Z)\,c'(k\theta) + D\,T_j(Z)\,c''(k\theta)\right. \\
& \left. - D\,T_j(Z)\,c(k\theta) - \iota\,\frac{Re_\delta}{4}h^2\,T_j(Z)\,c(k\theta)\right] \\
+ \; & 2V_{jk}\left[T_j(Z)\,s'(k\theta) + (1-Z)\frac{h'(\theta)}{h(\theta)}\,T_j'(Z)\,s(k\theta)\right] \\
+ \; & \iota P_{jk}\frac{Re_\delta}{2}h(\theta)\sqrt{D}\left[T_j(Z)\,s'(k\theta) + (1-Z)\frac{h'(\theta)}{h(\theta)}\,T_j'(Z)\,s(k\theta)\right] = 0\,, \\
\sum_{j=0}^{m}\sum_{k=0}^{n} V_{jk} & \left[A\,T_j''(Z)\,s(k\theta) + B\,T_j'(Z)\,s(k\theta) + C\,T_j'(Z)\,s'(k\theta) + D\,T_j(Z)\,s''(k\theta)\right. \\
& \left. - D\,T_j(Z)\,s(k\theta) - \iota\,\frac{Re_\delta}{4}h^2\,T_j(Z)\,s(k\theta)\right] - \\
- \; & 2W_{jk}\left[T_j(Z)\,c'(k\theta) + (1-Z)\frac{h'(\theta)}{h(\theta)}\,T_j'(Z)\,c(k\theta)\right] \\
- \; & \iota P_{jk}\frac{Re_\delta}{2}h(\theta)\,T_j'(Z)\,s(k\theta) = 0\,,
\end{aligned} \tag{5.38}$$

$$\sum_{j=0}^{m}\sum_{j=0}^{n} \quad V_{jk} \quad \left[T_j'(Z)\, s(k\theta) - \sqrt{D}T_j(Z)\, s(k\theta)\right]$$

$$-W_{jk} \quad \left[T_j(Z)\, c'(k\theta) + (1-Z)\frac{h'(\theta)}{h(\theta)} T_j'(Z)\, c(k\theta)\right] = 0\,, \qquad (5.39)$$

subject to the boundary conditions

$$\begin{aligned}
\sum_{j=0}^{m}\sum_{k=0}^{n} V_{jk}\, T_j(1)\, s(k\theta) &= \sin\theta\,, \\
\sum_{j=0}^{m}\sum_{k=0}^{n} W_{jk}\, T_j(1)\, c(k\theta) &= \cos\theta\,, \\
\sum_{j=0}^{m}\sum_{k=0}^{n} V_{jk}\, T_j(-1)\, s(k\theta) &= 0\,, \\
\sum_{j=0}^{m}\sum_{k=0}^{n} W_{jk}\, T_j(-1)\, c(k\theta) &= 0\,. \qquad (5.40)
\end{aligned}$$

Similarly to case (a), satisfying the governing equations and the continuity equation at a certain number of the collocation points and considering the boundary equations produces the discretized algebraic equations for the coeffcients, V_{jk}, W_{jk} and P_{jk}. Considering the obtained coefficients, which are the complex, the fluid-dynamic parameters in the physical domain can be evaluated completely by the coordinate transformations.

5.2.2 Shear Stress and Resultant Viscous Forces

The hydrodynamic forces, which can be separated into self-added-mass and viscous-damping terms, acting on the inner cylinder can be calculated by line integration of the stress components including pressure, as shown in Chapter 2. For the present analysis in cylindrical coordinates, the stress component can be rewritten as

$$\begin{aligned}
\tau_{rr} &= -p^* + 2\mu\frac{\partial v^*}{\partial r}\,, \\
\tau_{r\Theta} &= \mu\left\{\frac{\partial w^*}{\partial r} + \frac{w^*}{r} + \frac{1}{r}\frac{\partial v^*}{\partial \Theta}\right\}\,, \qquad (5.41)
\end{aligned}$$

where the unsteady pressure and unsteady-flow velocities are determined in terms of Chebyshev polynomials and Fourier expansions through the spectral collocation method.

The resultant forces, acting on the inner cylinder per unit length, in the direction of oscillatory motion can be calculated by circumferential integration of the stress components on the wall as

$$F_I = \int_0^{2\pi} a(\tau_{rr}\mid_{r=a}\cos\Theta - \tau_{r\Theta}\mid_{r=a}\sin\Theta)\,d\Theta\,,$$
$$G_I = \int_0^{2\pi} a(\tau_{rr}\mid_{r=a}\sin\Theta + \tau_{r\Theta}\mid_{r=a}\cos\Theta)\,d\Theta\,, \qquad (5.42)$$

where F_I and G_I stands for the cases (a) and (b), respectively, and the stress components on the surface of the inner cylinder can be expanded as

$$\tau_{rr} = -\rho a^2\omega^2\hat{e}e^{\iota\omega t}\sum_{j=0}^{m}\sum_{k=0}^{n}\left[P_{jk}T_j(1)c(k\theta) + \frac{4\iota}{Re_s h}V_{jk}T_j'(1)c(k\theta)\right]\,, \qquad (5.43)$$

$$\tau_{r\Theta} = \rho a^2\omega^2\hat{e}e^{\iota\omega t}\sum_{j=0}^{m}\sum_{k=0}^{n}\frac{\iota}{Re_s}\left[\frac{-2}{h}W_{jk}T_j'(1)s(k\theta) + W_{jk}T_j(1)s(k\theta) + V_{jk}T_j(1)c'(k\theta)\right]\,,$$

for case (a) and

$$\tau_{rr} = -\rho a^2\omega^2\hat{g}e^{\iota\omega t}\sum_{j=0}^{m}\sum_{k=0}^{n}\left[P_{jk}T_j(1)s(k\theta) + \frac{4\iota}{Re_s h}V_{jk}T_j'(1)s(k\theta)\right]\,, \qquad (5.44)$$

$$\tau_{r\Theta} = \rho a^2\omega^2\hat{g}e^{\iota\omega t}\sum_{j=0}^{m}\sum_{k=0}^{n}\frac{\iota}{Re_s}\left[\frac{-2}{h}W_{jk}T_j'(1)c(k\theta) + W_{jk}T_j(1)c(k\theta) + V_{jk}T_j(1)s'(k\theta)\right]\,,$$

for case (b), where the unknown coefficients are determined in complex form from the algebraic system of equations. Thus, the hydrodynamic forces can be separated into real and imaginary components. Substituting equation (5.43) and (5.44) into equation (5.42), these forces can be expressed in the form

$$F_I = -\rho\pi a^2 C_M\frac{\partial^2 e_I}{\partial t^2} - C_v\frac{\partial e_I}{\partial t} = \rho\pi a^2\omega^2 a\hat{e}\,e^{\iota\omega t}[\Re(\hat{F}) + \iota\Im(\hat{F})]\,,$$

$$G_I = -\rho\pi a^2 C_M\frac{\partial^2 g_I}{\partial t^2} - C_v\frac{\partial g_I}{\partial t} = \rho\pi a^2\omega^2 a\hat{g}\,e^{\iota\omega t}[\Re(\hat{G}) + \iota\Im(\hat{G})]\,, \qquad (5.45)$$

where C_M and C_v represent the added-mass and viscous-damping coefficients, respectively, and e_I and g_I denote the displacements of the moving cylinder in cases (a) and (b), respectively; the nondimensional fluid-dynamic forces, $\hat{F}$ and $\hat{G}$, are expressed in

complex form as

$$\begin{aligned}
\hat{F} &= -\sum_{j=0}^{m}\left\{P_{j1}+\frac{\iota}{Re_s}[V_{j1}^{\dagger}-W_{j1}^{\dagger}+W_{j1}-V_{j1}\right\}T_j(1)\,,\\
\hat{G} &= -\sum_{j=0}^{m}\left\{P_{j1}+\frac{\iota}{Re_s}[V_{j1}^{\ddagger}+W_{j1}^{\ddagger}-W_{j1}-V_{j1}\right\}T_j(1)\,,
\end{aligned} \tag{5.46}$$

where

$$\begin{aligned}
\sum_{j=0}^{m}\sum_{k=0}^{n}\frac{4}{h}V_{jk}\,T_j'(Z)\,c(k\theta) &= \sum_{j=0}^{m}\sum_{k=0}^{n}V_{jk}^{\dagger}\,T_j(Z)\,c(k\theta)\,,\\
\sum_{j=0}^{m}\sum_{k=0}^{n}\frac{2}{h}W_{jk}\,T_j'(Z)\,s(k\theta) &= \sum_{j=0}^{m}\sum_{k=0}^{n}W_{jk}^{\dagger}\,T_j(Z)\,s(k\theta)\,,\\
\sum_{j=0}^{m}\sum_{k=0}^{n}\frac{4}{h}V_{jk}\,T_j'(Z)\,s(k\theta) &= \sum_{j=0}^{m}\sum_{k=0}^{n}V_{jk}^{\ddagger}\,T_j(Z)\,s(k\theta)\,,\\
\sum_{j=0}^{m}\sum_{k=0}^{n}\frac{2}{h}W_{jk}\,T_j'(Z)\,c(k\theta) &= \sum_{j=0}^{m}\sum_{k=0}^{n}W_{jk}^{\ddagger}\,T_j(Z)\,c(k\theta)\,.
\end{aligned}$$

From equation (5.45), by definition, the added-mass and damping coefficients can be written as

$$\begin{aligned}
C_M = \Re(\hat{F})\,, \qquad C_v &= -\rho\pi a^2\omega\Im(\hat{F})\,, \qquad \text{in case (a)}\,,\\
C_M = \Re(\hat{G})\,, \qquad C_v &= -\rho\pi a^2\omega\Im(\hat{G})\,, \qquad \text{in case (b)}\,.
\end{aligned} \tag{5.47}$$

Similarly to the case of potential-flow theory, the hydrodynamic forces normal to oscillatory motion are zero.

5.2.3 Numerical Results for Viscous Fluid-dynamic Forces

To illustrate the influence of viscosity of the fluid on added mass and viscous damping for the problem of harmonic oscillatory motion of the inner cylinder in an eccentric annulus, the calculations have been conducted while varying the oscillatory Reynolds number, Re_s, the ratio of radii, b/a, and relative eccentricity, $e/(b-a)$.

In these calculations, the collocation points $(m-1)$ along the radial direction are clustered near the wall using equation (4.24) to obtain good accuracy and computing efficiency, when the penetration depth is relatively small *vis-à-vis* the annular space,

$\delta_p/(b-a) < 0.1$. In other cases, the calculations have been conducted with equally distributed collocation points along the radial direction. Along the circumferential direction, equally distributed collocation points $(n+1)$ are selected, but with $F_k(\theta) \neq 0$ to avoid the pseudo-singularity problem.

For concentric configurations, the nondimensional flow velocities, $v^*(\Theta = 0°)/e_v$ and $w^*(\Theta = 90°)/e_v$ are ploted in Figure 5.5 along the radial direction for selected values of the nondimensional parameters ($Re_s = 50, 1740$ and $b/a = 1.25$, with $m = 8$). In this figure, the dotted line represents the circumferential-flow velocity obtained by the present potential-flow theory. Considering equation (5.41) together with this figure, it is expected that the skin-friction force becomes larger as the oscillatory Reynolds number is increased. The distribution of the real parts of complex-flow velocity in the circumferential direction has a parabolic shape for low values of Re_s, while it has a shape similar to that for turbulent flow at relatively high Re_s.

The pressure distribution along the radial direction is nearly constant for annular configurations and its amplitude in nondimensional form is almost of the same order as the added-mass coefficients. Hence, these results are not presented.

When Re_s is 50, 500 and 5000, and b/a is varied from 1.25 to 4, the added-mass and viscous-damping coefficients for concentric configurations are shown in Figure 5.6. It is found that the coefficients are strongly dependent on the oscillatory Reynolds number; as it increases, these coefficients decrease. Physically, for fixed values of the ratio of radii, b/a, and the viscosity of fluid, ν, these coefficients decrease with increasing the frequency of oscillatory motion, ω. The two coefficients exponentially increase with decreasing b/a for the fixed oscillatory Reynolds number. Particularly for narrow annular flow, it is necessary to take into account the viscous damping, even if the oscillatory Reynolds number is high, corresponding to the case of low-viscosity fluid or high-circular frequency. With increasing values of the oscillatory Reynolds number, the added-mass coefficient is influenced less by the viscosity of the fluid, and not much different from the result obtained by the potential-flow theory.

The influence of the relative eccentricity on the nondimensional pressure in com-

plex form is illustrated in Figure 5.7 for $b/a = 1.25$ and $Re_s = 50$ in the case of oscillatory motion in the plane of symmetry and in Figure 5.8 in the case of oscillatory motion normal to the plane of symmetry. The real part of it, which is related to the added mass, is compared with the result (open circles for concentric configurations and filled circles for eccentric ones $e/(b-a) = 0.4$) shown in Figure 5.1 for potential flow. The character of the variation of $\Re(\hat{p})$ and $\Im(\hat{p})$ with the eccentricity is similar to that for potential flow.

In Figure 5.9 for the case of $b/a = 1.25$ and $Re_s = 500$ with the relative eccentricity, the shear stress and unsteady pressure effects on the added-mass and damping coefficients are investigated and the added-mass coefficients are compared with the corresponding ones for potential flow. It is found that these coefficients are mainly influenced by the unsteady pressure, rather than by the shear stress, but the coefficients are slightly increased by the effect of the skin friction. The added-mass and viscous-damping coefficients are shown in Figure 5.10 for the oscillatory motion in the plane of symmetry and Figure 5.11 for the motion normal to the plane of symmetry. The effect of the relative eccentricity, $e/(b-a)$, on the coefficients is investigated with the selected oscillatory Reynold number ($Re_s = 50,\ 5000$) and the ratios of radii ($b/a = 1.25,\ 2$). The numerical results have been calculated with $m < 6$ and $n < 6$ in case of $Re_s = 50$ and with $m < 10$ and $n < 4$ in case of $Re_s = 5000$, in order to minimize the round-off error which may increase with the size of the matrix obtained from the algebraic equations. In general, it is necessary to increase the number of terms in the Fourier expansion with increasing eccentricity, and the number of Chebyshev polynomials with increasing annular space. As the eccentricity increases, the magnitudes of these coefficients increase and, due to the viscosity, the added-mass coefficients increase as the oscillatory Reynolds number decreases.

5.3 REMARKS

The spectral method is applied in this chapter to the unsteady potential and viscous flows generated by the small-amplitude harmonic translational motion of a cylinder in

an annulus. The numerical results are presented to evaluate the general characteristics of the added masses for both flows and the viscous damping for viscous flow in terms of the radius ratio b/a with the eccentricity $e/(b-a)$. For viscous flow, the oscillatory Reynolds number Re_s is an important parameter, as shown in equation (5.31).

To assess the validity of the results for potential flow, the present results are compared with the analytical results given by Chung and Chen [9] for eccentric configurations and by Fritz [7] for concentric ones. The numerical results for both potential and viscous flows are compared. The difference between the two sets of results can be explained by the viscous effects caused by the shear stress and the unsteady pressure drop in circumferential direction.

Considering the results obtained by potential and viscous flow theories for translational motion of the inner cylinder in an annulus, the following remarks should made: (a) the present collocation method has been validated by comparing results with analytical ones. Therefore, the present method can be adapted for use in more complicated unsteady flow problems, which remain unsolved at present; (b) the linear theory presented in this analysis is based on the assumption of small amplitudes (as a result, the added-mass and viscous-damping coefficients are independent of the amplitude); (c) the added-mass and viscous-damping coefficients are dependent on the oscillatory Reynolds number, and these coefficients are influenced by the relative eccentricity; with decreasing oscillatory Reynolds number and increasing eccentricity, these coefficients increase; (d) for the high oscillatory Reynolds number, the added-mass coefficients can be estimated approximately by potential-flow theory, but the viscous-damping coefficients, even for high oscillatory Reynolds number, should be considered in the hydrodynamic forces for narrow annuli; (e) for narrow configurations, the added mass is insensitive to variations of the oscillatory Reynolds number; however, the damping is sensitive to it.

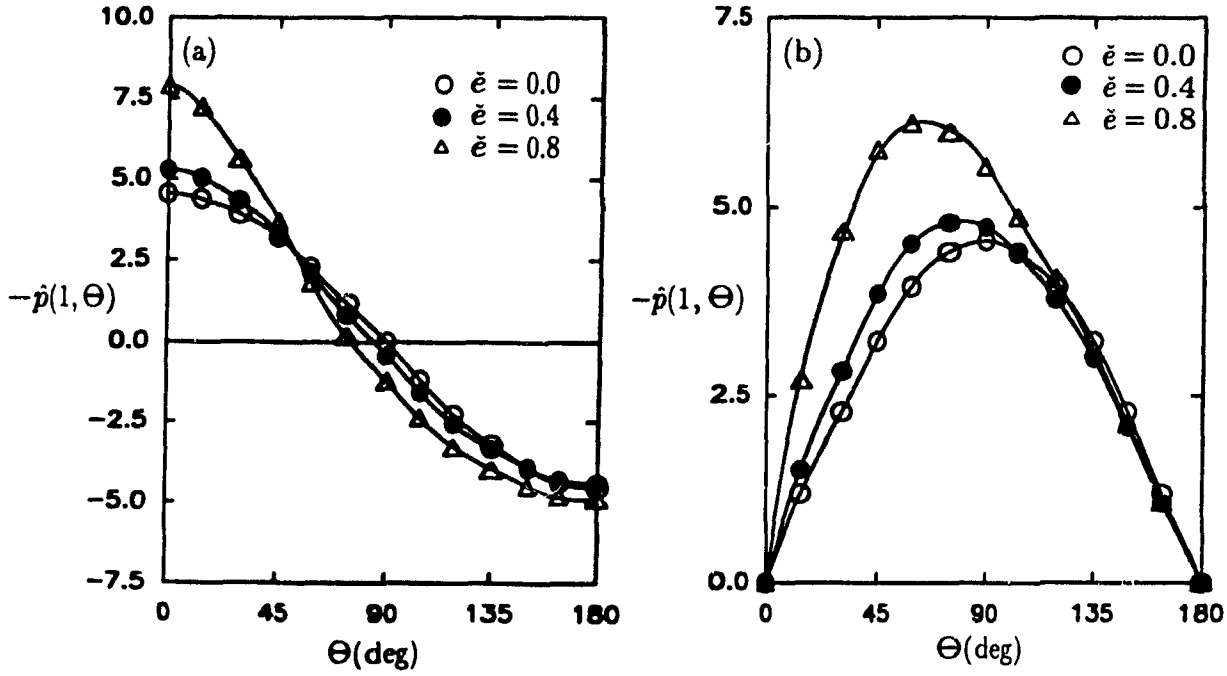

Figure 5.1: The unsteady pressure in nondimensional form, $\hat{p}(1,\theta)$, on the oscillating inner cylinder for various relative eccentricities $\check{e} = e/(b-a)$ and for $b/a = 1.25$. (a) Case of oscillations in the plane of symmetry; (b) case of oscillations normal to the symmetry plane.

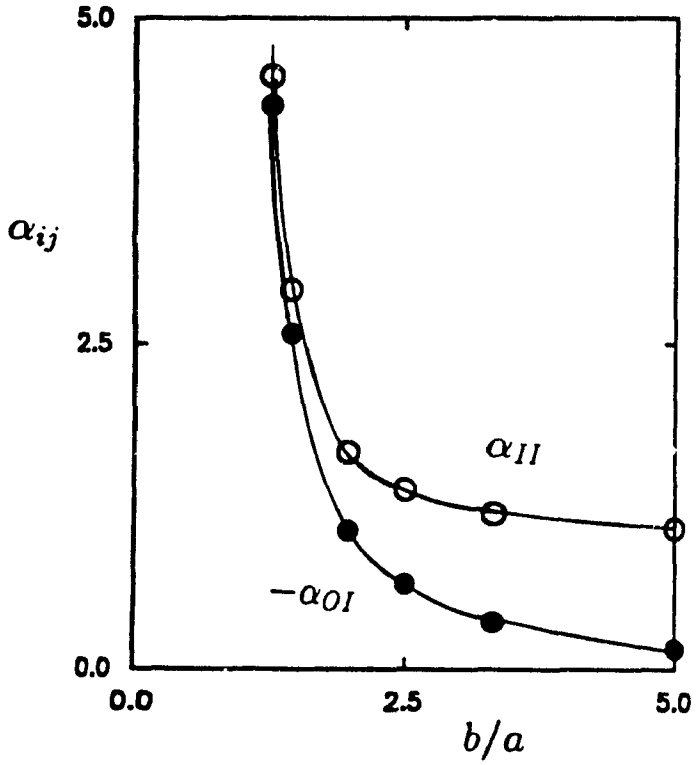

Figure 5.2: The added-mass coefficients, α_{II} and α_{OI}, for concentric configurations, as functions of the radius ratio, b/a. Comparison between the present solution and Fritz's solution: o, α_{II}; •, α_{OI}; —, Fritz's analytical solution.

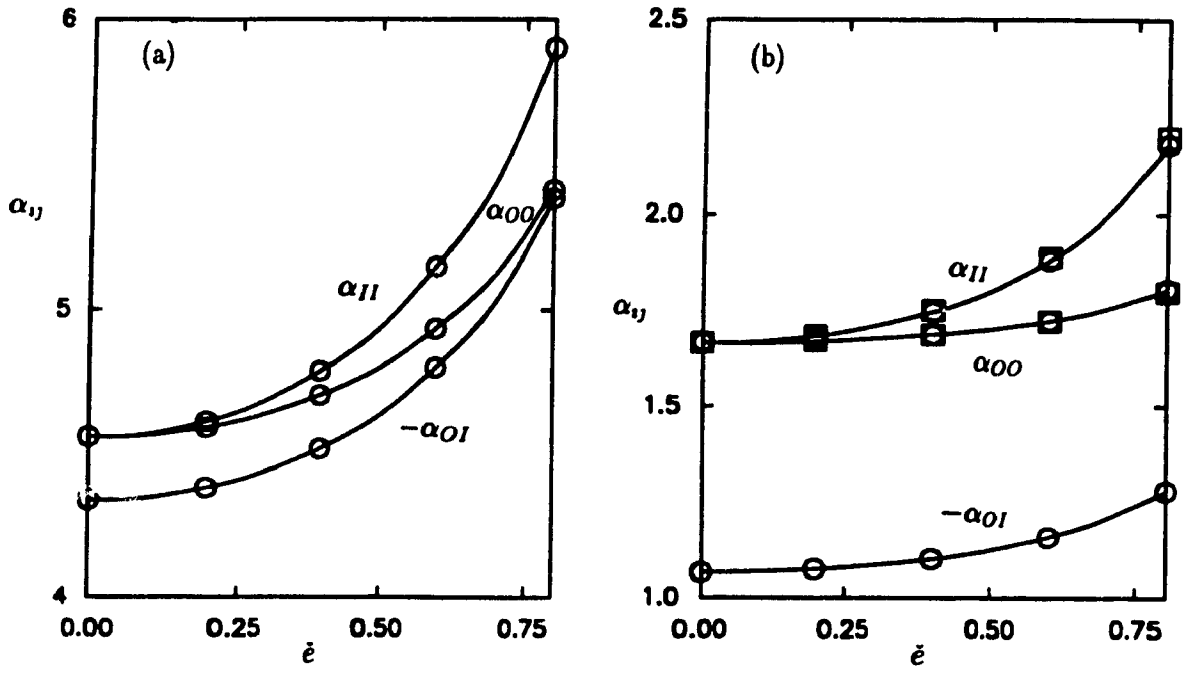

Figure 5.3: The added-mass coefficients, α_{II}, α_{OO} and α_{OI}, for oscillations in the plane of symmetry, as functions of the relative eccentricity $\bar{e} = e/(b-a)$ for the cases: (a) $b/a = 1.25$ and (b) $b/a = 2$. Comparison between the present solution(-o-) and Chung and Chen's solution(□).

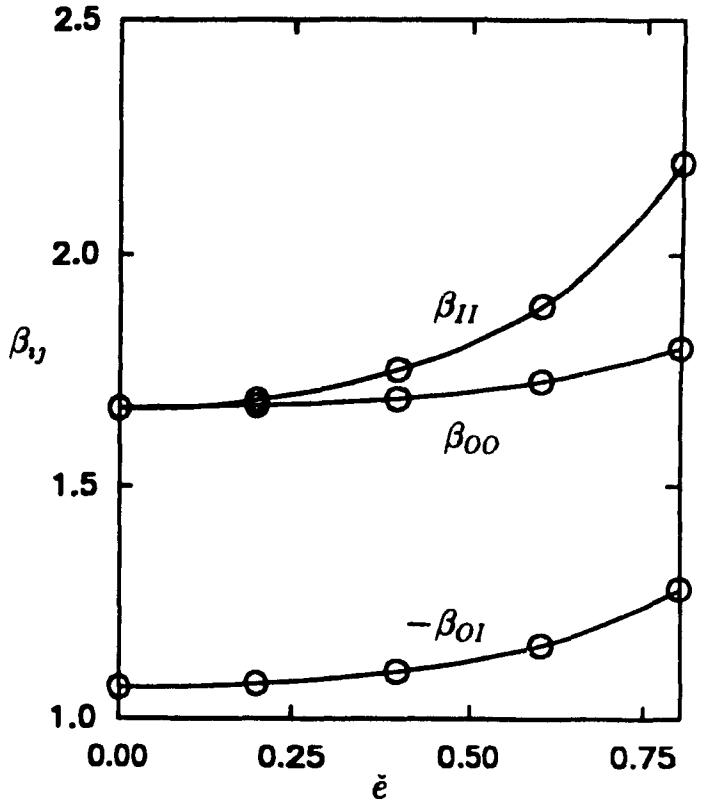

Figure 5.4: The added-mass coefficients, β_{II}, β_{OO} and β_{OI}, for oscillations normal to the symmetry plane, as functions of the relative eccentricity $\check{e} = e/(b-a)$ for $b/a = 2$.

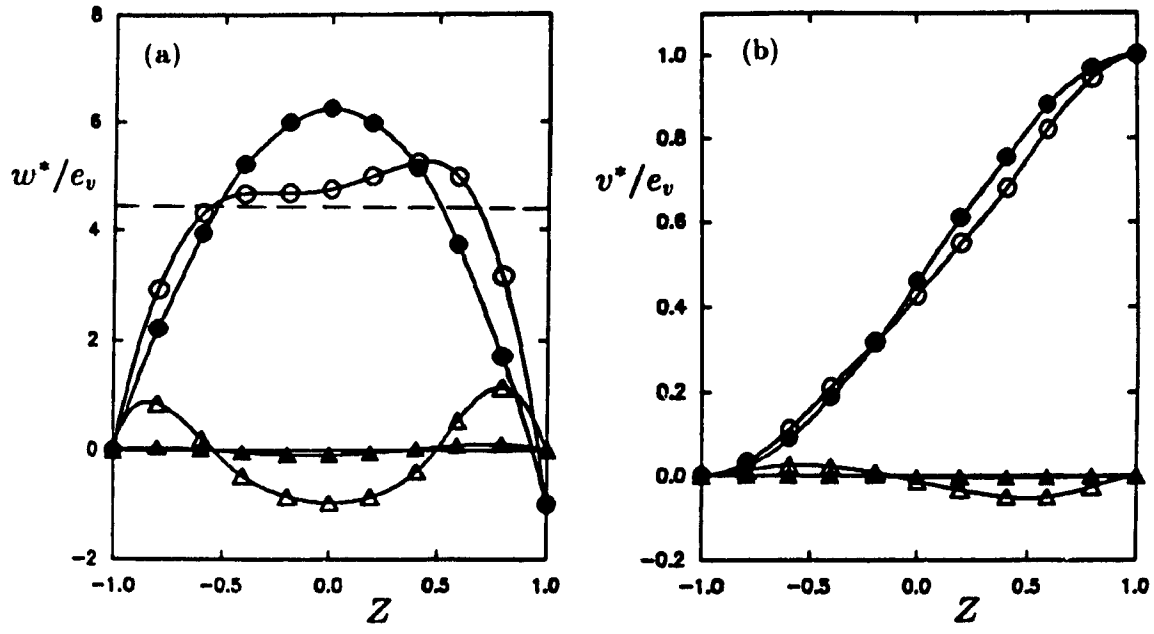

Figure 5.5: The distribution of the nondimensional amplitude of the unsteady flow velocity for $b/a = 1.25$, $Re_s = 50$(filled symbols) and $Re_s = 1,740$(open symbols) across the annular space; (a) the circumferential and (b) the radial components. Viscous theory; ○●, real part; △▲, imaginary part; - - - -, circumferential components obtained for present potential flow.

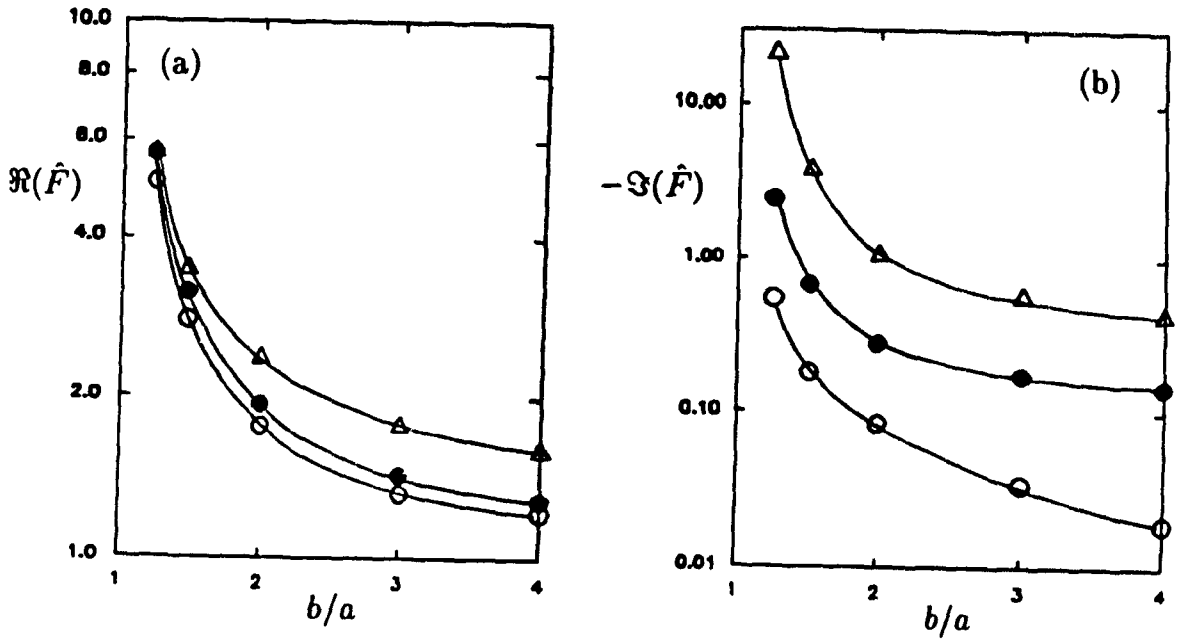

Figure 5.6: The (a) real and (b) imaginary components of the nondimensional fluid-dynamic forces versus the radius ratio, b/a, for the selected oscillatory Reynolds number:Δ, $Re_s = 50$; $\bullet$, $Re_s = 500$; o, $Re_s = 5000$.

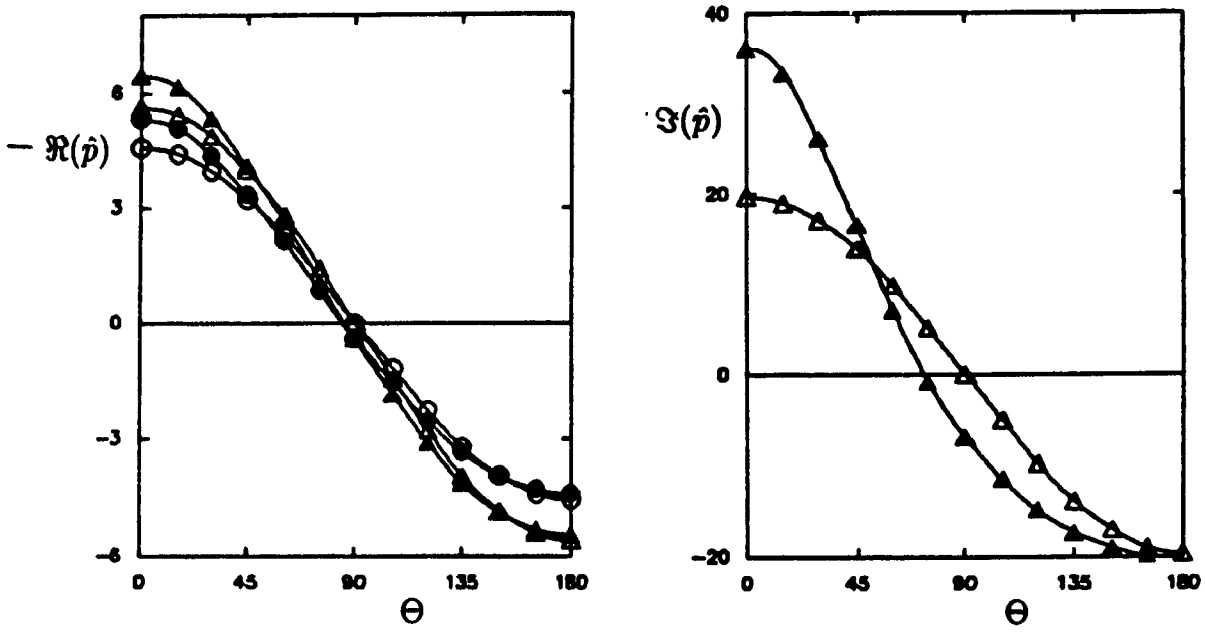

Figure 5.7: Influence of eccentricity on the nondimensional pressure, $\hat{p}$, obtained by the present potential(o, •) and viscous($\triangle$, $\blacktriangle$; $Re_s = 50$) theories for oscillations in the plane of symmetry and for the case $b/a = 1.25$. Open symbols, $\check{e} = e/(b-a) = 0$; filled symbols, $\check{e} = 0.4$.

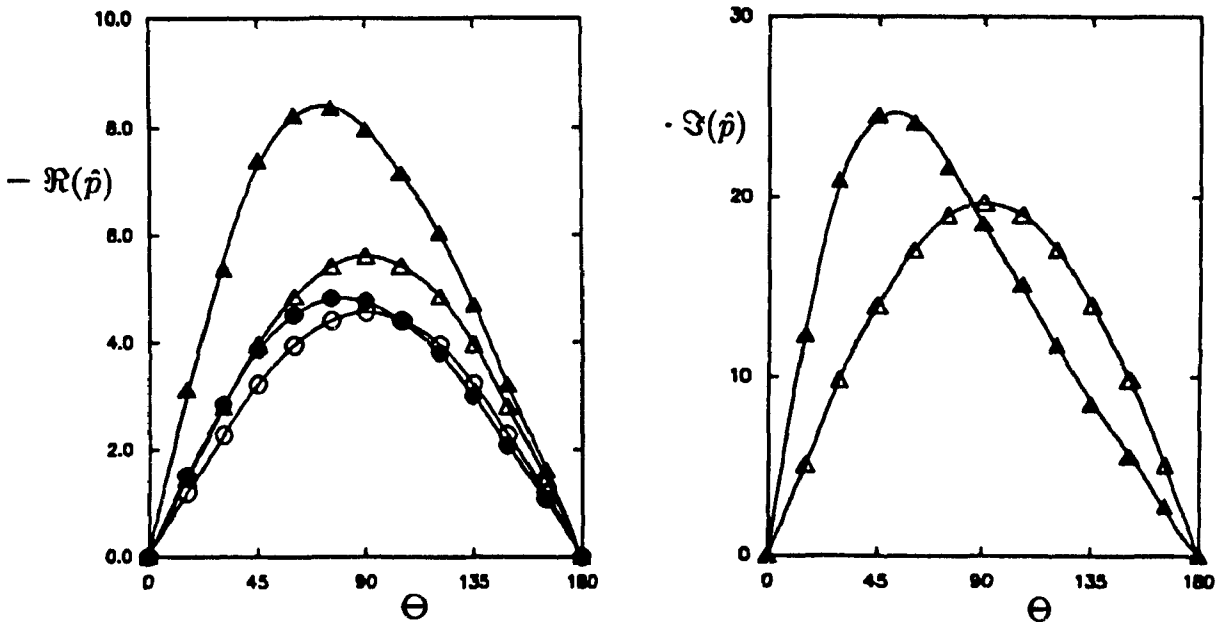

Figure 5.8: Influence of eccentricity on the nondimensional pressure, $\hat{p}$, obtained by the present potential(o, •) and viscous(Δ, $\blacktriangle$; $Re_s = 50$) theories for oscillations normal to the symmetry plane and for the case $b/a = 1.25$. Open symbols, $\tilde{e} = e/(b-a) = 0$; filled symbols, $\tilde{e} = 0.4$.

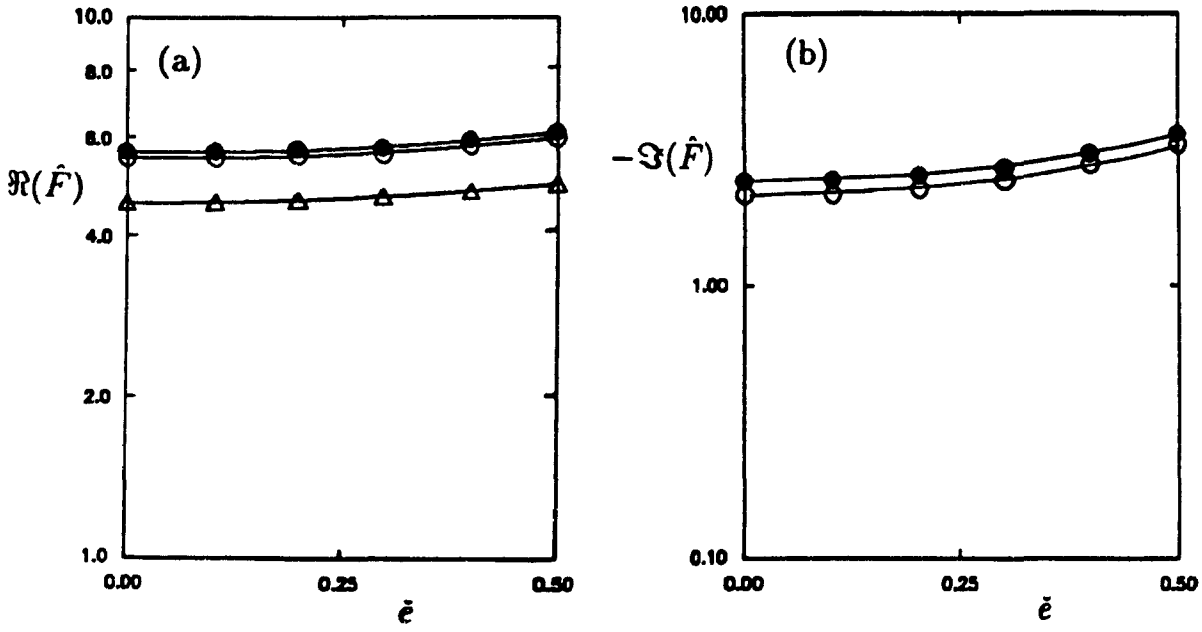

Figure 5.9: Viscous effects on the (a) real and (b) imaginary components of the nondimensional fluid-dynamic forces for oscillations in the plane of symmetry for different eccentricities $\tilde{e} = e/(b-a)$ and for $b/a = 1.25$, obtained by the viscous theory($Re_s = 500$):-o-, only pressure considered; -•-, full viscous effects considered. —Δ—, Results obtained by the potential theory.

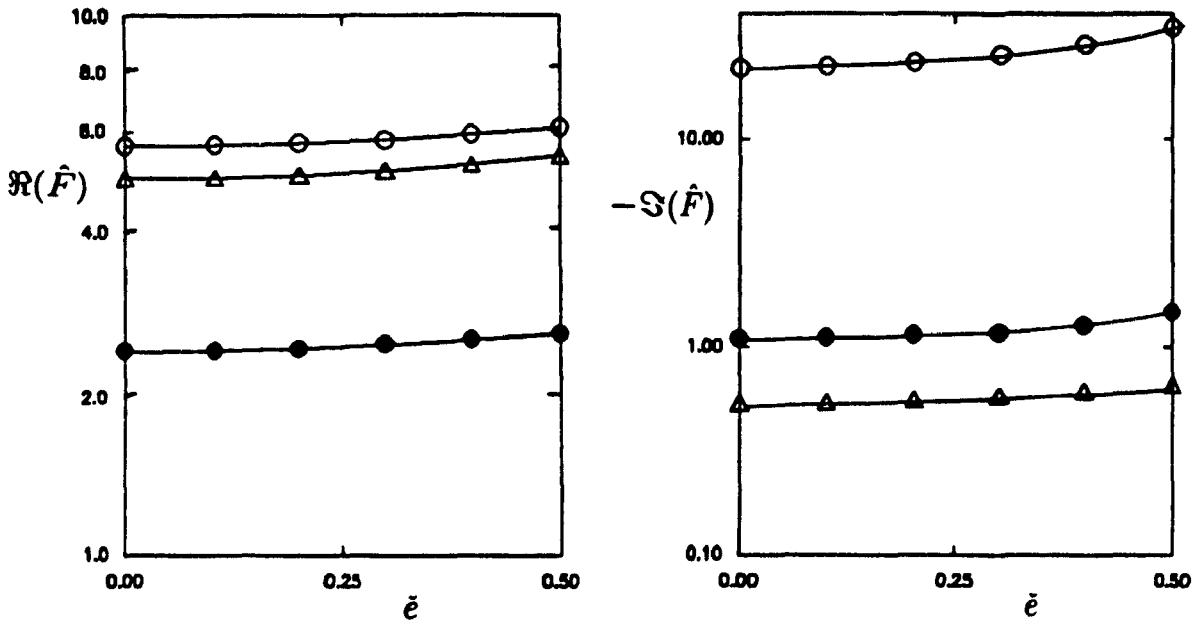

Figure 5.10: Influence of the relative eccentricity $\check{e} = e/(b-a)$ on the nondimensional fluid-dynamic forces considering full viscous effects for oscillations in the plane symmetry: —o—, $Re_s = 50$ and $b/a = 1.25$; —•—, $Re_s = 50$ and $b/a = 2$; —△—, $Re_s = 5000$ and $b/a = 1.25$.

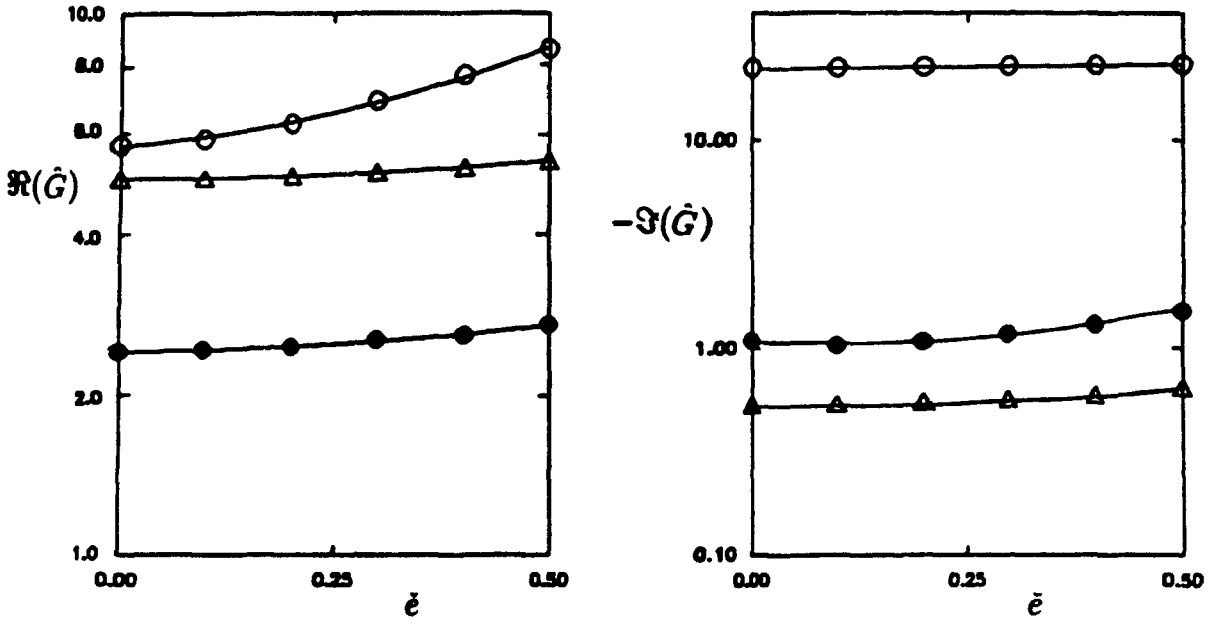

Figure 5.11: Influence of the relative eccentricity $\check{e} = e/(b-a)$ on the nondimensional fluid-dynamic forces considering full viscous effects for oscillations normal to symmetry plane: —o—, $Re_s = 50$ and $b/a = 1.25$; —•—, $Re_s = 50$ and $b/a = 2$; —△—, $Re_s = 5000$ and $b/a = 1.25$.

Chapter 6

Study of Three-dimensional Unsteady Viscous Flows

In connection with the spectral method, the governing equations were discretized through the collocation method for unsteady fluid flow. In the previous chapter, the convective terms and the axial components of the diffusion terms were not considered for the translational motion of a cylinder without steady axial flow. For a system consisting of a flexible cylinder subjected to axial flow, it is obvious that these terms must be considered.

The fluid-dynamic forces acting on a flexible cylinder have been formulated by the hybrid collocation finite-difference method, as well as by approximate semi-analytical methods. In the present analysis, the steady viscous forces derived from the longitudinal frictional force and from the pressurization of the flow are not considered; only the unsteady fluid-dynamic forces are investigated. The numerical results are compared to the semi-analytical results.

The inner cylinder subjected to steady axial flow in a concentric annulus is assumed to have a simple flexural motion, as a clamped-clamped beam. In order to simplify the problem and to get general information, only the first mode of the beam is considered for the oscillatory motion of the flexible cylinder. This cylinder has length L and radius a. The radius of the outer cylinder is b; hence the annular space between two cylinders is $H = b - a$. The motions are assumed to be small.

6.1 COLLOCATION FINITE-DIFFERENCE METHOD

To formulate this three-dimensional problem with the spectral method, another interpolation function is needed for the axial variation. Thus, the unknown coefficients are also dependent on the axial coordinate. When a system of equations is obtained by the collocation method with n interpolation functions for the axial variation, the discretized-system equations might become n times larger, when the same number of collocation points are selected for the radial and circumferential coordinates. As shown in the previous chapters, the solutions given by the spectral method converged fast. However, difficulties are encounted in the three-dimensional problem due to a relatively large full matrix system, which might produce singularity problems in the mathematical procedure. In order to avoid this difficulty, a finite-difference method based on a hybrid scheme is adapted for axial variations, which is characterized by an artificial viscosity which helps to achieve convergence of the solution.

The hybrid scheme is related only to the axial domain, while the collocation method is still used for the radial and circumferential domains. As a result, the axial domain is subdivided into a certain number of grid points, where spectral expansions for the fluid parameters are defined. The numerical details of the collocation method, which remain the same as for the two-dimensional flow discussed in the previous chapter, have not been repeated in this chapter. However, an attempt has been made to clearly point out and emphasize the details of the finite-difference method for the present analysis.

Based on the collocation finite-difference method, the governing equations of the unsteady flow, obtained from the appropriate Navier-Stokes and continuity equations, reduce to a system of algebraic equations leading to a block-tridiagonal system. Each row of the matrix is concerned with three grid points based on the finite-difference method, and the submatrices are related to the corresponding collocation points based on the spectral method. To obtain a solution of the system, the LU decomposition

method based on the factorization scheme given in Appendix F is used.

In most of the previous studies, the fluid-dynamic forces acting on the oscillating cylinder subjected to axial flow have been developed based on uniform axial flow. Therefore, the effect of laminar axial flow is still difficult to quantify systematically. In this section, the fluid-dynamic forces have been formulated from the Navier-Stokes equations, accounting for unsteady viscous flow effects much more fully than the semi-empirical and approximate formulations utilized heretofore. Far upstream, the axial flow is fully developed and its velocity can be calculated using the spectral method as shown in Chapter 4. In order to formulate the unsteady viscous problem, the results for steady viscous flow are utilized.

6.1.1 Hybrid Method Formulation

In this section, the basic concepts needed in the formulation of the hybrid scheme are presented. The hybrid scheme was introduced by Spalding under the name "High-lateral-flux modification" for the finite difference method [56]. The significance of the hybrid scheme can be understood by observing that it is identical to the central-difference scheme for the mesh Reynolds number range $-2 < Re_m(= (U\Delta x)/\nu) < 2$, and outside this range with an upwind scheme. As mentioned before, the axial components of the diffusion terms and convective terms related with the steady axial flow velocity must be considered for the present analysis. The addtion of these terms does not alter the form of the discretized equations, when the axial derivative terms are relatively small by the assumption of small amplitude motion.

Although the convection and diffusion terms connected to the axial variation are the only new terms in this section, its formulation is not very straightforward. The convection term has an inseparable connection with the diffusion term and, therefore, the two terms need to be handled as one unit. Considering the connection between the two terms, the hybrid scheme has been developed to easily converge to solution. On the use of the central-difference scheme, there is one real constraint which will be discussed further. Sometimes, it creates difficulties in obtaining convergent solutions.

To simplify matters, only the convection and diffusion terms are considered for a one-dimensional problem. The governing differential equation is

$$\frac{\partial}{\partial x}(\rho U f) = \frac{\partial}{\partial x}\left(\mu \frac{\partial f}{\partial x}\right) , \tag{6.1}$$

where U represents the steady-flow velocity in the axial direction and f denotes any flow-field parameter, which will be obtained. As shown in Chapter 4, the axial-flow velocity, U, can be obtained from the Navier-Stokes equations for the steady flow, which is separated from the full Navier-Stokes equations that include the unsteady components based on small-amplitude motion. At this stage, our task is to obtain a solution for f, which will be the unsteady fluid quantities in the present analysis. For concentric configurations, the steady-flow velocity does not depend on the axial coordinate under consideration.

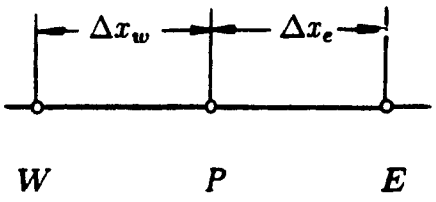

Figure 6.1: Typical grid-points cluster for the axial variation

Using the central difference scheme with order $(\Delta x)^2$ over the control volume shown in the above figure, the first and second partial derivatives can be written as

$$\begin{aligned}
\left(\frac{\partial f}{\partial x}\right)_P &= \frac{f_E - f_W}{\Delta x_e + \Delta x_w} , \\
\left(\frac{\partial^2 f}{\partial x^2}\right)_P &= \frac{2f_E}{(\Delta x_e + \Delta x_w)\Delta x_e} - \frac{2f_P}{\Delta x_e \Delta x_w} + \frac{2f_W}{(\Delta x_e + \Delta x_w)\Delta x_w} ,
\end{aligned} \tag{6.2}$$

where the subscripts E and W present east and west sides with respect to the central grid point P in the axial domain.

For incompressible flow, substituting equation (6.2) into equation (6.1) with the aid of the following continuity equation

$$\frac{\partial}{\partial x}(\rho U) = 0 \,, \tag{6.3}$$

the discretized equation becomes

$$a_P f_P = a_E f_E + a_W f_W \,, \tag{6.4}$$

where

$$\begin{aligned} a_E &= \frac{\mu}{\Delta x_e} - \frac{\rho U}{2} \,, \\ a_W &= \frac{\mu}{\Delta x_w} + \frac{\rho U}{2} \,, \\ a_P &= a_E + a_W \,. \end{aligned}$$

Reflecting on the implications of equation (6.4) which gives f_P relative to f_W and f_E, it is realized that a_E and a_W should both be positive to properly imply the expected behaviour of a viscous fluid. The expected behaviour would be such that a decrease in the variable, f, of the fluid below or above the point P would distribute toward a decrease in the variable, f, at the point P, through the effect of viscosity. Also, the negative coefficient would imply that a_P, which equals $a_E + a_W$, is less than $| a_E + a_W |$, which fails to satisfy the Scarborough criterion [62]. Then, a point-by-point solution of the discretized equation may diverge. This is the reason why all the early attempts to solve convective problems by the central difference scheme were limited to low mesh Reynolds number.

To keep a_E and a_W, shown in equation (6.4), positive in value requires

$$Re_m = \frac{U \Delta x}{\nu} < 2 \,, \tag{6.5}$$

which confirms our suspicion that the "correct" representation is one that permits viscous-like behaviour. The inequality can be satisfied for a sufficiently fine mesh which, of course, is achieved at convergence. For some flow, the constraint of equation (6.5) tends to require the use of an excessively large number of grid points. This has

motivated several investigators to consider ways of altering the difference scheme to eliminate the mesh-Reynolds-number constraint.

The simplest remedy to the problem of the mesh-Reynolds-number constraint is to introduce the hybrid scheme for the convective term as a "high lateral flux" correction. The name 'hybrid scheme' is indicative of a combination of the central-difference scheme for the mesh Reynolds number range $-2 < Re_m < 2$ and the upwind scheme outside this range. The truncation error associated with the upwind scheme creates an artificial viscosity which tends to enhance viscous-like behaviour. In other words, the formulation of the diffusion terms is left unchanged, but the convective terms are calculated according to the mesh Reynolds number. Based on the upwind scheme, the first-order derivative with order (Δx) can be expressed as

$$\left(\frac{\partial f}{\partial x}\right)_P = \frac{2(f_P - f_W)}{\Delta x_e + \Delta x_w} \qquad \text{if} \qquad U > 0\,. \tag{6.6}$$

In the present analysis, the axial-flow velocity is always positive; there is no adverse pressure gradient in a constant width annular space.

Using the hybrid scheme, the discretized convective-diffusion equation can now written as

$$a_P f_P = a_E f_E + a_W f_W \qquad \text{if} \qquad U > 0\,, \tag{6.7}$$

where

$$\begin{aligned} a_E &= \frac{\mu}{\Delta x_e} + [\![0,\ -\frac{\rho U}{2}]\!]\,, \\ a_W &= \frac{\mu}{\Delta x_w} + [\![\rho U,\ \frac{\rho U}{2}]\!]\,, \\ a_P &= a_E + a_W\,, \end{aligned}$$

where $[\![p,q]\!]$ represents p for the upwind scheme ($Re_m > 2$) or q for the central-difference scheme ($-2 < Re_m < 2$).

6.1.2 Formulation of the System Equation for Unsteady Viscous Flow

The unsteady fluid-dynamic forces acting on the inner cylinder are formulated by the numerical method, considering the unsteady pressure and shear stresses. Using the collocation finite difference method, a system of discretized equations is obtained from the appropriate Navier-Stokes and continuity equations with the boundary conditions. Based on small-amplitude motions of the cylinder, the governing equations can be linearized, as shown in Chapter 2.

The inner cylinder, surrounded by incompressible viscous-fluid flow, has periodic flexural motion in a concentric annulus. The vibrating motion is assumed to be simple harmonic, with circular frequency ω. For the three-dimensional problem with steady axial flow, the unsteady governing equations are obtained by subtracting the steady terms from the full Navier-Stokes equations. The linearized Navier-Stokes equations and the continuity equation in cylindrical coordinates for the present analysis can be reduced

$$\frac{\partial u^*}{\partial t} + v^*\frac{\partial U}{\partial r} + \frac{w^*}{r}\frac{\partial U}{\partial \Theta} + U\frac{\partial u^*}{\partial x} + \frac{1}{\rho}\frac{\partial p^*}{\partial x} = \nu\left[\frac{1}{r}\frac{\partial}{\partial r}\left(r\frac{\partial u^*}{\partial r}\right) + \frac{1}{r^2}\frac{\partial^2 u^*}{\partial \Theta^2} + \frac{\partial^2 u^*}{\partial x^2}\right],$$

$$\frac{\partial w^*}{\partial t} + U\frac{\partial w^*}{\partial x} + \frac{1}{\rho}\frac{1}{r}\frac{\partial p^*}{\partial \Theta} = \nu\left[\frac{1}{r}\frac{\partial}{\partial r}\left(r\frac{\partial w^*}{\partial r}\right) + \frac{1}{r^2}\frac{\partial^2 w^*}{\partial \Theta^2} + \frac{\partial^2 w^*}{\partial x^2} - \frac{w^*}{r^2} + \frac{2}{r^2}\frac{\partial v^*}{\partial \Theta}\right],$$

$$\frac{\partial v^*}{\partial t} + U\frac{\partial v^*}{\partial x} + \frac{1}{\rho}\frac{\partial p^*}{\partial r} = \nu\left[\frac{1}{r}\frac{\partial}{\partial r}\left(r\frac{\partial v^*}{\partial r}\right) + \frac{1}{r^2}\frac{\partial^2 v^*}{\partial \Theta^2} + \frac{\partial^2 v^*}{\partial x^2} - \frac{v^*}{r^2} - \frac{2}{r^2}\frac{\partial w^*}{\partial \Theta}\right], \quad (6.8)$$

$$\frac{\partial u^*}{\partial x} + \frac{\partial w^*}{\partial \Theta} + \frac{\partial}{\partial r}(rv^*) = 0, \quad (6.9)$$

where u^*, v^* and w^* denote the unsteady flow velocities in the axial, radial and circumferential directions, respectively. In the above equations, the production terms between the unsteady components are neglected for small-amplitude motion, and the circumferential variation of steady axial flow is zero for concentric configurations.

Considering the no-slip condition at the interface between fluid and cylinder, the boundary conditions on the fixed ($r = b$) and moving ($r = a$) cylinders can be expressed as

$$u^*(x, b, \Theta, t) = v^*(x, b, \Theta, t) = w^*(x, b, \Theta, t) = 0,$$

$$
\begin{aligned}
u^*(x,a,\Theta,t) &= 0 \\
v^*(x,a,\Theta,t) &= e_v(x,t)\,\cos\Theta = \frac{e_I(x,t)}{\partial t}\cos\Theta\,, \\
w^*(x,a,\Theta,t) &= -e_v(x,t)\,\sin\Theta = -\frac{e_I(x,t)}{\partial t}\sin\Theta\,,
\end{aligned} \tag{6.10}
$$

where $e_v(x,t)$ represents the lateral velocity of the moving inner cylinder and $e_I(x,t)$ denotes the corresponding displacement which can be expressed in terms of the eigenfunction $\psi_1(x)$ of the first normal mode for a clamped-clamped beam

$$
e_I(x,t) = E(x)e^{\iota\omega t} = a_1\psi_1(x)e^{\iota\omega t}\,. \tag{6.11}
$$

The present problem is generalized by the following nondimensional parameters, which are similar in form to those in Chapter 5;

$$
X = \frac{x}{L}\,, \qquad l = \frac{L}{a}\,, \qquad h = \frac{H}{a}\,, \qquad \hat{U} = \frac{U}{\bar{U}}\,, \qquad \hat{p} = \frac{p^*}{\rho a^2\omega^2\epsilon_{1/2}e^{\iota\omega t}}\,,
$$

$$
\hat{u} = \frac{u^*}{\iota a\omega\epsilon_{1/2}e^{\iota\omega t}}\,, \qquad \hat{v} = \frac{v^*}{\iota a\omega\epsilon_{1/2}e^{\iota\omega t}}\,, \qquad \hat{w} = \frac{w^*}{\iota a\omega\epsilon_{1/2}e^{\iota\omega t}}\,,
$$

$$
\hat{e}(X) = \frac{e_v(X,t)}{\iota a\omega e^{\iota\omega t}}\,, \qquad \hat{e}_r(X) = \frac{\hat{e}(X)}{\hat{e}_{1/2}}\,, \qquad Re = \frac{\bar{U}\,2ha}{\nu}\,, \qquad Re_s = \frac{\omega a^2}{\nu}\,, \tag{6.12}
$$

where $\hat{e}(X)$ denotes the nondimensional amplitude of velocity or displacement of the moving cylinder and $\bar{U}$ represents the mean axial flow velocity. As shown in the above equations, the nondimensional unsteady velocities and pressure are defined in terms of $\epsilon_{1/2} = \hat{e}_{1/2}$, where the subscript 1/2 stands for the corresponding local value at $X = 1/2$.

Considering the coordinate transformation with the nondimensional parameters, the governing equations (6.8) and (6.9), can be rewritten in the computational domain (Z,θ) in the nondimensional form

$$
\begin{aligned}
\iota\frac{Re_s}{4}h^2\hat{u} \;-\; \iota\frac{Re_s}{4}\frac{h^2}{l}\frac{\partial\hat{p}}{\partial X} + \frac{Re}{8}\left\{\frac{h}{l}\hat{U}\frac{\partial\hat{u}}{\partial X} - 2\hat{v}\frac{\partial\hat{U}}{\partial Z}\right\} = \\
\left[\frac{\partial^2\hat{u}}{\partial Z^2} - \sqrt{D}\frac{\partial\hat{u}}{\partial Z} + D\frac{\partial^2\hat{u}}{\partial\theta^2} + \frac{h^2}{4l^2}\frac{\partial^2\hat{u}}{\partial X^2}\right]\,, \\
\iota\frac{Re_s}{4}h^2\hat{w} \;-\; \iota\frac{Re_s}{2}h\sqrt{D}\,\frac{\partial\hat{p}}{\partial\theta} + \frac{Re}{8}\frac{h}{l}\hat{U}\frac{\partial\hat{w}}{\partial X} =
\end{aligned}
$$

$$\left[\frac{\partial^2\hat{w}}{\partial Z^2} - \sqrt{D}\frac{\partial\hat{w}}{\partial Z} + D\frac{\partial^2\hat{w}}{\partial\theta^2} + \frac{h^2}{4l^2}\frac{\partial^2\hat{u}}{\partial X^2} - D\left\{\hat{w} - 2\frac{\partial\hat{v}}{\partial\theta}\right\}\right],$$

$$\iota\frac{Re_s}{4}h^2\hat{v} + \iota\frac{Re_s}{2}h\frac{\partial\hat{p}}{\partial Z} + \frac{Re}{8}\frac{h}{l}\hat{U}\frac{\partial\hat{v}}{\partial X} =$$

$$\left[\frac{\partial^2\hat{v}}{\partial Z^2} - \sqrt{D}\frac{\partial\hat{v}}{\partial Z} + D\frac{\partial^2\hat{w}}{\partial\theta^2} + \frac{h^2}{4l^2}\frac{\partial^2\hat{u}}{\partial X^2} - D\left\{\hat{v} + 2\frac{\partial\hat{w}}{\partial\theta}\right\}\right], \quad (6.13)$$

$$\frac{\partial\hat{v}}{\partial Z} - \sqrt{D}\hat{v} - \sqrt{D}\frac{\partial\hat{w}}{\partial\theta} - \frac{h}{2l}\frac{\partial\hat{u}}{\partial X} = 0, \quad (6.14)$$

where $D = \{h/[2+h(1-Z)]\}^2$. For a concentric annulus, the nondimensional annular space, h, is constant.

In order to get the system equations based on the collocation finite difference method, the nondimensional parameters can be expressed in terms of Chebyshev polynomials and Fourier expansions, as shown in the previous chapter. As compared to the previous expansion forms, the unknown coefficients are dependent on the axial coordinate. Using the spectral expansion for the flexural motion of the inner cylinder, the following types of expansions can be considered for the fluid-dynamic properties in the three-dimensional annular space

$$\begin{aligned}
\hat{u} &= \sum_{j=0}^{m} U_j(X)\,T_j(Z)\cos\theta, \\
\hat{w} &= \sum_{j=0}^{m} W_j(X)\,T_j(Z)\sin\theta, \\
\hat{v} &= \sum_{j=0}^{m} V_j(X)\,T_j(Z)\cos\theta, \\
\hat{p} &= \sum_{j=0}^{m-2} P_j(X)\,T_j(Z)\cos\theta, \quad (6.15)
\end{aligned}$$

where the unknown coefficients U_j, W_j, V_j and P_j can be decomposed into real and imaginary components.

Taking account of the expansion forms shown in the above equations, the governing equations and continuity equation can be expressed based on the hybrid scheme as

$$\sum_{j=0}^{m}\begin{pmatrix} U_j\left[T_j''(Z) - \sqrt{D}\,T_j'(Z) - D\,T_j(Z) - \iota\frac{Re_s}{4}h^2\,T_j(Z)\right. \\ -(\frac{h}{l})^2\frac{1}{2(\Delta X_e\,\Delta X_w)}T_j(Z) - \frac{Re}{4}\frac{h}{l}\frac{\hat{U}}{\Delta X_e+\Delta X_w}[\![1,0]\!]\,T_j(Z)] \\ +V_j\frac{Re}{4}\hat{U}'T_j(Z) \end{pmatrix}_P$$

$$+\sum_{j=0}^{m}\begin{pmatrix} U_j\left[\frac{1}{2(\Delta X_e+\Delta X_w)\Delta X_e}(\frac{h}{l})^2-\frac{Re}{8}\frac{h}{l}\frac{\hat{U}}{\Delta X_e+\Delta X_w}[\![0,1]\!]\right]T_j(Z) \\ +\iota P_j\frac{Re_s}{4}\frac{h^2}{l}\frac{1}{\Delta X_e+\Delta X_w}T_j(Z)\end{pmatrix}_E$$

$$+\sum_{j=0}^{m}\begin{pmatrix} U_j\left[\frac{1}{2(\Delta X_e+\Delta X_w)\Delta X_w}(\frac{h}{l})^2+\frac{Re}{8}\frac{h}{l}\frac{\hat{U}}{\Delta X_e+\Delta X_w}[\![2,1]\!]\right]T_j(Z) \\ -\iota P_j\frac{Re_s}{4}\frac{h^2}{l}\frac{1}{\Delta X_e+\Delta X_w}T_j(Z)\end{pmatrix}_W = 0\,,$$

$$\sum_{j=0}^{m}\begin{pmatrix} W_j\left[T_j''(Z)-\sqrt{D}\,T_j'(Z)-2D\,T_j(Z)\right. \\ -\iota\frac{Re_s}{4}h^2\,T_j(Z)-(\frac{h}{l})^2\frac{1}{2(\Delta X_e\Delta X_w)}T_j(Z)-\left.\frac{Re}{4}\frac{h}{l}\frac{\hat{U}}{\Delta X_e+\Delta X_w}[\![1,0]\!]\,T_j(Z)\right] \\ -2V_jT_j(Z)-\iota P_j\frac{Re_s}{2}h\sqrt{D}T_j(Z)\end{pmatrix}_P$$

$$+\sum_{j=0}^{m}\left(W_j\left[\frac{1}{2(\Delta X_e+\Delta X_w)\Delta X_e}(\frac{h}{l})^2-\frac{Re}{8}\frac{h}{l}\frac{\hat{U}}{\Delta X_e+\Delta X_w}[\![0,1]\!]\right]T_j(Z)\right)_E$$

$$+\sum_{j=0}^{m}\left(W_j\left[\frac{1}{2(\Delta X_e+\Delta X_w)\Delta X_w}(\frac{h}{l})^2+\frac{Re}{8}\frac{h}{l}\frac{\hat{U}}{\Delta X_e+\Delta X_w}[\![2,1]\!]\right]T_j(Z)\right)_W = 0\,,$$

$$\sum_{j=0}^{m}\begin{pmatrix} V_j\left[T_j''(Z)-\sqrt{D}\,T_j'(Z)-2D\,T_j(Z)\right. \\ -\iota\frac{Re_s}{4}h^2\,T_j(Z)-(\frac{h}{l})^2\frac{1}{2(\Delta X_e\Delta X_w)}T_j(Z)-\left.\frac{Re}{2}\frac{h}{l}\frac{\hat{U}}{\Delta X_e+\Delta X_w}[\![1,0]\!]\,T_j(Z)\right] \\ -2W_j\,T_j(Z)-\iota P_j\frac{Re_s}{2}h\,T_j'(Z)\end{pmatrix}_P$$

$$+\sum_{j=0}^{m}\left(V_j\left[\frac{1}{2(\Delta X_e+\Delta X_w)\Delta X_e}(\frac{h}{l})^2-\frac{Re}{8}\frac{h}{l}\frac{\hat{U}}{\Delta X_e+\Delta X_w}[\![0,1]\!]\right]T_j(Z)\right)_E$$

$$+\sum_{j=0}^{m}\left(V_j\left[\frac{1}{2(\Delta X_e+\Delta X_w)\Delta X_w}(\frac{h}{l})^2+\frac{Re}{8}\frac{h}{l}\frac{\hat{U}}{\Delta X_e+\Delta X_w}[\![2,1]\!]\right]T_j(Z)\right)_W = 0\,, \qquad (6.16)$$

$$\sum_{j=0}^{m}\left(V_j\left[T_j'(Z)-\sqrt{D}T_j(Z)\right]-\sqrt{D}\,W_jT_j(Z)\right)_P-\sum_{j=0}^{m}\left(U_j\,\frac{h}{l}\frac{1}{2(\Delta X_e+\Delta X_w)}T_j(Z)\right)_E$$

$$+\sum_{j=0}^{m}\left(U_j\,\frac{h}{l}\frac{1}{2(\Delta X_e+\Delta X_w)}T_j(Z)\right)_W = 0\,. \qquad (6.17)$$

subject to the boundary conditions

$$\sum_{j=0}^{m}U_j(X)T_j(1) = 0\,,$$

$$\sum_{j=0}^{m}V_j(X)T_j(1) = \dot{e}_r(X)\,,$$

$$\sum_{j=0}^{m} W_j(X)\, T_j(1) = -\hat{e}_r(X)\,,$$
$$\sum_{j=0}^{m} U_j(X)\, T_j(-1) = 0\,,$$
$$\sum_{j=0}^{m} V_j(X)\, T_j(-1) = 0\,,$$
$$\sum_{j=0}^{m} W_j(X)\, T_j(-1) = 0\,, \tag{6.18}$$

where the prime and the double prime denote, respectively, the first and second derivatives with respect to the coordinates concerned; for example, $\hat{U}' = d\hat{U}/dZ$ and $T'' = d^2T/dZ^2$.

In the present analysis, a system of linear algebraic equations can be obtained by satisfying the above equations at a finite number of collocation points in the computational domain (Z, Θ), and applying the equations at a finite number of grid points distributed in the axial domain. As a result, the system of equations can be expressed, as a block-tridiagonal system, in the general form

$$S\Delta Q = R\,, \tag{6.19}$$

where ΔQ and R are the vectors for the unknown coefficients and the boundary conditions, respectively. The matrix S represents the block-tridiagonal matrix expressed as

$$S = \begin{bmatrix} P_1 & W_1 & 0 & 0 & 0 & 0 & 0 & 0 \\ E_2 & P_2 & W_2 & 0 & 0 & 0 & 0 & 0 \\ 0 & E_3 & P_3 & W_3 & 0 & 0 & 0 & 0 \\ 0 & 0 & \cdot & \cdot & \cdot & 0 & 0 & 0 \\ 0 & 0 & 0 & \cdot & \cdot & \cdot & 0 & 0 \\ 0 & 0 & 0 & 0 & E_{t-2} & P_{t-2} & W_{t-2} & 0 \\ 0 & 0 & 0 & 0 & 0 & E_{t-1} & P_{t-1} & W_{t-1} \\ 0 & 0 & 0 & 0 & 0 & 0 & E_t & P_t \end{bmatrix}, \tag{6.20}$$

where E_i, P_i and W_i are matrices of order $2 \times [(m-1)+3\times(m+1)]$, concerned with the ith grid point, and the subscript t denotes the number of total grid points considered.

When smooth variations of fluid quantities along the axial direction are expected, it is convenient to have uniformly distributed grid points, $\Delta X_e = \Delta X_w$. In the present analysis with the flexible cylinder, which experiences small-amplitude oscillations, it is

possible to use a uniform mesh space. With this uniform step size, the submatrix can be expressed as

$$\begin{aligned} E_1 &= E_2 = E_3 = \cdots = E_t \,, \\ P_1 &= P_2 = P_3 = \cdots = P_t \,, \\ W_1 &= W_2 = W_3 = \cdots = W_t \,. \end{aligned} \tag{6.21}$$

Therefore, the storage required for the system equations can be reduced. For the two-dimensional viscous-flow problem presented in the previous chapter, the system of equations can be obtained by eliminating the convective terms and the axial derivatives of the diffusion terms, eventually to be expressed as only submatrix P.

To obtain the numerical solution, the LU decompsition method is utilized, as mentioned before. The LU decomposition method, which is one of the direct methods, gives the solution in a finite and predeterminable number of operations. This method has proven to be a very useful and efficient tool for solving the block-tridiagonal system of equations.

6.1.3 Stress Components and Formulation of Fluid-Dynamic Forces

In order to formulate the fluid-dynamic forces acting on the moving cylinder, the stress components including the unsteady pressure, generated by the flexural motion, are considered, as shown in the previous chapter. By circumferential line integration of the stress components, the unsteady fluid-dynamic forces are obtained. The analysis has now sufficiently progressed to evaluate the unsteady lateral forces.

The resulting fluid-dynamic forces, acting on the cylinder in the direction of oscillatory motion, can be calculated by the following equation

$$F_l(x,t) = \int_0^{2\pi} a \left(\tau_{rr} \,|_{r=a} \cos\Theta - \tau_{r\Theta} \,|_{r=a} \sin\Theta + \tau_{rx} \,|_{r=a} \, \frac{de_l}{dx} \right) d\Theta \,, \tag{6.22}$$

where the stresses are expressed as

$$\tau_{rr}(x,r,\Theta,t) = -p^* + 2\mu \frac{\partial v^*}{\partial r} \,,$$

$$\tau_{r\Theta}(x,r,\Theta,t) = \mu\left\{\frac{\partial w^*}{\partial r} + \frac{w^*}{r} + \frac{1}{r}\frac{\partial v^*}{\partial \Theta}\right\},$$
$$\tau_{rx}(x,r,\Theta,t) = \mu\left\{\frac{\partial u^*}{\partial r} + \frac{\partial v^*}{\partial x}\right\}, \qquad (6.23)$$

The integral effect of the stress component τ_{rx}, acting in x-direction on a surface whose normal vector points in r-direction, on the fluid-dynamic forces is null.

Using the same procedure as in the previous chapter for viscous fluid, the resulting forces can be expressed as

$$f_j(x,t) = \rho\pi a^2\omega^2 a\hat{e}_{1/2}\left\{\Re[\hat{F}(x)] + \iota\Im[\hat{F}(x)]\right\}e^{\omega t}, \qquad (6.24)$$

where the nondimensional fluid-dynamic force, $\hat{F}(x)$, in complex form, is

$$\hat{F}(x) = -\sum_{j=0}^{m}\left\{P_j(x) + \frac{\iota}{Re_s}[V_j^\dagger(x) - W_j^\dagger(x) + W_j(x) - V_j(x)\right\}T_j(1), \qquad (6.25)$$

in which

$$V_j^\dagger(x) = \frac{8}{hc_j}\sum_{q=j+1}^{m-1} qV_q(x), \qquad j+q = \text{odd},$$
$$W_j^\dagger(x) = \frac{8}{hc_j}\sum_{q=j+1}^{m-1} qW_q(x), \qquad j+q = \text{odd}, \qquad (6.26)$$

where $c_0 = 2$ and $c_j = 1 (j > 0)$. The real and imaginary components of the resulting forces, shown in the above equation are in-phase and in quadrature with displacement, respectively.

6.1.4 Numerical Results

For studying the unsteady viscous flow generated by the oscillating inner cylinder subjected to axial flow, first typical distributions of unsteady velocities and then the unsteady fluid-dynamic forces are presented. In order to show the rate of convergence of the numerical solution, the calculations have been conducted for various mesh spacings defined for the finite-difference method. For self-excited flexural motion, it is of interest to estimate the fluid-dynamic forces acting on a slender cylinder. The fluid-dynamic forces obtained by the present numerical method are compared with the results given

by the approximate method in the next section. In the present work, the length-to-radius ratio remains constant, $l = L/a = 15$. The program used for calculating the fluid-dynamic forces and typical results are presented in Appendix G.

As shown before, the fluid-dynamic forces are decomposed into real and imaginary parts. The imaginary component, which is associated with the damping force, is proportional to the velocity of the moving cylinder. The real component is due to inertial excitation and fluid elastic effects. In this analysis, the effects of steady axial flow and oscillatory Reynolds number on the unsteady fluid-dynamic forces will be discussed. Taking account of the nondimensional governing equations (6.13) and (6.14), the nondimensional fluid variables are influenced by the Reynolds number Re, as well as by the oscillatory Reynolds number Re_s.

The variation of the calculated fluid dynamic forces with various mesh spacings between two grid points is shown for the case of $b/a = 1.05$, $Re = 300$ and $Re_s = 5,000$ in Figure 6.2 and 6.3 (the results are obtained with $m = 8$). In Figure 6.2, the results at certain grid points ($X = x/L = 0.25$, 0.5 and 0.75) are presented. As the spacing is decreased, the results appear to converge to a certain value, and then abruptly diverge. The character of these results might be caused by a truncation error for coarse mesh spacings and by a round-off error for fine mesh spacings. In other words, the truncation error might decrease slightly with decreasing mesh space; however, the round-off error, which is usually generated for a large matrix system, becomes larger and eventually dominates. The influence of mesh size, $\Delta X = 0.083$, 0.1, 0.125 and 0.143, on the fluid-dynamic forces along the axial coordinate is shown in Figure 6.3. Even though its effect in the range of the present mesh spacing is small, the imaginary component is more influenced than the real one by the spacing. Also, the effect of the mesh spacing is slightly larger at upstream points ($X < 0.5$) than at downstream ones ($X > 0.5$) – this tendency might be due to the mathematical procedure based on the LU decomposition method. Considering these results, the suitable mesh spacing for the given problem can be selected. For the present case, the optimized spacing should be $\Delta X = 0.1$.

Typical results of the nondimensional amplitude of the unsteady velocities across

the annular space are shown in Figure 6.4(a,b,c) for the case of $b/a = 1.25$, $Re = 626$ and $Re_s = 5,000$ with $m = 8$ at $X = 0.3$, 0.5 and 0.7. As compared to the results given for translational motion without axial steady flow (given in the previous chapter), the (a) circumferential and (b) radial components have similar distributions; the distributions of the axial ones are shown in Figure 6.4(c). By inspection of equations (6.24) and (6.25), the nondimensional pressure $\hat{p} = p^*/(\rho a^2 \omega^2 a \hat{e}_{1/2} e^{i\omega t})$ has almost the same order of magnitude as the forces; this means that the resulting forces are mainly affected by unsteady pressure. Thus, the pressure distribution along the axial direction is not shown in the present work.

The influence of the Reynolds number ($Re = 0$, 626 and 1,256) on the forces along the axial direction is presented in Figure 6.5 for $b/a = 1.25$ and $Re_s = 5,000$ for a mesh spacing $\Delta X = 0.1$. It is found that the real component of fluid dynamic forces is only slightly dependent on the Reynolds number; however, the imaginary one is strongly influenced by the Reynolds number. As shown in the figure, it is obvious that the real components are proportional to the acceleration of the moving cylinder, mainly influenced by the inertia force. The damping forces, related to the imaginary component, might be caused by the combined effects of the unsteady viscous drag and the equivalent Coriolis force due to the mean flow (associated with cylinder-motion-induced rotation of the fluid, superposed on the axial velocity). For flexural motion in the first mode, the viscous drag and the Coriolis terms are symmetric and antisymmetric with respect to the middle ($X = 1/2$), respectively, since the former is in phase with displacement of the cylinder, while the other is proportional to the first derivative of the displacement. With increasing Reynolds number (i.e., increasing axial flow velocity), the equivalent Coriolis term becomes larger.

Calculations have been conducted to investigate the effect of the oscillatory Reynolds number ($Re_s = 500$, 5,000 and 10,000) for $b/a = 1.25$ and $Re = 626$ with $\Delta X = 0.1$ and $m = 6$. The results are shown in Figure 6.6. For the low value of $Re_s = 500$, the effect on the real part of the force (including the viscous effect as shown in the previous chapter) is relatively large. The ratio of the imaginary component to

the real one becomes smaller with increasing oscillatory Reynolds number; its effect on the forces is less than 15% in the case of $b/a = 1.25$ with $Re_s = 5,000$ or $10,000$. However, the viscous effect on the damping force is important for very narrow annular configurations.

6.2 APPROXIMATE SEMI-ANALYTICAL METHOD

The principal aim of this section is to estimate the fluid-dynamic forces acting on the flexible inner cylinder with a simplified method. The numerical results obtained in the previous section will be compared to the approximate results obtained in this section. This is one of the necessary procedures to validate the newly develped numerical method, since there are no other previous results to be used for comparison. For this purpose, the approximate analytical method, developed in Chapter 2, will be modified to obtain an improved unsteady viscous-flow solution.

The fluid-dynamic forces are formulated, first assuming the case of an unsteady potential(inviscid) flow, and then considering also the main effects of fluid viscosity. The unsteady inviscid force will be obtained by the numerical approach based on the spectral method with the aid of the separation of variables method, which is more rigorous than the previous analytical method; however, the viscous effects are approximated analytically by the same principles as in Chapter 2. This is the reason why the method is called semi-analytical. This analysis for potential flow is less restrictive on the size of the annular passage, which will be shown later. The present results are also compared to ones obtained by the previous analytical method discussed in Chapter 2, especially for narrow annular configurations.

Based on the assumption of small-amplitude oscillations of the flexible centrebody in an annulus, the two flow fields, potential and viscous, are considered to simplify the approach of this problem. The unsteady viscous forces are formulated by considering the mean-circumferential-flow velocity obtained by potental flow theory. The direction of the mean-flow velocity, which is considered to oscillate, is then deter-

mined, and the unsteady viscous pressure drop along the circumferential direction and the shear stress acting on the wall are evaluated.

The axial steady flow is assumed to be a fully developed laminar flow characterized by the mean-flow velocity $\bar{U}$, static pressure P_∞ and the fluid density ρ, which is considered constant.

6.2.1 Derivation of the Inviscid Force

With no separation in the annular flow, the inviscid forces are derived by potential flow theory. For incompressible fluid, the unsteady governing equation is expressed in terms of the unsteady velocity potential ϕ, in the form of the Laplace equation:

$$\nabla^2\phi = \frac{\partial^2\phi}{\partial x^2} + \frac{\partial^2\phi}{\partial r^2} + \frac{1}{r}\frac{\partial\phi}{\partial r} + \frac{1}{r^2}\frac{\partial^2\phi}{\partial\Theta^2} = 0\,, \tag{6.27}$$

subject to the boundary conditions

$$\begin{aligned} \left.\frac{\partial\phi}{\partial r}\right|_{r=a} &= \frac{\partial e_r}{\partial t} + \left[\frac{\partial\phi}{\partial x}\frac{\partial e_r}{\partial x} + \frac{1}{r}\frac{\partial\phi}{\partial\Theta}\frac{1}{r}\frac{\partial e_r}{\partial\Theta}\right]\,, \\ \left.\frac{\partial\phi}{\partial r}\right|_{r=b} &= 0\,, \qquad\qquad \left.\frac{\partial\phi}{\partial x}\right|_{x=-\infty} = \bar{U}\,, \end{aligned} \tag{6.28}$$

where the radial displacement, $e_r(x,\Theta,t)$, is expressed in terms of the eigenfunctions, ψ_k, of the corresponding beam - see equations (2.29) and (2.30).

Using the separation of variables method, the velocity potential $\phi(x,r,\Theta,t)$ may be written in the form

$$\phi(x,r,\Theta,t) = \sum_k a_k\hat{\phi}_k(x,r)\cos\Theta e^{i\omega t}\,, \tag{6.29}$$

where the reduced potentials $\hat{\phi}_k(x,r)$ can be expressed as

$$\hat{\phi}_k(x,Z) = f_k(x)F_k(Z)\,, \tag{6.30}$$

in terms of new coordinate $Z = 1 - 2(r-a)/H$.

Taking into account the coordinate transformation, the reduced potentials, $\hat{\phi}_k(x,Z)$, must satisfy the Laplace equation in the computational domain (Z,θ), *i.e.*

$$\frac{a^2h^2}{4}\frac{\partial^2\hat{\phi}_k}{\partial x^2} + \frac{\partial^2\hat{\phi}_k}{\partial Z^2} - \sqrt{D}\frac{\partial\hat{\phi}_k}{\partial Z} - D\,\hat{\phi}_k = 0\,, \tag{6.31}$$

with the boundray conditions

$$\left.\frac{\partial\hat{\phi}_k}{\partial Z}\right|_{Z=-1} = 0\,, \qquad \left.\frac{\partial\hat{\phi}_k}{\partial Z}\right|_{Z=1} = -\frac{ah}{2}[\iota\omega\psi_k(x) + \bar{U}\psi_k'(x)]\,, \tag{6.32}$$

where the prime denotes differentiation with respect to x, the nondimensional annular space is expressed as $h = (b-a)/a = H/a$ and D is shown in equation (4.5). Comparing the above equations with equations (2.35) and (2.36), it is obvious that this potential theory is not restricted to very narrow annuli. Considering the normal-mode expansion for the motion of cylinder, which can be separated into trigonometric and hyperbolic components, it is more convenient to define the reduced-motion potentials, $\hat{\phi}_{1k}$ and $\hat{\phi}_{2k}$, as follows:

$$\hat{\phi}_k(x,Z) = \sum_{s=1}^{2} f_{sk}(x)F_{sk}(Z) = \hat{\phi}_{1k}(x,Z) + \hat{\phi}_{2k}(x,Z)\,, \tag{6.33}$$

where

$$\hat{\phi}_{1k}(x,Z) = [A_a\cos\beta_k x + A_b\sin\beta_k x]\sum_j \hat{\Phi}_{1kj}T_j(Z)\,,$$

$$\hat{\phi}_{2k}(x,Z) = [B_a\cosh\beta_k x + B_b\sinh\beta_k x]\sum_j \hat{\Phi}_{2kj}T_j(Z)\,,$$

in terms of the eigenvalues, $\beta_k L$, of the eigenfunctions and the expansion forms of Chebyshev polynomials, $T_j(Z)$. In the above equations, the subscripts 1 and 2, stand for the trigonometric and hyperbolic terms, respectively.

Substituting the reduced-motion potentials into the governing equation leads to

$$\sum_{j=0}^{m}\hat{\Phi}_{ikj}T_j''(Z) - \sqrt{D}\hat{\Phi}_{ikj}T'(Z) - \left[D \pm \left(\frac{ah\beta_k}{2}\right)^2\right]\hat{\Phi}_{ikj}T_j(Z) = 0\,, \tag{6.34}$$

subject to the boundray conditions

$$\sum_{j=0}^{m}\sum_{s=1}^{2} f_{sk}(x)\hat{\Phi}_{skj}T_j'(-1) = 0\,,$$

$$\sum_{j=0}^{m}\sum_{s=1}^{2} f_{sk}(x)\hat{\Phi}_{skj}T_j'(1) = -\frac{ah}{2}\sum_{s=1}^{2}[\iota\omega\psi_{sk}(x) + \bar{U}\psi_{sk}'(x)]\,, \tag{6.35}$$

where the two sets of solutions, $s = 1$ and 2, arising from $+\beta_k^2$ and $-\beta_k^2$ in the above equations can each be associated with either ψ_{1k} or ψ_{2k}, defined in equation (2.31) for the trigonometric and hyperbolic components of the eigenfunctions, respectively.

Considering the $+\beta_k^2$ case for the trigonometric components, the boundary conditions can be rewritten

$$-\frac{ah}{2}[\iota\omega\psi_{1k}(x)+\bar{U}\psi'_{1k}(x)] = [A_a\cos\beta_k x + A_b\sin\beta_k x]\sum_{j=0}^{m}\hat{\Phi}_{1kj}T'_j(1)\,, \qquad (6.36)$$

through which the constants, A_a and A_b, may be determined. Proceeding similarly, the constants, B_a and B_b associated with $-\beta_k^2$, may also be determined. Hence, the unknown constants are found to be

$$A_a = -\frac{ah}{2}[-\iota\omega+\bar{U}\sigma_k\beta_k]\,, \qquad A_b = -\frac{ah}{2}[\iota\omega\sigma_k+\bar{U}\beta_k]\,,$$

$$B_a = -\frac{ah}{2}[\iota\omega-\bar{U}\sigma_k\beta_k]\,, \qquad B_b = -\frac{ah}{2}[-\iota\omega\sigma_k+\bar{U}\beta_k]\,, \qquad (6.37)$$

and the boundary conditions are reduced to

$$\sum_{j=0}^{m}\hat{\Phi}_{ekj}T'_j(1) = 1\,, \qquad \sum_{j=0}^{m}\hat{\Phi}_{ekj}T'_j(-1) = 0\,, \qquad (6.38)$$

where σ_k was defined in equation (2.31).

Imposing the governing equation (6.34) at a finite number $(m-1)$ of collocation points, equally distributed in the radial direction and considering the above boundary conditions, the solution of the reduced potential $\hat{\phi}_k$ can be completely determined from the algebraic equation obtained. Thus, the reduced potential can be evaluated on the surface of the moving cylinder $(Z=1)$:

$$\hat{\phi}_k(x,1) = -a\sum_{e=1}^{2}G_{ek}[\iota\omega\psi_{ek}(x)+\bar{U}\psi_{ek}(x)]\,, \qquad (6.39)$$

where

$$G_{1k} = \frac{h}{2}\sum_{j=0}^{m}\hat{\Phi}_{1kj}\,, \qquad G_{2k} = \frac{h}{2}\sum_{j=0}^{m}\hat{\Phi}_{2kj}\,. \qquad (6.40)$$

Substituting the solution of the unsteady velocity potential into the unsteady Bernoulli equation (2.5) with the aid of $d\phi_e/dx = \bar{U}$ and integrating around the circumference of the inner cylinder, the unsteady inviscid force is found to be

$$F_p(x,t) = -\rho\pi a^2 e^{\iota\omega t}\sum_k a_k(-\omega^2 P_{k2}+\iota\omega P_{k1}+P_{k0})\,, \qquad (6.41)$$

where

$$P_{k2} = \sum_{s=1}^{2} G_{sk}\psi_{sk}, \quad P_{k1} = 2\bar{U}\sum_{s=1}^{2} G_{sk}\psi'_{sk}, \quad P_{k0} = \bar{U}^2\beta_k^2\sum_{s=1}^{2}(-1)^s G_{sk}\psi_{sk}\ . \tag{6.42}$$

The inviscid forces are expressed as the general form shown in Appendix A, where the added mass χ is dependent only on the cross-sectional geometry of the slender body. However, in the present theory which is applicable to cylinders of small length-to-radius ratio, the added mass is dependent on the eigenfunctions of the beam as well as the geometry, as described in the above equation. Therefore, the G_{sk} are equivalent added mass coefficients in this analysis. The inviscid forces are linearly dependent on the lateral displacement of the moving cylinder and on its derivatives with respect to x.

6.2.2 Determination of the Viscous Forces

As shown in the simplified unsteady viscous model of Chapter 2, perturbation terms due to unsteady viscous effects are superimposed on the unsteady terms obtained above; thus, the nondimensional pressure perturbation with respect to $\rho\bar{U}^2$ is defined by

$$\check{p}(x, r, \Theta, t) = \check{p}_v(x, r; \Theta, t) + \check{p}_p(x, r, \Theta, t), \tag{6.43}$$

and simlarly, for the nondimessional velocity components with respect to the mean axial flow velocity, $\check{u}$, $\check{v}$ and $\check{w}$, where the components, $\check{u}_v$, $\check{v}_v$, $\check{w}_v$, and $\check{p}_v$, associated with viscous effects are considered to depend only slightly on Θ and t.

It was found in Chapter 2 that, for laminar flow, the gradient of the pressure perturbation $\check{p}_v$ due to the unsteady viscous effect is expressed as

$$\frac{\partial \check{p}_v}{\partial \xi} = -\frac{24}{h}\frac{1}{Re} = -\frac{c_f}{h} \simeq \frac{\partial P_m}{\partial x}\frac{a}{\rho\bar{U}^2}\ , \tag{6.44}$$

where P_m denotes mean pressure, the nondimensional friction coefficient c_f is defined by

$$c_f = \frac{24}{Re}\ , \tag{6.45}$$

and $Re = \rho\bar{U}D_H/\mu$ is the Reynolds number based on the hydraulic diameter $D_H = 2ha$. In the above equation, ξ is a coordinate directed by the total mean flow velocity, which

fluctuates circumferentially through a small angle ϑ calculated as

$$\sin\vartheta = \bar{w} = \frac{1}{H}\int_{r=a}^{r=b} \breve{w}dr = \sum_k \frac{a_k}{2\bar{U}}\left[\sum_{s=1}^{2} f_{sk}W_{sk}\right]\sin\Theta e^{\iota\omega t}\,, \tag{6.46}$$

where

$$f_{sk} = G_{sk}[\iota\omega\psi_{sk}(x) + \bar{U}\psi'_{sk}(x)]\,,$$

and

$$W_{sk} = \sum_{j=0}^{m}\int_1^1 \frac{2}{2-h(Z-1)}\hat{\Phi}_{skj}T_j(Z)\,dZ\,.$$

The dimensional shear stress on the cylinder in the circumferential direction is found to be

$$\tau_\Theta = \tau\sin\vartheta, \tag{6.47}$$

where

$$\tau = \rho\bar{U}^2\frac{12}{Re} = c_f\frac{1}{2}\rho\bar{U}^2.$$

Now, the unsteady lateral viscous force F_{vl} can be evaluated

$$\begin{aligned} F_{vl} &= -\int_0^{2\pi}[\tau_\Theta\sin\Theta + \rho\bar{U}^2\breve{p}_v\cos\Theta]ad\Theta\,, \\ &= -\rho\pi a^2 e^{\iota\omega t}\sum_k a_k(\iota\omega\bar{P}_{k1} + \bar{P}_{k0})\,, \end{aligned} \tag{6.48}$$

where

$$\bar{P}_{k1} = -\frac{c_f\bar{U}}{2}\frac{2+h}{ah^2}\sum_{s=1}^{2}G_{sk}W_{sk}\psi_{sk}\,,\quad \bar{P}_{k0} = -\frac{c_f\bar{U}^2}{2}\frac{2+h}{ah^2}\sum_{s=1}^{2}G_{sk}W_{sk}\psi'_{sk}\,. \tag{6.49}$$

By inspection of the above equation, it is clear that the lateral viscous forces are dependent on the Reynolds number and the geometry of the system. As mentioned in Chapter 2, the effect of the pressure perturbation is $2/h$ times that of the shear stress, considering the numerator, $2+h \simeq 2$, in the above equation.

Considering the inviscid and lateral viscous forces without taking into account the steady longitudial force, the fluid-dynamic forces are expressed in complex form as

$$F = F_p + F_{vl} = \rho\pi a^2\omega^2 a_1\psi_1(L/2)e^{\iota\omega t}[\Re(\hat{F}) + \iota\Im(\hat{F})]\,, \tag{6.50}$$

where $a_1\psi_1(L/2)e^{\iota\omega t}$ denotes the lateral displacement of the moving cylinder at $x = L/2$.

6.2.3 Comparison with Previous Solutions

The equivalent added-mass coefficients defined in equation (6.40), G_{sk} are predicted by the present theory and then compared with those obtained by the previous theory described in Chapter 2 for situations where both should be applicable. The equivalent added-mass coefficients obtained by the present inviscid-flow theory are presented for slender cylinders ($l = L/a = 20$) with radius ratios, $b/a = 1.05$ and 1.1 ($m = 6$). As shown in Table 6.1, it is seen that there is better agreement for a narrower annulus ($b/a = 1.05$), where the narrow-annulus simplification of the previous theory applies best. The added-mass coefficients obtained by slender-body theory [21], $\chi = [(1+h)^2+1]/[(1+h)^2-1]$. are also presented to compare with the results — see Appendix A (χ is independent on the eigenfunctions as compared to the present results).

Table 6.1 Comparison of equivalent added mass coefficients for concentrically narrow annular flow; $l = L/a = 20$, (a)$b/a = 1.05$ and (b) $b/a = 1.1$

(a)	Previous Results(1)		Present Results(2)		Rel. Diff(%) [(2) − (1)]/(2)	
k	G_{1k}	G_{2k}	G_{1k}	G_{2k}	ΔG_{1k}	ΔG_{2k}
1	18.49	20.68	19.38	21.79	4.5	5.1
2	16.92	23.08	17.66	24.47	4.2	5.2
3	14.99	27.97	15.57	30.05	3.7	6.9

$\lambda = 20.51$

(b)	Previous Results(1)		Present Results(2)		Rel. Diff(%) [(2) − (1)]/(2)	
k	G_{1k}	G_{2k}	G_{1k}	G_{2k}	$1k$	$2k$
1	9.04	10.11	9.92	11.21	8.8	9.9
2	8.27	11.28	9.00	12.67	8.1	11.0
3	7.34	13.66	7.90	15.76	7.2	13.3

$\lambda = 10.52$

In order to compare the present results with those obtained by the collocation finite-difference method, the fluid-dynamic forces including this inviscid force are presented. Before comparing the present approximate results to the numerical results, the nondimensional fluid-dynamic forces, $\Re(\dot{F})$ and $\Im(\dot{F})$, obtained by the present approx-

imate method are compared with those of the approximate analytical method shown in Chapter 2 for $l = 15$ and $Re_s = 5,000$ ($m = 6$). In Figure 6.7, the result is calculated for $b/a = 1.05$ and $Re = 300$, while in Figure 6.8 for $b/a = 1.1$ and $Re = 400$. It is found that the discrepancy becomes smaller for the narrower case, where the both theories are quite applicable. Hence, the present approximate results can be compared with confidence to the present numerical results obtained in Section 6.1.

The present approximate results are compared to the numerical results with $\Delta X = 0.1$ and $m = 7$ for $b/a = 1.05$, $Re = 300$ and $Re_s = 5,000$, where the two theory can be applicable. Good agreement between two results is shown in Figure 6.9. Even for a high oscillatory Reynolds number ($Re_s = 5,000$), the viscous damping force is important for very narrow annular configurations.

6.3 REMARKS

Using the collocation finite difference method, it is possible to predict the fluid-dynamic forces acting on the moving cylinder, systematically. The fluid-dynamic force is dependent on the oscillatory Reynolds number, as well as the ordinary Reynolds number. However, the results cannot be expressed in terms of the oscillatory motion of cylinder explicitly, which would be desirable for the stability analysis of the system.

The strength of the present semi-analytical theory is that the unsteady inviscid forces are predicted numerically without the limitation, shown in the previous analytical theory, of a narrow annular space. Thus, for the system where unsteady inviscid forces are dominant over fluid-dynamic forces, the semi-analytical theory is fairly applicable, for of a finite-length of cylinder and a slightly confined flow. The viscous effects on the fluid-dynamic forces for narrow annular configurations can be estimated by the present approximate method.

A number of significant observations may be made from the results. First, with increasing axial-flow velocity, the Coriolis term, which is associated with the anti-symmetric component of the damping forces with respect to $X = 1/2$ in the present work, becomes larger, almost linearly with flow velocity. This could be important for

wave-propagation studies. The second point of interest is that the fluid-dynamic forces for relatively wide annuli with high oscillatory Reynolds number can be estimated by potential-flow theory: the viscous effect is negligible in this case. However, for very narrow annuli, the damping forces are stronger. These significant damping forces are mainly caused by the unsteady viscous drag, which is more or less linearly dependent on the amplitude of oscillatory motion. Finally, the effect of the unsteady pressure perturbation on the fluid-dynamic forces becomes dominant with respect to the shear stress effect with decreasing annular space.

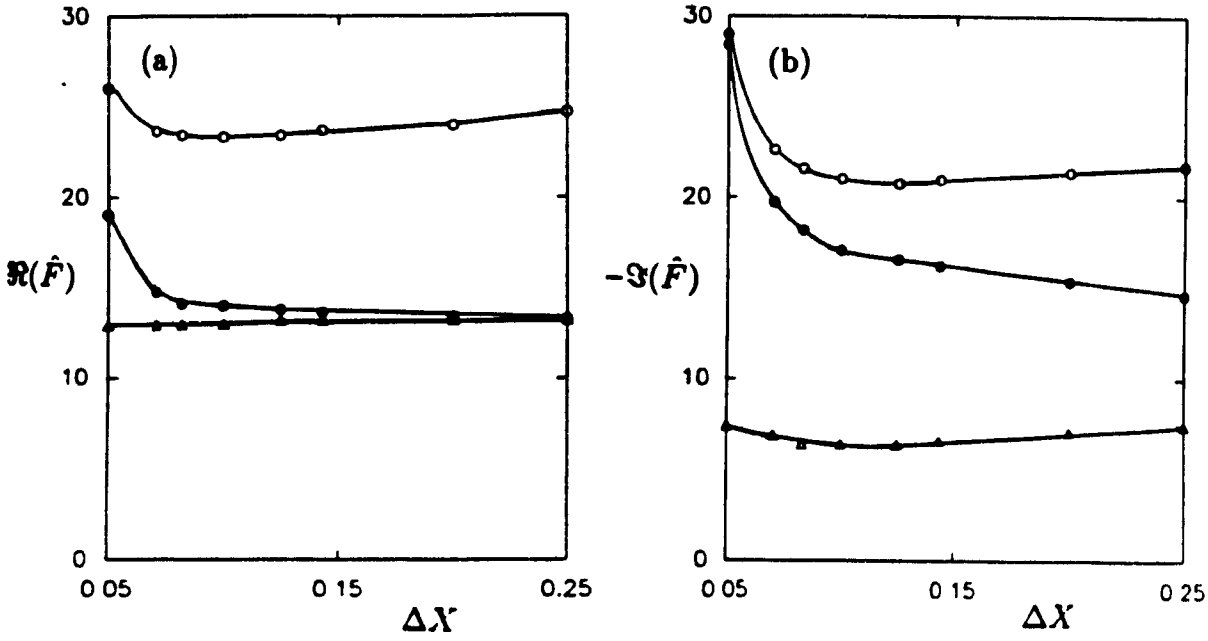

Figure 6.2: Variaton of (a) the real and (b) the imaginary components of the nondimensional fluid-dynamic forces versus the mesh space ΔX for $b/a = 1.05$, $Re = 300$ and $Re_s = 5,000$ ($m = 8$) at various axial positions: •, $X = x/L = 0.25$; o, $X = 0.5$;Δ, $X = 0.75$.

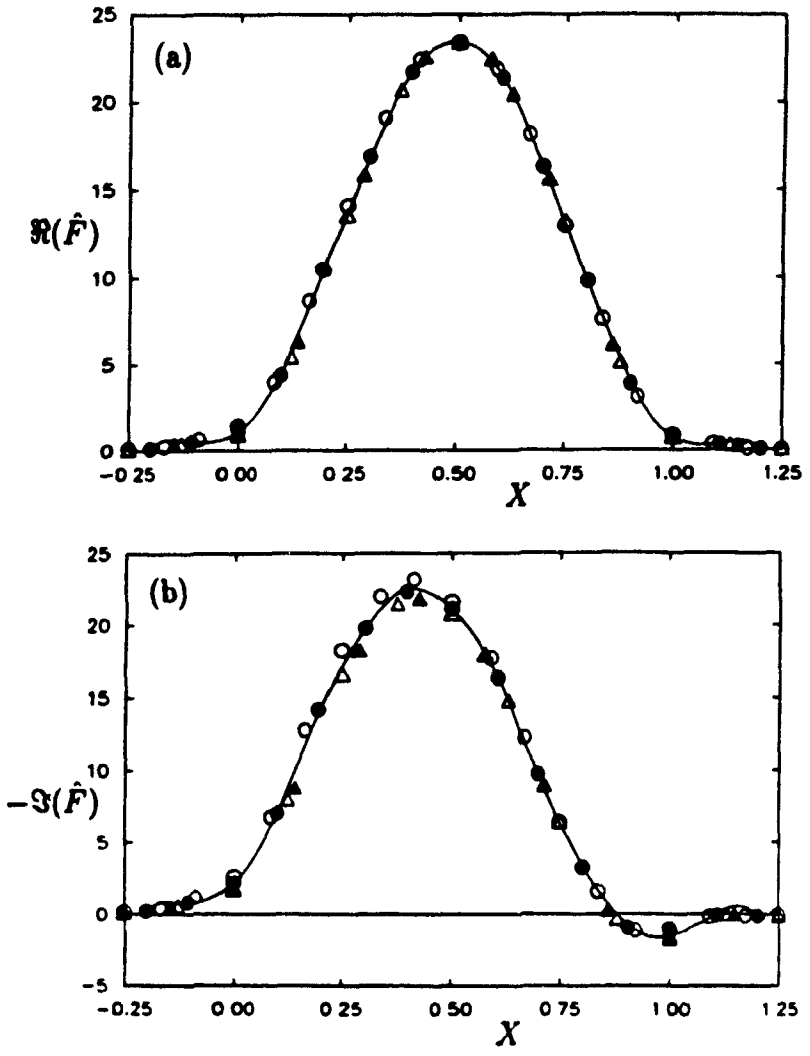

Figure 6.3: Variaton of (a) the real and (b) the imaginary components of the nondimensional fluid-dynamic forces versus axial positions, $X = x/L$, for $b/a = 1.05$, $Re = 300$ and $Re_s = 5,000$ ($m = 8$) with various mesh space: ○, $\Delta X = 0.083$; ●, $\Delta X = 0.1$; △, $\Delta X = 0.125$; ▲, $\Delta X = 0.143$.

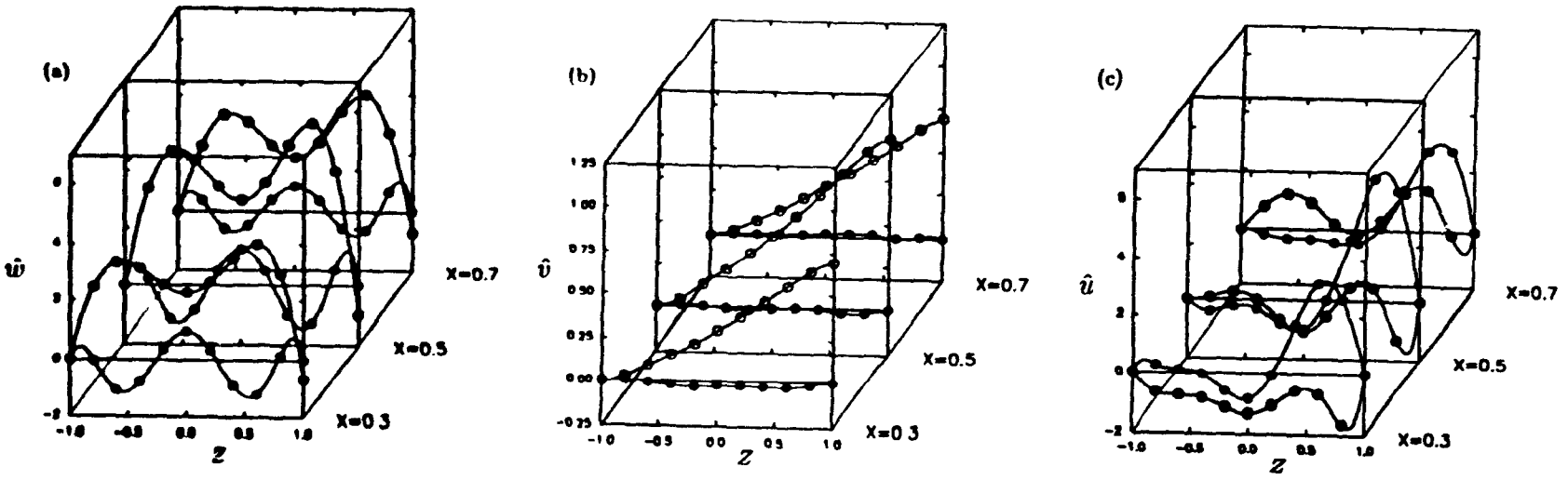

Figure 6.4: The nondimensional amplitude distribution of the unsteady flow velocities for $b/a = 1.25$, $Re = 626$ and $Re_s = 5,000$ across the annular space; (a) the circumferential, (b) radial and (c) axial components. o, real part; •, imaginary part.

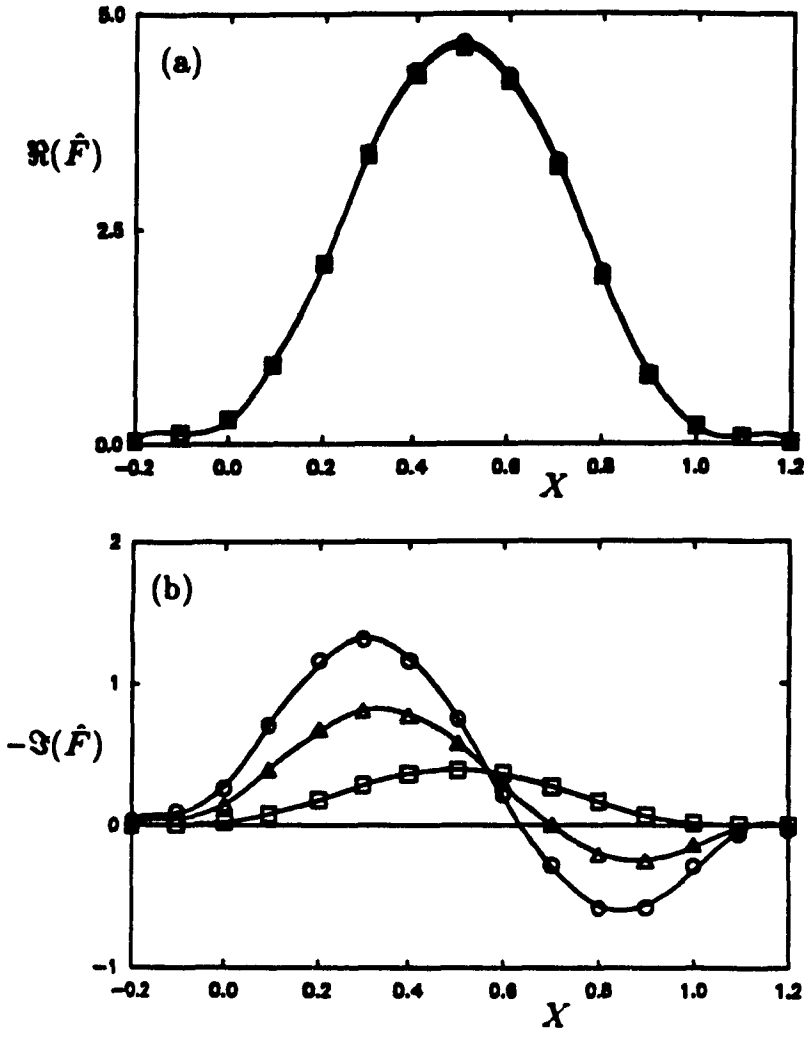

Figure 6.5: Influence of axial flow velocity on (a) the real and (b) the imaginary components of the nondimensional fluid-dynamic forces for $b/a = 1.25$, $L/a = 15$, and $Re_s = 5,000$ with $\Delta X = 0.1$: □, $Re = 0$; △, $Re = 626$; ○, $Re = 1,256$.

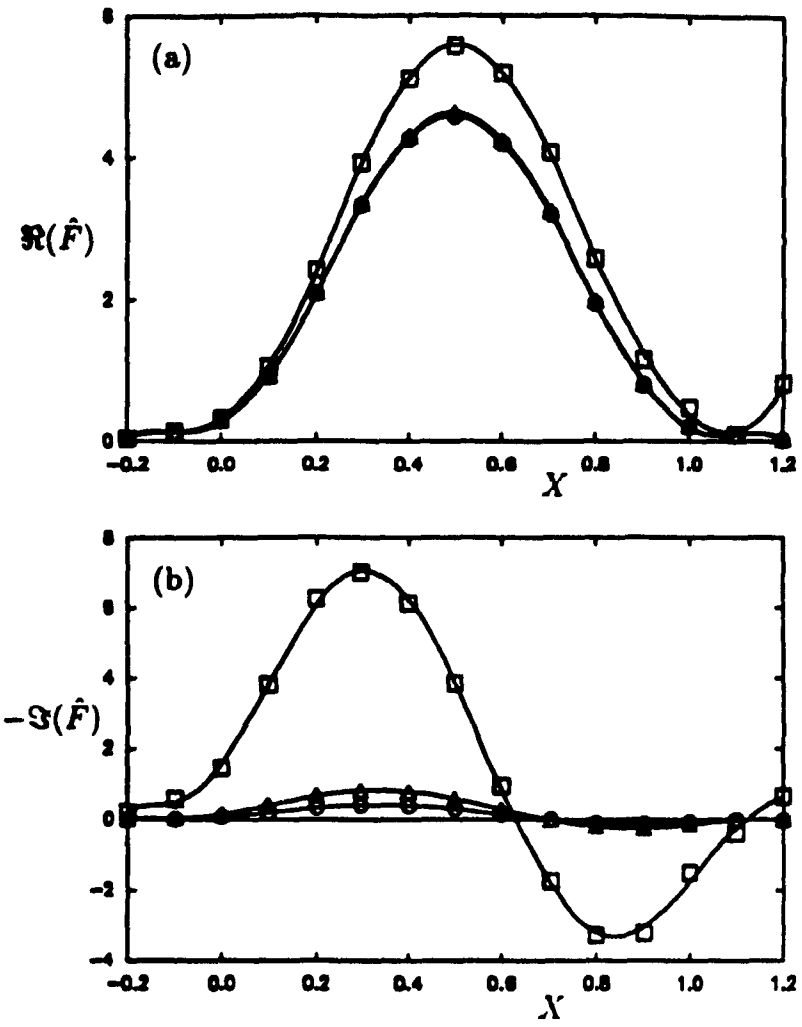

Figure 6.6: Influence of the oscillatory Reynolds number on (a) the real and (b) the imaginary components of the nondimensional fluid-dynamic forces for $b/a = 1.25$, $L/a = 15$, and $Re = 626$ with $\Delta X = 0.1$: □, $Re_s = 500$; △, $Re_s = 5,000$; ○, $Re_s = 10,000$.

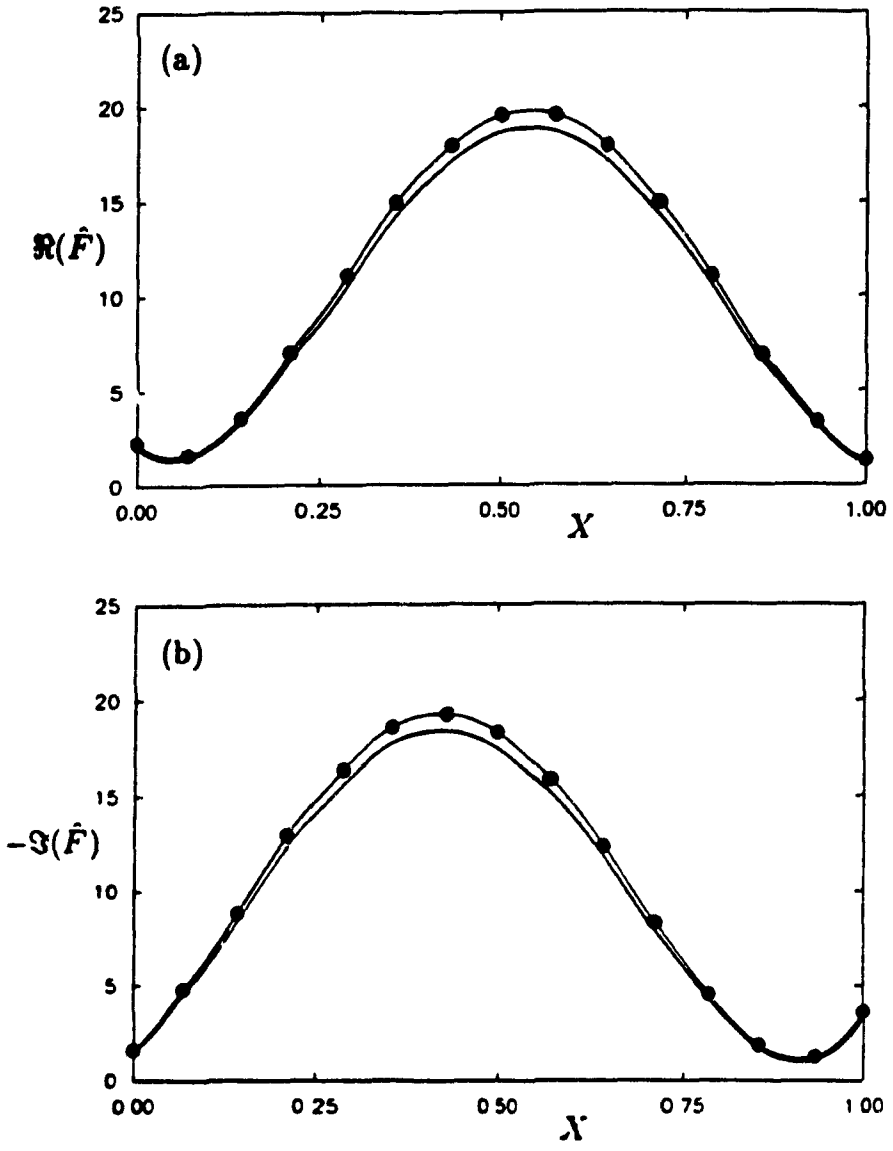

Figure 6.7: Comparison of (a) the real and (b) the imaginary components of the nondimensional fluid-dynamic forces for $b/a = 1.05$, $L/a = 15$, $Re = 300$ and $Re_s = 5,000$, obtained by two methods: $-\bullet-$, the present semi-analytical method; -, the previous analytical method.

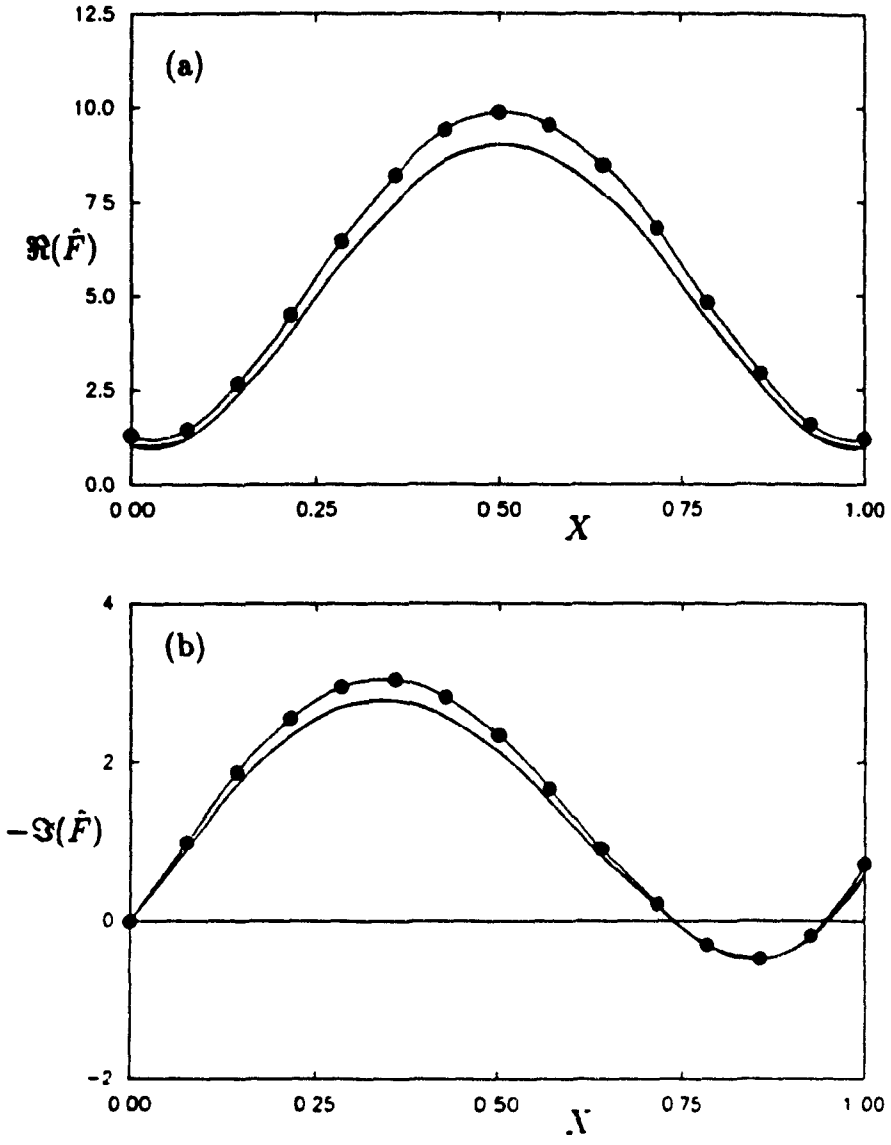

Figure 6.8: Comparison of (a) the real and (b) the imaginary components of the nondimensional fluid-dynamic forces for $b/a = 1.1$, $L/a = 15$, $Re = 400$ and $Re_s = 5,000$, obtained by two methods: $-\bullet-$, the present semi-analytical method; -, the previous analytical method.

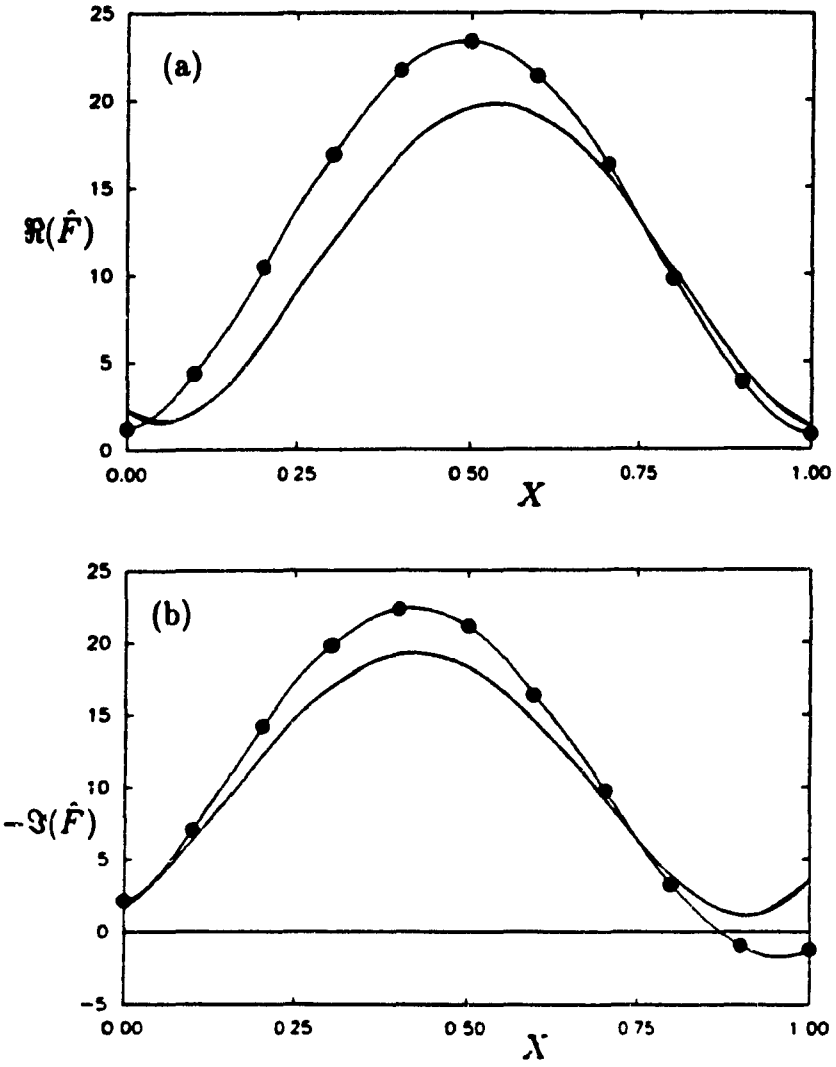

Figure 6.9: Comparison of (a) the real and (b) the imaginary components of the nondimensional fluid-dynamic forces for $b/a = 1.05$, $L/a = 15$, $Re = 300$ and $Re_s = 5,000$, obtained by two methods: $-\bullet-$, the numerical method; -, the semi-analytical method.

Chapter 7

Damping Forces Obtained by a Simplified Analytical Method

When a cylinder vibrates in viscous fluid, the fluid-dynamic forces acting on the moving cylinder are influenced by the fluid properties, including axial-flow velocity, and by the geometry of the system. In general, the resulting forces become larger with the confinement of the annulus. According to the results given in Chapter 5, the added-mass coefficient is mainly affected by the geometry for narrow configurations, especially in the case of a relatively high oscillatory Reynolds number Re_s. The effect of Re_s itself on the added mass is relatively small. Thus, the added mass for narrow annuli can be estimated by potential theory.

In contrast to the added mass, the damping coefficient is strongly dependent on the oscillatory Reynolds number, as well as on the geometry of system. Specially for narrow annular passages, the effect of viscous damping on the fluid-dynamic forces should be considered for the analysis of stability, even if the viscosity of the fluid is relatively small. Due to the confinement, the viscous drag force due to unsteady viscous flow is an important component of the fluid forces.

As shown in the previous chapters, higher-order terms in the Chebyshev polynomials are clearly needed as the oscillatory Reynolds number is increased, since the penetration depth, defined by $\delta_p = \sqrt{2\nu/\omega}$, is very small compared to the annular space between the two cylinders. Thus a very large system of equations is necessary for such problems. Potential-flow theory can of course be utilized to obtain the added

mass, but the viscous forces cannot easily be estimated, because of the large size of the matrices obtained by viscous-flow theory in the spectral collocation method. This is a reason why the approximate method for obtaining the viscous forces with axial flow was developed in Chapter 2 and subsequently in Section 6.2.

By assuming a relatively low frequency and Reynolds number, the previous analytical theories, of Chapters 2 and 6 for the flexural motion of cylinder subject to axial flow, have been formulated to estimate the fluid-dynamic forces. To approximate the viscous force, a parabolic radial distribution of the unsteady circumferential flow velocity in the annular flow was introduced. In the previous chapters devoted to the spectral method, it was shown that the unsteady-flow velocity profile is different from the parabolic one when the ratio of the penetration depth with respect to the annular space is relatively small. The initial motivation was to modify the analytical method and reduce this limitation.

For the future purpose of stability analysis, it is convenient to express the damping forces as explicit functions of the oscillatory frequency and motion of the moving cylinder. With the full viscous theories shown in the previous chapters, the damping coefficient contains the effect of the oscillatory Reynolds number, but the coefficient was calculated when the oscillatory Renolds number was given. Thus, an iteration procedure is required to obtain the eigenfrequencies of a system. On the other hand, it is more convenient to obtain the damping force through an analytical method.

In this chapter, an approximate analytical method has been developed to estimate the damping force for relatively narrow annular configurations: when (i) an inner(rigid) cylinder executes translational oscillation in the plane of symmetry in an eccentric annulus (in Section 7.1), and (ii) a flexible cylinder vibrates in its first mode as a clamped-clamped beam in axial flow (in Section 7.2). This theory is developed for both high and low oscillatory Reynolds numbers. To validate this theory, the results are compared with those obtained by the full viscous theory in the previous chapters.

7.1 UNSTEADY VISCOUS DRAG FORCE DUE TO TRANSLATIONAL OSCILLATION

To develop the present analytical theory, the previously obtained results are carefully examined. According to these results, the unsteady pressure variation across the annular gap is very small and the mean value of the unsteady-flow velocity in the circumferential direction (in phase with the velocity of the moving cylinder) is approximately equal to the velocity obtained by the potential-flow theory. Moreover, the second-order term of Chebyshev polynomials defined for the circumferential-flow velocity is quite large for low oscillatory Reynolds numbers, which means that the distribution of the velocity has a parabolic profile in this case. For high oscillatory Reynolds numbers, the amplitude of the velocity at a certain point, which is situated near the wall ($r = a + \delta_p$ or $r = b - \delta_p$), is almost the same as the corresponding one given by potential-flow theory.

In the present analysis, the unsteady radial-flow velocity is not considered, in order to simplify the problem, so that its effect on the drag forces is neglected. Physically, the unsteady skin friction on the surface is induced mainly by the unsteady circumferential-flow velocity. Also, the unsteady pressure drop in the circumferential direction is affected by the skin friction. Under these considerations, a drastically simplified form of the Navier-Stokes equations is obtained; from that starting point, the problem is formulated to evaluate the viscous drag force.

7.1.1 Formulation

Considering the assumptions defined for the present problem, the simplified momentum equation is obtained, by integrating the Navier-Stokes equation across the annular space for the element shown in Figure 7.1, as

$$-\frac{H}{r}\frac{\partial p^*}{\partial \Theta} - \tau_a - \tau_b = \int_a^b \left[\frac{1}{r}\frac{\partial}{\partial \Theta}(\rho w^{*2}) - \frac{\partial w^*}{\partial t}\right]_{\Theta+\Delta\Theta} dr - \int_a^b \left[\frac{1}{r}\frac{\partial}{\partial \Theta}(\rho w^{*2}) - \frac{\partial w^*}{\partial t}\right]_{\Theta} dr , \tag{7.1}$$

where the skin frictions on the surfaces of the inner and outer cylinder are given by

$$\tau_a = \mu \left.\frac{\partial w^*}{\partial r}\right|_{r=a}, \qquad \tau_b = -\mu \left.\frac{\partial w^*}{\partial r}\right|_{r=b}, \tag{7.2}$$

where w^* denotes the unsteady circumferential flow velocity. By the assumption of small amplitude motion of the cylinder in a narrow annular passage, the right-hand side of equation (7.1) can be neglected.

Introducing the dimensionless parameters, $\hat{p} = p^*/(\rho a^2 \omega^2 \epsilon e^{\iota\omega t})$ and $\hat{w} = w^*/(\iota a \omega \epsilon e^{\iota\omega t})$ as defined in Chapter 5, with the aid of a coordinate transformation, the governing equation for a narrow annulus are nondimensionlized as

$$\frac{\partial \hat{p}}{\partial \theta} = \iota \frac{2}{Re_s} \frac{1 + h/2}{h^2} \left[\left.\frac{\partial \hat{w}}{\partial Z}\right|_{Z=1} - \left.\frac{\partial \hat{w}}{\partial Z}\right|_{Z=-1} \right], \tag{7.3}$$

and the shear stress is obtained by

$$\tau = \mu \frac{\partial w'}{\partial r} = -\iota \rho a^2 \omega^2 \epsilon e^{\iota\omega t} \frac{2}{h Re_s} \frac{\partial \hat{w}}{\partial Z}, \tag{7.4}$$

where the oscillatory Reynolds number is defined by $Re_s = \omega a^2/\nu$ and the nondimensional coordinate $Z = 1 - 2(r - a)/H$.

For the purpose of this simplified analysis, the mean-flow velocity $\bar{w}^*$ across the gap will be calculated by the potential theory given in Chapter 5. From the velocity potential ϕ and the relationship $(w^* = 1/r)\,(\partial\phi/\partial\Theta)$, one can obtain by integrating over the gap

$$\bar{w}^* = \frac{1}{H} \int_a^b \frac{1}{r} \frac{\partial \phi}{\partial \Theta} dr = \frac{1}{a} \int_{-1}^{1} \frac{1}{2 - h(Z-1)} L(\phi) dZ, \tag{7.5}$$

where the operator $L(\phi)$ can be expressed as $L(\phi) = \partial\phi/\partial\theta$ for a narrow annulus or an annulus of relatively small eccentricity.

In the above equation, an analytical potential theory such as the previous one for concentric configurations can be used to obtain the velocity potential ϕ. However, in the present analysis, the numerical solutions based on the following expansion form are utilized

$$o = \iota \omega a^2 \epsilon e^{\iota\omega t} \sum_{j=0}^{m} \sum_{k=0}^{n} \Phi_{jk} T_j(Z) F_k(\theta), \tag{7.6}$$

which have already been defined in Chapter 5. For the present problem, the Fourier function F_k may be expressed as cosine functions as shown in Chapter 5 due to the flow symmetry with respect to the plane of eccentricity. Considering the expansion form with dimensionless parameters, the dimensionless mean-flow velocity, $\bar{\tilde{w}} = \bar{w}^*/(\iota a\omega\epsilon e^{\iota\omega t})$, can be obtained from equation (7.5) as

$$\bar{\tilde{w}} = \sum_{k=0}^{n} k\, s(k\theta) \int_{-1}^{1} \frac{-1}{2-h(Z-1)} \sum_{j=0}^{m} \Phi_{jk} T_j(Z) dZ = \sum_{k=0}^{n} \bar{W}_k\, s(k\theta)\,, \qquad (7.7)$$

where $s(k\theta)$ denotes $\sin k\theta$. By potential theory, the coefficients Φ_{jk} have already been obtained. Hence, the coefficients $\bar{W}_k$ can be determined.

To solve the pressure drop along the circumferential direction, the shear stress on the surface of the cylinders is considered by carefully investigating the distribution of the unsteady circumferential-flow velocity across the annular space for both cases: when (a) the ratio of the penetration depth with respect to annular gap is relatively large and (b) the ratio is relatively small. This ratio is related to the oscillatory Reynolds number by the definition, $\delta_p/H = \sqrt{2/Re_s}\cdot a/H$, where δ_p is the penetration depth.

(a) Case of relatively low oscillatory Reynolds number

As discussed before, the circumferential-flow velocity w^* has a parabolic profile in this case. In this method, the dimensionless flow velocity $\hat{w}$ may be approximated in the following form

$$\hat{w}(Z,\theta) = \sum_{k=0}^{n} (W_{2k}^{\dagger} Z^2 + W_{1k}^{\dagger} Z + W_{0k}^{\dagger})\, s(k\theta)\,, \qquad (7.8)$$

subject to the boundary conditions – see equation (5.36)

$$\sum_{k=0}^{n} (W_{2k}^{\dagger} Z^2 + W_{1k}^{\dagger} Z + W_{0k}^{\dagger})\, s(k\theta)\,|_{Z=1} = -\sin\theta\,,$$

$$\sum_{k=0}^{n} (W_{2k}^{\dagger} Z^2 + W_{1k}^{\dagger} Z + W_{0k}^{\dagger})\, s(k\theta)\,|_{Z=-1} = 0\,.$$

Hence, the mean value, $\bar{\tilde{w}}$, may be obtained by integrating $\hat{w}$ over the annular gap

$$\bar{\tilde{w}} = \frac{1}{2} \sum_{k=0}^{n} \int_{-1}^{1} (W_{2k}^{\dagger} Z^2 + W_{1k}^{\dagger} Z + W_{0k}^{\dagger})\, s(k\theta)\, dZ = \sum_{k=0}^{n} \left(\frac{1}{3} W_{2k}^{\dagger} + W_{0k}^{\dagger}\right) s(k\theta)\,. \qquad (7.9)$$

Taking account of two boundary conditions and of the above equation together with equation (7.7), the three-unknown coefficients could clearly be expressed in terms of W_k in the form

$$W_{2k}^{\dagger} = -\frac{3}{2}\bar{W}_k - \frac{3}{4}\delta\,, \qquad W_{1k}^{\dagger} = -\frac{1}{2}\delta\,, \qquad W_{0k}^{\dagger} = \frac{3}{2}\bar{W}_k + \frac{1}{4}\delta\,, \tag{7.10}$$

where $\delta = 0$ when $k \neq 1$, or $\delta = 1$ when $k = 1$; from which the skin friction on the surface can be obtained. In view of equation (7.3), one ought to derive the following equation from equation (7.8) with the known coefficients $W_{2k}^{\dagger}$, $W_{1k}^{\dagger}$ and $W_{0k}^{\dagger}$, to obtain the pressure distribution,

$$\left.\frac{\partial \hat{w}}{\partial Z}\right|_{Z=1} = -(3\bar{W}_k + 2\delta)\, s(k\theta)\,, \qquad \left.\frac{\partial \hat{w}}{\partial Z}\right|_{Z=-1} = (3\bar{W}_k + \delta)\, s(k\theta)\,. \tag{7.11}$$

(b) Case of relatively high oscillatory Reynolds number

By inspection of the distribution of the unsteady circumferential-flow velocity across the annular space for this case (see Figure 5.5), the radial derivative of the velocity in phase with the velocity of the moving cylinder can be approximated in terms of the penetration depth as

$$\left.\frac{\partial w^*}{\partial r}\right|_{r=a} = \frac{\bar{w}^* + e_v \sin\Theta}{\delta_p}\,, \qquad \left.\frac{\partial w^*}{\partial r}\right|_{r=b} = -\frac{\bar{w}^*}{\delta_p}\,, \tag{7.12}$$

through which the unsteady pressure drop shown in equation (7.1) may be determined. In the above equation, the mean-flow velocity $\bar{w}^*$ has already been obtained by potential theory as shown in equation (7.5). To consider the boundary condition on the surface of the moving inner cylinder, the lateral velocity of the moving cylinder, e_v, is added to the left-hand side of the first equation.

Utilizing the dimensionless parameters in the transformed domain, the above equation can be rewritten in nondimensional form

$$\left.\frac{\partial \hat{w}}{\partial Z}\right|_{Z=1} = -\frac{ah}{2\delta_p}\sum_{k=0}^{n}(\bar{W}_k + \delta)\, s(k\theta)\,,$$

$$\left.\frac{\partial \hat{w}}{\partial Z}\right|_{Z=-1} = \frac{ah}{2\delta_p}\sum_{k=0}^{n}\bar{W}_k\, s(k\theta)\,, \tag{7.13}$$

where the coefficients for the nondimensional mean-flow velocity, $\bar{W}_k$, are defined in equation (7.7). Thus, the unsteady pressure drop and the skin friction on the surfaces of the cylinders can be estimated, considering equations (7.1) and (7.2).

7.1.2 Unsteady Drag force

Having determined skin friction on the surfaces, the unsteady pressure disribution along the circumference may now be found for both the relatively low and high oscillatory Reynolds number. Then the unsteady drag force can be obtained by considering the skin friction on the surface of the moving cylinder and the pressure drop along the circumference of the inner cylinder.

For the case (a) of low oscillatory Reynolds number, substituting equation (7.11) into equation (7.3) leads to

$$\frac{\partial \hat{p}}{\partial \theta} = -\iota \frac{12}{Re_s} \frac{1+h/2}{h^2} \sum_{k=0}^{n} (\bar{W}_k + \delta/2)\, s(k\theta)\,. \tag{7.14}$$

Proceeding similarly with equation (7.13), for the case (b) of high oscillatory Reynolds number, the nondimensional pressure is expressed as

$$\frac{\partial \hat{p}}{\partial \theta} = -\iota \sqrt{\frac{2}{Re_s}} \frac{1+h/2}{h} \sum_{k=0}^{n} (\bar{W}_k + \delta/2)\, s(k\theta)\,. \tag{7.15}$$

Taking account of the pressure and skin friction, the viscous drag forces may be obtained by integrating its components around the cylinder as

$$F_d = -a \int_0^{2\pi} \left(p^* \cos\Theta + \mu \left. \frac{\partial w^*}{\partial r} \right|_{r=a} \sin\Theta \right) d\Theta\,. \tag{7.16}$$

However, some manipulation is required to bring p^*, which is an implicit function of Θ, into a convenient form. In this respect, $p^* \cos\Theta$ is modified as

$$p^* \cos\Theta = \frac{d}{d\Theta}(p^* \sin\Theta) - \frac{dp^*}{d\Theta} \sin\Theta\,. \tag{7.17}$$

The integral of the first term of the right-hand side in the above equation is equal to zero. Hence, the equation of the drag force can be expressed in the nondimensional form

$$\begin{aligned} F_d &= \rho a^2 \omega^2 a \dot{e} e^{\iota\omega t} \int_0^{2\pi} \left(\frac{\partial \hat{p}}{\partial \theta} + \iota \frac{2}{h Re_s} \left. \frac{\partial \hat{w}}{\partial Z} \right|_{Z=1} \right) \sin\theta d\theta \\ &= \iota \rho \pi a^2 \omega^2 a \dot{e} e^{\iota\omega t} \hat{F}_d\,, \end{aligned} \tag{7.18}$$

where $a\hat{e}e^{i\omega t}$ denotes the lateral displacement of oscillatory motion of the cylinder and $\hat{F}_d$ is the nondimensional viscous-damping force.

Substituting equations (7.11) and (7.14) into the above equation for case (a) leads to

$$\hat{F}_d = \hat{F}_{vp} + \hat{F}_{vs} , \tag{7.19}$$

where

$$\hat{F}_{vp} = \frac{-12}{Re_s}\frac{1+h/2}{h^2}(\bar{W}_1 + 1/2) ,$$
$$\hat{F}_{vs} = \frac{-6}{Re_s}\frac{1}{h}(\bar{W}_1 + 2/3) , \tag{7.20}$$

in which the subscripts vp and vs stand for the unsteady pressure and the skin friction terms, respectively. Thus, the damping coefficient due to the viscous drag can be expressed as

$$C_{vd} = -\rho\pi a^2\omega\hat{F}_d . \tag{7.21}$$

Similarly, for case (b),

$$\hat{F}_{vp} = -\sqrt{\frac{2}{Re_s}}\frac{1+h/2}{h}(\bar{W}_1 + 1/2) ,$$
$$\hat{F}_{vs} = -\sqrt{\frac{1}{2Re_s}}\bar{W}_1 . \tag{7.22}$$

Considering these results, the viscous drag force is expressed in terms of an explicit function of the oscillatory Reynold number, since the coefficients Φ_{jk} and $\bar{W}_k$, determined by the potential theory, are dependent on only the geometry of system.

7.2 UNSTEADY DAMPING FORCES DUE TO FLEXURAL OSCILLATION OF A CYLINDER

By inspection of the results given by the full viscous theory based on the collocation-finite-difference method, the added-mass coefficient can be approximately calculated by potential-flow theory for narrow annular configurations since it is mainly affected by the geometry of the system. However, the damping forces are dependent on fluid

properties as well as geometry. In general, it is well known that the damping force acting on a flexible cylinder subject to an axial flow is decomposed into two terms: the viscous-damping force due to the fluid viscosity, as can be seen in the previous section, and a force due to the Coriolis effect associated with the axial flow.

According to the results given in the full viscous theory, the circumferential velocity is almost linearly dependent on the velocity of the flexible cylinder and the profile of this velocity along the radial direction is similar to that obtained in the two-dimensional problem discussed in Chapter 5. Therefore, the viscous-damping forces can be approximated by considering the unsteady pressure drop mainly due to the radial derivative of the unsteady circumferential-flow velocity in annular flow. Hence, the viscous-drag force due to flexural motion of the inner cylinder can be calculated by considering the viscous-damping force F_d obtained by the approximate method for the two-dimensional problem based on the lateral displacement, $e_I(L/2,t)$, as

$$F_{d3} = F_d \frac{e_I(x,t)}{e_I(L/2,t)} , \tag{7.23}$$

where subscript 3 stands for the three-dimensional problem and the lateral displacement $e_I(x,t)$ of the inner cylinder is expressed in terms of eigenfunction, $\psi_1(x)$, which is the first-mode expansion for a clamped-clamped beam as shown in Chapter 2,

$$e_I(x,t) = E(x)\, e^{\iota\omega t} = a_1\psi_1(x)\, e^{\iota\omega t} . \tag{7.24}$$

Thus, the viscous-damping forces can be rewritten in the following form

$$F_{d3} = \iota\rho\pi a^2\omega^2 a\hat{e}(L/2)\, e^{\iota\omega t}\hat{F}_{d3} , \tag{7.25}$$

where $\hat{e} = e_I/(ae^{\iota\omega t})$ and

$$\hat{F}_{d3} = \hat{F}_d \frac{e_I(x,t)}{e_I(L/2,t)} ,$$

in which $\hat{F}_d = \hat{F}_{vp} + \hat{F}_{vo}$ has already been obtained in the previous section as a function of the oscillatory Reynolds numbers.

Taking account of the potential-flow theory based on the slender-body assumption, the damping force due to the axial-flow, which is related to the Coriolis force,

may be estimated by the following equation

$$F_c = -2\rho\pi a^2 \bar{U} \frac{\partial^2 e_I(x,t)}{\partial x \, \partial t} \chi \,, \tag{7.26}$$

where the mean axial flow velocity $\bar{U}$ is obtained by integrating the axial-flow velocity over the annular space and the ratio of confinement is equal to the added-mass coefficient determined by the slender-body potential-flow theory, as $\chi = (b^2 + a^2)/(b^2 - a^2)$.

Utilizing the normal-mode expansion for the flexural motion, the equivalent Coriolis force can be expressed as

$$F_c = \iota\rho\pi a^2 \omega^2 a\hat{e} e^{\omega t} \hat{F}_c \,, \tag{7.27}$$

where

$$\hat{F}_c = -2\frac{\bar{U}\beta_1}{\omega}\chi\frac{\psi_1'(x)}{\psi_1(L/2)} \,,$$

in which the prime denotes differentiation with respect to x, and $\beta_1 L$ represents the eigenvalue for the first mode of the flexible cylinder.

Considering the viscous drag force and the equivalent Coriolis force, the total damping force acting on the flexible cylinder subject to steady axial flow in a narrow annulus can be calculated approximately by

$$F_{dt} = \iota\rho\pi a^2 \omega^2 a\hat{e} e^{\omega t} (\hat{F}_{d3} + \hat{F}_c) \,. \tag{7.28}$$

7.3 RESULTS AND DISCUSSION

The main purpose of this section is to validate the approximate methods developed for estimating the damping force as influenced by the oscillatory Reynolds number, the geometry of system and the Reynolds number. For that purpose, the present results obtained by the approximate methods are compared to the results given by the viscous theory shown in Chapters 5 and 6.

When the inner cylinder executes translational motion in the plane of symmetry, the calculations have been conducted for the cases of various ratios of the radii, b/a, with a selected oscillatory Reynolds number, rather than attempting an exhaustive

parametric study. In order to investigate the effect of axial flow on the damping force acting on the inner cylinder in a narrow annulus, the damping force has been calculated with the chosen Reynolds number based on hydraulic diameter $2ha$. As shown before, the governing equations formulated for the viscous theories are nondimensionalized in terms of the Reynolds number.

In this study, we are mostly concerned with forces on the centre body *per unit length* and their variation with length. With regard to the Coriolis force, it should be remarked that the integrated force (for $x \in (0, L)$) is zero – although its variation with x is of interest and will be shown in the results that follows.

The viscous-drag force with increasing oscillatory Reynolds number will be discussed for $b/a = 1.25$ and $b/a = 1.4$. The viscous-drag coefficient $\hat{F}_d$ obtained for cases of both low and high oscillatory Reynolds number is shown in Table 7.1, where the results are compared to the corresponding numerical results based on the spectral collocation method. The drag coefficient $\hat{F}_d$ has the same definition as the imaginary one $\Im(\hat{F})$ defined in the previous numerical method.

From the results, it is found that the transition region, where both approximate methods give approximately same value, is situated around $\delta_p/H = 0.2$. Above this ratio of penetration depth, the method developed for low oscillatory Reynolds numbers can be used, while the other one is more suitable for high Re_s. Thus, it is true that the viscous-drag force is dependent on the ratio of the penetration depth to the annular space, which affects the circumferential flow velocity profile in the radial direction.

In Figure 7.2, the nondimensional damping forces for various oscillatory Reynolds numbers ($Re_s = 50, 500, 5,000$ and $50,000$) are illustrated for concentric annular configurations to show the effect of b/a. The results denoted by closed symbols represent the nondimensional force $\hat{F}_{vp}$ obtained by considering only the unsteady pressure. The overall results $\hat{F}_d$, including the effect of skin friction, are denoted by the open symbols. According to the results, the effect of skin friction is relatively small; however, the relative magnitude of the effect of the skin friction versus the unsteady pressure becomes larger with increasing radius ratio b/a. By inspection of equations (7.20) and

(7.22), this can be expected: the ratio between the two results is of the order of h. As compared to the numerical results obtained by viscous-flow theory with the spectral collation method of Chapter 5, good agreement is found between these results and the numerical results.

Table 7.1 Comparison of the drag coefficients $\hat{F}_d$ obtained by the approximate method developed for (a) low and (b) high oscillatory Reynolds number and by the numerical method with various ratios of the penetration depth to the annular space.

b/a	Re_s	δ_p/H	Approximate Result $\hat{F}_d$		Numerical Results $\hat{F}_d$
			(a)	(b)	
1.25	5000	0.08	0.22	0.52	0.53
	1000	0.18	1.08	1.16	1.46
	500	0.25	2.17	1.65	2.44
	100	0.57	10.8	3.68	11.0
	50	0.80	21.7	5.21	22.1
1.4	5000	0.05	0.06	0.26	0.25
	500	0.16	0.64	0.82	0.96
	100	0.36	3.18	1.84	3.34
	50	0.50	6.35	2.60	6.61

When the inner cylinder has translational motion in the plane of axis symmetry in an eccentric annulus, the nondimensional overall drag force $\hat{F}_d$ is presented in Figure 7.3 for $b/a = 1.25$, with oscillatory Reynolds numbers (a) $Re_s = 50$ and (b) $Re_s = 5,000$. For the former case, the calculation is done by the method developed for low oscillatory Reynolds numbers and for the latter case by the method developed for high oscillatory Reynolds numbers. These results are also compared to the numerical solutions. The present approximate method (developed in Section 7.1) is found to be adequate.

In Figure 7.4, the overall damping force including the effect of the axial flow ($Re = 626$ and $1,256$) given by the present approximate method (developed in Section 7.2) is compared to the numerical results shown in Chapter 6 in case of $b/a = 1.25$. As shown in the figure, the nondimensional damping force may be decomposed into

two components for the given flexural motion (the first mode vibration as a clamped-clamped beam): (i) the symmetric component with respect to the middle point $x = L/2$, which is related to the unsteady viscous-drag force and (ii) the antisymmetric one, which is associated with the Coriolis force (axial flow effect). It is shown in Figure 7.4(a) that the antisymmetric component becomes large with increasing Reynolds number. The damping force, containing the effect of the unsteady viscous drag and the axial flow, predicted by the approximate method agrees well with the numerical ones, which means the full viscous theory shown in Chapter 6 is validated indirectly; however the comparisons have been conducted for a special case – slender cylinders subject to narrow annular flow.

Taking account of the above results, the interesting remarks are as follows; (i) the present approximate method can be utilized for estimating the damping force, especially for narrow configurations where the damping force has an important role in the dynamics of system and the virtual mass can be estimated by potential theory; (ii) the damping force can be expressed in terms of the circular frequency of the moving cylinder explicitly through the approximate method – this expression is very convenient to analyse the stability of the system; (iii) the unsteady viscous drag force is propotional to $1/Re_s$ for relatively low oscillatory numbers and to $1/\sqrt{Re_s}$ for relatively high ones.

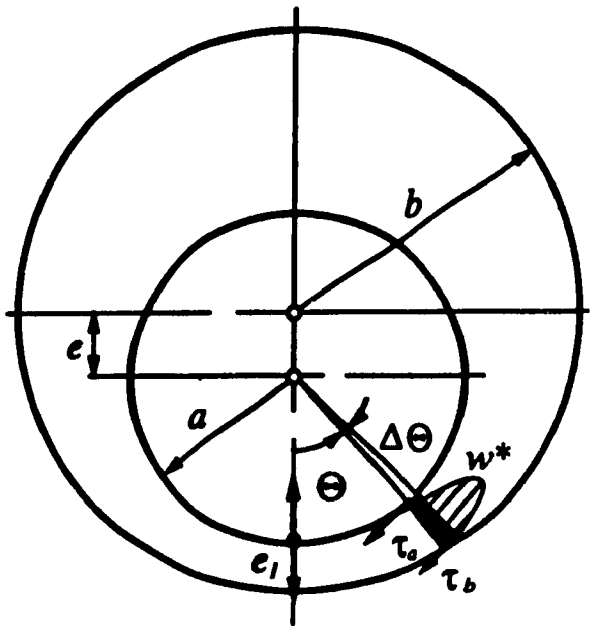

Figure 7.1: The shear stress acting on surface elements of the inner and outer cylinders due to the unsteady circumferential-flow velocity.

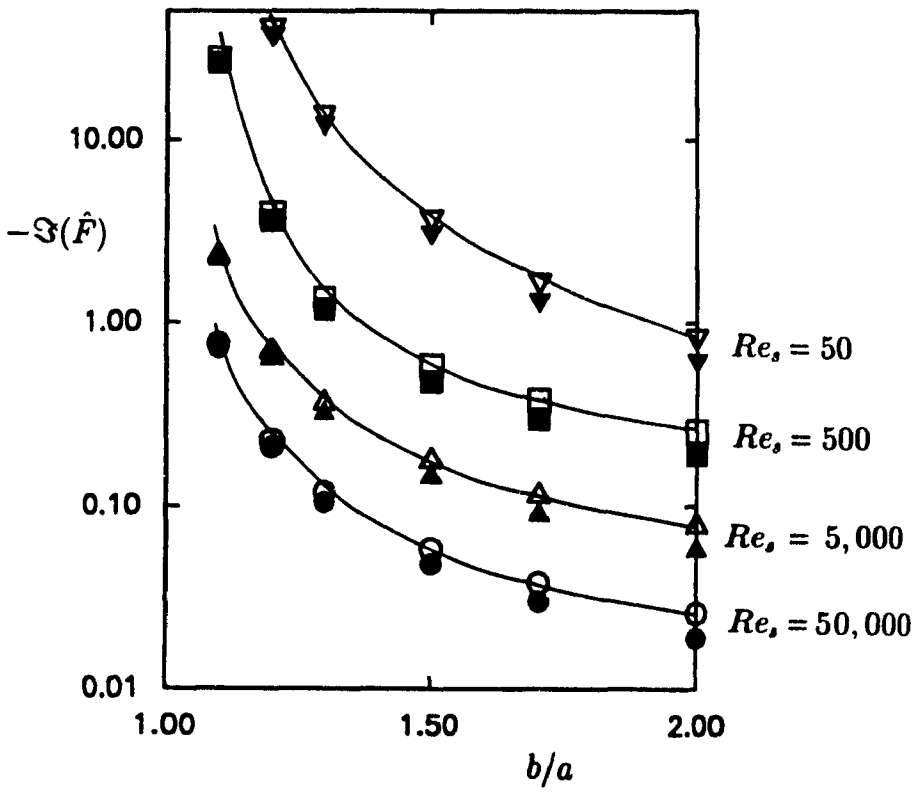

Figure 7.2: Nondimensional viscous-damping force obtained by the approximate method for the translational motion of the inner cylinder in concentric configurations; considering only unsteady pressure(closed symbols), and unsteady shear stress and pressure(open symbols). —, numerical results obtained with the spectral method of Chapter 5.

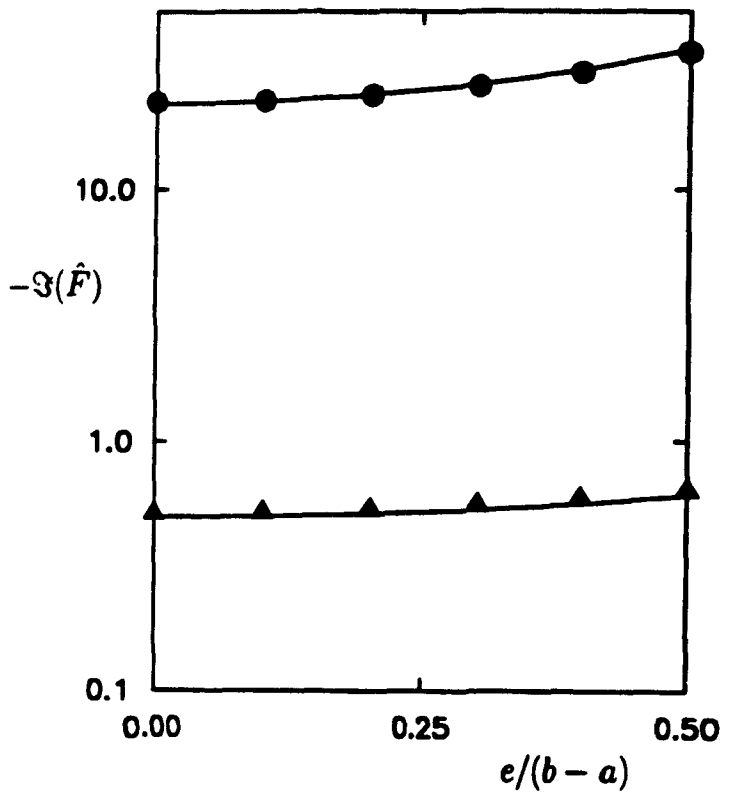

Figure 7.3: Effect of annular eccentricity on the viscous-damping force obtained by the approximate method for the translational motion of the inner cylinder and for $b/a = 1.25$: •, $Re_s = 50$; ▲, $Re_s = 5,000$. Compared with the numerical results obtained with the spectral collocation method of Chapter 5 (—).

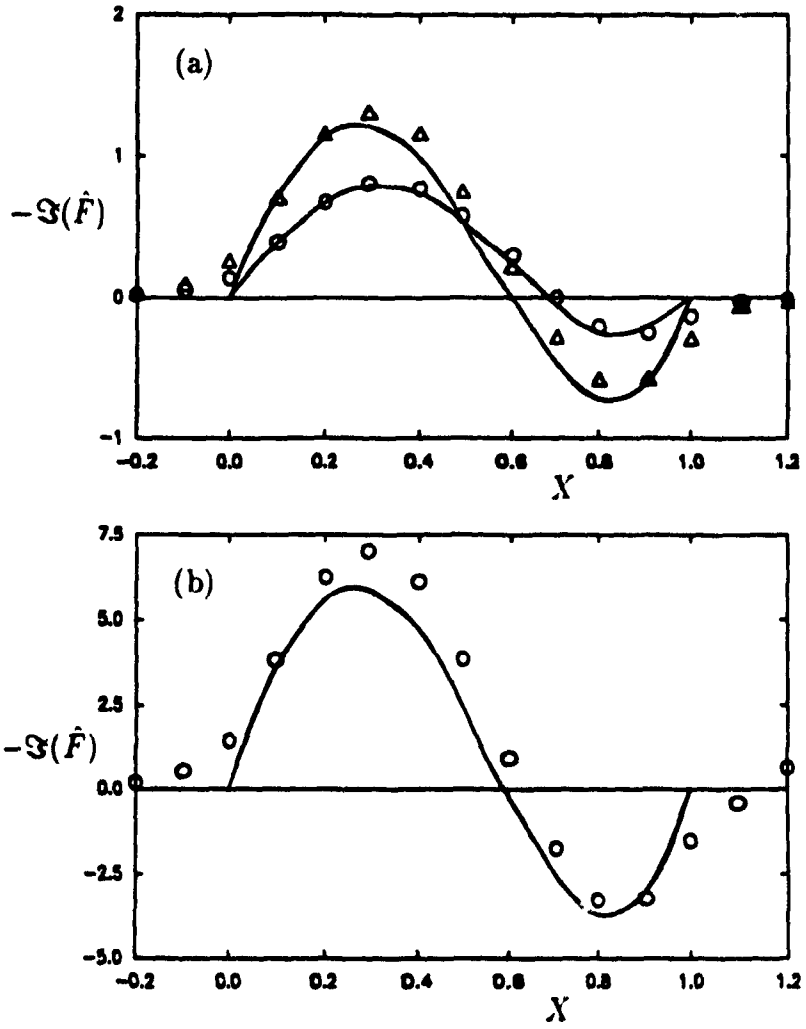

Figure 7.4: Nondimensional viscous-damping force obtained by the approximate method (—) and by the collocation finite-difference method of Chapter 6 (o, $Re = 626$; Δ, $Re = 1,256$), for the first-mode flexural oscillations of the inner cylinder: (a) $Re_s = 5,000$; (b) $Re_s = 500$.

Chapter 8

Experimental Investigations and Comparison with Theory

In parallel to the foregoing theoretical models of which the ultimate objective is to predict the unsteady flow field in annular flow—either turbulent or laminar, the problem has also been studied experimentally; the results of the experimental investigations are presented in this chapter.

Experiments have been performed partly to validate the theory which has been developed for the present problem in the foregoing. For this purpose, the unsteady pressure generated by the oscillatory motion of the outer cylinder in the annular configurations was measured on the surface of the fixed inner cylinder, to compare with the theoretical results. This was found to be a reliable and convenient way of testing the theory. Once the motion-related unsteady pressure is known, the forces acting on the moving parts of the annular flow passage may be easily calculated by adding the shear stress effect; hence, the stability of the centre-body may then be evaluated.

Using an earlier experimental apparatus designed for concentric configurations, experimental investigations were made to study flow-induced-vibration problems [35, 60]. In that set of experiments also, the quantity that was measured was the unsteady pressure. In those tests, a rigid, cylindrical centre-body was forced to oscillate in a rocking mode about a hinge point with air flow in the annulus, while the outer conduit was rigid and immobile. The experiments in this other apparatus have been characterized by high axial-flow velocities, which permitted the validation of the theory

developed for turbulent flow in concentric annuli. In contrast, no experiments were performed with that apparatus for unsteady laminar flows, which may be important especially in very narrow annuli. The evaluation of the eccentricity effects on the unsteady pressure analyzed in Chapter 5 for the translational motion could not be examined using the earlier apparatus. This was the reason why a new apparatus was constructed, where rocking and lateral(translation) motions would be equally feasible, with low flow velocity as well as high flow velocity.

In the design, the following important modifications, as opposed to the previous apparatus, were introduced: (a) the possibility of conducting experiments for eccentric arrangements, with the oscillation either in the plane of eccentricity or normal to it; (b) the facility of having very low flow velocity, so that the flow in the annulus could be laminar rather than turbulent. For future works, this new apparatus has the possibility of having axial variations in the annular passage, either smooth or abrupt.

To accommodate all these possibilities, it was found convenient, in this new apparatus, to oscillate part of the outer cylindrical conduit, while the centre-body remains immobile. In the present experimental tests, the rigid outer cylinder, containing quiescent fluid or steady axial flow(laminar flow), executes a rocking motion in concentric configurations or a translational motion in eccentric configurations.

To eliminate the viscous-flow-related effects, such as flow separation and/or vortex shedding which are not considered in the present theory, a smooth transition between cylindrical and annular flows is assumed both upstream and downstream. This is insured by connecting smooth ogives to the fixed centre-body at both ends as shown in Figure 8.1. The constant cross-section, from the upstream ogive to the test section where the pressure was measured, is long enough to obtain developed laminar flow. Also, the tests have been conducted at low amplitudes of oscillation, characterized by an amplitude/gap ratio smaller than 0.15.

In view of the theoretical results shown in Chapter 5, it is obvious that the fluid-dynamic forces are mainly influenced by the geometry of the system for high oscillatory Reynolds number, $Re_s = (\omega a^2)/\nu$. The radius ratio b/a, for the present experimental

results, was 1.21. For simplicity of design, the test was performed in air rather than in water.

8.1 EXPERIMENTAL APPARATUS

As mentioned before, the unsteady pressure generated by the forced vibration of the outer cylinder was measured and then compared to the theoretical results given by the present theory based on the numerical approach.

The test section consists of a rigid cylindrical centre-body of uniform cross-section connected to the fixed ogives at the upstream and downstream ends, as depicted in Figure 8.1. The ogive, together with a mesh and a honeycomb, placed near upstream end, help to render the annular flow as uniform as possible. The constant-cross-section moving outer conduit was oscillated harmonically. In the basic configuration of the annular gap, two cylinders were either concentric or eccentric, in the plane of oscillation or normal to it. Obviously, there was relative motion between the oscillating part of the outer cylinder and the rest of the outer cylindrical conduit, which was immobile. Various flange designs, as shown in Figure 8.2(a, b and c), were tried to reduce the effect of this relative motion. A fuller explanation will be given later.

The unsteady pressure was measured by six pressure transducers situated at different locations along the length of the centre-body, $X = x/L = 0.342, 0.421, 0.5, 0.578$ and 0.657 ($L = 965$ mm), as shown in Figure 8.3. In the middle, $X = 0.5$, two transducers were located at diametrally opposed locations in order to compare the corresponding measured unsteady pressures; for example, the phase difference between two signals might be 180° for concentric configurations, when the cylinder executed either translational or rocking motion. At each axial location, the transducer was installed inside the hollow centre-body in a recessed housing hole, with a very small hole (0.8 mm diameter and 3.2 mm deep) used for measuring the pressure in the annulus, to minimize the effect of the hole on the flow field. To measure the pressure distribution along the azimuthal direction, the inner cylinder was designed to be rotated.

According to previously obtained experimental results, the relative difference be-

tween the pressures measured on the walls of the outer and inner cylinders was found to be very small for narrow annuli; this was also found to be the case in the present theoretical results. For this reason, the pressure on the surface of the outer cylinder was not measured in the present tests.

The outer conduit itself was oscillated by means of an electro-dynamic shaker and its displacement was measured by an accelerometer mounted on the base plate of the shaker. The oscillation of the shaker is transmitted to the moving outer cylinder via a set of yokes designed for the translational or rocking motion. For the rocking motion experiments, the hinge was located at $X = 0.237$ and the shaker was connected to the outer cylinder at $X = 0.815$. In the case of translational motion, the moving cylinder is connected in the middle ($X = 0.5$) to keep its weight balanced.

The signals from the pressure transducers and the accelerometer were processed through a dual-channel FFT digital signal analyzer. Utilizing the present apparatus, the following parameters were varied in the experiments: (a) oscillation frequency; (b) oscillation amplitude; (c) eccentricity of the annulus; (d) axial-flow velocity. The test can also be conducted for various hinge points and axial locations of the pressure transducers. The possible range of oscillation frequency and amplitude were limited by the dynamical characteristic of the system. In order to have a meaningful comparison with the theoretical results and to avoid impacts between the inner and outer cylinders, the amplitude of motion was not very high.

To describe the apparatus in detail, its different components are presented separately as follows: (1) the external conduit including the oscillating outer-cylinder; (2) the fixed centre-body connected to the ogives; (3) the "transmission" mechanism linking the shaker to the outer cylinder; (4) the blower and the connecting flow system.

8.1.1 The External Conduit

The external pipe consists of two main sections, oscillating and fixed parts. The inner radius of the pipe was $b = 53.8$ mm and its wall thickness was 3.2 mm. The central section, which executes the oscillatory motion, was 965 mm long. The central section was

allowed to oscillate in a one-degree-of-freedom motion provided by the electromagnetic exciter assembly.

The fixed cylindrical conduit of the same diameter as the moving portion continued on either side, and housed the ogives as well as the fixed centre-body. The inlet axial flow was regularized with the aid of several meshes, a honeycomb screen and an ogive, to eventually obtain the developed laminar flow as mentioned before or at high velocity a uniform turbulent flow. These parts were secured on the vertical plates which were fixed on a long I-beam at certain locations along the axial direction. The system was made horizontal rather than vertical (as was the case with the previous apparatus).

As discussed before, it is necessary to overcome the problem of a discontinuity arising from the relative motion between the oscillatory and fixed parts of the outer cylinder. The "obvious" solution of using flexible rubber seals was found unsatisfactory, because locked-in stresses in the rubber seals combined with the slight flexibility in the shaker actuator gave rise to small but important asymmetries to the desired motion. Utilizing a sponge instead of rubber, as a "felt" shown in Figure 8.2(a), the problem was improved but not entirely solved especially for high-amplitude oscillatory motion. The arrangement shown in Figure 8.2(b) using two larger-diameter flanges separated by a very small gap was found to be the best solution to the problem, although it dose not achieve total sealing. The closed arrangement of Figure 8.2(c) was occasionally used, but only with zero mean flow in the annulus.

8.1.2 The Fixed Centre-body

The fixed centre-body is comprised of three parts: the central test section, facing by the oscillating outer cylinder, and the upstream and downstream sections. The pressure transducers were mounted in the central test section. The fixed upstream and downstream sections were composed of two parts: an ogival part and a constant cross-section part. The constant cross-section part was connected to the test section. The ogival part was shaped so as to have varying parabolic profile; it was designed to

allow a smooth and uniform transition from cylindrical to annular flow, or vice-verse. Thus, fully developed annular flow to the test section is allowed through the constant cross-section part.

The central test section of the centre-body was made up of two sections(split longitudiually to mount the pressure transducer inside the cylinder) and was connected to the upstream and downstream sections at both ends in sliding contact (male and female) to allow rotation to the central test section for measuring the unsteady pressures at various azimuthal locations. An O-ring between the male and female parts prevented any air leakage into the hollow inner cylinder. Undesired rotations were prevented with the aid of a set of screws. The radius of the inner cylinder(apart from the ogives) was constant $a = 44.8$ mm. The length of the test section was 965 mm and the upstream and downstream sections, including the constant cross-section part, were 1000 mm long. The contant cross-section part between the ogive and the test section was 500 mm long, so that the ratio of the entrance length, from the ogive to the test section, with respect to the annular space was 50, which might be enough to obtain a sufficiently developed laminar flow.

Each of the upstream and downstream bodies was held in place at two locations. This was accomplished by a set of screws, which were secured into pairs of reinforcing half rings to the outer pipe, at each location. Utilizing the set of screws with a spindle, and measuring the lead of the screw(calibrated appropriately), one could adjust the eccentricity.

8.1.3 Shaker and Transmission

The harmonic oscillation was generated by a Brüel & Kjaer electromagnetic shaker (exciter body B&K 4801 mounted with exciter head B&K 4812). The maximum peak-to-peak amplitude limit was 12.7 mm, the maximum force rating was 445 N, and the possible frequency range was from 5 Hz to 10 kHz effectively.

The harmonic signals generated by the shaker controller (B&K exciter control type 1047) were fed into a power amplifier (B&K 2707) that amplified them to levels

appropriate to drive the shaker. The shaker controller controlled the frequency and the displacement amplitude of the shaker moving element. In order to make use of the frequency-constant-parameter programming capability, an accelerometer was fixed on the base plate of the shaker head and its signal was fed back into the shaker controller through a charge amplifier, the latter conditioning the accelerometer signal into a form suitable for the shaker controller feed-back input circuit.

The oscillatory motion of the central outer cylinder was restricted by a pair of vertical rigid plates parallel to each other, which were placed between the shaker and the cylinder, as a yoke, to give purely transverse transtion. For rocking motion about a hinge, the oscillation was executed via a rigid plate with two pivot points or, in the latest version of the experimental apparatus, via a flexible slender plate. The pivoting points or the flexibility of the yoke were designed to allow rocking(rotational motion), and to avoid problems associated with trying to impose purely vertical motion(which then tends to move the hinge and produces rattling).

8.1.4 The Blower and the Connecting Flow System

The flow through the annulus was provided by an external air source. In the present work, to compare with the theory developed for laminar flow, a vacuum-cleaner type blower was used in the suction mode for generating laminar or low-velocity turbulent flow in the annulus.

It was found that, for turbulence-level flow, the noise level generated by the blower was relatively small as compared to the expected pressure signal. Thus, without using an acoustic filter, the signal acquired from the pressure transducers could be processed by a signal analyzer.

The flow rate was measured by means of an orifice plate mounted near the downstream end of a straight pipe(3 m long and 40 mm in diameter) which was secured at its other end to the downstream section of the outer pipe. This length was required to obtain the fully developed flow near the inlet of the orifice plate. The flow rate was controlled by means of the circumferential slots located at the downstream end near

the blower.

8.2 INSTRUMENTATION FOR MEASUREMENT

During each test, the following physical parameters have to be measured: the unsteady pressure, the displacement of the centre-body with a certain circular frequency, and the flow velocity. As mentioned before, the pressure as well as the displacement were analysed by means of signal processing through a FFT(Fast Fourier Transform) digital signal analyzer, from which the pressure amplitude and the phase angle with respect to the displacement could be obtained.

In the present experiments, the following instruments were used to obtain the required data: (1) six piezoelectric pressure transducers; (2) one accelerometer; (3) one digital spectrum FFT analyzer; (4) one differential alcohol manometer.

8.2.1 Piezoelectric Pressure Transducer

In previous tests [35], a differential-pressure transducer was used for the concentric case. In the present work, the differential-pressure transducer was no longer useful for eccentric configurations, since the unsteady component of the pressure is no longer antisymmetric at diametrally opposed points. In other words, through the differential-pressure transducer, the eccentric effect on the pressure could not be measured. This was the main reason for which the piezoelectric pressure transducer(112A23) was chosen for these experiments instead of the differential-pressure transducer.

The main specifications of the piezoelectric pressure transducer are as follows:

Output Range:	2.5 V
Useful overrange:	344.7 kPa (50 psi)
Resolution:	6.89 Pa (0.001 psi)
Sensitivity:	7.25 ± 1.45 mV/kPa (50 ± 10 mV/psi)
Resonant Frequency:	250 kHz
Linearity:	1.0

Utilizing this pressure transducer, the steady or static component has been undetectable and the signal had an acceptable level without special conditioning, which is a distinct advantage for the present work.

8.2.2 Accelerometer

The displacement of the centre-body was measured by an accelerometer(B&K type 4381) which was m unted on the shaker head. The accelerometer signal was first fed into the charge amplifier(B&K type 2624). One of two-output signals from the charge amplifier was used for the constant displacement control through the feedback loop of the shaker controller system, while the other was monitored by the spectrum analyzer which gave the centre-body displacement.

As opposed to the earlier apparatus [35], it was not necessary to consider the flexibility of the transmission yoke, since the transmission components were relatively simple and more directly connected; moreover, the transmisson was sufficiently rigid in the moving direction. As a result, the difference of the accelerations measured on the base plate and on the surface of the moving cylinder was small enough to be considered negligible.

8.2.3 Spectrum Analyzer

A dual-channel FFT digital spectrum analyzer(Hewlett-Packard 3582A) was used to monitor the signals from the pressure transducers and from the accelerometer. In Figure 8.4, a schematic of signal processing is shown. The amplitude of either signal could be obtained from the power spectrum, while the phase difference between pressure and acceleration could similarly be obtained from the cross-spectrum of the those two quantities. The information was available for each individual spectral component by means of a cursor that can be positioned accordingly.

The main advantage of using the FFT analyzer was that the signal due to the secondary effects (*e.g.* the nonlinearlity of fluid motion, unexpected secondary motions

of the cylinder, the random noise from turbulence, and acoustic wave pressure components) can be adequately separated from the main signal. The other advantage of this instrument is that it can accept signals down to μV range without special signal conditioning, which was very useful, since the signal levels in these experiments were just above the resolution of the pressure tranducer.

The frequency range of the dual-channel digital analyzer is 0.02 to 25 kHz. With suitable frequency spans in the range of 5 Hz up to 25 kHz, to provide better frequency resolution, the signal can be analysed. The instrument can measure inputs from 31.6 volts down to 1 μV, without resorting to external signal conditioning. Its dynamic range is 70 dB. The use of this analyzer permitted us to obtain the transducer and accelerometer readings accurately in the frequency range of 20-70 Hz, in which the present experimental tests were performed.

8.2.4 Differential Alcohol Manometer

To calculate the flow rate, the pressure drop across the orifice plate was measured by a differential Lambrecht alcohol manometer, the range of which was 0-200 mm of alcohol. Its two taps were connected upstream and downstream of the orifice plate. The calculation of the flow rate, from which the mean-flow velocity and the Reynolds number in the annulus can be determined, will be described in the next section as part of the preliminary experimental work.

8.3 PRELIMINARY EXPERIMENTAL WORK

In order to obtain the signal with a desired accuracy, every aspect of data acquisition was studied for each parameter to be measured, and the pressure transducer and the accelerometer were appropriately calibrated. Special attention was paid to the measurements of the pressure signal, the centre-body displacement and the annular flow rate. As mentioned before, the unsteady pressure was influenced by the type of connection between the moving and fixed parts of the outer pipes. After several trial tests, the most suitable connection was found.

8.3.1 Calibration of the Instruments

To assess the dynamical behaviour of the instrumentation with an accuracy relevant to the order of magnitude of the signals, appropriate calibration procedures are required, especially for the pressure transducer and the accelerometer, as well as for the orifice plate; however, in the present work, the discharge coefficient of the commercial orifice plate as a function of Reynolds number was taken from the calibration data for the commercial orifice plate, which was already verified during a previous test.

(a) The pressure transducer

Before the dynamic calibration started, it was necessary to have a pressure transducer with known sensitivity. A PCB 106B pressure transducer (sensitivity 43.51 mV/kPa and resolution 0.69 Pa) was used as a reference pressure transducer, since it has a higher sensitivity and lower resolution than the actual transducer to be calibrated.

The experimental apparatus for dynamic calibration, shown in Figure 8.5, consists of a plexiglass cylinder of which the free end is covered by a rubber membrane and the fixed end has two pressure transducer housing holes. The membrane was held tightly by a ring against the edges of the cylinder by means of eight screws in order to prevent air leakage. Two small circular plates of diameters slightly less than the inside diameter of the cylinder provide an oscillatory displacement of the membrane by means of a yoke which was clamped to the base plate of the electromagnetic shaker (B&K 4801).

The reference pressure transducer was flush-mounted to the fixed end of the cylinder and the pressure transducer to be calibrated was mounted in another housing hole which had the same configuration as in the actual measurements on the centre-body. As mentioned before, both were installed recessed. The electrical output signal proportional to the deflection of the membrane was generated by the harmonic oscillatory motion of the shaker. Using the reference signal from the flush-mounted one, the sensitivities of the actual pressure transducers were found to be in the range of $6.09 - 7.25$ mV/kPa.

(b) The accelerometer

Taking into account the actual measurement configurations, the accelerometer

was calibrated by the aid of a B&K accelerometer calibration Exciter (B&K 4294), acceleration of which is fixed (10 m/s^2 with 59.2 Hz). To calibrate the accelerometer, it was mounted on the device and then connected to the charge amplifier with the cable in the same arrangement as for actual measurements. The sensitivity of the accelometer was measured to be 1.02 mV/(m/s^2).

8.3.2 Measurement of Flow Velocity

In the present work, it was expected that the actual flow rate was slightly larger the measured one due to the leakage at the flanges between the fixed and the moving parts of the outer pipe. However, as mentioned before, the air leakage was minimized by keeping the gap very small. For this purpose, the radial width of the flanges was relatively large with respect to the gap. This, together with the relatively low pressure difference with respect to the ambient, insured that the leakage flow was quite small.

Looking at Figure 8.1, an orifice plate was installed at the downstream end, near the pump, between two flanges to measure the flow rate. The flow in the basic duct of diameter D was forced through an obstruction of diameter d, as shown in Figure 8.6. The ratio of the radii $\beta = d/D$ is a key parameter. For the present work, the diameters were $D = 40.0$ mm and $d = 12.7$ mm so that $\beta = 0.318$

Applying the Bernoulli and continuity equations for incompressible steady frictionless flow to estimate the pressure changes, one obtains

$$\frac{\pi}{4}D^2V_1 = \frac{\pi}{4}d^2V_2,$$

$$p_o = p_1 + \frac{1}{2}\rho V_1^2 = p_2 + \frac{1}{2}\rho V_2^2. \tag{8.1}$$

Eliminating V_1, one can obtain the flow velocity V_2 in terms of the pressure change $(p_1 - p_2)$; thus,

$$V_2 = \left[\frac{2(p_1 - p_2)}{\rho(1 - \beta^4)}\right]^{1/2}, \tag{8.2}$$

where the pressure difference was calculated by reading the manometer. However, this is surely inaccurate because of the friction due to the viscosity which was neglected.

Thus, an experimental calibration of the device must be carried out to fit the relation

$$V_2 = c_d \left[\frac{2(p_1 - p_2)}{\rho(1 - \beta^4)} \right]^{1/2}, \tag{8.3}$$

where the dimensionless discharge coefficient c_d accounts for the discrepancies in the above approximate analysis. By dimensional analysis, it is expected that the coefficient is expressed as

$$c_d = f(\beta, Re_D), \tag{8.4}$$

where

$$Re_D = \frac{V_1 D}{\nu}.$$

Utilizing the discharge coefficient given for the commercial orifice with $D : 0.5D$ tapping shown in Figure 8.6, the flow velocity V_2 can be calculated through an iteration procedure. Thus, it is not difficult to obtain the Reynolds number in the annulus from the calculated flow rate, with the aid of the continuity equation.

8.4 EXPERIMENTAL RESULTS AND COMPARISON WITH THE THEORY

Unsteady pressure at each pressure transducer location was measured, when the outer-cylinder, subject to axial flow or in quiescent fluid, executed the translational motion, in the plane of eccentricity or normal to it; or, alternatively, when it was subjected to the rocking motion about a hinge point. Experiments have been conducted with the following arrangements: (1) with the centre-body concentrically mounted vis-à-vis the outer pipe, for both cases; (2) with the centre-body eccentrically mounted, for the former case only.

Before the results are presented, attention will be brought to a point that proved to have some importance, experimentally. It was found that the repeatability of the results was not good when the fixed and moving outer cylinders were connected by rubber or sealed by a sponge between the flanges, due to the shear stresses coming from its deformation. However, in the limited range of frequency 25 – 45 Hz with

the sponge, the repeatability of the results was acceptable. Fixed blockades as shown in Figure 8.2(c), in smooth contact with the moving cylinder, were used (at the two ends of the moving portion) in the case of translational motion without axial flow; grease was added liberally between the moving cylinder and the blockades to reduce the surface friction forces as well as to prevent air leakage. For other cases, two flanges of large diameter were used, and a very small gap between them (less than 1mm). With these arrangements, it was found that the repeatability of the results for the present work were pretty good and the results for low axial flow velocity can be considered acceptable.

The ultimate objective of the analytical effort is to develop theoretical models for accurately predicting the flow field in annular flow, either turbulent or laminar. The latter situation is especially important in applications involving very narrow annuli. For high turbulent flows, the experimental experimental test had been conducted with pretty good comparison to the theoretical result using the previous apparatus. It was therefore important to have experimental data for systems in laminar flow, or low-intensity turbulent flow. In the present experiments with axial flow, the flow velocity was low ($\bar{U} \simeq 2.2$ m/s), so that $Re = \bar{U}2H/\nu \simeq 2{,}900$. Although, this is not low enough for laminar flow, it nevertheless represents a low turbulence-level flow.

A final remark concerns the presentation of the results. The pressure presented here is actual unsteady pressure, (raher than differential pressure in the previous experiments). Moreover, unlike the previous results, the nondimensional unsteady pressure, $\hat{p}$ was plotted versus the azimuthal angle Θ for various frequencies $f = \omega/(2\pi)$. The dimensionless pressure $\hat{p}$ was defined in the previous chapters as

$$\hat{p}(r,\theta) = \frac{p^*(r,\Theta,t)}{\rho\omega^2 a^2 \epsilon e^{i\omega t}}, \quad \text{and} \quad \hat{p}(x,r,\theta) = \frac{p^*(x,r,\Theta,t)}{\rho\omega^2 a^2 \epsilon_{1/2} e^{i\omega t}}, \tag{8.5}$$

for the translational and the rocking motion, respectively, where the nondimensional displacement, ϵ and $\epsilon_{1/2}$, were defined with respect to the radius of the inner cylinder a and the subscript $1/2$ stands for the local value at the middle point $X = 1/2$, as shown in Chapter 6. In fact, the dimensionless parameter $\hat{p}$ is independent of the small

amplitude of the moving cylinder as shown in the previous chapters, either for viscous flow or for inviscid flow.

The experimental results are compared with the theoretical ones obtained with the spectral method for potential theory. As discussed by Chen *et al.* [9] for sufficiently high values of the oscillatory Reynolds number, $Re_s > 15,000$ approximately, it is possible to neglect viscous effects with little loss of accuracy. For the case of these experiments, $29,000 < Re_s < 56,860$ is clearly sufficiently large. Also it was shown in Chapter 6 that in the case of the three-dimensional problem and $b/a = 1.25$, $Re_s = 10,000$, the effect of low flow velocity was small compared to the inertia effect, and the unsteady pressure was linearly dependent on the vibration amplitude. Thus, the theoretical results, to which experiments will be compared, were obtained without considering the flow velocity of laminar flow, by means of two-dimensional-flow theory, where the pressure is taken to be linearly proportional to the amplitude of motion.

As a preliminary result without axial flow, the amplitudes of the dimensional unsteady pressure p^* versus the frequency are presented in Figure 8.7, when the outer cylinder executes rocking motion with an amplitude of 1 mm at the shaking position, 558 mm from the hinge. The pressure was measured at the middle $X = 1/2$, while the sponge as a felt was filled between the fixed and the moving flanges. It was found that the pressure distributions along the length of the cylinder are proportional to the acceleration of the moving body, in parabolic shape versus the frequency, which means that inertia effects are dominant, as expected. Discrepancies between the experimental and theoretical results are most marked at low and high frequencies. The discrepancy at high frequencies is probably associated with end effects, for example due to shear deformation of sponge. For low-frequency oscillation, the low level of the pressure signal is probably the cause of these discrepancy, since high noise/signal level almost certainly affects the accuracy. Because of this, in the cases where the axial flow effect is expected to be minimal, the tests have been conducted with either a very small gap or with a closed arrangement as discussed before.

The experimental dimensionless pressure, exerted on the inner cylinder, versus

the azimuthal angle $\theta = \Theta$ are shown in Figures 8.8 – 8.10, to compare with the theoretical ones. The amplitudes of the oscillations were 1 mm (at 41.6 Hz), 0.5 mm (at 52 Hz) and 0.3 mm (at 66.4 Hz). For eccentric annuli, the motions were executed in the plane of the symmetry of the eccentric configurations (Figure 8.9) and normal to it (Figure 8.10).

Several features should be noted, as follows:

1. The measured unsteady pressure distributions are symmetric about $\Theta = 0$ in Figures 8.8 for concentric configurations and in Figure 8.9 for an eccentric arrangement with translational motion in the plane of eccentricity, or they are skew-symmetric in Figure 8.10 for an eccentric arrangement with oscillation normal to the plane of eccentricity, as expected.

2. The pressure readings increase with frequency; however, the nondimensional pressure is almost constant with it. Considering the present results, it was found that the nondimensional unsteady pressure, $\hat{p}$, depend more or less on the geometry and it can be assumed that p^* is linearly proportional to vibration amplitude in cases of high-frequency oscillation—the viscous effects were found to be minimal in the present tests.

3. At these low flow velocities and for the translational motion, the effect of the axial flow velocity is very small and can be neglected, as expected. This means that the unsteady pressure field for purely transverse flow is dominated by the oscillation-induced cross-flow.

4. Agreement between theory and experiment was found to be good.

Figure 8.11 presents the axial variation of the dimensionless unsteady pressure with distance away from the hinge, along the centre-body. The amplitude of oscillation was 1 mm with 34.4 Hz oscillation for the result of Figure 8.11(a) and 0.75 mm with 42.6 Hz oscillation for those of Figure 8.11(b) at the point of shaking. The following

observations may be made with respect to the experimental results for the rocking motion:

1. As discussed before, the pressure increases more or less linearly with distance from the hinge-point. In the case of the higher frequency, Figure 8.11(b), agreement with this linearity condition is better; this is at least partially due to the slightly higher pressure reading, and hence better signal-to-noise ratio.

2. There is little difference in the reading for zero and non-zero annular flow velocity for the present case with low flow velocity.

3. Agreement between theory and experiment is seen to be good, except for the two readings in of the low-frequency test, Figure 8.11(a), close to the ends of the moving pipe, which were probably affected by end effects due to local discontinuities, as well as low signal-to-noise ratio in the case of small x/L.

For these experiments, the phase difference for the motion of the cylinder is not presented and no comparisons with theory have been made. The reason for this is twofold: (a) the theoretical phase difference including the flow-velocity effect was less than 10° for the high values of Re_s involved; (b) it was difficult to determine the phase difference with the desired accuracy, in the experiments. The cause of this latter difficulty is related to the fact that the pressure levels were generally rather low and hence signal-to-noise ratios were not as high as desired.

Agreement between the experimental and numerical results was found to be within 10%, except the two readings close to the ends of the moving pipe shown in Figure 8.11(b). The range of uncertainty in the results, i.e. the maximum variation between pressure measurements from the six transducers, was less than ± 0.4 nondimensional units of $\hat{p}$ defined by equation 8.5.

Considering experimental results, what should be stressed here is the importance of the "end effects". In lateral transverse motion of the outer cylinder, the local discontinuities at the two ends could make a great deal of difference to the pressure reading, especially in the vicinity of these discontinuities, but sometimes considerably further

in. Similarly, in the rocking mode experiments, the inevitable protrusion of the ends of the oscillating outer-cylinder generated pressure readings which were quite different from the theoretical prediction, the theory having been developed for uniform or at least smooth flow.

Also concerning the experimental results, the viscous effects and the low-flow-velocity effect on the pressure were not visible for the present annular passage; however, they might be important for estimating the stability of a system in a very narrow annular passage. By inspection of the theoretical results shown in the previous chapters, it is clear that the viscous damping becomes larger with decreasing the annular passage. Thus, future experiments will have to be done to measure the unsteady pressure for narrower annular configurations. In this respect, another inner cylinder and set of ogives of larger diameter have to be manufactured to obtain a narrower annular configuration.

Finally, for engineering applications, the theory and experimental tests for nonuniform and/or discontinuous annular passages, such as a body protruding into the annular flow must be dealt with in future work. A recent paper of Hobson and Jedwab [61] shows how intricate and challenging the flow can be in non-uniform annular passage.

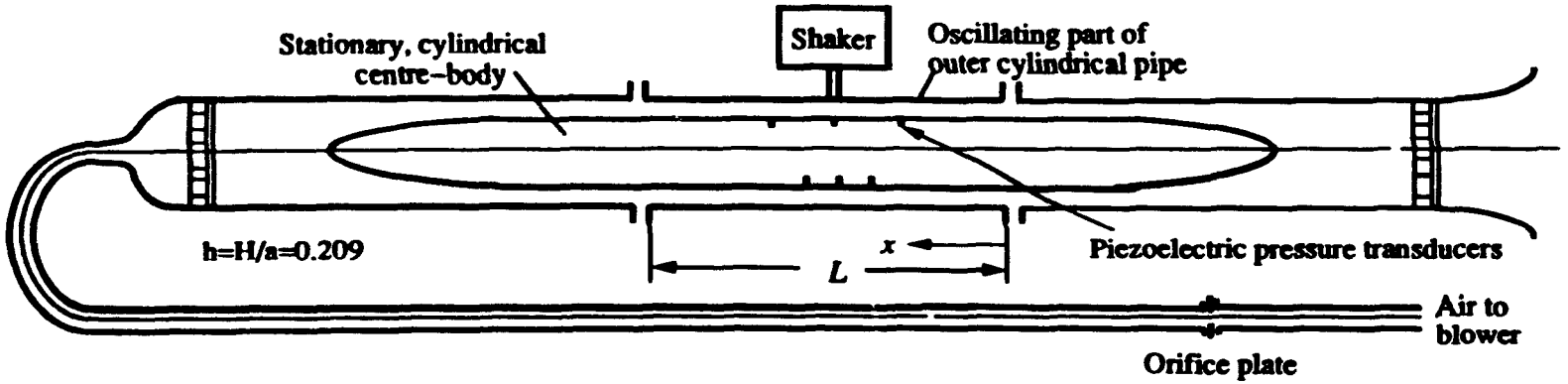

Figure 8.1: Schematic diagram of the experimental apparatus in which either transverse or rocking motion of the central part of the outer pipe could be imposed by the shaker.

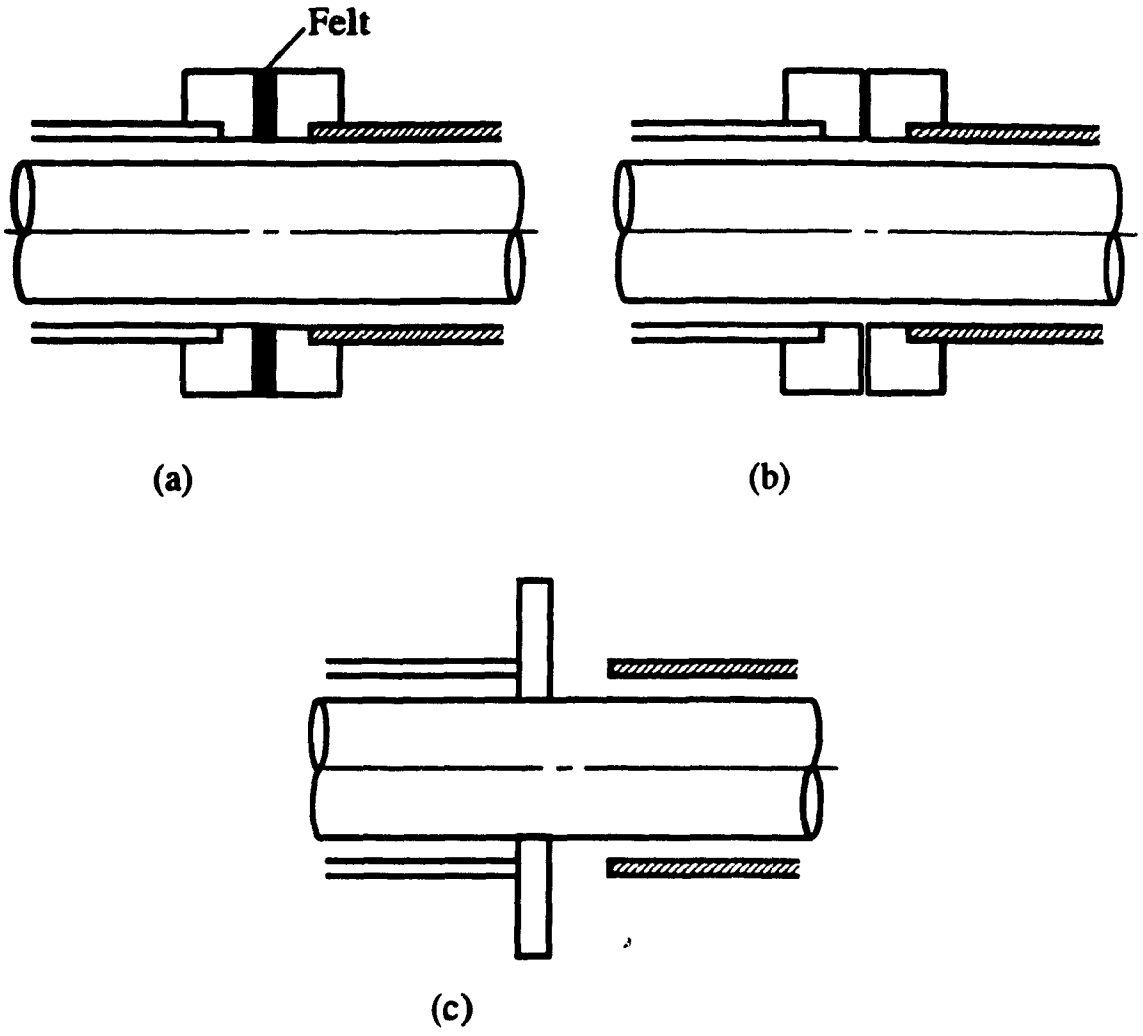

Figure 8.2: Sealing arrangements between the moving and stationary parts of the outer pipe: (a) felt rings between flanges; (b) close-fitting flanges; (c) flange with lubricated rubbing contact with oscillating cylinders(for zero axial flow only).

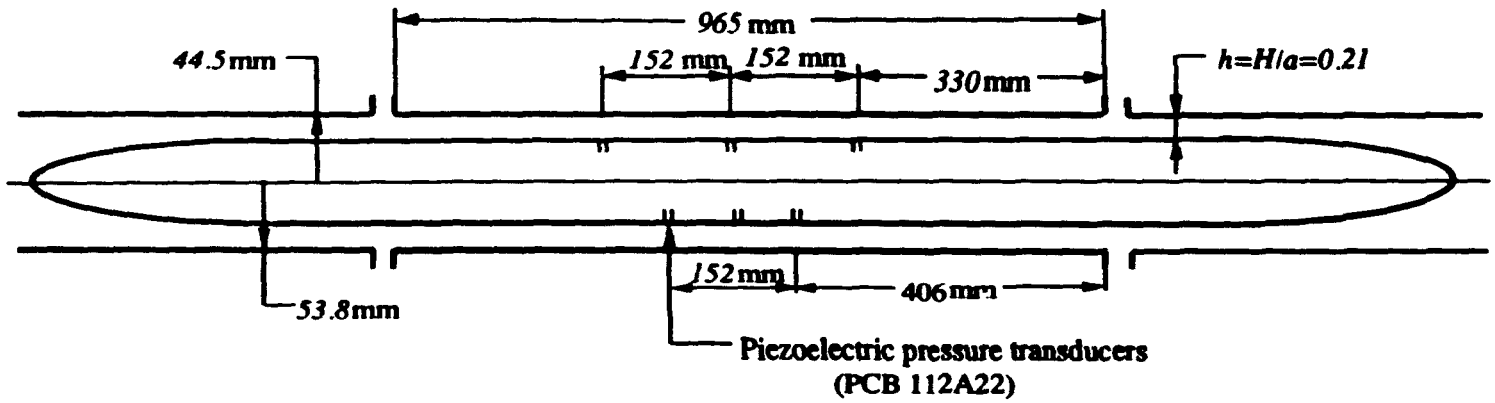

Figure 8.3: Schematic diagram of the central portion of the apparatus, showing dimensions and location of the pressure tranducers.

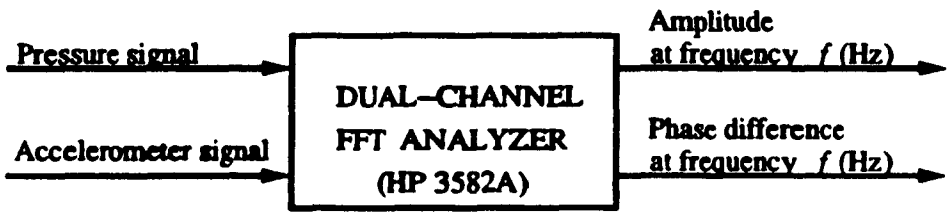

Figure 8.4: Diagram showing signal processing utilized.

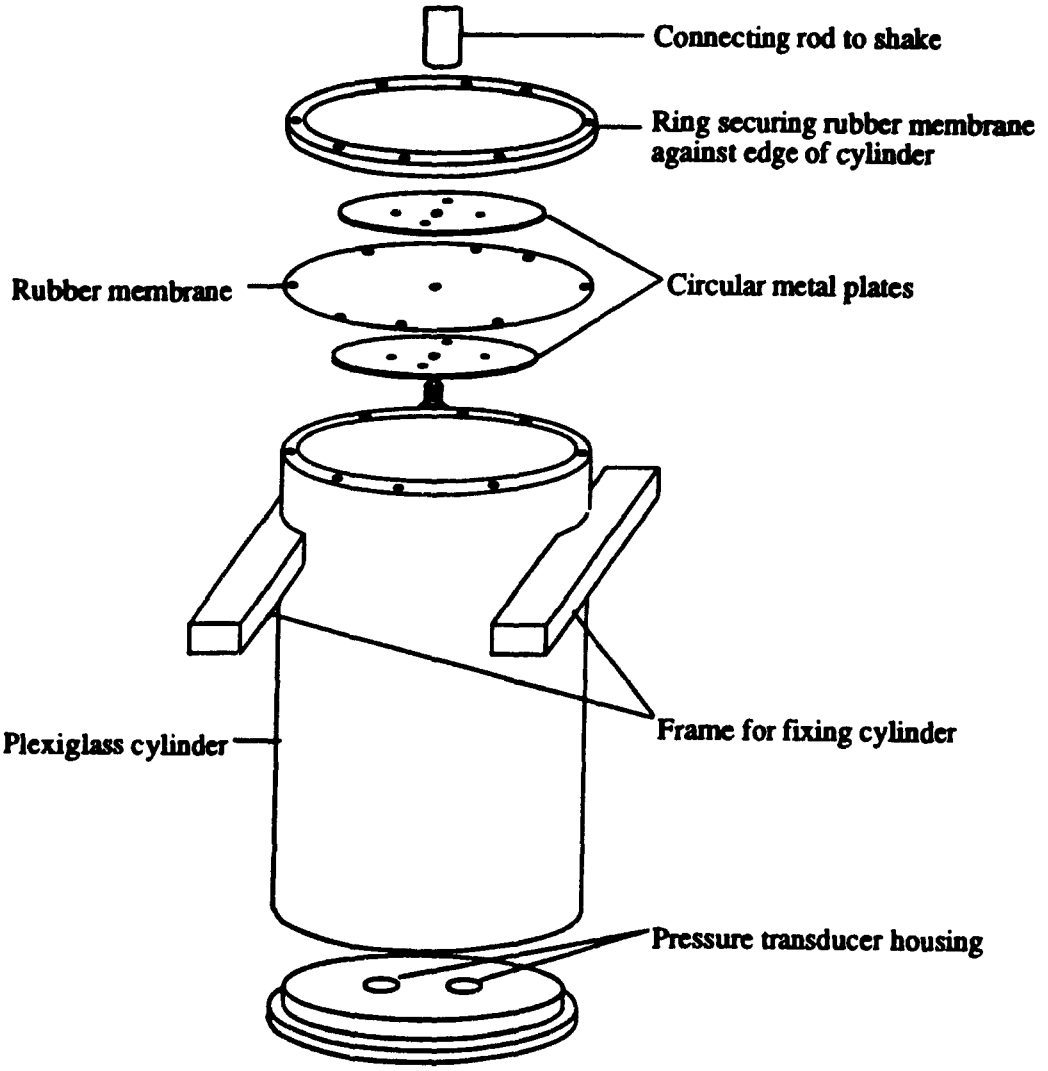

Figure 8.5: Schematic diagram of the chamber used for pressure transducer calibration.

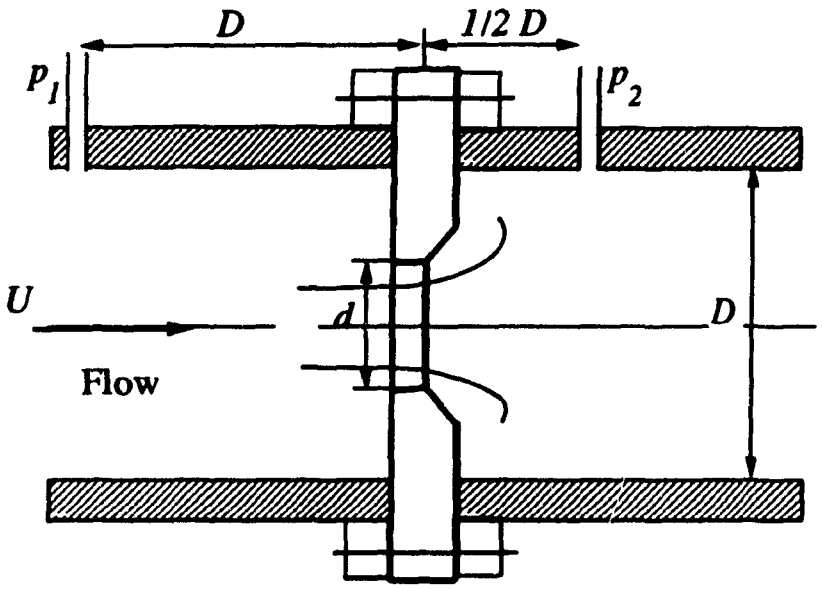

Figure 8.6: Schematic diagram of the orifice plate used in the experiments (D = 40.0 mm; d = 12.7 mm).

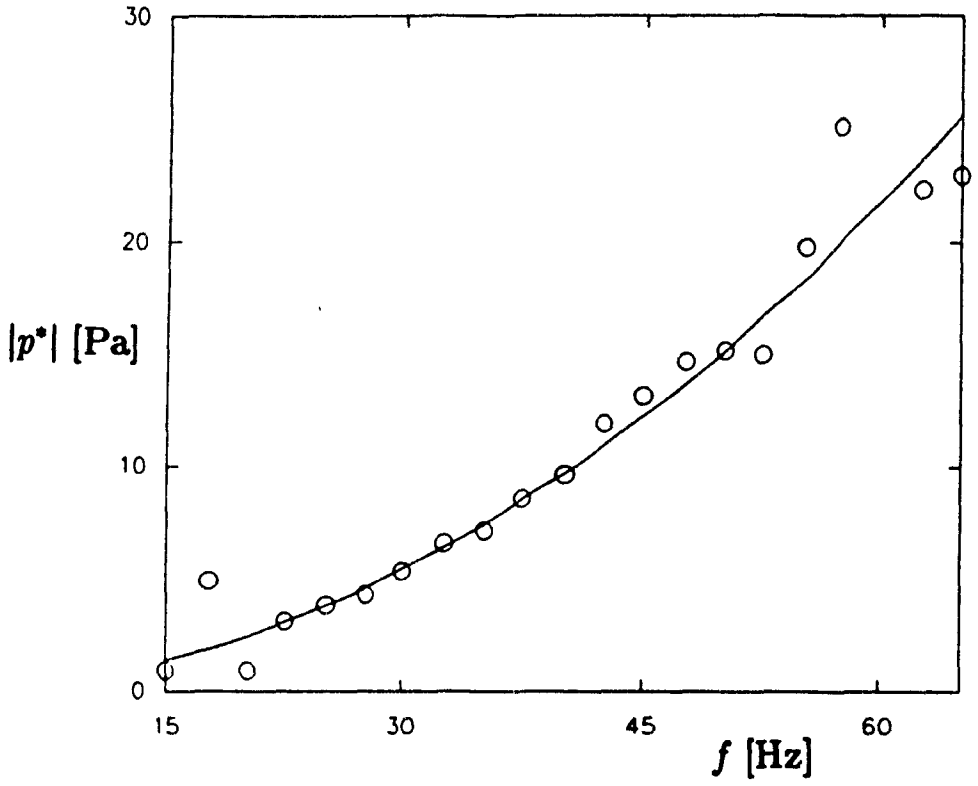

Figure 8.7: Unsteady pressure measurements $X = 1/2$ versus oscillatory frequency f, in translational motion for a concentric arrangement with felt rings between flanges (see part (a) of Figure 8.2).

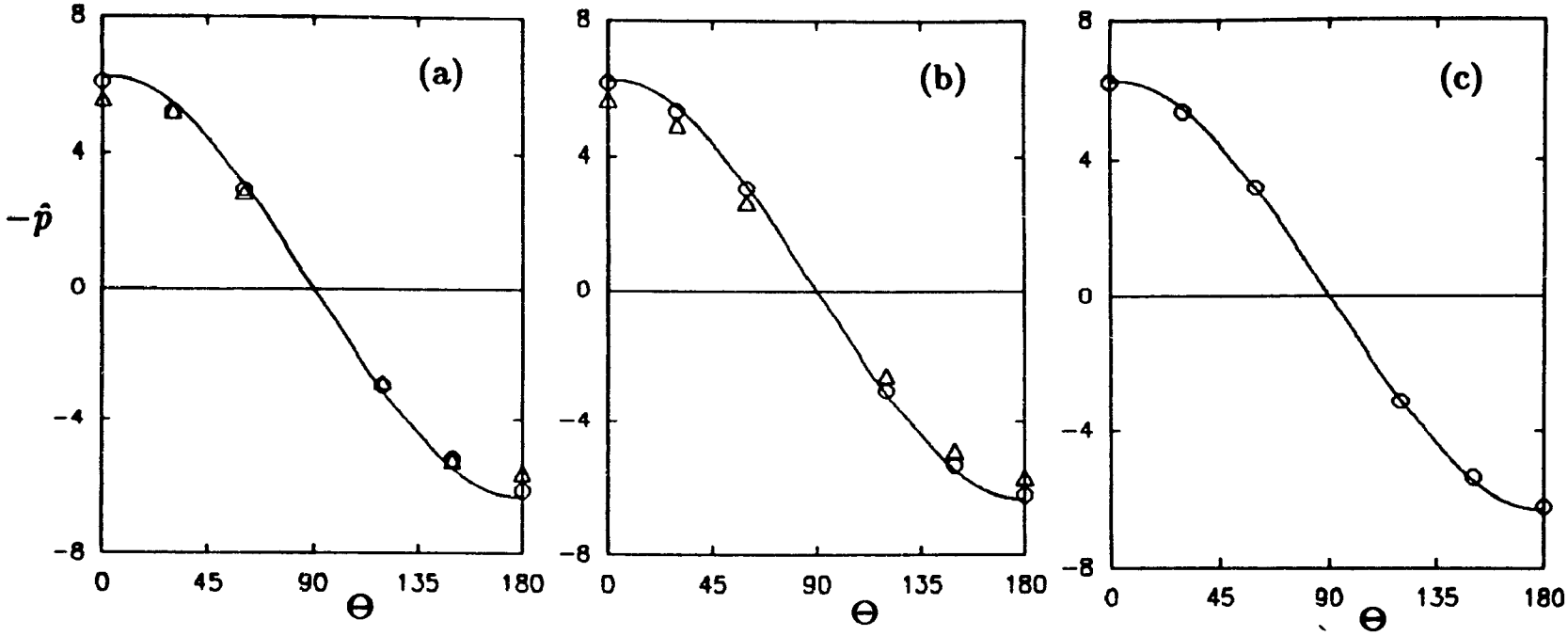

Figure 8.8: Unsteady dimensionless pressure versus the azimuthal angle Θ, in translational motion for a concentric arrangement. Oscillating frequency: (a) $f = 41.6$Hz; (b) $f = 52.0$Hz; (c) $f = 66.4$Hz. —, potential flow theory; o,experimental results without axial flow; $\triangle$,experimental results with axial flow $Re \simeq 2,900$.

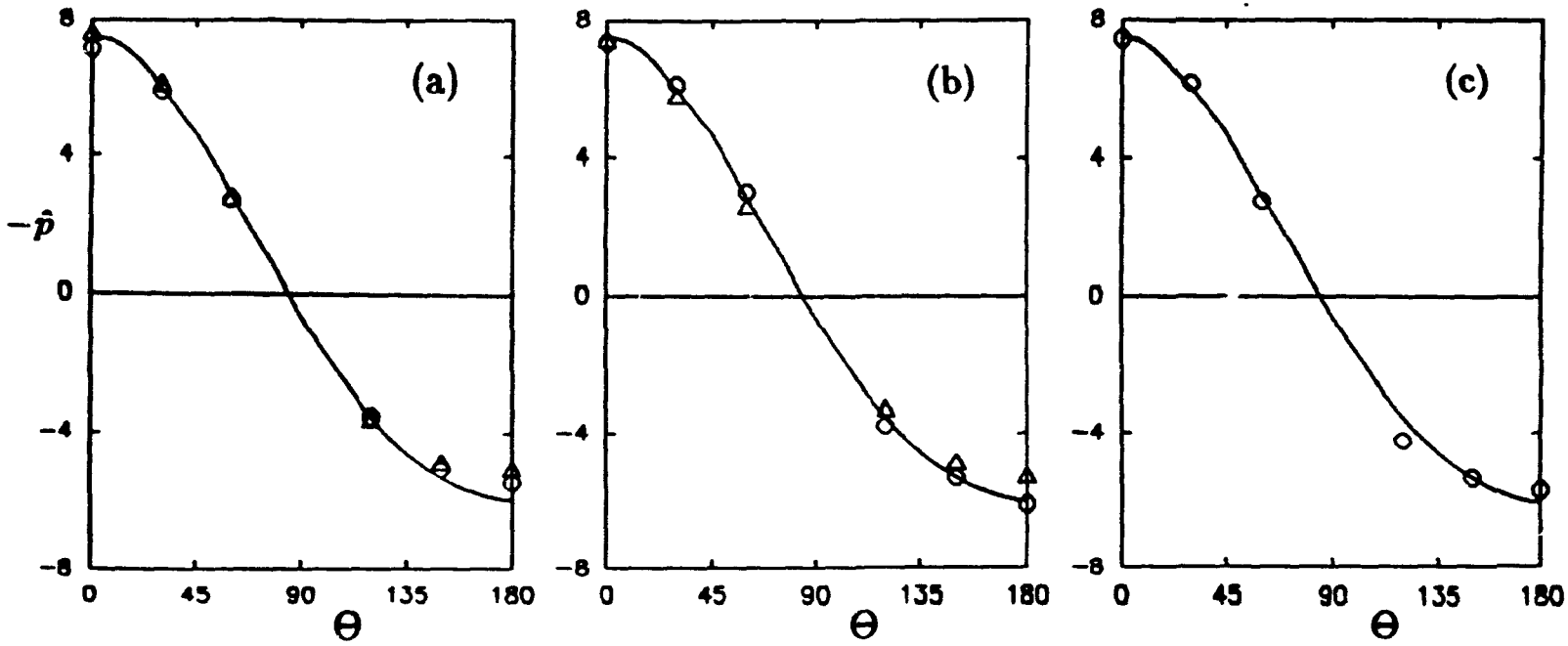

Figure 8.9: Unsteady dimensionless pressure versus the azimuthal angle Θ, in translational motion for an eccentric arrangement with oscillation in the plane of eccentricity; nondimensional eccentricity $e/(b-a) = 0.5$. Oscillating frequency: (a) $f = 41.6$Hz; (b) $f = 52.0$Hz; (c) $f = 66.4$Hz. —, potential flow theory; o, experimental results without axial flow; Δ, experimental results with axial flow $Re \simeq 2,900$.

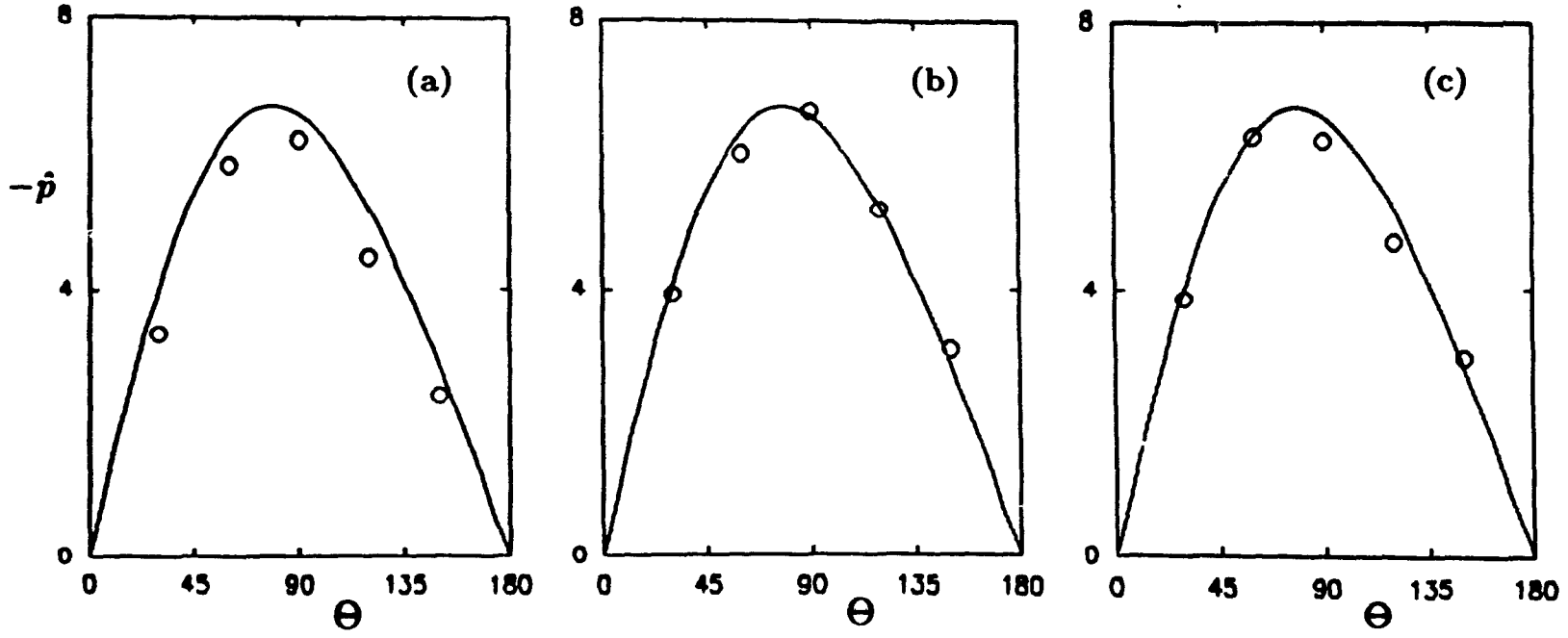

Figure 8.10: Unsteady dimensionless pressure versus the azimuthal angle Θ, in translational motion for an eccentric arrangement with oscillation normal to plane of eccentricity; nondimensional eccentricity $e/(b-a) = 0.5$. Oscillating frequency: (a) $f = 41.6$Hz; (b) $f = 52.0$Hz; (c) $f = 66.4$Hz. —, potential flow theory; o, experimental results without axial flow.

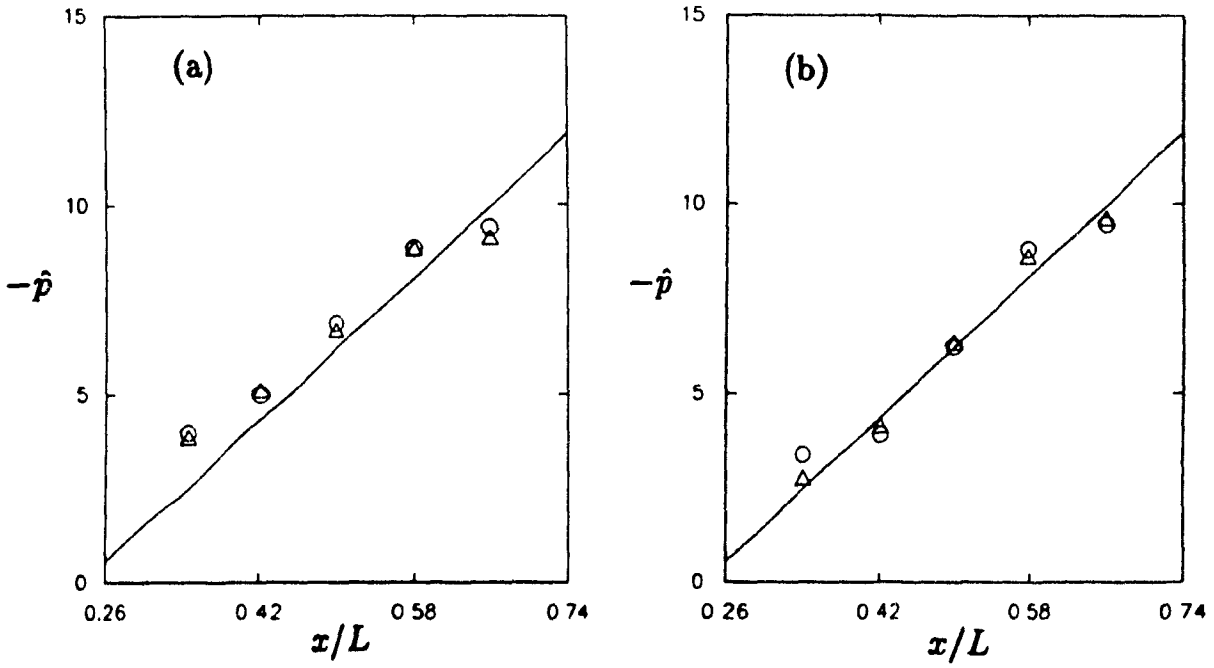

Figure 8.11: Measured unsteady dimensionless pressure versus position along the centre-body in rocking motion, for L_o = 229 mm (L = 965 mm) and for frequencies of oscillation (a) f = 34.4Hz (Re_s = 29,460) and (b) f = 42.6Hz (Re_s = 36,480). —, potential flow theory; o,experimental results with no axial flow; △,experimental results with axial flow $Re \simeq 2{,}900$.

Chapter 9

Conclusions

9.1 DISCUSSION AND SUMMARY

The unsteady flows generated by the oscillatory motion of cylinder in an annulus have been studied by a newly developed numerical method. The main aim of this study is to evaluate the fluid-dynamic forces acting on a cylinder immersed in inviscid or viscous fluid for concentric and eccentric configurations. This new numerical method, based on a spectral collocation, is capable of taking fully into account unsteady viscous effects and of predicting the viscous forces for complex geometries, rigorously rather than approximately. For the purpose of verification of the numerical method, semi-analytical and simplified analytical methods have been developed to estimate the forces.

The spectral method has first been applied to a system having translational motion(two-dimensional problem) in quiescent flow for eccentric configurations and then to a system having flexural motion in axial flow for concentric configurations, with the aid of a hybrid scheme, also involving a finite-difference method (three-dimensional problem). In the former case, cylinders were taken to be infinite rigid bodies, while in the latter case the flexible inner cylinder was considered to be clamped at both extremities. In both problems, the fluid-dynamic parameters are expressed as spectral expansions involving Chebyshev polynomials, Fourier series and exponential functions. These expansions contain *a priori* unknown coefficients which are determined by a collocation approach from the governing equations and the boundary conditions of the flow; these expansions are perfomed in a convenient computational domain, obtained with

the aid of a coordinate transformation, in which the governing equations are imposed at appropriatly chosen collocation points. For the three-dimensional problem, the LU decompsition method is utilized to solve a block-tridiagonal system of equations, while the submatrices are treated with the Gauss-Seidel iteration method.

The spectral collocation method has been validated by applying it to several types of steady and unsteady flows for which analytical solutions are available: (a) the steady viscous flow between two fixed eccentric cylinders; (b) the steady viscous flow generated by the steady rotational motion of one of the cylinders in a concentric annular space; (c) the unsteady viscous flow between two parallel plates which have oscillatory motion; (d) the unsteady viscous flow generated by oscillatory rotational motion of cylinders in an concentric annular space. Excellent agreement was found, in all these typical flow problems, between the spectral solutions and the analytical ones. Therefore, one can conclude that the present spectral collocation method might be applied to the analysis of the unsteady viscous flow problems in annular configurations with confidence.

The spectral collocation method has now been applied to the potential flow generated by the translational motion of cylinder, in order to verify the method for flow-induced vibration problem. The numerical results obtained for the inviscid case have been compared to the available analytical solutions given by Chung and Chen [9] for eccentric configurations and by Fritz [7] for concentric configurations. With meaningful comparison under the same considerations, the numerical method has been validated.

The fluid-dynamic forces were formulated under the assumption of small amplitudes of motion. As a result, linearized equations were derived from the Laplace equation for inviscid flow and from the Navier-Stokes and continuity equations for viscous flow. The resulting forces have been calculated while varying (i) the geometry of the system, including the eccentricity, (ii) the oscillatory Reynolds number, representing the product of the Reynolds number and the reduced frequency, and (iii) the Reynolds number based on the hydraulic diameter.

It should be remarked that, in the present analysis, the flow in the narrow annular

passage is assumed to be a fully developed laminar flow. The velocity distribution in the eccentric annular domain has been obtained by the spectral method and then the results are utilized for developing the unsteady flow model.

In parallel to the numerical models, the semi-analytical and simplified analytical approaches have been developed to estimate the fluid-dynamic forces and the viscous damping forces, respectively, as mentioned before. The fluid-dynamic forces are formulated by the semi-analytical method, considering the inviscid effects and the main effects of fluid viscosity. This semi-analytical method can be applicable to a system of narrow annular flow; moreover, the inviscid fluid-dynamic forces are predicted, rigorously, without the restriction about annular space. By inspection of the velocity distribution of the circumferential flow velocity across the annular space, the viscous damping forces are approximated by a simplified analytical method for either low or high oscillatory Reynolds numbers. The big advantage of this simplified method is that the fluid-dynamic forces can be easily estimated for very narrow annular flow, where the forces can be expressed as explicit function of the circular frequency of the moving cylinder; this is useful for future studies of the stability of such systems. The results obtained by these methods are compared to the numerical results to validate the newly developed numerical method. Good agreement was shown for narrow annular configurations.

With the aid of the present numerical theory and the approximated analytical theories, both qualitative and quantitative aspects of the results have already been discussed in the corresponding chapters in fair detail. A number of significant results were obtained, as follows.

1. The ratio of the penetration depth to the annular space width, which is related to the oscillatory Reynolds number Re_s and the nondimensional annular space h, is an important parameter for characterizing the unsteady viscous fluid motion; *e.g.*, the unsteady viscous drag force is proportioal to either $1/Re_s$ for low oscillatory Reynolds numbers or $1/\sqrt{Re_s}$ for high ones.

2. The viscous effects on the fluid-dynamic forces can be neglected for sufficiently high oscillatory Reynolds number; however, the viscous damping forces are important for very narrow annuli, as expected.

3. The viscous damping forces are mainly influenced by the unsteady viscous drag due to the oscillatory motion for low axial flow velocity.

4. The viscous effects are caused by the unsteady viscous pressure perturbation rather than shear stress effects. This tendency becomes larger with decreasing annular space.

It is interesting to note that the pressure variation across the narrow annular space is negligible. Also it is found that the fluid-dynamic forces are exponentially increased with decreasing the anular space.

Although, the treatment of the viscous effect is based on translational motion or flexural motion of the clamped-clamped beam, these conclusions may be considered to be reasonable as an attempt to assess the influence of the viscous effect on the fluid-dynamic forces for any boundary conditions.

Comparison of this numerical theory with the closest analytical available ones validated all aspects that could be compared. However, as expected, the key element which is unique to this theory in three-dimensional viscous flow problems, *i.e.*, the prediction of the unsteady fluid-dynamic forces is different and superior to those of previous theories, by taking into account the viscous related changes in the unsteady flow field. In the present analysis, the viscous effects are more rigorously considered by an adaptation of the formulation applicable to more complex geometries including eccentricity or relatively wide annuli, and the effect of axial(laminar) flow on the unsteady flow field is predicted systematically rather than approximately by means of a numerical solution of the Navier-Stokes equations. Hence, for the fluid-dynamic forces acting on an oscillating flexible cylinder, this theory is superior to the previously available ones. However, for future stability analysis, the simplified analytical methods can be utilized rather easily to estimate the forces, including viscous effects, with a very

good computational efficiency.

Experiments described in the last part of this thesis have been conducted partly to test the validity of the presented numerical theory. The unsteady pressure generated by the oscillation of the outer cylinder was measured on the wall of the fixed inner cylinder at various axial azimuthal locations. This was found to be a reliable and convenient way of testing the theory. Either lateral translation or rocking motion was imposed. In the equilibrium configurations the two bodies are either concentric or eccentric, in the plane of oscillation or normal to it. The experiments have been performed for high values of the oscillatory Reynolds number. As discussed in the numerical results for sufficiently high values of the oscillatory number, it is possible to neglect viscous effects with little loss of accuracy.

Experiments have shown that the effect of the axial flow velocity on the unsteady pressure is minimal for low flow velocities($Re \simeq 2,900$) and low amplitudes (displacement/radius$\simeq$0.04). The pressure is more or less linearly dependent on the amplitude of the moving cylinder, which means that linear theory is applicable, based on the assumption of small amplitude motion; moreover, the viscous effects can be negligible for high values of the oscillatory Reynolds number. It should be remarked here that local discontinuities at both ends of the moving part could make a great deal of difference to pressure readings, mainly in the vicinity of these discontinuities.

The experimental results are compared with the theoretical ones obtained by the potential flow theory based on the spectral method. It was seen that that agreement between theory and experiment is good and potential-flow theory was found to be adequate for the high values of the oscillatory Reynolds number.

9.2 MAIN CONTRIBUTIONS OF THIS THESIS

The main aim of this thesis is to present a newly developed numerical approach, based on a spectral collocation method, for solving confined viscous flows with oscillating boundaries, which are related to the flow-induced-vibration problems. This approach uses suitable spectral expansions for the fluid-dynamic paremeters, as discussed before.

The main contributions of the present work can be summarized as follows.

1. A new and efficient numerical model has been developed to accurately evaluate the unsteady flow field and the fluid-dynamic forces on oscillating rigid centre-bodies or outer cylinders in eccentric annuli.

2. A hybrid collocation finite-difference method was developed for three-dimensional unsteady flow problems, specifically for obtaining the fluid-dynamic forces on flexible centre-bodies oscillating in concentric annuli.

3. Alternative approaches, semi-analytical and simplified analytical, are presented for the determination of the unsteady fluid-dynamic forces, with extensive discussion on their applicability to various systems; they are used for the validation of the numerical models mentioned above, and can be efficiently applied in the analysis of the fluid-elastic instabilities.

4. A detailed experimental investigation for eccentric configurations was first undertaken as part of this thesis, to author's best knowledge. The numerical results were validated with these experimental results.

Furthermore, the following important advantages of the various approaches developed in this thesis were established.

1. The fluid-dynamic forces, including viscous effects, can be evaluated more rigorously by the numerical methods developed than by analytical theories; moreover, the accuracy of the numerical solution converges fast, exponentially, with the number of collocation points.

2. The semi-analytical approach is fairly applicable for the system where unsteady inviscid forces are dominant in the fluid-dynamic forces (*e.g.*, for high values of the oscillatory Reynolds number), even in the case of a finite length of cylinder and only slightly confined flow. This analysis is less restricted in the size of the annular space as compared to the previous analytical models [54].

3. The damping force is estimated rather easily by the simplified analytical method; this approach is very useful for very narrow annular configurations, where the added mass is mainly influenced by the geometry, although the viscous damping forces are very important, even in this case.

This numerical approach is expected to be a very useful tool in the analysis of other, similar fluid-structure interaction problems, involving oscillatory boundaries.

9.3 SUGGESTIONS FOR FUTURE WORK

In order to determine the fluid-dynamic forces acting on a flexible cylinder, the problem has been formulated based on the assumption of laminar flow and a simple mode shape of vibration in uniform annular passage. Therefore, there are several possible directions in which this work can be extended. In this sense, it is suggested that the present numerical analysis should be extended for turbulent flow and for systems with discontinuous geometries, such as a step variation of the annular passage. Also, the study of the stability of the system should be undertaken by using numerical and analytical tools developed here.

In view of the difficulty of the experiments involving flexural motion of a slender cylinder subjected to narrowly confined axial flow, the numerical results obtained here are not compared with experimental results; however, this comparison is very interesting from the point of view of the flow-induced vibration and stability analysis. Obviously, it is necessary to have experimental verification, showing how good the present theory is, especially in evaluating the viscous effects on the fluid-dynamic forces. To get sufficiently large pressure signals, even for low oscillation frequencies, so as to see the viscous effects, it is suggested to have experimental tests in narrower annuli filled with water.

The experimental results highlight the importance of the end effects, which are also present in engineering systems; hence, a possible next phase of work should deal with nonuniform and/or discontinuous annular flow passages. An attempt should be

made to extend the theory for this problem, the importance of which is self-evident.

Bibliography

[1] Chen, S. S., 1977, "Flow Induced Vibrations of Circular Cylindrical Structure, Part I: Stationary Fluid and Parallel Flow", *Shock and Vibration Digest*, Vol.9(10), pp. 25-38.

[2] Chen, S. S., 1981, "Fluid Damping for Circular Cylindrical Structures", *Nuclear Engineering and Design*, Vol.63(1), pp. 81-100.

[3] Païdoussis, M. P., 1981, "Fluidelastic Vibration of Cylinder Arrays in Axial And Cross Flow: State of Art", *Journal of Sound and Vibration*, Vol.76(3), pp. 329-360.

[4] Païdoussis, M. P., 1987, "Flow-induced Instabilities of Cylindrical Structures", *ASME Applied Mechanics Reviews*, Vol.40(2), pp. 163-175.

[5] Stokes, G. G., 1843, "On Some Cases of Fluid Motion", *Proceedings of the Cambridge Philosophical Society*, Vol.8, pp. 105-137.

[6] Muga, B. J. and Wilson, J. F., 1970, "Dynamic Analysis of Ocean Structures", Plenum Press, New York-London.

[7] Fritz, R. J., 1972, "The Effect of Liquids on the Dynamic Motions of Immersed Solids", *ASME Journal of Engineering for Industry*, Vol.94, pp. 167-173.

[8] Au-Yang, M. K., 1976, "Free Vibration of Fluid-coupled Coaxial Cylindrical Shells of Different Lengths", *Journal of Applied Mechanics*, Vol.43, pp. 480-484.

[9] Chung, H. and Chen, S. S., 1977, "Vibratioin of a Group of Circular Cylinders in a Confined Fluid", *Journal of Applied Mechanics*, Vol.44, pp. 213-217.

[10] Chen, S. S., 1972, "Free Vibration of a Coupled Fluid/Structural System", *Journal of Sound and Vibration*, Vol.21(4), pp. 387-398.

[11] Chen, S. S., Wambsganss, M. W. and Jendrzejczyk, J. A., 1976, "Added Mass and Damping Vibrating Rod in Confined Viscous Fluid", *Journal of Applied Mechanics*, Vol.43, pp. 325-329.

[12] Yeh, T. T. and Chen, S. S., 1977, "Dynamics of a Cylindrical Shell system Coupled by Viscous Fluid", *Journal of the Acoustical Society of America*, Vol.62(2), pp. 262-270.

[13] Yeh, T. T. and Chen, S. S., 1978, "The Effect of Fluid Viscosity on Coupled Tube/Fluid Vibrations", *Journal of Sound and Vibration*, Vol.59(3), pp. 453-467.

[14] Mulcahy, T. M., 1980 "Fluid Forces on Rods Vibrating in Finite Length Annular Regions", *Journal of Applied Mechanics*, Vol.47, pp. 234-240.

[15] Païdoussis, M. P., 1966, "Dynamics of Flexible Slender Cylinders in Axial Flow; Part I: Theory", *Journal of Fluid Mechanics*, Vol.26, pp. 717-736.

[16] Païdoussis, M. P., 1966, "Dynamics of Flexible Slender Cylinders in Axial Flow; Part II: Experiments", *Journal of Fluid Mechanics*, Vol.26, pp. 737-751.

[17] Lighthill, M. J., 1960, "Note on the Swimming of Slender Fish", *Journal of Fluid Mechanics*, Vol.9, pp. 305-317.

[18] Taylor, G. I., 1952, "Analysis of the Swimming of Long and Narrow Animals", *Proceedings of the Royal Society (London)*, A214, pp. 158-183.

[19] Hawthorne, W. R., 1961, "The Early Development of the Dracone Flexible Barge", *Proceedings of the Institution of Mechanical Engineers*, Vol.175, pp. 52-83.

[20] Païdoussis, M. P., 1968, "Stability of Towed, Totally Submerged Flexible Cylinders", *Journal of Fluid Mechanics*, Vol.34, pp. 273-297.

[21] Païdoussis, M. P., 1973, "Dynamics of Cylindrical Structures Subjected to Axial Flow", *Journal of Sound and Vibration*, Vol.29(3), pp. 365-385.

[22] Païdoussis, M. P. and Pettigrew, M. J., 1979, "Dynamics of Flexible Cylinders in Axisymmetrically Confined Axial Flow", *Journal of Applied Machanics*, Vol.46, pp. 37-44.

[23] Chen, S. S., 1975, "Vibrations of a Row of Circular Cylinders in a Liquid", *ASME Journal of Engineering for Industry*, Vol.97(4) Series B, pp. 1212-1218.

[24] Païdoussis, M. P. and Suss, S., 1977, "Stability of a Cluster of Flexible Cylinders in Bounded Axial Flow", *Journal of Applied Mechanics*, Vol.44, pp. 401-408.

[25] Païdoussis, M. P. and Ostoja-Starzewski, M., 1981, "Dynamics of a Flexible Cylinder in Subsonic Axial Flow", *AIAA Journal*, Vol.19(11), pp. 1467-1475.

[26] Dowell, E. H. and Widnall, S. E., 1966, "Generalized Aerodynamic Forces on an Oscillating Cylindrical Shell; Subsonic and Supersonic Flow", *AIAA Journal*, Vol.4, pp. 607-610.

[27] Chen, S. S. and Wambsganss, M. W., 1972, "Parallel-flow-induced Vibration of Fuel Rods", *Nuclear Engineering and Design*, Vol.18, pp. 253-278.

[28] Wambsganss, M. W. and Zaleski, P. L., 1970, "Measurement, Interpretation and Characterization of Near-field Flow Noise", *Proceedings Conference on Flow-induced Vibrations in Reactor System Components*, Argonne, Illinois, ANL-7685, pp. 112-137.

[29] Hobson, D. E., 1982, "Fluid-elastic Instabilities Caused by Flow in an Annulus", *In Proceedings of BNES 3rd International Conference on Vibration in Nuclear Plant*, Keswic, U. K., pp. 440-463.

[30] Spurr, A. and Hobson, D. E., 1984, "Forces on the Vibrating Centrebody of an Annular Diffuser", *ASME Symposium on Flow-induced Vibration*, Vol.4: Vibration

Induced by Axial and Annular Flows (eds. M. P. Païdoussis and M. K. Au-Yang), pp. 41-52.

[31] Hobson, D. E., 1984, "Instabilities of the AGR Fuel Assembly during On-rod Refueling", *ASME Symposium on Flow-induced Vibration*, Vol.4: Vibration Induced by Axial and Annular Flows (eds. M. P. Païdoussis and M. K. Au-Yang), pp. 25-39.

[32] Mateescu, D. and Païdoussis, M. P., 1985, "The Unsteady Potential Flow in an Axially Variable Annulus and Its Effect on the Dynamics of the Oscillating Rigid Centre-body", *ASME Journal of Fluids Engineering*, Vol.107, pp. 421-427.

[33] Mateescu, D. and Païdoussis, M. P., 1987, "Unsteady Viscous Effects on the Annular-flow-induced Instabilities of a Rigid Cylindrical Body in a Narrow Duct", *Journal of Fluids and Structures*, Vol.1, pp. 197-215.

[34] Mateescu, D., Païdoussis, M. P. and Bélanger, F., 1988, "Unsteady Pressure Measurements on an Oscillating Cylinder in Narrow Flow", *Journal of Fluids and Structures*, Vol.2, pp. 615-628.

[35] Mateescu, D., Païdoussis, M. P. and Bélanger, F., 1989, "A Theoretical Model Compared with Experiments for the Unsteady Pressure on a Cylinder Oscillating in a Turbulent Annular Flow", *Journal of Sound and Vibration*, Vol.135(3), pp. 487-498.

[36] Mateescu, D., Païdoussis, M. P. and Sim, W.-G., 1987, "Flow-induced Instability of a Flexible Cylinder in a Narrow Pipe Conveying Fluid", *CANCAM*, Edmonton, pp. B150-151.

[37] Païdoussis, M. P., Mateescu, D. and Sim, W.-G., 1990, "Dynamics and stability of a Flexible Cylinder in a Narrow Coaxial Cylindrical Duct Subjected to Annular Flow", *Journal of Applied Mechanics*, Vol.57, pp. 232-240.

[38] Païdoussis, M. P., 1965, "Vibration of Flexible Cylinders with Supported Ends, Induced by Axial Flow", *Proceedings of the Institution of Mechanical Engineers*, Vol.180(3J), pp. 268-279.

[39] Grotberg, J. B. and Reiss, E. L., 1982, "A Subsonic Flutter Anomaly", *Journal of Sound and Vibration* Vol.80, pp. 444-446.

[40] Païdoussis, M. P., Suss, S. and Pustejovsky, M., 1977, "Free Vibration of Cylinders in Liquid-filled Channels", *Journal of Sound and Vibration*, Vol.55, pp. 443-459.

[41] Zienkiewicz, O. C. and Nath, B., 1963, "Earthquake Hydrodynamic Pressures on Arch Dams - an Electric Analogue Solution", *Proceedings of the Institution of Civil Engineers*, Vol.25, pp. 165-176.

[42] Chenault, D. W., 1970, "Motion of a Ship at the Free Surface", *M. S. Thesis*, Naval Postgradute School, Monterey, Calif..

[43] Newton, R. E., Chenault, D. W. and Smith, D. A., 1974, "Finite Element Solution for Added Mass and Damping", *Proceedings of the International Symposium on Finite Element Methods in Flow Problems*, Swansea.

[44] Edelstein, W. S., Chen, S. S. and Jendrzejczyk, J. A., 1986, "A Finite Element Computation of the Flow-induced Oscillations in a Cantileved Tube", *Journal of Sound and Vibration*, Vol.107(1), pp. 121-129.

[45] Yang, C. I. and Moran T. J., 1979, "Finite-Element Solution of Added Mass and Damping of Oscillation Rods in Viscous Fluids", *Journal of Applied Mechanics*, Vol.46, pp. 519-523.

[46] Mateescu, D., Païdoussis, M. P. and Bélanger, F., 1991, "Computational Solutions Based on a Finite Difference Formulation for Unsteady Internal Flow", *AIAA 29th Aerospace Science Meeting*, Reno, AIAA Paper No. 91-0724.

[47] Orszac, S. A., 1971, "Numerical Simulation of Incompressible Flows within Simple Boundaries, Part I", *Studies in Applied Mathematics*, Vol.50, pp. 293-327.

[48] Orszac, S. A., 1972, "Comparison of Pseudospectral and Spectral Approximations", *Studies in Applied Mathematics*, Vol.51, pp. 253-259.

[49] Orszag, S. A., 1971, "Galerkin Approximations to Flows within Slabs, Spheres and Cylinders", *Physical Review Letters*, Vol.26, pp. 1100-1103.

[50] Marcus, P. S., 1984, "Simulation of Taylor-Couette Flow, Part I", *Journal of Fluid Mechanics*, Vol.146, pp. 45-64.

[51] Marcus, P. S., 1984, "Simulation of Taylor-Couette Flow, Part II", *Journal of Fluid Mechanics*, Vol.146, pp. 65-113.

[52] Piercy, N. A. V., Hooper, M. S. and Winny, H. F., 1933, "Viscous Flow through Pipes with Cores", *The Philosophical Magazine*, Vol.15(7), pp. 647-676.

[53] Snyder, W. T., and Goldstein, G. A., 1965, "An Analysis of Fully Developed Laminar Flow in an Eccentric Annulus", *American Institute of Chemical Engineers*, Vol.11(3), pp. 462-467.

[54] Sim, W.-G., 1987, "Stability of a Flexible Cylinder in Axistmmetrically Confined Flow", *M. Eng. Thesis*, Department of Mech. Eng., McGill University.

[55] Schlicting, H., 1979, "Boundary-Layer Theory", McGraw-Hill Book Co., 7th Edition, New York.

[56] Spalding, D. B., 1972, "A Novel Finite-difference Formulation for Differential Expressions Involving both First and Second Derivatives", *International Journal for Numerical Method in Engineers*, Vol.4, pp. 551-559.

[57] Brighton, J. A. and Jones, J. B., 1964, "Fully Developed Turbulent Flow in Annulus", *ASME Journal of Basic Engineering*, Vol.86, pp. 835-844.

[58] Jonsson, V. K. and Sparrow, E. B., 1965, "Experiments on Turbulent Flow Phenomena in Eccentric Annular Ducts", *Journal of Fluid Mechanics*, Vol.25(1), pp. 65-86.

[59] Hood, P. and Taylor, C., 1974, "Navier-Stokes Equations Using Mixed Interpolation, Finite Element Method in Flow Problems", The University of Alabama in Huntsville Press (eds. Oden, J. J., etc).

[60] Taheri, A. H., 1985, "An Experimental Investigation of the Unsteady Pressure Exerted on a Cylindrical Rigid Body Oscillating in a Cylindrical Pipe Conveying Fluid", *B. Eng. Thesis with " Honours"*, Department of Mech. Eng., McGill University.

[61] Hobson, D. E. and Jedwab, M., 1990, "Investigations of the Effect of Eccentricity on the Unsteady Fluid Forces on the Centrebody of an Annular Diffuser", *Journal of Fluids and Structures*, Vol. 4., pp. 155-169.

[62] Patankar, S. V., 1980, "Numerical Heat Transfer and Fluid Flow", McGraw-Hill Book Co., New York.

Appendix A

The Approximate Method Based on Inviscid Slender-body Theory and Comparison of Critical Flow Velocities

The system consists of a flexible inner cylinder, which has radius a, cross-sectional area $A_s = \pi a^2$, length L, density ρ_s and flexural rigidity EI. The radius of the confining duct is $a_d = a + H$, and the undisturbed flow velocity is $\tilde{U}$.

Considering small lateral motions of the flexible cylinder immersed in inviscid flow, the equation of motion based on slender body theory is given by

$$EI\frac{\partial^4 e_l}{\partial x^4} + \rho_s A_s \frac{\partial^2 e_l}{\partial t^2} = -M\left(\frac{\partial}{\partial t} + \tilde{U}\frac{\partial}{\partial x}\right)^2 e_l = F_p\,, \tag{A.1}$$

in terms of the displacement of the moving cylinder, e_l, as proposed by Lighthill [17], where F_p represents the inviscid fluid-dynamic forces. In the above equation, the virtual mass, M is expressed as $\chi\rho A$, where ρ is fluid density. For concentrically confined flow, χ is expressed as follows:

$$\chi = \frac{(a+H)^2 + a^2}{(a+H)^2 - a^2}\,, \tag{A.2}$$

where H denotes the annular space between the two cylinders. Thus, it is clear that the added mass increases with confinement.

Thus, the inviscid fluid-dynamic forces can be expressed as

$$F_p = -\left(M\frac{\partial^2 e_l}{\partial t^2} + C_v\frac{\partial e_l}{\partial t} + k e_l\right)\,, \tag{A.3}$$

where the damping coefficient, C_v, and the stiffness coeficient, k, are related to the centrifugal and Coriolis forces, respectively. Hence, it should be remarked that the system is generally nonconservative; hence, inviscid theory contains a component related to damping(Coriolis force). Nevertheless, the effect of this force is null for cylinder supported at both ends(as is the case here). Considering thes equation (A.1), it is obvious that the coefficients C_v and k depend on the flow velocity.

At this stage, the critical flow velocity, where the system loses stability by buckling, may be found particularly easily, considering Euler's method of equilibrium. Eliminating the time derivatives from equation (A.1) yields

$$EI\frac{\partial^4 e_l}{\partial x^4} + M\bar{U}^2\frac{\partial^2 e_l}{\partial x^2} = 0\,, \tag{A.4}$$

where $e_l = \sum a_k e^{i\alpha x}$ (the destabilizing force in this case is propotional to $M\bar{U}^2$).

As a result, a system with clamped ends loses stability by divergence, of which the critical flow velocity can be approximated by Païdoussis [21] in a simple form, because of the simplicity of the slender-body formulation, as

$$\bar{U}_{cr} = 2\pi\sqrt{\frac{1}{\chi}}\sqrt{\frac{EI}{\rho AL^2}}\,. \tag{A.5}$$

Table A Comparison of the nondimensional critical flow velocity $\bar{U}_{cn}$ obtained with the potential-flow verisons of the slender-body theory [21] and the inviscid version of previous theory [37]

$l = L/a$	$h = H/a$	Vaule of $\bar{U}_{cn}$		Percent discrepancy based on first column
		Slender-body theory	Previous theory	
20	0.05	1.39	1.49	7.2
	0.10	1.94	2.13	9.8
	0.15	2.34	2.64	12.8
100	0.01	0.627	0.631	0.7
	0.05	1.387	1.425	2.7

It is instructive to compare the results with those given by the previous analytical theory [37], which was developed based on the assumption of narrow annulus as shown in Chapter 2, but considering only the inviscid fluid-dynamic forces. For this purpose, the nondimensional critical flow velocity, $\bar{U}_{cn} = \bar{U}_{cr}/\sqrt{(EI)/(\rho AL^2)}$, are calculated by

both methods and then the typical results are shown in Table A for narrow annulus. The difference between two results becomer with increasing L/a and decreasing the annular gap H/a, where slender-body theory and the narrow-annular simplification of the previous theory, respectively, apply best.

Appendix B

An Analysis of Fully Developed Laminar Flow between Two Eccentric Cylinders

An analysis, developed for fully developed laminar flow in an eccentric annulus by Piercy *et al.* [52] and more recently by Snyder *et al.* [53], is presented to validate the present numerical method. By the analytical method based on the bipolar transformation, an exact solution for the velocity distribution is calculated and then compare with that obtained by the numerical method shown in Chapter 4.

The geometry considered in the analysis is presented in the Figure B. The radii of two infinitely-long cylinder are a and b. Because of the asymmetry of the geometry, solution is obtained in bipolar coordinate system rather than in cylindrical coordinate system.

The Navier-Stokes equations in this essentially two-dimensional problem reduce to the Poisson equation, which may be expressed in the rectangular coordinates, x, y and z, in the form

$$\nabla^2 U = \frac{\partial^2 U}{\partial y^2} + \frac{\partial^2 U}{\partial z^2} = 4\frac{Q}{a^2}, \tag{B.1}$$

where

$$Q = \frac{a^2}{4\mu}\frac{dP}{dx}$$

in which $U(y,z)$ is the axial flow velocity, $P(x)$ is the pressure and $\mu = \rho\nu$ is the fluid viscosity. In the analysis, the pressure gradient in the axial direction, dP/dx,

is constant because of the the assumption of fully developed laminar flow and the viscosity is assumed constant. The above equation is subjected to the usually no-slip boundary conditions expressed by $U = 0$ at the inner and outer surfaces.

Using a plane harmonic function expressed as

$$\Psi = U - \frac{Q}{a^2}(y^2 + z^2)\,, \tag{B.2}$$

the governing equation (B.1) can be rewritten

$$\nabla^2\Psi(y,z) = \frac{\partial^2\Psi}{\partial y^2} + \frac{\partial^2\Psi}{\partial z^2} = 0\,. \tag{B.3}$$

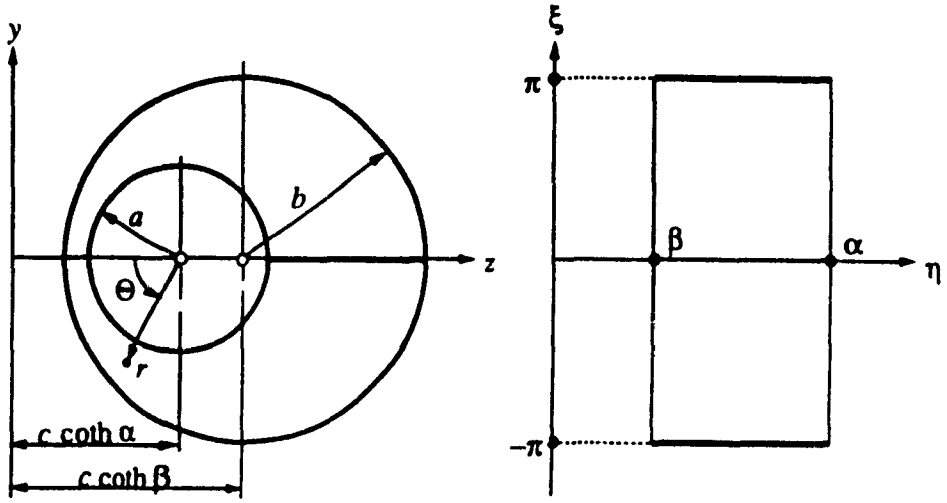

Figure B. Eccentric annulus geometry in the physical plane (y, z) and in the bipolar plane (ξ, η).

This solution must satisfy the following equation, due to the flow symmetry with respect to the plane of the eccentricity, as

$$\left.\frac{\partial\Psi}{\partial y}\right|_{y=0} = 0\,. \tag{B.4}$$

To solve the problem, the bipolar coordinates (ξ, η) are defined by the transformation

$$y + \imath z = c\tan\frac{\xi + \imath\eta}{2}\,, \tag{B.5}$$

where c is a constant. Thus, one can get relations between the physical and bipolar coordinates in the form

$$y = \frac{c\sin\xi}{\cosh\eta + \cos\xi}\,, \qquad z = \frac{c\sinh\eta}{\cosh\eta + \cos\xi}\,, \tag{B.6}$$

$$\tan\xi = -\frac{2cy}{y^2+z^2-c^2}\,, \qquad e^{2\eta} = \frac{y^2+(z+c)^2}{y^2+(z-c)^2}\,, \tag{B.7}$$

$$y^2 + [z - c\coth\eta]^2 = \frac{c^2}{\sinh^2\eta}\,, \tag{B.8}$$

where

$$c = a\sinh\alpha = b\sinh\beta\,, \tag{B.9}$$

with

$$\cosh\alpha = \frac{b^2-a^2-e^2}{2ae}\,, \quad \cosh\beta = \frac{b^2-a^2+e^2}{2be}\,, \tag{B.10}$$

and y and z are related to the cylindrical coordinates r and Θ, as

$$y = -r\sin\Theta\,, \qquad z = c\coth\alpha - r\cos\Theta\,. \tag{B.11}$$

Equation (B.8) shows that lines of constant η represent circles in the physical plane with centre at $(c\coth\eta, 0)$ and and radius $c/\sinh\eta$. The inner and and outer surface of the annulus are thus represented by lines of constant η which will be designed as α and β, respectively.

Tranforming equation (B.3) into bipolar coordinates, one gets

$$\nabla^2\Psi(\xi,\eta) = \frac{\partial^2\Psi}{\partial\xi^2} + \frac{\partial^2\Psi}{\partial\eta^2} = 0\,, \tag{B.12}$$

subject to the boundary conditions

$$\Psi(\xi,\alpha) = \frac{Qc^2}{a^2}\left[1 - \frac{2\cosh\alpha}{\cosh\alpha+\cos\xi}\right]\,, \quad \text{at the surface of the inner cylinder}\,,$$

$$\Psi(\xi,\beta) = \frac{Qc^2}{a^2}\left[1 - \frac{2\cosh\beta}{\cosh\beta+\cos\xi}\right]\,, \quad \text{at the surface of the outer cylinder}\,, \tag{B.13}$$

and the equation (B.4) can be expressed in the new coordinates (ξ,η) as

$$\left.\frac{\partial\Psi}{\partial\xi}\right|_{\xi=0} = 0\,, \qquad \left.\frac{\partial\Psi}{\partial\xi}\right|_{\xi=\pm\pi} = 0\,. \tag{B.14}$$

Considering the geometry of the system and equation (B.14), the solution to equation (B.12) may be assumed in the form

$$\Psi = E_0 + E_1\eta + \sum_{n=1}^{\infty}[A_n e^{n\eta} + B_n e^{-n\eta}]\cos n\xi\,, \tag{B.15}$$

The unknown coefficients can be determined, applying the boundary conditions expressed in the expanded form as

$$\Psi(\xi,\alpha) = \frac{Qc^2}{a^2}\left[1 - 2\coth\alpha\left\{1 + 2\sum_{n=1}^{\infty}(-1)^n e^{-n\alpha}\cos n\xi\right\}\right],$$

$$\Psi(\xi,\beta) = \frac{Qc^2}{a^2}\left[1 - 2\coth\beta\left\{1 + 2\sum_{n=1}^{\infty}(-1)^1 e^{-n\alpha}\cos n\xi\right\}\right], \qquad \text{(B.16)}$$

with the aid of the comparison of its order n. Thus, the unknown coefficients are

$$E_0 = 2\frac{Qc^2}{a^2}\frac{\coth\beta - \coth\alpha}{\alpha - \beta},$$

$$E_1 = \frac{Qc^2}{a^2}\left[1 - 2\frac{\alpha\coth\beta - \beta\coth\alpha}{\alpha - \beta}\right],$$

$$A_n = 4\frac{Qc^2}{a^2}(-1)^n\frac{\coth\beta - \coth\alpha}{e^{2n\alpha} - e^{2n\beta}},$$

$$B_n = 4\frac{Qc^2}{a^2}(-1)^n\frac{e^{2n\beta}\coth\beta - e^{2n\alpha}\coth\alpha}{e^{2n\alpha} - e^{2n\beta}}. \qquad \text{(B.17)}$$

Substituting equation (B.15) into equation (B.2), the general solution is obtained in the form

$$U(\xi,\eta) = E_0 + E_1\eta + \sum_{n=1}^{\infty}[A_n e^{n\eta} + B_n e^{-n\eta}]\cos n\xi + \frac{Qc^2}{a^2}\left[1 - \frac{2\cos\xi}{\cosh\eta + \cos\xi}\right], \qquad \text{(B.18)}$$

where the last terms come from

$$y^2 + z^2 = 1 - \frac{2\cos\xi}{\cosh\eta + \cos\xi},$$

with the aid of the coordinate transformation.

The velocity profile in cylindrical coordinates must be expressed in terms of the bipolar coordinates (ξ,η), utilizing the relations between the two coordinates shown in equations (B.6) and (B.11).

Appendix C

Steady and Unsteady Annular Viscous Flows between Rotating Cylinders

An annular viscous flow between two concentric cylinders of radii a and $b = a + H$, where $H = ah$ is the annular space, is generated by the steady or oscillatory rotation of one of the cylinders, while the other is fixed. The present spectral collocation method, presented in Chapter 4, is used to slove the problem and then the results are compared with these analytical results to validate the numerical method.

In this case, by eliminating the radial flow velocity and the circumferential variation of fluid dynamic parameters from full Navier-Stokes equations, the governing equations reduce drastically to

$$\rho \frac{W^{*2}}{r} = \frac{dP}{dr} , \tag{C.1}$$

$$\frac{1}{\nu}\frac{\partial W^*}{\partial t} = \frac{1}{r}\frac{\partial}{\partial r}\left(r\frac{\partial W^*}{\partial r}\right) + \frac{W^*}{r^2} , \tag{C.2}$$

where W^* denotes the circumferential velocity. Equation (C.1) determines the radial pressure distribution resulting from the motion.

Introducing a new coordinate defined by

$$r = e^q , \qquad \text{or} \qquad q = \ln r , \tag{C.3}$$

the radial derivatives are expressed as

$$r\frac{\partial W^*}{\partial r} = \frac{\partial W^*}{\partial q} , \qquad r\frac{\partial^2 W^*}{\partial r^2} = \frac{\partial^2 w}{\partial q^2} - \frac{\partial W^*}{\partial q} . \tag{C.4}$$

Substituting the above equations into the equation (C.2), the governing equation can reduce, in nondimensional form, to

$$\frac{\partial^2 \hat{w}}{\partial q^2} - \left(1 + \frac{(ar^*)^2}{\nu}\frac{\partial}{\partial t}\right)\hat{w} = 0\,, \tag{C.5}$$

with the aid of $\hat{w} = W^*/W_r$ and $r^* = r/a$ where W_r represents reference flow velocity.

C.1 STEADY ROTATIONAL FLOW

In the case when the moving cylinder is rotating with a steady peripheral velocity W_b, equation (C.5) is rewritten

$$\frac{d^2 \hat{w}}{dq^2} - \hat{w} = 0\,, \tag{C.6}$$

subject to the boundary conditions

$$\hat{w}|_{r^*=1} = 1 - \delta\,, \qquad \hat{w}|_{r^*=1+h} = \delta\,, \tag{C.7}$$

where $\delta = 0$ or 1 accordingly as the inner or outer cylinder is rotating, and where the nondimensional circumferential velocity is defined by

$$\hat{w} = W/W_b\,. \tag{C.8}$$

Analytically, the general solution of the above equation is in the form

$$\hat{w} = C_1 e^q + C_2 e^{-q}\,; \tag{C.9}$$

thus, in the physical domain, it is expressed, considering the coordinate transformation shown in equation (C.3), as

$$\hat{w} = C_1 a r^* + C_2 \frac{1}{ar^*}\,, \tag{C.10}$$

where the unknown coefficients, C_1 and C_2 can be determined by the boundary conditions.

The analytical solution for this steady rotation case can be obtained as

$$\hat{w}(r^*) = \frac{1}{h(2+h)}\left\{\delta(1+h)\left(r^* - \frac{1}{r^*}\right) - (1-\delta)\left[r^* - \frac{(1+h)^2}{r^*}\right]\right\}\,. \tag{C.11}$$

C.2 OSCILLATORY ROTATIONAL FLOW

The unsteady flow, generated by an harmonic oscillatory motion of a cylinder with the peripheral(*i.e.* tangential) velocity $w^* = W_o e^{\iota\omega t}$ in annulus, will be discussed. For this case, equation (C.5) reduces to

$$\frac{d^2\hat{w}}{dq^2} - \left[1 + \iota Re_s r^{*2}\right]\hat{w} = 0\,, \tag{C.12}$$

where the nondimensional reduced velocity is defined by

$$\hat{w}(r^*) = \frac{w(r,t)}{W_o e^{\iota\omega t}}\,,$$

and the oscillatory Reynolds number by

$$Re_s = \frac{\omega a^2}{\nu}\,, \tag{C.13}$$

which is explained as the product between the Reynolds number based on the peripheral velocity amplitude of the cylinder, $Re = W_o a/\nu$ and the reduced frequency, $\Omega = \omega a/W_o$. The differential equation (C.12) is subjected to the boundary conditions, equation (C.7), where again $\delta = 0$ or 1 for the case of inner or outer cylinder oscillation, respectively.

Thus, the analytical solution may be expressed for the case of very narrow annular clearance $h \ll 1$ or $r^* \approx 1$, in the form

$$\hat{w} = A_1 e^{\alpha q} + A_2 e^{-\alpha q}\,, \tag{C.14}$$

where α^2 denotes

$$\alpha^2 = (1 + \iota Re_s) = \left(1 + Re_s^2\right)^{1/2}(\cos\beta + \iota\sin\beta)\,, \tag{C.15}$$

in terms of $\beta = \arctan Re_s$.

Taking into account of the boundary conditions, the approximate analytical solution is obtained

$$\hat{w}(r^*) = \frac{1}{(1+h)^{2\alpha} - 1}\left[\delta(1+h)^{\alpha}\left(r^{*\alpha} - \frac{1}{r^{*\alpha}}\right) - (1-\delta)\left(r^{*\alpha} - \frac{(1+h)^{2\alpha}}{r^{*\alpha}}\right)\right]\,, \tag{C.16}$$

where the complex constant, α, is expressed as

$$\alpha = \left(1 + Re_s^2\right)^{1/4} (\cos \beta/2 + \iota \sin \beta/2) \,. \tag{C.17}$$

Appendix D

Unsteady Viscous Motion between Oscillating Parallel Plates

A further example which leads to a simple exact solution of the Navier-Stokes equations is afforded by the unsteady flow between two infinitely long plates, $2H$ apart, one of which executes harmonic oscillation parallel to itself with a velocity $u_1^*(t) = U_b e^{\iota\omega t}$ while the other plate is fixed ($u_2^* = 0$) or has an antiphase motion, $u_2^* = -U_b e^{\iota\omega t}$. Let y denote the coordinate perpendicular to tha wall, measured from mid-distance between the plates. In this case, the Navier-Stokes equations reduce to

$$\frac{\partial u^*}{\partial t} = \nu \frac{\partial^2 u^*}{\partial y^2} , \tag{D.1}$$

where ν is the kinematic viscosity of fluid; since, the flow velocity normal to the wall and the derivatives of dynamic fluid parameters in the direction of the motion can be eliminated in the equation. This equation may further be reduced to the form

$$\frac{\partial^2 \dot{u}}{\partial Z^2} - \iota Re_s \dot{u} = 0 , \tag{D.2}$$

subject to the boundary conditions

$$\dot{u}|_{Z=1} = 1 ,$$

$$\dot{u}|_{Z=-1} = \delta ,$$

where $\delta = 0$ in case when the lower plate ($Z = -1$) is fixed, or $\delta = -1$ when it oscillates in antiphase with respect to the upper one ($Z+1$). In the above equations, $Z = y/H$ is

a nondimensional coordinate, $Re_s = \omega H^2/\nu$ is the oscillatory Reynolds number, which can be viewed as the product between the Reynolds number based on plate-velocity amplitude $Re = U_b H/\nu$ and the reduced frequency defined by $\Omega = \omega H/U_b$; $\hat{u}$ represents a nondimensional is reduced velocity defined by

$$\hat{u}(Z) = \frac{u(z,t)}{U_b e^{\iota\omega t}} \,. \tag{D.3}$$

The analytical solution to equation (D.2) for this unsteady flow is

$$\hat{w} = A_1 e^{\alpha Z} + A_2 e^{-\alpha Z} \,, \tag{D.4}$$

where the complex constant α is expressed as as

$$\alpha = (1+\iota)\sqrt{Re_s/2} \,. \tag{D.5}$$

Considering the boundary conditions on the oscillating and fixed plates, the complex constants A_1 and A_2 are determined. The resulting analytical solution is

$$\hat{u}(Z) = \frac{\sinh[\alpha(Z+1)]}{\sinh(2\alpha)} \,, \tag{D.6}$$

for the case the upper plate ($Z = 1$) oscillating with respect to a fixed lower one ($Z = -1$), or

$$\hat{u}(Z) = \frac{\sinh[\alpha(Z+1)] + \sinh[\alpha(Z-1)]}{\sinh(2\alpha)} \,, \tag{D.7}$$

for the case when the two plates oscillate in antiphase.

Appendix E

Inviscid Fluid-dynamic Forces on A Cylinder in Concentric Annular Configurations

The presence of fluid can significantly affect the dynamic motion of a cylinder in annular configurations. A method for evaluating fluid-dynamic forces for use in the dynamic analysis of moving cylinder immersed in incompressible, frictionless fluid was developed by Fritz, for small amplitude motion. However, the theory can be adapted to several unsteady fluid-dynamic problems, and the results associated with the present problem in concentric annulus are presented to estimate these forces. In this analysis, the cylinder is assumed to execute translational motion.

A frictionless, incompressible fluid in irrotational motion will have no loss of potential energy and may be called an inertial Lagrangian system. The fluid-dynamic forces F_i acting on a cylinder are given by Lagrange's equation:

$$F_i = -\frac{d}{dt}\frac{\partial T_f}{\partial \dot{x}_i} + \frac{\partial T_f}{\partial x_i} , \tag{E.1}$$

where x_j are the generalized coordinates of motion and T_f is the fluid kinematic energy. By the assumption of small amplitude motion, it is reasonable to neglect the nonlinear contributions associated with the last term in equation (E.1). Hence, the equation reduces to

$$F_i = -\frac{d}{dt}\frac{\partial T_f}{\partial \dot{x}_i} . \tag{E.2}$$

For the present analysis, the system consists of cylinders of which radii are a and b as shown in Figure E.1. The displacements of the moving inner and outer cylinders are denoted by e_I and e_O, respectively.

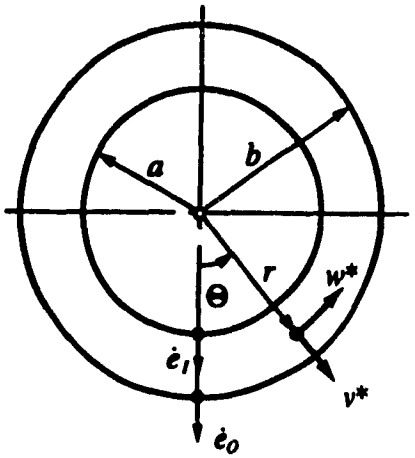

Figure E. Two-cylinder motion with fluid coupling

Hence, the kinematic energy per unit length of system is

$$T_f = \int_a^b \int_0^{2\pi} \frac{1}{2}\rho r \, dr \, d\Theta (v^{*2} + w^{*2}) \,, \tag{E.3}$$

where the radial and circumferential velocities, respectively, are expressed as

$$v^* = \left(\frac{B}{r^2} - A\right)\cos\Theta \,,$$

$$w^* = \left(\frac{B}{r^2} + A\right)\sin\Theta \,, \tag{E.4}$$

with

$$A = \frac{1}{b^2 - a^2}\left(a^2\frac{de_I}{dt} - b^2\frac{de_O}{dt}\right) \,,$$

$$B = \frac{b^2a^2}{b^2 - a^2}\left(\frac{de_I}{dt} - \frac{de_O}{dt}\right) \,.$$

Substituting equation (E.3) into equation (E.2) yields

$$\begin{aligned} F_I &= -\rho\pi a^2 a_{II}\frac{d^2e_I}{dt^2} + \rho\pi\frac{a^2+b^2}{2}a_{IO}\frac{d^2e_O}{dt^2} \,, \\ F_O &= -\rho\pi b^2 a_{OO}\frac{d^2e_O}{dt^2} + \rho\pi\frac{a^2+b^2}{2}a_{OI}\frac{d^2e_I}{dt^2} \,, \end{aligned} \tag{E.5}$$

where F_O and F_I are the fluid-dynamic forces acting on the inner and outer cylinders, respectively. The self-added(α_{II} and α_{OO}) and mutual-added(α_{IO} and α_{OI}) coefficients are given by

$$\alpha_{OI} = \alpha_{OI} = \frac{2}{1+(b/a)^2}\left(1+\frac{a^2+b^2}{b^2-a^2}\right) ,$$

$$\alpha_{OO} = \alpha_{II} = \frac{a^2+b^2}{b^2-a^2} , \tag{E.6}$$

where, *i.e,*, α_{OI} is the mutual-added mass coefficient acting on the outer cylinder due to oscillatory motion of the inner cylinder. As compared with the approach based on slender-body theory shown in Appendix A, the self-added mass coefficients are in the same form. Typical results and comparison with the present numerical results are presented in Chapter 5.

Appendix F

Block-tridiagonal System of Equations

When a system of partial differential equations is approximated by an implicit formulation involving three grid points at each level, a block-tridiagoral system is produced. A block-tridiagonal is one whose only non-zero submatrices are in the diagonal and either side of it. In the present analysis, a system of linear algebraic equations can be obtained by applying the governing equations to a finite number of grid points distributed in the axial domain, based on the hybrid scheme. As a result, the system of equations can be expressed as a block-tridiagonal system in the general form

$$S\Delta Q = R\,, \tag{F.1}$$

where ΔQ and R are the vectors for the unknown coefficients and the boundary conditions, respectively. S represents the block-tridiagonal matrix expressed as

$$S = \begin{bmatrix} A_1 & C_1 & 0 & 0 & 0 & 0 & 0 & 0 \\ B_2 & A_2 & C_2 & 0 & 0 & 0 & 0 & 0 \\ 0 & B_3 & A_3 & C_3 & 0 & 0 & 0 & 0 \\ 0 & 0 & \cdot & \cdot & \cdot & 0 & 0 & 0 \\ 0 & 0 & 0 & \cdot & \cdot & \cdot & 0 & 0 \\ 0 & 0 & 0 & 0 & B_{t-2} & A_{t-2} & C_{t-2} & 0 \\ 0 & 0 & 0 & 0 & 0 & B_{t-1} & A_{t-1} & C_{t-1} \\ 0 & 0 & 0 & 0 & 0 & 0 & B_t & A_t \end{bmatrix}, \tag{F.2}$$

where A_t, B_t and C_t are matrices of order m.

To solve the system of equations, the elimination method with factorization, is utilized. In the first equation, $A_1\,\Delta Q_1 + C_1\,\Delta Q_2 = R_1$, involves only ΔQ_1 and ΔQ_2.

Using this equation and the second one to eliminate ΔQ_2, the new second equation involves only ΔQ_2 and ΔQ_3. Continuing this procedure to the last equation where ΔQ_{t-1} has been eliminated, the new last equation only involes ΔQ_t. Therefore, ΔQ_t can be determined and the result is applied to the new $(t-1)$th equation to determine ΔQ_{t-1}. Applying the solution of the ith equation to the $(i-1)$th equation up to $i=2$, ΔQ_{i-1} is determined. The algorithm for doing all of this will now be described.

Let us consider the following factorization,

$$S = LU =$$

$$\begin{bmatrix} \Gamma_1 & 0 & 0 & 0 & 0 & 0 & 0 & 0 \\ B_2 & \Gamma_2 & 0 & 0 & 0 & 0 & 0 & 0 \\ 0 & B_3 & \Gamma_3 & 0 & 0 & 0 & 0 & 0 \\ 0 & 0 & \cdot & \cdot & 0 & 0 & 0 & 0 \\ 0 & 0 & 0 & \cdot & \cdot & 0 & 0 & 0 \\ 0 & 0 & 0 & 0 & B_{t-2} & \Gamma_{t-2} & 0 & 0 \\ 0 & 0 & 0 & 0 & 0 & B_{t-1} & \Gamma_{t-1} & 0 \\ 0 & 0 & 0 & 0 & 0 & 0 & B_t & \Gamma_t \end{bmatrix} \begin{bmatrix} \Lambda_1 & 0 & 0 & 0 & 0 & 0 & 0 & 0 \\ I & \Lambda_2 & 0 & 0 & 0 & 0 & 0 & 0 \\ 0 & I & \Lambda_3 & 0 & 0 & 0 & 0 & 0 \\ 0 & 0 & \cdot & \cdot & 0 & 0 & 0 & 0 \\ 0 & 0 & 0 & \cdot & \cdot & 0 & 0 & 0 \\ 0 & 0 & 0 & 0 & I & \Lambda_{t-2} & 0 & 0 \\ 0 & 0 & 0 & 0 & 0 & I & \Lambda_{t-1} & 0 \\ 0 & 0 & 0 & 0 & 0 & 0 & I & \Lambda_t \end{bmatrix}, \tag{F.3}$$

where I is the identity matrix of order m. The square matrices Γ_i and Λ_i are determined as follows:

$$\Gamma_1 = A_1 , \qquad \text{and} \qquad \Lambda_1 = A_1^{-1} C_1 ,$$

$$\Gamma_i = A_i - B_i \Lambda_{i-1} , \qquad \text{for} \quad i = 2, 3, 4, \cdots, t ,$$

and

$$\Lambda_i = A_i^{-1} C_i , \qquad \text{for} \quad i = 2, 3, 4, \cdots, t-1 .$$

The system of equations given by equation (F.1) is now equivalent to

$$L\Upsilon = R , \tag{F.4}$$

where

$$\Upsilon = U\Delta Q . \tag{F.5}$$

Rewriting equation (F.4), one obtains

$$\begin{bmatrix} \Gamma_1 & 0 & 0 & 0 & 0 & 0 & 0 & 0 \\ B_2 & \Gamma_2 & 0 & 0 & 0 & 0 & 0 & 0 \\ 0 & B_3 & \Gamma_3 & 0 & 0 & 0 & 0 & 0 \\ 0 & 0 & \cdot & \cdot & 0 & 0 & 0 & 0 \\ 0 & 0 & 0 & \cdot & \cdot & 0 & 0 & 0 \\ 0 & 0 & 0 & 0 & B_{t-2} & \Gamma_{t-2} & 0 & 0 \\ 0 & 0 & 0 & 0 & 0 & B_{t-1} & \Gamma_{t-1} & 0 \\ 0 & 0 & 0 & 0 & 0 & 0 & B_t & \Gamma_t \end{bmatrix} \begin{bmatrix} Y_1 \\ Y_2 \\ Y_2 \\ \cdot \\ \cdot \\ Y_{t-2} \\ Y_{t-1} \\ Y_t \end{bmatrix} = \begin{bmatrix} R_1 \\ R_2 \\ R_2 \\ \cdot \\ \cdot \\ R_{t-2} \\ R_{t-1} \\ R_t \end{bmatrix}, \qquad \text{(F.6)}$$

from which

$$Y_1 = \Gamma_1^{-1} R_2 ,$$

and

$$Y_i = \Gamma_i^{-1}(R_i - B_i Y_{i-1}) , \qquad \text{for} \quad i = 2, 3, 4, \cdots, t .$$

Equation (F.5) is then expressed as

$$\begin{bmatrix} I & \Lambda_1 & 0 & 0 & 0 & 0 & 0 & 0 \\ 0 & I & \Lambda_2 & 0 & 0 & 0 & 0 & 0 \\ 0 & 0 & I & \Lambda_3 & 0 & 0 & 0 & 0 \\ 0 & 0 & 0 & \cdot & \cdot & 0 & 0 & 0 \\ 0 & 0 & 0 & 0 & \cdot & \cdot & 0 & 0 \\ 0 & 0 & 0 & 0 & 0 & I & \Lambda_{t-2} & 0 \\ 0 & 0 & 0 & 0 & 0 & 0 & I & \Lambda_{t-1} \\ 0 & 0 & 0 & 0 & 0 & 0 & 0 & I \end{bmatrix} \begin{bmatrix} \Delta Q_1 \\ \Delta Q_2 \\ \Delta Q_2 \\ \cdot \\ \cdot \\ \Delta Q_{t-2} \\ \Delta Q_{t-1} \\ \Delta Q_t \end{bmatrix} = \begin{bmatrix} Y_1 \\ Y_2 \\ Y_2 \\ \cdot \\ \cdot \\ Y_{t-2} \\ Y_{t-1} \\ Y_t \end{bmatrix}, \qquad \text{(F.7)}$$

from which

$$\Delta Q_t = Y_t ,$$

and

$$\Delta Q_i = Y_i - \Lambda_i \Delta Q_{i+1} , \qquad \text{for} \quad i = t, t-2, t-3, t-4, \cdots, 2, 1 .$$

In the present analysis, the submatrices of equation (F.2) become for equal axial spacing

$$\begin{aligned} A_1 &= A_2 = A_3 = \cdots = A_t , \\ B_1 &= B_2 = B_3 = \cdots = B_t , \\ C_1 &= C_2 = C_3 = \cdots = C_t . \end{aligned} \qquad \text{(F.8)}$$

Therefore, the system of equations is drastically simplified and the storage required for the system of equations can be substantially reduced.

Appendix G

The Computer Program and Typical Results

The program is used for calculating the fluid-dynamic parameters including the unsteady pressure generated by the oscillatory motion of the inner cylinder, eventually computing the fluid-dynamic forces acting on the inner cylinder. The system, presented in Chapter 6, consists of a flexible inner cylinder, as a clamped-clamped beam, subjected to axial flow in a concentric annulus. The fluid-dynamic forces can be studied for different geometries and fluid properties. This program has been modified to tackle the two-dimensional problem discussed in Chapter 5.

The whole program is written in FORTRAN. It can be run on a personal digital computer. All calculations are carried out in real and complex arithmetic with double precision. The program is composed of a main program and sub-programs. The main program is subdivided into four parts. In the first part, the axial flow velocity is calculated for laminar flow. Considering the results of steady axial flow velocity and using the collocation method for discretizing the governing equations, the submatrices W, P, E(see section 6.1.2) are obtained by the finite-difference method and the inverse matrix, P^{-1} and its determinant are computed in the second part. Utilizing the LU decomposition method, the unknown coefficients for the fluid parameters in expanded form under the spectral method, are determined in part three. Finally, the fluid-dynamic parameters and the resulting forces are calculated.

The sub-program consists of subroutines SHORTEN, AMPLY and DISP. The

inversion and determinant of matrix A are computed in the subroutine SHORTEN by the shortened method based on the Gauss-Seidel iteration procedure with respect to pivot point. The subroutine AMPLY is used for complex matrix multiplication. The lateral displacements of the moving flexible cylinder based on the first mode expansion are calculated in the subroutine DISP. The value of Chebyshev polynomials for given Z are computed in the subfunction CBSP.

A sample listing of the program and its output results (for $b/a = 1.25$, $L/a = 15$, $dP/dx = -5\,\mathrm{Pa/m}$, $\mu = 0.0015\,\mathrm{Pa{\cdot}s}$, $\rho = 1000\,\mathrm{kg/m^3}$, $e/(b-a) = 0$ and $Re_s = 500$) are shown in the pages that follow. In the program, the input data(*e.g.* RA, FRE, FM) are used to calculate the nondimensional parameters(as numerical input data) shown in equation (6.12). For example, the frequency FRE is not used explicitly, but only to calculate Re_s.

The output should be read as follows. First, the radial variation of the axial flow velocity, which is used to formulate the unsteady flow problem, is presented with its unknown coefficients U_{j1} – see equation (4.7); in the output, "r" denotes the real(*e.g.* in Ur) and "i" the imaginary part, and the different columns correspond the different values of j above. Second, the complex dimensional unsteady flow parameters, *e.g* u^* in m/s and p^* in Pa, are calculated at specific positions (X, Z, $F_1(\Theta) = 1$), considering the corresponding unknown coefficients presented. Finally, the complex dimensionless fluid-dynamic forces $\hat{F}$ are presented along the axial locations X. Of the four numbers given, *e.g.* CM(X), the first involves only the contribution of pressure, whereas the last involves also all shear stress effects.

```
$STORAGE:2
$NOFLOATCALLS
$LARGE
CC
******** MAIN PROGRAM **********
CC
      PROGRAM UEIL
      IMPLICIT REAL*8 (A-H,O-Z)
      IMPLICIT INTEGER (I-N)
      PARAMETER (MC=8,MF=1,NF=60,NF1=61,MX=43)
      DIMENSION UMS(MF,MC),DR(MF,MC),DI(MF,MC),QNT(NF)
      DIMENSION RR(MF,MC),RI(MF,MC),Q(NF),QT(NF),QN(NF,MX)
      DIMENSION XR(MF,MC),XI(MF,MC),PR(MF,MC),PI(MF,MC)
      DIMENSION A(NF,NF1),AA(NF,NF1),B(NF,NF),C(NF,NF)
      DIMENSION DSR(MF,MC),DSI(MF,MC),RSR(MF,MC),RSI(MF,MC)
      DIMENSION AP(NF,NF),Y(NF,NF)
      EQUIVALENCE (AA(1,1),QN(1,1))
      EQUIVALENCE (Y(1,1),AP(1,1))
      EQUIVALENCE (B(1,1),XR(1,1)),(B(1,2),DR(1,1)),(B(1,3),RR(1,1))
      EQUIVALENCE (B(1,4),XI(1,1)),(B(1,5),DI(1,1)),(B(1,6),RI(1,1))
      EQUIVALENCE (B(1,7),PR(1,1)),(B(1,8),DSR(1,1)),(B(1,9),RSR(1,1))
      EQUIVALENCE (B(1,10),PI(1,1)),(B(1,11),DSI(1,1))
      EQUIVALENCE (B(1,12),RSI(1,1))
      COMMON A,AA
C
      CHARACTER*10 FNAME2
  448 FORMAT(A)
      WRITE(*,452)
  452 FORMAT(' OUTPUT FILE NAME-'\)
      READ(*,448) FNAME2
      OPEN(6,FILE=FNAME2,STATUS='NEW')
C
C
    1 WRITE(*,500)
      READ(*,*) RB,RA,FRE,ADP,VF,FM,EO,EC
      WRITE(*,502) RB,RA,FRE,ADP,VF,FM,EO,EC
      WRITE(*,504)
      READ(*,*) IANS
      IF(IANS.EQ.2) GO TO 1
      WRITE(6,502) RB,RA,FRE,ADP,VF,FM,EO,EC
C
    3 WRITE(*,507)
      READ(*,*)MN,MJ,ML,XL,NU,ND
      WRITE(*,508)MN,MJ,ML,XL,NU,ND
      WRITE(*,504)
      READ(*,*) IANS
      IF(IANS.EQ.2) GO TO 3
      WRITE(6,508)MN,MJ,ML,XL,NU,ND
      NM=8*MN*MJ-4*MN
      NM1=NM+1
      DV=VF/FM
      PIE=2.D0*DASIN(1.D0)
      OMG=FRE*2.D0*PIE
      EON=EO/OMG/RA
      XD=1.D0/DBLE(ML-NU-ND)
      RAN=RA/RB
      ECN=EC/RB
      ECC=EC/(RB-RA)
      CK=-.25D0*ADP/VF
      S=OMG*RA**2/DV
```

```
      WRITE(6,506)RAN,ECC,S
      CD=DBLE(MN-1)
      IF(DABS(CD).LT.1.D-13) CD=1.D13
      SOD=.9D0*PIE/CD
      SOZ=2.D0/DBLE(MJ-3)
CC
CCCCCCCCCCCCCCCCCCCCCCCCCCCCCCCCCCCCCCCCCCCCCCC
C                PART ONE                      C
CCCCCCCCCCCCCCCCCCCCCCCCCCCCCCCCCCCCCCCCCCCCCCC
      JN=MN*MJ
      JN1=JN+1
      ND2=NM/2
      L=0
      IF(DABS(CK).LT.1.D-13) GO TO 11
      DO 22 I=1,MN
       DEG=SOD*DBLE(I-1)+.005D0*PIE
       CA=1.D0-ECN**2*(DSIN(DEG))**2
       RO=-EC*DCOS(DEG)+RB*CA**.5
       H=-1.D0+RO/RA
       CB=.5D0*RB*ECN**2*DSIN(2.D0*DEG)*CA**(-.5)
       DHT=(EC*DSIN(DEG)-CB)/RA
       CB=.25D0*RB*ECN**4*(DSIN(2.D0*DEG))**2*CA**(-1.5)
       CB=CB+RB*ECN**2*DCOS(2.D0*DEG)*CA**(-.5)
       D2HT=(EC*DCOS(DEG)-CB)/RA
       DO 22 LZ=1,MJ-2
        Z=SOZ*DBLE(LZ-1)-1.D0
        H1=H/(2.D0+H*(1.D0-Z))
        AS=((1.D0-Z)/H*DHT)**2
        BS=2.D0*(Z-1.D0)/(H**2)*DHT**2+(1.D0-Z)/H*D2HT
        CS=2.D0*(1.D0-Z)/H*DHT
        D1=1.D0+H1**2*AS
        D2=-H1-H1**2*BS
        D3=H1**2*CS
        D4=H1**2
        IF(LZ.EQ.1.OR.LZ.EQ.MJ-2) GO TO 12
        GO TO 15
   12   L=L+1
        WRITE(*,*)L
        A(L,JN1)=0.D0
        DO 16 J1=1,MJ
         J=J1-1
         DJ=DBLE(J)
         CJ=1.D0
         IF(J.EQ.0) CJ=2.D0
         TJ=CBSP(J,Z)
         DO 16 KF=1,MN
          DK1=DBLE(KF-1)
          MKF=(KF-1)*MJ+J1
          DC=DCOS(DK1*DEG)
          IF(EC.LT.1.D-14)DC=1.D0
          A(L,MKF)=A(L,MKF)+TJ*DC
   16   CONTINUE
   15   L=L+1
        WRITE(*,*)L
        A(L,JN1)=CK*(RA*H)**2
       DO 26 J1=1,MJ
        J=J1-1
        DJ=DBLE(J)
        CJ=1.D0
        IF(J.EQ.0) CJ=2.D0
```

```
          TJ=CBSP(J,Z)
          J2=J+2
          DO 25 KF=1,MN
           DK1=DBLE(KF-1)
           DC=DCOS(DK1*DEG)
           DS=DSIN(DK1*DEG)
           IF(EC.LT.1.D-13) DC=1.D0
           IF(EC.LT.1.D-13) DS=1.D0
           IF(EC.LT.1.D-13) DK1=1.D0
           DO 28 JP=J2,MJ-1,2
            DJP=DBLE(JP)
            MKF=(KF-1)*MJ+JP+1
            A(L,MKF)=A(L,MKF)+TJ*DJP*(DJP**2-DJ**2)/CJ*DC*D1
   28      CONTINUE
           DO 29 JP=J1,MJ-1,2
            DJP=DBLE(JP)
            MKF=(KF-1)*MJ+JP+1
            A(L,MKF)=A(L,MKF)+2.D0*TJ/CJ*DJP*D2*DC
            A(L,MKF)=A(L,MKF)-DK1*2.D0*TJ/CJ*DJP*D3*DS
   29     CONTINUE
          MKF=(KF-1)*MJ+J1
          A(L,MKF)=A(L,MKF)-DK1**2*TJ*D4*DC
   25     CONTINUE
   26     CONTINUE
   22     CONTINUE
          CALL SHORTEN(JN,JN1)
          K=0
          DO 32 I=1,MN
           DO 32 J=1,MJ
            K=K+1
            UMS(I,J)=AA(K,JN1)
   32     CONTINUE
          WRITE(6,512) MJ,MN
          WRITE(6,516)((UMS(I,J),J=1,MJ),I=1,MN)
          MJ2=14
          SOZ1=2.D0/DBLE(MJ2-1)
C
          DO 34 I=1,MN
           DEG=PIE/CD*DBLE(I-1)
           DJ=1.8D2*DEG/PIE
           CC=1.D0-ECN**2*(DSIN(DEG))**2
           RO=-EC*DCOS(DEG)+RB*CC**.5
           H=-1.D0+RO/RA
           DO 34 J=1,MJ2
            Z=SOZ1*DBLE(J-1)-1.D0
            U=0.D0
            DO 36 KS1=1,MJ
             KS=KS1-1
             TS=CBSP(KS,Z)
             DO 36 KQ=1,MN
              FQ=DCOS(DEG*DBLE(KQ-1))
              U=U+UMS(KQ,KS1)*FQ*TS
   36       CONTINUE
           WRITE(6,514) DJ,U
   34     CONTINUE
CC
CCCCCCCCCCCCCCCCCCCCCCCCCCCCCCCCCCCCCCCCCCCCCCCCCC
C                    PART TWO                     C
CCCCCCCCCCCCCCCCCCCCCCCCCCCCCCCCCCCCCCCCCCCCCCCCCC
          DO 35 I=1,JN
```

```
      DO 35 J=1,JN1
       A(I,J)=0.D0
   35 CONTINUE
   11 ND2=NM/2
      L=0
      DO 42 I=1,MN
       DEG=SOD*DBLE(I-1)+.005D0*PIE
       CA=1.D0-ECN**2*(DSIN(DEG))**2
       RO=-EC*DCOS(DEG)+RB*CA**.5
       H=-1.D0+RO/RA
       CB=.5D0*RB*ECN**2*DSIN(2.D0*DEG)*CA**(-.5)
       DHT=(EC*DSIN(DEG)-CB)/RA
       CB=.25D0*RB*ECN**4*(DSIN(2.D0*DEG))**2*CA**(-1.5)
       CB=CB+RB*ECN**2*DCOS(2.D0*DEG)*CA**(-.5)
       D2HT=(EC*DCOS(DEG)-CB)/RA
       DO 42 LZ=1,MJ-2
        Z=SOZ*DBLE(LZ-1)-1.D0
        IF(S.GT.2.D3)X=PIE/DBLE(MJ-3)*DBLE(LZ-1)
        IF(S.GT.2.D3)Z=-DCOS(X)
        H1=H/(2.D0+H*(1.D0-Z))
        AS=((1.D0-Z)/H*DHT)**2
        BS=2.D0*(Z-1.D0)/(H**2)*DHT**2+(1.D0-Z)/H*D2HT
        CS=2.D0*(1.D0-Z)/H*DHT
        D1=1.D0+H1**2*AS
        D2=-H1+H1**2*BS
        D3=H1**2*CS
        D4=H1**2
        IF(LZ.EQ.1) GO TO 37
        IF(LZ.EQ.MJ-2) GO TO 38
        GO TO 39
   37   L=L+6
        WRITE(*,*)L
        A(L,NM1)=0.D0
        A(L-1,NM1)=0.D0
        A(L-2,NM1)=0.D0
        A(L-3,NM1)=0.D0
        A(L-4,NM1)=0.D0
        A(L-5,NM1)=0.D0
        DO 40 J1=1,MJ
         J=J1-1
         CJ=1.D0
         IF(J.EQ.0) CJ=2.D0
         TJ=CBSP(J,Z)
         DO 40 KF=1,MN
          DK1=DBLE(KF-1)
          DK=DBLE(KF)
          DC=DCOS(DK1*DEG)
          DS=DSIN(DK*DEG)
          IF(EC.LT.1.D-13) DC=1.D0
          IF(EC.LT.1.D-13) DS=1.D0
          MKF=(KF-1)*MJ+J1
          A(L,MKF)=A(L,MKF)+TJ*DC
          A(L-1,MKF+ND2)=A(L-1,MKF+ND2)+TJ*DC
          A(L-2,MKF+JN)=A(L-2,MKF+JN)+TJ*DS
          A(L-3,MKF+ND2+JN)=A(L-3,MKF+ND2+JN)+TJ*DS
          A(L-4,MKF+2*JN)=A(L-4,MKF+2*JN)+TJ*DC
          A(L-5,MKF+ND2+2*JN)=A(L-5,MKF+ND2+2*JN)+TJ*DC
   40   CONTINUE
        GO TO 39
   38   L=L+6
```

```
      WRITE(*,*)L
      A(L,NM1)=0.D0
      A(L-1,NM1)=0.D0
      A(L-2,NM1)=-DSIN(DEG)
      IF(EC.LT.1.D-13) A(L-2,NM1)=-1.D0
      A(L-3,NM1)=0.D0
      A(L-4,NM1)=DCOS(DEG)
      IF(EC.LT.1.D-13) A(L-4,NM1)=1.D0
      A(L-5,NM1)=0.D0
      DO 41 J1=1,MJ
       J=J1-1
       CJ=1.D0
       IF(J.EQ.0) CJ=2.D0
       TJ=CBSP(J,Z)
       DO 41 KF=1,MN
        DK1=DBLE(KF-1)
        DK=DBLE(KF)
        DC=DCOS(DK1*DEG)
        DS=DSIN(DK*DEG)
        IF(EC.LT.1.D-13) DC=1.D0
        IF(EC.LT.1.D-13) DS=1.D0
        MKF=(KF-1)*MJ+J1
        A(L,MKF)=A(L,MKF)+TJ*DC
        A(L-1,MKF+ND2)=A(L-1,MKF+ND2)+TJ*DC
        A(L-2,MKF+JN)=A(L-2,MKF+JN)+TJ*DS
        A(L-3,MKF+ND2+JN)=A(L-3,MKF+ND2+JN)+TJ*DS
        A(L-4,MKF+2*JN)=A(L-4,MKF+2*JN)+TJ*DC
        A(L-5,MKF+ND2+2*JN)=A(L-5,MKF+ND2+2*JN)+TJ*DC
 41    CONTINUE
 39    L=L+8
      WRITE(*,*)L
      A(L,NM1)=0.D0
      A(L-1,NM1)=0.D0
      A(L-2,NM1)=0.D0
      A(L-3,NM1)=0.D0
      A(L-4,NM1)=0.D0
      A(L-5,NM1)=0.D0
      A(L-6,NM1)=0.D0
      A(L-7,NM1)=0.D0
      U=0.D0
      UZ=0.D0
      UF=0.D0
     DO 461 J1=1,MJ
      J=J1-1
      DJ=DBLE(J)
      CJ=1.D0
      IF(J.EQ.0) CJ=2.D0
      TJ=CBSP(J,Z)
      DO 461 KF=1,MN
       DK1=DBLE(KF-1)
       DC=DCOS(DK1*DEG)
       DS1=DSIN(DK1*DEG)
       IF(EC.LT.1.D-13) DC=1.D0
       IF(EC.LT.1.D-13) DS1=1.D0
       IF(EC.LT.1.D-13) DK1=0.D0
       DO 481 JP=J1,MJ-1,2
        DJP=DBLE(JP)
        CA=2.D0*TJ/CJ*DJP*DC
        UZ=UZ+CA*UMS(KF,JP+1)
481    CONTINUE
```

```
        CA=-DK1*DS1*TJ
        UF=UF+CA*UMS(KF,J1)
        U=U+UMS(KF,J1)*TJ*DC
461   CONTINUE
      UZ=UZ/RA/OMG
      U=U/RA/OMG
      UF=UF/RA/OMG
      DO 46 J1=1,MJ
       J=J1-1
       DJ=DBLE(J)
       CJ=1.D0
       IF(J.EQ.0) CJ=2.D0
       TJ=CBSP(J,Z)
       J2=J+2
       DO 45 KF=1,MN
        DK1=DBLE(KF-1)
        DK=DBLE(KF)
        DC=DCOS(DK1*DEG)
        DS=DSIN(DK*DEG)
        DC1=DCOS(DK*DEG)
        DS1=DSIN(DK1*DEG)
        IF(EC.LT.1.D-13) DC=1.D0
        IF(EC.LT.1.D-13) DS=1.D0
        IF(EC.LT.1.D-13) DC1=1.D0
        IF(EC.LT.1.D-13) DS1=1.D0
        IF(EC.LT.1.D-13) DK1=1.D0
        IF(EC.LT.1.D-13) DK=1.D0
        DO 48 JP=J2,MJ-1,2
         DJP=DBLE(JP)
         CA=TJ*DJP*(DJP**2-DJ**2)/CJ*D1
         MKF=(KF-1)*MJ+JP+1
         A(L,MKF)=A(L,MKF)+CA*DC
         A(L-1,MKF+ND2)=A(L-1,MKF+ND2)+CA*DC
         A(L-2,MKF+JN)=A(L-2,MKF+JN)+CA*DS
         A(L-3,MKF+JN+ND2)=A(L-3,MKF+JN+ND2)+CA*DS
         A(L-4,MKF+2*JN)=A(L-4,MKF+2*JN)+CA*DC
         A(L-5,MKF+2*JN+ND2)=A(L-5,MKF+2*JN+ND2)+CA*DC
48      CONTINUE
       DO 49 JP=J1,MJ-1,2
        DJP=DBLE(JP)
        CA=2.D0*TJ/CJ*DJP*D2
        MKF=(KF-1)*MJ+JP+1
        A(L,MKF)=A(L,MKF)+CA*DC
        A(L-1,MKF+ND2)=A(L-1,MKF+ND2)+CA*DC
        A(L-2,MKF+JN)=A(L-2,MKF+JN)+CA*DS
        A(L-3,MKF+JN+ND2)=A(L-3,MKF+JN+ND2)+CA*DS
        A(L-4,MKF+2*JN)=A(L-4,MKF+2*JN)+CA*DC
        A(L-5,MKF+2*JN+ND2)=A(L-5,MKF+2*JN+ND2)+CA*DC
        CA=2.D0*TJ/CJ*DJP*D3*DK1
        CB=2.D0*TJ/CJ*DJP*D3*DK
        A(L,MKF)=A(L,MKF)-CA*DS1
        A(L-1,MKF+ND2)=A(L-1,MKF+ND2)-CA*DS1
        A(L-2,MKF+JN)=A(L-2,MKF+JN)+CB*DC1
        A(L-3,MKF+ND2+JN)=A(L-3,MKF+ND2+JN)+CB*DC1
        A(L-4,MKF+2*JN)=A(L-4,MKF+2*JN)-CA*DS1
        A(L-5,MKF+2*JN+ND2)=A(L-5,MKF+2*JN+ND2)-CA*DS1
        CA=4.D0*TJ/CJ*DJP*H1**2*(1.D0-Z)/H*DHT
        A(L-2,MKF+2*JN)=A(L-2,MKF+2*JN)+CA*DC
        A(L-3,MKF+2*JN+ND2)=A(L-3,MKF+2*JN+ND2)+CA*DC
        A(L-4,MKF+JN)=A(L-4,MKF+JN)-CA*DS
```

```
      A(L-5,MKF+ND2+JN)=A(L-5,MKF+ND2+JN)-CA*DS
      CA=2.D0*TJ/CJ*DJP
      A(L-6,MKF+2*JN)=A(L-6,MKF+2*JN)+CA*DC
      A(L-7,MKF+2*JN+ND2)=A(L-7,MKF+2*JN+ND2)+CA*DC
      CA=2.D0*TJ/CJ*DJP*H1*(1.D0-Z)/H*DHT
      A(L-6,MKF+JN)=A(L-6,MKF+JN)-CA*DS
      A(L-7,MKF+ND2+JN)=A(L-7,MKF+ND2+JN)-CA*DS
      IF(JP.GT.MJ-3) GO TO 49
      MKF=(KF-1)*(MJ-2)+JP+1
      CB=-TJ/CJ*DJP*S*H1*(1.D0-Z)*DHT
      A(L-2,MKF+3*JN)=A(L-2,MKF+3*JN)+CB*DC
      A(L-3,MKF+3*JN+ND2)=A(L-3,MKF+3*JN+ND2)+CB*DC
      CB=TJ/CJ*DJP*S*H
      A(L-4,MKF+3*JN)=A(L-4,MKF+3*JN)+CB*DC
      A(L-5,MKF+3*JN+ND2)=A(L-5,MKF+3*JN+ND2)+CB*DC
49    CONTINUE
      CA=-DK1**2*TJ*D4
      CB=-DK**2*TJ*D4
      MKF=(KF-1)*MJ+J1
      A(L,MKF)=A(L,MKF)+CA*DC
      A(L-1,MKF+ND2)=A(L-1,MKF+ND2)+CA*DC
      A(L-2,MKF+JN)=A(L-2,MKF+JN)+CB*DS
      A(L-3,MKF+JN+ND2)=A(L-3,MKF+JN+ND2)+CB*DS
      A(L-4,MKF+2*JN)=A(L-4,MKF+2*JN)+CA*DC
      A(L-5,MKF+2*JN+ND2)=A(L-5,MKF+2*JN+ND2)+CA*DC
      CA=-S*H**2/4.D0*TJ
      A(L,MKF+ND2)=A(L,MKF+ND2)-CA*DC
      A(L-1,MKF)=A(L-1,MKF)+CA*DC
      A(L-2,MKF+JN+ND2)=A(L-2,MKF+JN+ND2)-CA*DS
      A(L-3,MKF+JN)=A(L-3,MKF+JN)+CA*DS
      A(L-4,MKF+2*JN+ND2)=A(L-4,MKF+2*JN+ND2)-CA*DC
      A(L-5,MKF+2*JN)=A(L-5,MKF+2*JN)+CA*DC
      A(L-2,MKF+JN)=A(L-2,MKF+JN)-H1**2*DS*TJ
      A(L-3,MKF+ND2+JN)=A(L-3,MKF+ND2+JN)-H1**2*DS*TJ
      A(L-4,MKF+2*JN)=A(L-4,MKF+2*JN)-H1**2*DC*TJ
      A(L-5,MKF+2*JN+ND2)=A(L-5,MKF+2*JN+ND2)-H1**2*DC*TJ
      A(L-6,MKF+2*JN)=A(L-6,MKF+2*JN)-H1*DC*TJ
      A(L-7,MKF+2*JN+ND2)=A(L-7,MKF+2*JN+ND2)-H1*DC*TJ
      A(L-2,MKF+2*JN)=A(L-2,MKF+2*JN)-2.D0*DK1*H1**2*DS1*TJ
      A(L-3,MKF+2*JN+ND2)=A(L-3,MKF+2*JN+ND2)-2.D0*DK1*H1**2*DS1*TJ
      A(L-4,MKF+JN)=A(L-4,MKF+JN)-2.D0*DK*H1**2*DC1*TJ
      A(L-5,MKF+ND2+JN)=A(L-5,MKF+ND2+JN)-2.D0*DK*H1**2*DC1*TJ
      A(L-6,MKF+JN)=A(L-6,MKF+JN)-H1*DK*DC1*TJ
      A(L-7,MKF+ND2+JN)=A(L-7,MKF+ND2+JN)-H1*DK*DC1*TJ
      CA=UZ*S*H/2.D0*DC*TJ
      A(L,MKF+2*JN)=A(L,MKF+2*JN)+CA
      A(L-1,MKF+2*JN+ND2)=A(L-1,MKF+2*JN+ND2)+CA
      CA=S*H**2/(2.D0+H*(1.D0-Z))/2.D0
      CA=CA*(UF+(1.D0-Z)/H*DHT*UZ)
      A(L,MKF+JN)=A(L,MKF+JN)-CA*TJ*DS
      A(L-1,MKF+JN+ND2)=A(L-1,MKF+JN+ND2)-CA*TJ*DS
      CA=-(H/XD/XL)**2/2.D0*TJ
      A(L,MKF)=A(L,MKF)+CA*DC
      A(L-1,MKF+ND2)=A(L-1,MKF+ND2)+CA*DC
      A(L-2,MKF+JN)=A(L-2,MKF+JN)+CA*DS
      A(L-3,MKF+JN+ND2)=A(L-3,MKF+JN+ND2)+CA*DS
      A(L-4,MKF+2*JN)=A(L-4,MKF+2*JN)+CA*DC
      A(L-5,MKF+2*JN+ND2)=A(L-5,MKF+2*JN+ND2)+CA*DC
      CA=(H/XD/XL)**2/4.D0*TJ
      B(L,MKF)=B(L,MKF)+CA*DC
```

```
      B(L-1,MKF+ND2)=B(L-1,MKF+ND2)+CA*DC
      B(L-2,MKF+JN)=B(L-2,MKF+JN)+CA*DS
      B(L-3,MKF+JN+ND2)=B(L-3,MKF+JN+ND2)+CA*DS
      B(L-4,MKF+2*JN)=B(L-4,MKF+2*JN)+CA*DC
      B(L-5,MKF+2*JN+ND2)=B(L-5,MKF+2*JN+ND2)+CA*DC
      C(L,MKF)=C(L,MKF)+CA*DC
      C(L-1,MKF+ND2)=C(L-1,MKF+ND2)+CA*DC
      C(L-2,MKF+JN)=C(L-2,MKF+JN)+CA*DS
      C(L-3,MKF+JN+ND2)=C(L-3,MKF+JN+ND2)+CA*DS
      C(L-4,MKF+2*JN)=C(L-4,MKF+2*JN)+CA*DC
      C(L-5,MKF+2*JN+ND2)=C(L-5,MKF+2*JN+ND2)+CA*DC
      CC=4.DO
      REP=S*U*XL*XD
      IF(REP.LT.2.DO)CC=8.DO
      CA=S*U*H**2/XD/XL/CC*TJ
      B(L,MKF)=B(L,MKF)+CA*DC
      B(L-1,MKF+ND2)=B(L-1,MKF+ND2)+CA*DC
      B(L-2,MKF+JN)=B(L-2,MKF+JN)+CA*DS
      B(L-3,MKF+JN+ND2)=B(L-3,MKF+JN+ND2)+CA*DS
      B(L-4,MKF+2*JN)=B(L-4,MKF+2*JN)+CA*DC
      B(L-5,MKF+2*JN+ND2)=B(L-5,MKF+2*JN+ND2)+CA*DC
      IF(REP.LT.2.DO)GO TO 421
      CA=-S*U*H**2/XD/XL/CC*TJ
      A(L,MKF)=A(L,MKF)+CA*DC
      A(L-1,MKF+ND2)=A(L-1,MKF+ND2)+CA*DC
      A(L-2,MKF+JN)=A(L-2,MKF+JN)+CA*DS
      A(L-3,MKF+JN+ND2)=A(L-3,MKF+JN+ND2)+CA*DS
      A(L-4,MKF+2*JN)=A(L-4,MKF+2*JN)+CA*DC
      A(L-5,MKF+2*JN+ND2)=A(L-5,MKF+2*JN+ND2)+CA*DC
      GO TO 422
421   CA=-S*U*H**2/XD/XL/CC*TJ
      C(L,MKF)=C(L,MKF)+CA*DC
      C(L-1,MKF+ND2)=C(L-1,MKF+ND2)+CA*DC
      C(L-2,MKF+JN)=C(L-2,MKF+JN)+CA*DS
      C(L-3,MKF+JN+ND2)=C(L-3,MKF+JN+ND2)+CA*DS
      C(L-4,MKF+2*JN)=C(L-4,MKF+2*JN)+CA*DC
      C(L-5,MKF+2*JN+ND2)=C(L-5,MKF+2*JN+ND2)+CA*DC
422   CA=H/XD/XL/4.DO*TJ
      B(L-6,MKF)=B(L-6,MKF)+CA*DC
      B(L-7,MKF+ND2)=B(L-7,MKF+ND2)+CA*DC
      C(L-6,MKF)=C(L-6,MKF)-CA*DC
      C(L-7,MKF+ND2)=C(L-7,MKF+ND2)-CA*DC
      IF(J1.GT.MJ-2) GO TO 45
      MKF=(KF-1)*(MJ-2)+J1
      CB=H*H1*DK1*S*TJ/2.DO
      A(L-2,MKF+3*JN)=A(L-2,MKF+3*JN)+CB*DS1
      A(L-3,MKF+3*JN+ND2)=A(L-3,MKF+3*JN+ND2)+CB*DS1
      CA=S*H**2/XD/XL/8.DO*TJ
      B(L,MKF+3*JN)=B(L,MKF+3*JN)+CA*DC
      B(L-1,MKF+ND2+3*JN)=B(L-1,MKF+ND2+3*JN)+CA*DC
      C(L,MKF+3*JN)=C(L,MKF+3*JN)-CA*DC
      C(L-1,MKF+ND2+3*JN)=C(L-1,MKF+ND2+3*JN)-CA*DC
 45   CONTINUE
 46   CONTINUE
 42   CONTINUE
     DO 321 I=1,NM
      Q(I)=A(I,NM1)
      DO 321 J=1,NM
       AP(I,J)=A(I,J)
321   CONTINUE
```

```
      CALL SHORTEN(NM,NM1)
      DO 322 I=1,NM
       DO 322 J=1,NM
        A(I,J)=AA(I,J)
  322 CONTINUE
CC
CCCCCCCCCCCCCCCCCCCCCCCCCCCCCCCCCCCCCCCCCCCCCCCCCCCC
C              PART THREE                            C
CCCCCCCCCCCCCCCCCCCCCCCCCCCCCCCCCCCCCCCCCCCCCCCCCCCC
      CALL AMPLY(A,C,AA,NM)
      DO 323 I=1,NM
       DO 323 J=1,NM
        C(I,J)=AA(I,J)
  323 CONTINUE
      CALL AMPLY(B,C,QN,NM)
      DO 324 I=1,NM
       DO 324 J=1,NM
        A(I,J)=-QN(I,J)+AP(I,J)
  324  CONTINUE
       CALL SHORTEN(NM,NM1)
       DO 328 I=1,NM
        DO 328 J=1,ML
        Y(I,J)=0.D0
  328  CONTINUE
       DO 330 I=2,ML
        X=-DBLE(NU)*XD+XD*DBLE(I-1)
        CALL DISP(EON,1,X,EX)
        IF(X.LT.0.D0) EX=0.D0
        IF(X.GT.1.D0) EX=0.D0
        DO 331 J=1,NM
         QT(J)=EX*Q(J)
         QNT(J)=0.D0
  331   CONTINUE
        DO 334 I1=1,NM
         DO 332 J1=1,NM
          QNT(I1)=QNT(I1)+B(I1,J1)*Y(J1,I-1)
  332    CONTINUE
         QNT(I1)=QT(I1)-QNT(I1)
  334   CONTINUE
        DO 336 I1=1,NM
         DO 336 J1=1,NM
          Y(I1,I)=Y(I1,I)+AA(I1,J1)*QNT(J1)
  336   CONTINUE
       WRITE(6,519)X,(Y(J,I),J=1,NM)
  330   CONTINUE
        DO 338 J=1,NM
         QN(J,ML)=Y(J,ML)
  338   CONTINUE
        DO 340 I=ML-1,1,-1
        X=-DBLE(NU)*XD+XD*DBLE(I-1)
         DO 341 J=1,NM
          QNT(J)=0.D0
  341    CONTINUE
         DO 342 I1=1,NM
          DO 344 J1=1,NM
           QNT(I1)=QNT(I1)+C(I1,J1)*QN(J1,I+1)
  344     CONTINUE
          QN(I1,I)=Y(I1,I)- QNT(I1)
  342    CONTINUE
        WRITE(*,519)X,(QN(J,I),J=1,NM)
```

```
      WRITE(6,519)X,(QN(J,I),J=1,NM)
  340 CONTINUE
CC
CCCCCCCCCCCCCCCCCCCCCCCCCCCCCCCCCCCCCCCCCCCCCCC
C            PART FOUR                          C
CCCCCCCCCCCCCCCCCCCCCCCCCCCCCCCCCCCCCCCCCCCCCCC
      DO 350 L=1,ML
      X=XD*DBLE(L-1)-DBLE(NU)*XD
      WRITE(6,526)X
      K=0
      DO 52 I=1,MN
       DO 52 J=1,MJ
        K=K+1
        XR(I,J)=QN(K,L)
        XI(I,J)=QN(K+ND2,L)
        DR(I,J)=QN(K+JN,L)
        DI(I,J)=QN(K+JN+ND2,L)
        RR(I,J)=QN(K+2*JN,L)
        RI(I,J)=QN(K+2*JN+ND2,L)
   52 CONTINUE
      K=0
      DO 53 I=1,MN
       DO 53 J=1,MJ-2
        K=K+1
        PR(I,J)=QN(K+3*JN,L)
        PI(I,J)=QN(K+3*JN+ND2,L)
   53 CONTINUE
      WRITE(6,516)((XR(I,J),J=1,MJ),I=1,MN)
      WRITE(6,516)((XI(I,J),J=1,MJ),I=1,MN)
      WRITE(6,516)((DR(I,J),J=1,MJ),I=1,MN)
      WRITE(6,516)((DI(I,J),J=1,MJ),I=1,MN)
      WRITE(6,516)((RR(I,J),J=1,MJ),I=1,MN)
      WRITE(6,516)((RI(I,J),J=1,MJ),I=1,MN)
      WRITE(6,517)((PR(I,J),J=1,MJ-2),I=1,MN)
      WRITE(6,517)((PI(I,J),J=1,MJ-2),I=1,MN)
C
C
      K1=5
      IF(MN.EQ.1) K1=1
      D1=DBLE(K1-1)
      IF(MN.EQ.1) D1=1
      DO 54 ID=1,K1
      DEG=PIE/D1*DBLE(ID-1)
      DJ=1.8D2*DEG/PIE
      DO 54 IZ=1,11
       Z=.2D0*DBLE(IZ-1)-1.D0
       RX=0.D0
       GX=0.D0
       RC=0.D0
       GC=0.D0
       RN=0.D0
       GN=0.D0
       RP=0.D0
       GP=0.D0
       DO 56 K=1,MN
        DK1=DBLE(K-1)
        DK=DBLE(K)
        DC=DCOS(DK1*DEG)
        DS=DSIN(DK*DEG)
        IF(EC.LT.1.D-13) DC=1.D0
```

```
      IF(EC.LT.1.D-13) DS=1.D0
      DO 56 J=1,MJ
       TJ=CBSP(J-1,Z)
       RX=RX+XR(K,J)*TJ*DC*RA*OMG
       GX=GX+XI(K,J)*TJ*DC*RA*OMG
       RC=RC+DR(K,J)*TJ*DS*RA*OMG
       GC=GC+DI(K,J)*TJ*DS*RA*OMG
       RN=RN+RR(K,J)*TJ*DC*RA*OMG
       GN=GN+RI(K,J)*TJ*DC*RA*OMG
       IF(J.GT.MJ-2) GO TO 56
       RP=RP+PR(K,J)*TJ*DC*FM*(OMG*RA)**2
       GP=GP+PI(K,J)*TJ*DC*FM*(OMG*RA)**2
   56  CONTINUE
       AX=DSQRT(RX**2+GX**2)
       AC=DSQRT(RC**2+GC**2)
       AN=DSQRT(RN**2+GN**2)
       APP=DSQRT(RP**2+GP**2)
       WRITE(6,520)DJ,Z,RX,GX,RC,GC,RN,GN,RP,GP,APP
   54 CONTINUE
  350 CONTINUE
C
      JN2=JN*2
      JN21=JN2+1
      DEX=1.58815D0*EO
      WRITE(6,526)DEX
      DO 81 I=1,NM
       DO 81 J=1,ML
        Y(I,J)=QN(I,J)
   81 CONTINUE
      DO 82 IL=1,ML
      X=XD*DBLE(IL-1)-DBLE(NU)*XD
      K=0
      DO 57 I=1,MN
       DO 57 J=1,MJ
        K=K+1
        XR(I,J)=Y(K,IL)
        XI(I,J)=Y(K+ND2,IL)
        DR(I,J)=Y(K+JN,IL)
        DI(I,J)=Y(K+JN+ND2,IL)
        RR(I,J)=Y(K+2*JN,IL)
        RI(I,J)=Y(K+2*JN+ND2,IL)
   57  CONTINUE
      K=0
      DO 58 I=1,MN
       DO 58 J=1,MJ-2
        K=K+1
        PR(I,J)=Y(K+3*JN,IL)
        PI(I,J)=Y(K+3*JN+ND2,IL)
   58  CONTINUE
      DO 59 I=1,JN2
       DO 59 J=1,JN21
        A(I,J)=0.D0
   59 CONTINUE
      L=0
      DO 60 I=1,MN
       DEG=SOD*DBLE(I-1)+.005D0*PIE
       CA=1.D0-ECN**2*(DSIN(DEG))**2
       RO=-EC*DCOS(DEG)+RB*CA**.5
       H=-1.D0+RO/RA
       DO 60 LZ=1,MJ
```

```
      Z=2.DO/DBLE(MJ-1)*DBLE(LZ-1)-1.DO
      L=L+2
      WRITE(*,*)L
      DO 62 J1=1,MJ
       J=J1-1
       CJ=1.DO
       IF(J.EQ.0) CJ=2.DO
       TJ=CBSP(J,Z)
       DO 62 KF=1,MN
        DK1=DBLE(KF-1)
        DC=DCOS(DK1*DEG)
        IF(EC.LT.1.D-13) DC=1.DO
        CA=0.DO
        CB=0.DO
        DO 64 JP=J1,MJ-1,2
         DJP=DBLE(JP)
         CA=CA+DJP*RR(KF,JP+1)
         CB=CB+DJP*RI(KF,JP+1)
64      CONTINUE
        MKF=(KF-1)*MJ+J1
        A(L,MKF)=A(L,MKF)+TJ*DC
        A(L-1,MKF+JN)=A(L-1,MKF+JN)+TJ*DC
        A(L,JN21)=A(L,JN21)+2.DO*TJ/CJ*DC/H*CA
        A(L-1,JN21)=A(L-1,JN21)+2.DO*TJ/CJ*DC/H*CB
62    CONTINUE
60   CONTINUE
     CALL SHORTEN(JN2,JN21)
     K=0
     DO 66 I=1,MN
      DO 66 J=1,MJ
       K=K+1
       RSR(I,J)=AA(K,JN21)
       RSI(I,J)=AA(K+JN,JN21)
66   CONTINUE
C
     DO 68 I=1,JN2
      DO 68 J=1,JN21
       A(I,J)=0.DO
68  CONTINUE
     L=0
     DO 70 I=1,MN
      DEG=SOD*DBLE(I-1)+.005DO*PIE
      CA=1.DO-ECN**2*(DSIN(DEG))**2
      RO=-EC*DCOS(DEG)+RB*CA**.5
      H=-1.DO+RO/RA
      DO 70 LZ=1,MJ
       Z=2.DO/DBLE(MJ-1)*DBLE(LZ-1)-1.DO
       L=L+2
       WRITE(*,*)L
       DO 72 J1=1,MJ
        J=J1-1
        CJ=1.DO
        IF(J.EQ.0) CJ=2.DO
        TJ=CBSP(J,Z)
        DO 72 KF=1,MN
         DK=DBLE(KF)
         DS=DSIN(DK*DEG)
         IF(EC.LT.1.D-13) DS=1.DO
         CA=0.DO
         CB=0.DO
```

```
         DO 74 JP=J1,MJ-1,2
          DJP=DBLE(JP)
          CA=CA+DJP*DR(KF,JP+1)
          CB=CB+DJP*DI(KF,JP+1)
 74      CONTINUE
         MKF=(KF-1)*MJ+J1
         A(L,MKF)=A(L,MKF)+TJ*DS
         A(L-1,MKF+JN)=A(L-1,MKF+JN)+TJ*DS
         A(L,JN21)=A(L,JN21)+2.DO*TJ/CJ*DS/H*CA
         A(L-1,JN21)=A(L-1,JN21)+2.DO*TJ/CJ*DS/H*CB
 72    CONTINUE
 70   CONTINUE
     CALL SHORTEN(JN2,JN21)
     K=0
     DO 76 I=1,MN
      DO 76 J=1,MJ
       K=K+1
       DSR(I,J)=AA(K,JN21)
       DSI(I,J)=AA(K+JN,JN21)
 76   CONTINUE
 80  FR1=0.DO
     FI1=0.DO
     FR2=0.DO
     FI2=0.DO
     FR3=0.DO
     FI3=0.DO
     FR4=0.DO
     FI4=0.DO
     DO 78 J1=1,MJ
      J=J1-1
      TJ=1.DO
      IF(J1.GT.MJ-2) GO TO 79
      FR1=FR1+PR(1,J1)*TJ
      FI1=FI1+PI(1,J1)*TJ
 79   FR2=FR2+(DR(1,J1)-2.DO*DSR(1,J1))*TJ
      FI2=FI2+(DI(1,J1)-2.DO*DSI(1,J1))*TJ
      FR3=FR3-RR(1,J1)*TJ
      FI3=FI3-RI(1,J1)*TJ
      FR4=FR4+4.DO*RSR(1,J1)*TJ
      FI4=FI4+4.DO*RSI(1,J1)*TJ
 78  CONTINUE
     WRITE(6,526)X
     FI=FI1*OMG*RA/DEX
     FR=FR1*OMG*RA/DEX
     WRITE(6,522)FI,FR
     CA=VF/(RA*DEX*FM)
     FI=FI+FI2*CA
     FR=FR+FR2*CA
     WRITE(6,522)FI,FR
     FI=FI+FI3*CA
     FR=FR+FR3*CA
     WRITE(6,522)FI,FR
     FI=FI+FI4*CA
     FR=FR+FR4*CA
     WRITE(6,522)FI,FR
 82  CONTINUE
C
CCCCCCCCCCCCCCCCCCCCCCCCCCCCCCCCCCCCCCCCCCCCCCCCCCCCCCCCCCCCCCCCCCCCCCCC
 500 FORMAT(/,9X,'ENTER? (1) RB:OUTER CYL.DIA.  (2) RA.INNER CYL.DIA '
    /,/,15X,'(3) FRE:FREQ.   (4) ADP:+P. DROP   (5) VF.VISC. FLUID',/,
```

```
     /15X'(6) FM:DENS FLUID   (7) EO:AMP.   (8)EC:ECCEN.')
 502 FORMAT(5X,'RB=',F9.5,5X,'RA=',F9.5,5X,'FRE=',F9.3,5X,'ADP=',F9.5,
     //,5X,'VF=',F9.5,5X,'FM='F9.3,5X,'EO=',F9.5,5X,'EC=',F9.5)
 504 FORMAT(/,10X,'** IS THIS TRUE ? ** YES=1, NO=2')
 506 FORMAT(/,10X,'a/b=',F7.3,5X,'e/(b-a)=',F7.3,5X,'S=',F9.2)
 507 FORMAT(/,5X,'ENTER? (1) MN: F EXP <5  (2) MJ: CB EXP <10   (3) ML:
     /AXIAL POS.',/,10X,'(4) XL: L/A',/,15X,'** NM=8*MJ*MN-4*MN <61',/,
     /10X,'(5)NU: NO OF UPSTREAM   (6)ND:NO OF DOWNSTREAM')
 508 FORMAT(/,5X,'MN=',I3,5X,'MJ=',I3,5X,'ML=',I3,/,5X,'XL=',F6.3,/,5X,
     /'NU=',I3,5X,'ND=',I3,5X,'ML=ND+NU+NXD')
 512 FORMAT(/,10X,'((UMS(I,J),J=0,',I2,'),I=0,',I2,')')
 513 FORMAT(/,2(3(6F10.5,/),4F10.5,/))
 514 FORMAT(5X,'DEG=',F8.2,5X,'U=',F9.4)
 516 FORMAT(8F10.4)
 517 FORMAT(6F10.4)
 519 FORMAT(/,5X,'X=',F7.4,/,2(3(8F10.5,/),6F10.5,/))
 520 FORMAT(F5.1,1X,F4.1,2X,2F8.5,2X,2F8.5,2X,2F8.5,2X,3F8.4)
 522 FORMAT(2X,'CM(X)=',F9.4,5X,'CV(X)=',F9.4)
 526 FORMAT(/,5X,'X=',F9.4)
CCCCCCCCCCCCCCCCCCCCCCCCCCCCCCCCCCCCCCCCCCCCCCCCCCCCCCCCCCCCCCCCCCCCCC
     STOP
     END
CC
******** SUB-PROGRAM ***************
CC
CCCCCCCCCCCCCCCCCCCCCCCCCCCCCCCCCCCCCCCCCC
C          AMPLY CM=AM*BM               C
CCCCCCCCCCCCCCCCCCCCCCCCCCCCCCCCCCCCCCCCCC
     SUBROUTINE AMPLY(AM,BM,CM,N)
     REAL*8 AM(60,61),BM(60,60),CM(60,61)
     INTEGER I,J,N,K
     DO 10 I=1,N
      DO 10 J=1,N
  10 CM(I,J)=0.D0
     DO 40 I=1,N
      DO 40 J=1,N
       DO 40 K=1,N
  40 CM(I,J)=CM(I,J)+AM(I,K)*BM(K,J)
     RETURN
     END
C
CCCCCCCCCCCCCCCCCCCCCCCCCCCCCCCCCCCCCCCCCC
C          DISP=AK*(ETK+EHK)            C
CCCCCCCCCCCCCCCCCCCCCCCCCCCCCCCCCCCCCCCCCC
     SUBROUTINE DISP(AK,K,X,EX)
     REAL*8 AK,ETK,EHK,SK,BK,X,EX
     BK=4.7300407
     SK=.9825022
     ETK=-DCOS(BK*X)+SK*DSIN(BK*X)
     EHK=DCOSH(BK*X)-SK*DSINH(BK*X)
     EX=AK*(ETK+EHK)
     RETURN
     END
C
CCCCCCCCCCCCCCCCCCCCCCCCCCCCCCCCCCCCCCCCCCCC
C          CHEBYSHEV POLYNOMIAL           C
CCCCCCCCCCCCCCCCCCCCCCCCCCCCCCCCCCCCCCCCCCCC
     FUNCTION CBSP(N,Y)
     REAL*8 TN,PIE,DZ,Z,CBSP,Y
     INTEGER I,N
```

```
      TN=1.DO
      PIE=2.DO*DASIN(1.DO)
      IF(N.EQ.0) GO TO 3
      DO 1 I=1,N
       DZ=(2.DO*DBLE(I)-1.DO)*PIE/(2.DO*DBLE(N))
       Z=DCOS(DZ)
    1  TN=(Y-Z)*TN
      TN=2.DO**(N-1)*TN
    3 CBSP=TN
      RETURN
      END
C
CCCCCCCCCCCCCCCCCCCCCCCCCCCCCCCCCCCCCCCCCCCCCCC
C              SHORTEN METHOD                  C
CCCCCCCCCCCCCCCCCCCCCCCCCCCCCCCCCCCCCCCCCCCCCCC
      SUBROUTINE SHORTEN(N,N1)
      IMPLICIT REAL*8 (A-H,O-Z)
      IMPLICIT INTEGER (I-N)
      PARAMETER (NF=60,NF1=61)
      DIMENSION A(NF,NF1),AA(NF,NF1),COL(NF),ROW(NF1),NC(NF1),NR(NF)
      COMMON A,AA
      DO 1 I=1,N1
      IF(I.GT.N) GO TO 1
      NR(I)=I
    1 NC(I)=I
      DET=1.DO
      DO 2 K=1,N
      CLARGE=0.0DO
      DO 3 I=K,N
       DO 3 J=K,N
       CLARGO=DABS(A(I,J))
       IF(CLARGO.LT.CLARGE) GO TO 3
       CLARGE=CLARGO
       IP=I
       JP=J
       PIVOT=A(I,J)
    3  CONTINUE
      IF(CLARGE.GT.1.D-12) GO TO 16
      WRITE(*,101)
      READ(*,*)IANS
      IF(IANS.EQ.2) GO TO 13
   16 WRITE(*,*)K,PIVOT
      IF(JP.EQ.K) GO TO 4
      J=NR(JP)
      NR(JP)=NR(K)
      NR(K)=J
C     * INTERCHANGE COLUMS *
      DO 5 I=1,N
      SAVE=A(I,JP)
      A(I,JP)=A(I,K)
    5 A(I,K)=SAVE
    4 IF(IP.EQ.K) GO TO 6
      I=NC(IP)
      NC(IP)=NC(K)
      NC(K)=I
C     * INTERCHANGE ROWS *
      DO 7 J=1,N1
      SAVE=A(IP,J)
      A(IP,J)=A(K,J)
    7 A(K,J)=SAVE
```

```
  6   DO 8 I=1,N1
      IF(I.GT.N)GO TO 8
       COL(I)=A(I,K)
  8     ROW(I)=A(K,I)
      DO 9 I=1,N
       DO 9 J=1,N1
  9    A(I,J)=A(I,J)-COL(I)*ROW(J)/PIVOT
      DO 10 I=1, N1
       IF(I.GT.N) GO TO 10
       A(I,K)=-COL(I)/PIVOT
  10   A(K,I)=ROW(I)/PIVOT
       A(K,K)=1.D0/PIVOT
   2   CONTINUE
      GO TO 15
  13  WRITE(*,*)K
      DO 14 J=K,N
  14   A(J,N1)=0.D0
C     * PLACE IN CORRECT ORDER *
  15   DO 11 I=1,N
        DO 11 J=1,N1
  11   AA(NR(I),NC(J))=A(I,J)
 101  FORMAT(3X,'DO YOU WANT TO HAVE MORE ITERATION ?  YES=1, NO=2')
      RETURN
      END
```

```
*************************************************************************
*    INPUT DATA used for obtaining the nondimensional parameters(numerical   *
*              input data), as shown in equation (6.12)                     *
*           RA:  radius of the inner cylinder, a                            *
*           RB:  radius of the outer cylinder, b                            *
*           FRE: oscillation frequency, f                                   *
*           ADP: steady pressure drop alnog the axial direction, - dP/dx    *
*           VF:  viscosity of fluid                                         *
*           FM:  density of fluid                                           *
*           EO:  lateral velocity of moving cylinder at X=1/2, ev/ak        *
*           EC:  eccentricity, e                                            *
*                                                                           *
*       Degree(order) of the interpolation functions considered             *
*           MN: Fourier series                                              *
*           MJ: Chebyshev polynomials                                       *
*                                                                           *
*       Number of the mesh points:   ML                                     *
*       Length-to-radius ratio:      XL                                     *
*       Oscillatory Reynolds number: S                                      *
*************************************************************************

    RB=   .05000     RA=   .04000     FRE=     .057     ADP=  5.00000
    VF=   .00115     FM= 1000.000     EO=   .00100     EC=   .00000
    MN=  1     MJ=  8     ML= 15
    XL=15.000

         a/b=    .800     e/(b-a)=    .000     S=   500.01

********** Radial variation of axial flow velocity ******

Uj1 j=0       1         2         3         4         5         6         7
  .0270     .0005    -.0270    -.0005     .0000     .0000     .0000     .0000
     Z=   -1.000     U=    .0000
     Z=    -.846     U=    .0149
     Z=    -.692     U=    .0274
     Z=    -.538     U=    .0376
     Z=    -.385     U=    .0453
     Z=    -.231     U=    .0506
     Z=    -.077     U=    .0535
     Z=     .077     U=    .0538
     Z=     .231     U=    .0515
     Z=     .385     U=    .0466
     Z=     .538     U=    .0391
     Z=     .692     U=    .0289
     Z=     .846     U=    .0158
     Z=    1.000     U=    .0000

***** Radial variations of unsteady fluid parameters *******
      (real, imaginary parts and amplitude(only for p*))

     X=    .0000
Ur-.0402    -.0058     .0272     .0065     .0133    -.0007    -.0003     .0000
 i .0053     .0069    -.0047    -.0079    -.0017     .0009     .0011     .0000
Wr 0383      .0023    -.0266    -.0018    -.0116    -.0005    - 0001     .0000
 i- 0055    -.0001     .0055     .0001     .0009     .0000    -.0008     .0000
Vr 0010      .0002    -.0012    -.0003     .0003     .0001     0000      .0000
 i-.0006    -.0001     .0008     .0001    -.0002     .0000     .0000     .0000
Pr .1539     .0006     .0001    -.0001     .0000     .0000
 i .0358    -.0001     .0000     .0001     .0000     .0000
```

Z	u*		w*		v*		p*		
-1.0	.00000	.00000	.00000	.00000	.00000	.00000	.0319	.0075	.0328
-.8	-.00054	-.00004	.00054	-.00006	.00000	.00000	.0319	.0075	.0328
-.6	-.00072	-.00004	.00075	-.00012	.00001	-.00001	.0319	.0075	.0328
-.4	-.00073	-.00002	.00079	-.00014	.00002	-.00001	.0319	.0075	.0328
-.2	-.00073	.00002	.00078	-.00014	.00003	-.00002	.0320	.0075	.0328
.0	-.00078	.00010	.00077	-.00013	.00004	-.00002	.0320	.0074	.0329
.2	-.00089	.00021	.00080	-.00014	.00004	-.00002	.0321	.0074	.0329
.4	-.00100	.00029	.00085	-.00015	.00003	-.00002	.0321	.0074	.0330
.6	-.00099	.00029	.00084	-.00013	.00002	-.00001	.0321	.0074	.0330
.8	-.00072	.00017	.00063	-.00006	.00001	.00000	.0321	.0074	.0330
1.0	.00000	.00000	.00000	.00000	.00000	.00000	.0321	.0074	0330

X=	.2000						
Ur-	.2087	-.2373	.0765	.2068	.1291	.0309	.0031	-.0005
i	.0478	.1130	-.0253	-.1194	-.0307	.0037	.0081	.0027
Wr	.2061	-.0038	-.1728	-.0154	-.0560	-.0025	.0012	.0002
i-	.0297	.0023	.0366	-.0010	-.0022	-.0010	-.0047	-.0002
Vr	.0254	.0245	-.0051	-.0031	.0010	.0000	.0001	.0001
i-	.0029	-.0006	.0039	.0009	-.0010	-.0002	.0000	.0000
Pr	.6549	.0052	.0011	-.0008	-.0003	.0000		
i	.2614	.0025	.0008	.0002	.0000	.0000		

Z	u*		w*		v*		p*		
-1.0	.00000	.00000	.00000	.00000	.00000	.00000	.1356	.0540	.1459
-.8	-.00007	-.00098	.00287	-.00025	.00003	-.00001	.1355	.0540	.1459
-.6	.00003	-.00137	.00419	-.00063	.00012	-.00003	.1355	.0541	.1459
-.4	-.00008	-.00125	.00459	-.00085	.00023	-.00006	.1355	.0541	.1459
-.2	-.00076	-.00064	.00462	-.00092	.00035	-.00009	.1357	.0542	.1461
.0	-.00230	.00049	.00464	-.00092	.00045	-.00011	.1360	.0542	.1464
.2	-.00475	.00199	.00478	-.00091	.00054	-.00011	.1363	.0543	.1468
.4	-.00766	.00338	.00490	-.00082	.00060	-.00010	.1367	.0545	.1472
.6	-.00974	.00388	.00455	-.00057	.00063	-.00006	.1371	.0546	.1476
.8	-.00854	.00272	.00301	-.00016	.00063	-.00002	.1373	.0549	.1479
1.0	.00000	.00000	-.00062	.00000	.00062	.00000	.1374	.0551	.1480

X=	.4000						
Ur-	.3771	-.5912	.0887	.5209	.2849	.0727	.0035	-.0024
i	.1676	.3133	-.0941	-.3341	-.0931	.0144	.0196	.0064
Wr	3405	-.0210	-.3327	-.0279	-.0626	-.0020	.0044	.0004
i-	.0503	.0091	.0805	-.0059	-.0239	-.0029	-.0064	-.0002
Vr	.0516	.0564	-.0015	-.0057	.0003	-.0003	.0000	.0000
i-	.0030	-.0012	.0041	.0018	-.0010	-.0005	.0000	.0000
Pr	.6305	.0034	.0013	-.0004	-.0002	.0000		
i	.5461	.0060	.0018	.0002	.0000	.0000		

Z	u*		w*		v*		p*		
-1.0	.00000	.00000	.00000	.00000	.00000	.00000	.1308	.1127	1727
-.8	.00192	-.00213	.00436	-.00022	.00005	.00000	.1307	.1127	.1726
-.6	.00304	-.00315	.00686	-.00099	.00018	-.00001	.1307	.1128	1726
-.4	.00299	-.00285	.00806	-.00166	.00036	-.00005	.1307	.1129	1727
-.2	.00127	-.00109	.00854	-.00204	.00056	-.00008	1307	.1131	.1729
.0	-.00266	.00215	.00874	-.00214	.00077	-.00012	.1309	.1133	1731
.2	-.00884	.00636	.00882	-.00196	.00097	-.00013	.1311	.1135	.1734
.4	-.01615	.01018	.00852	-.00146	.00116	-.00012	.1314	.1138	.1738
.6	-.02149	.01144	.00727	-.00067	.00131	-.00008	.1317	.1142	1743
.8	-.01909	.00804	.00421	.00014	.00142	-.00003	.1319	.1147	.1748
1.0	.00000	.00000	-.00146	.00000	.00146	.00000	.1321	.1153	.1753

X=	.6000						
Ur	-.3495	-.6306	.0525	.5639	.2976	.0695	-.0006	-.0029
i	.2854	.3962	-.1876	-.4306	-.1213	.0288	.0235	.0055
Wr	.2591	-.0288	-.2996	-.0227	-.0140	.0008	.0041	.0002
i	-.0323	.0141	.0819	-.0107	-.0476	-.0035	-.0020	.0000
Vr	.0460	.0558	.0057	-.0048	-.0012	-.0005	-.0001	.0000
i	-.0002	-.0012	.0002	.0017	.0000	-.0005	.0000	.0000
Pr	.0810	-.0019	.0004	.0004	.0001	.0000		
i	.5522	.0057	.0018	.0001	.0000	.0000		

Z	u*		w*		v*		p*		
-1.0	.00000	.00000	.00000	.00000	.00000	.00000	.0172	.1141	.1154
-.8	.00269	-.00175	.00288	.00020	.00003	.00001	.0172	.1141	.1154
-.6	.00431	-.00268	.00510	-.00051	.00011	.00003	.0171	.1141	.1154
-.4	.00453	-.00214	.00659	-.00142	.00023	.00003	.0170	.1142	.1155
-.2	.00279	.00033	.00745	-.00210	.00038	.00002	.0169	.1143	.1156
.0	-.00150	.00473	.00780	-.00231	.00057	-.00001	.0168	.1145	.1158
.2	-.00831	.01022	.00766	-.00193	.00077	-.00003	.0167	.1148	.1160
.4	-.01631	.01485	.00689	-.00106	.00099	-.00004	.0165	.1151	.1163
.6	-.02207	.01589	.00522	.00003	.00120	-.00004	.0165	.1155	.1167
.8	-.01958	.01091	.00242	.00073	.00138	-.00002	.0165	.1160	.1171
1.0	.00000	.00000	-.00146	.00000	.00146	.00000	.0167	.1165	.1177

X=	.8000						
Ur	-.1366	-.3037	-.0108	.2791	.1516	.0262	-.0042	-.0015
i	.2904	.2686	-.2262	-.3015	-.0792	.0322	.0150	.0007
Wr	.0527	-.0182	-.1071	-.0058	.0321	.0026	.0009	-.0001
i	.0136	.0122	.0293	-.0105	-.0464	-.0019	.0035	.0002
Vr	.0154	.0234	.0079	-.0016	-.0017	-.0003	-.0001	.0000
i	.0024	-.0005	-.0033	.0008	.0009	-.0003	.0000	.0000
Pr	-.3555	-.0045	-.0006	.0007	.0003	.0000		
i	.2720	.0018	.0008	.0000	.0000	.0000		

Z	u*		w*		v*		p*		
-1.0	.00000	.00000	.00000	.00000	.00000	.00000	-.0732	.0564	.0924
-.8	.00148	-.00009	.00014	.00062	-.00001	.00002	-.0732	.0564	.0924
-.6	.00263	-.00014	.00089	.00043	-.00002	.00005	-.0733	.0563	.0924
-.4	.00314	.00060	.00178	-.00019	-.00001	.00008	-.0734	.0564	.0925
-.2	.00253	.00270	.00247	-.00077	.00002	.00010	-.0736	.0564	.0927
.0	.00043	.00609	.00276	-.00095	.00008	.00010	-.0738	.0564	.0929
.2	-.00311	.00995	.00253	-.00058	.00018	.00008	-.0741	.0565	.0932
.4	-.00729	.01273	.00179	.00019	.00030	.00005	-.0744	.0566	.0935
.6	-.01026	.01260	.00073	.00093	.00043	.00002	-.0747	.0568	.0938
.8	-.00911	.00824	-.00029	.00106	.00056	.00000	-.0749	.0570	.0941
1.0	.00000	.00000	-.00062	.00000	.00062	.00000	-.0748	.0572	.0941

X=	1.0000						
Ur	.0309	-.0151	-.0548	.0171	.0265	-.0020	-.0026	.0000
i	.1819	.0880	-.1701	-.1065	-.0155	.0207	.0038	-.0021
Wr	-.0315	-.0029	.0127	.0018	.0200	.0013	-.0012	-.0002
i	.0404	.0061	-.0222	-.0060	-.0218	-.0002	.0036	.0001
Vr	-.0018	.0000	.0024	.0001	-.0006	.0000	.0000	.0000
i	.0016	-.0001	-.0023	.0002	.0007	-.0001	-.0001	.0000
Pr	-.1588	-.0009	-.0003	.0001	.0001	.0000		
i	.0469	-.0006	.0000	.0001	.0000	.0000		

Z	u*		w*		v*		p*		
-1.0	.00000	.00000	.00000	.00000	.00000	.00000	-.0329	.0099	.0344
-.8	.00016	.00082	-.00057	.00062	-.00001	.00001	-.0329	.0099	.0344
-.6	.00068	.00140	-.00071	.00084	-.00003	.00003	-.0329	.0098	.0344
-.4	.00127	.00212	-.00059	.00075	-.00005	.00005	-.0329	.0098	.0343
-.2	.00166	.00330	-.00041	.00058	-.00006	.00006	-.0329	.0098	.0344
.0	.00166	.00480	-.00033	.00054	-.00007	.00007	-.0330	.0098	.0344
.2	.00124	.00612	-.00042	.00070	-.00006	.00006	-.0330	.0097	.0344
.4	.00058	.00658	-.00064	.00098	-.00005	.00004	-.0331	.0097	.0345
.6	-.00004	.00569	-.00082	.00111	-.00003	.00002	-.0332	.0097	.0345
.8	-.00030	.00335	-.00069	.00082	-.00001	.00001	-.0332	.0096	.0346
1.0	.00000	.00000	.00000	.00000	.00000	.00000	-.0332	.0096	.0346

******* Nondimensional Fluid-dynamic forces, F^ **********
* CM(X): real part, CV(X): -imaginary part *
****

X=	-.1000			X=	.6000		
CM(X)=	.1382	CV(X)=	.5448	CM(X)=	5.0849	CV(X)=	.7270
CM(X)=	.1382	CV(X)=	.5632	CM(X)=	5.1827	CV(X)=	.9399
CM(X)=	.1382	CV(X)=	.5632	CM(X)=	5.1827	CV(X)=	.9380
CM(X)=	.1382	CV(X)=	.5632	CM(X)=	5.1827	CV(X)=	.9380
'X=	.0000			X=	.7000		
CM(X)=	.3246	CV(X)=	1.4026	CM(X)=	3.9663	CV(X)=	-1.8255
CM(X)=	.3237	CV(X)=	1.4496	CM(X)=	4.0661	CV(X)=	-1.7356
CM(X)=	.3237	CV(X)=	1.4496	CM(X)=	4.0661	CV(X)=	-1.7370
CM(X)=	.3237	CV(X)=	1.4496	CM(X)=	4.0661	CV(X)=	-1.7370
X=	.1000			X=	.8000		
CM(X)=	1.0492	CV(X)=	3.6792	CM(X)=	2.4948	CV(X)=	-3.2657
CM(X)=	1.0514	CV(X)=	3.8129	CM(X)=	2.5844	CV(X)=	-3.2821
CM(X)=	1.0514	CV(X)=	3.8127	CM(X)=	2.5844	CV(X)=	-3.2829
CM(X)=	1.0514	CV(X)=	3.8127	CM(X)=	2.5844	CV(X)=	-3.2829
X=	.2000			X=	.9000		
CM(X)=	2.4064	CV(X)=	5.9965	CM(X)=	1.0814	CV(X)=	-3.1474
CM(X)=	2 4213	CV(X)=	6.2484	CM(X)=	1.1507	CV(X)=	-3.2198
CM(X)=	2.4213	CV(X)=	6.2476	CM(X)=	1.1507	CV(X)=	-3.2200
CM(X)=	2.4213	CV(X)=	6.2476	CM(X)=	1.1507	CV(X)=	-3 2200
X=	.3000			X=	1.0000		
CM(X)=	3.8894	CV(X)=	6.6844	CM(X)=	.4205	CV(X)=	-1.4513
CM(X)=	3.9252	CV(X)=	7.0199	CM(X)=	.4720	CV(X)=	-1.5041
CM(X)=	3.9252	CV(X)=	7.0185	CM(X)=	.4720	CV(X)=	-1.5041
CM(X)=	3.9252	CV(X)=	7.0185	CM(X)=	.4720	CV(X)=	-1.5041
X=	.4000			X=	1.1000		
CM(X)=	5.0337	CV(X)=	5.7644	CM(X)=	.0606	CV(X)=	-.3659
CM(X)=	5.0945	CV(X)=	6.1226	CM(X)=	.0936	CV(X)=	-.3880
CM(X)=	5.0945	CV(X)=	6.1208	CM(X)=	.0936	CV(X)=	-.3880
CM(X)=	5.0945	CV(X)=	6.1208	CM(X)=	.0936	CV(X)=	-.3880
X=	.5000						
CM(X)=	5.4754	CV(X)=	3.5379				
CM(X)=	5.5588	CV(X)=	3.8502				
CM(X)=	5.5588	CV(X)=	3.8482				
CM(X)=	5.5588	CV(X)=	3.8482				